STUDY OF APPLICATIONS OF A TRACKING FILTER TO STABILIZE LARGE FLEXIBLE LAUNCH VEHICLES

PHASE I FINAL TECHNICAL REPORT
PREPARED UNDER CONTRACT NAS8-20080

N66 34702
217
1
CR-77353
07

GPO PRICE $ ____________

CFSTI PRICE(S) $ ____________

Hard copy (HC) $6.00

Microfiche (MF) 1.25

ff 653 July 65

SPERRY PHOENIX COMPANY, PHOENIX, ARIZONA

SPERRY
DIVISION OF
SPERRY RAND
CORPORATION

STUDY OF APPLICATIONS OF A TRACKING FILTER TO STABILIZE LARGE FLEXIBLE LAUNCH VEHICLES

David C. Cunningham
Robert L. Schaeperkoetter

Sperry Phoenix Company
Division of Sperry Rand Corporation
Phoenix, Arizona

Phase I Final Technical Report
Contract No. NAS8-20080
Procurement Request No. DCN 1-5-40-56156-01
May 1966

Prepared for

George C. Marshall Spaceflight Center
NASA, Huntsville, Alabama

Pub. No. LJ-1201-0609

COPY 5

TABLE OF CONTENTS

LIST OF ILLUSTRATIONS

LIST OF ILLUSTRATIONS (cont)

LIST OF ILLUSTRATIONS (cont)

LIST OF ILLUSTRATIONS (cont)

LIST OF ILLUSTRATIONS (cont)

LIST OF ILLUSTRATIONS (cont)

LIST OF ILLUSTRATIONS (cont)

LIST OF ILLUSTRATIONS (cont)

LIST OF TABLES

LIST OF SYMBOLS

Symbol	Definition
e_{in}	Adaptive Tracking Filter Input (volts)
e_{out}	Adaptive Tracking Filter Output (volts)
e	Difference Between Adaptive Tracking Filter Output and Input (volts)
e_r	Demodulator Reference (volts)
e_d	Demodulator Output (volts)
e_1	Output of Second Integrator in Adaptive Tracking Filter (volts)
ω_a, ω_b	Frequencies of Oscillatory Components of Adaptive Tracking Filter Input (rad/sec)
A, B	Amplitudes of Oscillatory Components of Adaptive Tracking Filter Input (volts)
ω_p	Frequency of Adaptive Tracking Filter Pole (rad/sec)
ω_z	Frequency of Adaptive Tracking Filter Zero (rad/sec)
ζ_p	Damping Ratio of Adaptive Tracking Filter Pole
ζ_z	Damping Ratio of Adaptive Tracking Filter Zero
K_a	Gain Constant of Frequency Tracking System (rad/sec^2 per volt)
$\lambda_a, \lambda_b, \lambda_c$	Feedforward Gains of Adaptive Tracking Filter
C	Amplitude of Demodulator Reference (volts)
ϕ	Phase Angle of Demodulator Reference (rad)
$G(s, \omega_p)$	Transfer Function of Adaptive Tracking Filter
$(\ )_o$	DC Component of ( )

LIST OF SYMBOLS (cont)

Symbol	Definition
θ_a,θ_b	Phase Angles of Oscillatory Components of Adaptive Tracking Filter Input (rad)
σ	Control Signal Input to First Mode Adaptive Tracking Filter (deg)
σ_1	Control Signal Input to Second Mode Adaptive Tracking Filter (deg)
σ_2	Control Signal Output of Second Mode Adaptive Tracking Filter (deg)
$\ddot{\phi}_R$	Angular Acceleration of Rigid Body (deg/sec^2)
α	Angle of Attack (deg)
β	Total Engine Deflection (deg)
ϕ_R	Attitude Error of Rigid Body Pitch (deg)
$\ddot{Y}_T$	Total Acceleration Sensed by Control Accelerometer (meter/sec^2)
$\ddot{z}$	Vehicle Acceleration Normal to Reference (meter/sec^2)
a_o	Attitude Error Gain (deg/deg)
a_1	Attitude Rate Gain (deg per deg/sec)
g_2	Accelerometer Control Gain (deg per meter/sec^2)
C_1	Aerodynamic Restoring Coefficient (1/sec^2)
C_2	Restoring Coefficient Due to Control Engine Deflection (1/sec^2)
F	Total Vehicle Thrust (kg)
R'	Thrust of Control Engines (kg)
D	Total Vehicle Drag (kg)

LIST OF SYMBOLS (cont)

Symbol	Definition
l_{cp}	Distance from Vehicle C.G. to Aerodynamic Center of Pressure (meter)
l_G	Distance from Vehicle C.G. to Gimbal Point (meter)
l_A	Distance from Vehicle C.G. to Accelerometer Station (meter)
I_x	Moment of Inertia in Pitch-Yaw Plane (kg-meter-sec^2)
$\ddot{Y}$	Acceleration of Vehicle C.G. Normal to Vehicle Centerline (meter/sec^2)
m	Total Vehicle Mass (kg sec^2/meter)
m_{sk}	Equivalent Slosh Mass of kth Tank (kg sec^2/meter)
M_i	Generalized Mass Associated With ith Bending Mode (kg sec^2/meter)
V_m	Vehicle Velocity (meters/sec)
η_i	Generalized Displacement of ith Bending Mode at Normalizing Point (meters)
$Y_i(x_G)$	Normalized Displacement of ith Bending Mode at Gimbal
$Y_i'(x_G)$	Normalized Slope of ith Bending Mode at Gimbal (meter^{-1})
$Y_i(x_{IU})$	Normalized Displacement of ith Bending Mode at Instrument Unit
$Y_i(x_j)$	Normalized Displacement of ith Bending Mode at Station x_j.
$Y_i(x_{sk})$	Normalized Displacement of ith Bending Mode at Equivalent Slosh Mass Attach Point of kth Tank
ξ_k	Displacement of Equivalent kth Tank Slosh Mass (meters)

LIST OF SYMBOLS (cont)

Symbol	Definition
ζ_{sk}	Relative Damping of kth Sloshing Mode
ζ_{Bi}	Relative Damping of ith Bending Mode
ω_{sk}	Natural Frequency of kth Sloshing Mode (rad/sec)
ω_{Bi}	Natural Frequency of ith Bending Mode (rad/sec)
l_{sk}	Distance Between Equivalent Slosh Mass Attach Point of kth Sloshing Mode and Vehicle C.G. (meters)
S_E	First Mass Moment of Swiveled Engine About Gimbal Point (kg-sec^2)
I_E	Engine Moment of Inertia About Gimbal Point (kg-meter-sec^2)
q	Dynamic Pressure (kg/meter^2)
S	Reference Area (meter^2)
V_w	Wind Velocity (meter/sec)
C_{N_α}	Nondimensional Aerodynamic Normal Force Coefficient
N'	Dimensional Aerodynamic Normal Force Coefficient (kg)

STUDY OF APPLICATIONS OF A TRACKING FILTER TO STABILIZE LARGE FLEXIBLE LAUNCH VEHICLES

David C. Cunningham
Robert L. Schaeperkoetter

Sperry Phoenix Company
Division of Sperry Rand Corporation
Phoenix, Arizona

INTRODUCTION

This report presents a technical summary of the work done during Phase I of Contract NAS8-20080. The purpose of the study was to develop an adaptive control system for the stabilization of structural bending modes in flexible launch vehicles. The adaptive portion of the control system utilizes an adaptive tracking filter developed by the Sperry Phoenix Company.

The program was divided into two basic areas of investigation. The first area involved a detailed analysis of the adaptive tracking filter. Results of this investigation include information which defines the operating characteristics of the filter and the development of techniques for improving the performance of the filter. The second area of investigation was studying the application of the adaptive tracking filter for stabilizing the first two bending modes of a flexible launch vehicle. To accomplish this, analytical studies and computer simulations were performed to design and evaluate two separate adaptive control systems for the Saturn IB, SA-201 launch vehicle. The first of these configurations provides gain stabilization of the first two structural bending modes; the second configuration provides phase stabilization of these two modes.

The purpose of this report is to present a description of the work accomplished, the technical results obtained, and the conclusions and recommendations resulting from the study. The body of this report is divided into two sections; the first section covers the analysis of the adaptive tracking filter, and the second section covers the application studies.

SUMMARY

The study of applications of the adaptive tracking filter to launch vehicle structural bending mode stabilization has been divided into two basic areas of investigation: 1) determination of the static and dynamic characteristics of the adaptive tracking filter, and 2) application of the adaptive tracking filter to the specific problem of gain- and phase-stabilizing the first two bending modes of the S-IB-201 launch vehicle.

The frequency tracking technique is based on detecting the phase angle between the input signal and a reference signal. The reference signal is obtained from a tunable second-order filter which is driven by the input signal. The phase angle of the reference signal is a function of the frequency of the input and the filter natural frequency, and the rate of change of the filter natural frequency is made proportional to the output of the phase detector. When the filter frequency equals the input frequency, the input and reference signals differ in phase by 90 degrees and a null condition exists at the phase detector output.

Dynamic analysis of the frequency adjustment loop has shown that the response of the filter natural frequency to a small change in input frequency is essentially that of a first-order lag network. (For large changes in frequency, the tracking response becomes nonlinear.) Because the response is exponential, frequency identification time is defined as the time required for the filter to track to 95 percent of its final value. For several frequency tracking system configurations and a single frequency input, equations have been derived for the 95 percent tracking time. With a multiple frequency input, the tracking time must be obtained using numerical integration.

Static analysis of the adaptive tracking filter has included the determination of output harmonics for both single and multiple frequency inputs. Harmonics are introduced through modulation of the control signals by high frequency components in the frequency tracking system. With a notch configuration, the predominant harmonic at the filter output is the third harmonic of the input signal frequency and is proportional to the tracking-loop gain. For a given application, the limiting value of this gain will be determined by the maximum allowable harmonic content of the filter output.

A detailed analysis was made of the multiple frequency input case to determine the frequency tracking error and the frequency discrimination of the system. For this study, it was assumed that

only two predominant frequency components were present in the input signal. The equation for a null condition to exist in the frequency adjustment loop was derived, and a digital computer program was written to solve the equation for the equilibrium filter natural frequency. The filter may, under certain conditions, track to a location near one or the other input frequencies, depending on its initial frequency. The availability of several reference signals for use in the frequency tracking system permits the filter to be designed to favor either the high or the low input frequency.

The damping ratio of the second-order filter pole has a significant influence on the frequency discrimination of the system. Lower damping ratios result in a more sharply tuned system which provides better discrimination; however, there is usually a conflicting requirement for using larger damping ratios to obtain more desirable characteristics for the control loop compensation. The conflicting requirements on the selection of the damping ratio would be eliminated if the tracking filter were configured to use two separate filters that were frequency slaved, in lieu of the single filter which must accomplish both identification and control.

Application studies of two adaptive tracking filters were conducted. The S-IB-201 launch vehicle configuration was used in these studies. The first three bending modes, fourth and fifth cluster modes, and the SIV-B Lox tank slosh mode were included in the vehicle model.

A basic control system using first and second mode adaptive tracking filters was developed. Except for the difference in the bending mode compensation in the attitude and the attitude rate loop, the adaptive system is the same as the conventional S-IB-201 vehicle control system. Fixed compensation consisting of a single four-radian lag network is used to provide gain stabilization of higher frequency bending and cluster modes. The requirement for this fixed compensation exists regardless of whether the first two bending modes are gain- or phase-stabilized.

For phase stabilization, the first and second bending mode adaptive tracking filters were configured as second-order, lag-lead networks. For gain stabilization, two notch filter configurations were used.

Fixed-point trajectory studies were conducted which demonstrated that both of the above configurations are capable of providing the required stabilization for nominal first and second bending mode parameters. Rigid body stability margins obtained with both the gain- and phase-stabilization configuration described above are essentially the same as those obtained with the conventional S-IB-201 control system.

A real-time trajectory simulation study was also conducted. In addition to evaluating the performance of the adaptive tracking filter in a dynamically changing vehicle environment, the effect of structural mode parameter variations on overall performance was ascertained. During evaluation of the phase-stabilization configuration, a tendency for the first mode adaptive tracking filter to track to the propellant slosh frequency was noted. This tendency was minimized by adding high-pass filters at both demodulator inputs to improve the frequency discrimination of the tracking filters.

The results of both analytical and simulation studies have verified that the objective of gain- and phase-stabilizing the first two bending modes using adaptive tracking filters has been accomplished. As a result of the combined effect of control sensor location, rigid body characteristics, and control system lags, the rigid body stability is basically the same for both the adaptive control system and the conventional control system. The adaptive system does show an advantage over the conventional system in that it maintains a more stable system for the bending modes whenever the bending mode parameters vary. The overall loop gain, however, is limited by the rigid body stability and not by the stability of the bending modes.

DESCRIPTION OF THE ADAPTIVE TRACKING FILTER

The adaptive tracking filter is a second-order compensator which is capable of adaptively changing its natural frequency to coincide with the frequency of the predominant harmonic component of its input. It is comprised of a tunable second-order filter and a frequency tracking system. Figure 1 presents some typical transfer functions which may be realized with the adaptive tracking filter. These transfer functions are obtained by summing selected signals from the circuit used to develop the tunable second-order filter. This is shown in figure 2, where the λ's determine the coefficients in the numerator polynomial of the transfer function generated. For example, if $\lambda_a = \lambda_c = 1$ and $\lambda_b = 0$, the notch characteristic of figure 1a is obtained.

The frequency tracking system adjusts the natural frequency of the tunable second-order filter by integrating a frequency error signal generated by a demodulator and supplying this to two ω_p multipliers in the second-order filter. The frequency error signal is produced by using a demodulator to detect the phase shift between the input and a reference signal obtained from the second-order filter. This reference signal is selected to have a phase characteristic which is a function of the ratio of the existing filter natural frequency (ω_p) and the frequency of the input (ω_a). When these two frequencies are the same, the phase shift of the reference is 90 degrees, and the average demodulator output is zero.

Characteristics of the tunable second-order filter are described first, followed by analyses of the operation of the adaptive tracking filter for single and multiple frequency inputs.

Characteristics of the Tunable Second-Order Filter

The differential equation of the tunable second-order filter is derived for a general time-varying filter natural frequency in Appendix A.

$$\omega_p \ddot{e}_{out} + (2\zeta_p\omega_p^2 - \dot{\omega}_p)\,\dot{e}_{out} + \omega_p^3\, e_{out}$$

$$= \lambda_a\omega_p^3\, e_{in} + (\lambda_b\omega_p^2 - \lambda_c\dot{\omega}_p)\,\dot{e}_{in} + \lambda_c\omega_p\,\ddot{e}_{in}$$

If the natural frequency of the filter is constant, this equation reduces to the general second-order transfer function.

$$G(s,\omega_p) = \frac{\lambda_c S^2 + \lambda_b \omega_p S + \lambda_a \omega_p^2}{S^2 + 2\zeta_p \omega_p S + \omega_p^2}$$

Gain and phase characteristics for specific values of λ_a, λ_b, and λ_c are illustrated in figure 1. Figures 1a and 1b represent the notch and complex lag-lead networks which were used in the application studies.

Figures 1c, d, and e present transfer functions which may be used to produce demodulator reference signals. Selection of a particular demodulator reference is determined by the setting of switches S1 and S2 shown in figure 2.

S1	S2	Demodulator Reference Transfer Function
Closed	Open	"high-pass", figure 1c
Open	Closed	"low-pass", figure 1d
Closed	Closed	"all-pass", figure 1e

The transfer functions shown in figures 1f and 1g represent all-pass and band-pass configurations which can also be obtained with the adaptive tracking filter.

Single Frequency Input Analysis

This section presents the results of an analysis of the adaptive tracking filter for the case where the input signal contains a single frequency.

$$e_{in} = A \sin (\omega_a t + \theta_a)$$

Throughout the analysis of the tracking filter system, a quasi steady-state condition is assumed in which the transient response of the tunable second-order filter is neglected. Thus, the amplitudes and phase angles of signals appearing in the second-order filter are found by evaluating steady-state transfer functions at the instantaneous filter natural frequency. Analog verification of the analysis has indicated this assumption to be valid for the values of the various system parameters considered in this study.

Characteristics of the Frequency Tracking System.- Three types of demodulators have been considered which are capable of detecting the phase angle between the input and reference signals. Figure 3 illustrates the operation of these demodulators when the natural frequency of the second-order filter is less than the input signal frequency. The reference signal, in this case, leads the input by an angle ϕ which is between zero and 90 degrees. (See figure 1c, d, e.) Figure 3 indicates that the average output of each demodulator is positive. Since the integral of this signal is proportional to the natural frequency of the second-order filter, the positive average output means that the filter frequency is increasing.

The output of each demodulator may be approximated by the first two terms of its Fourier expansion. (This representation is exact for the multiplier demodulator with a sinusoidal input.) Table 1 lists the Fourier coefficients obtained when the inputs to the demodulators are:

$$e_{in} = A \sin \omega_a t$$

$$e_r = C \sin (\omega_a t + \phi)$$

Note that when the phase angle ϕ is 90 degrees (filter natural frequency equal to input signal frequency), the average output is zero, and the component at twice the input frequency is a maximum.

The amplitude C and phase angle ϕ of the reference are obtained by evaluating the transfer function relating the reference to the input $G(s,\omega_p)$ at the input signal frequency ($s = j\omega_a$). Table 2 summarizes the amplitude and phase angle obtained for each of the three demodulator reference transfer functions. Substituting these expressions into the average demodulator output equations (table 1), a relationship is obtained which relates the frequency ratio (ω_p/ω_a), to the dc signal generated by the frequency tracking system. This relationship is given in table 3 for the nine possible combinations of demodulators and demodulator reference transfer functions. Note that the frequency error characteristics of the chopper and double chopper demodulators are independent of the reference signal selected. Figures 4 through 8 are normalized plots of these functions for several values of the filter pole damping ratio ζ_p.

The demodulator output is related to the rate of change of the adaptive tracking filter natural frequency by the tracking gain K_a, and the tracking time can be obtained from the frequency error functions using:

$$t_2 - t_1 = \int_{\omega_p(t_1)}^{\omega_p(t_2)} \frac{1}{\dot{\omega}_p}\, d\omega_p \approx \int_{\omega_{po}(t_1)}^{\omega_{po}(t_2)} \frac{1}{\dot{\omega}_{po}}\, d\omega_{po}$$

In the second integral above, the subscript "o" is used to indicate that the second (and higher) harmonics are neglected.

Equations have been derived for the tracking time associated with the multiplier type of demodulator. These are presented in table 4 and are plotted in figures 9, 10, and 11 to provide a graphical solution for the time required for the frequency tracking system to track to 95 percent of its final value. Given the ratio of the initial filter frequency to the input frequency $(\omega_p/\omega_a) = X$ the identification time can be computed by multiplying the value given in the appropriate figure $f(X)$ by $(2\omega_a/A^2K_a)$. (Note that the symmetry of figures 4, 5, and 6 is not carried through to figures 9, 10, and 11.)

Figures 12a and b are analog computer recordings showing the adaptive tracking filter tracking from 1 to 2 radians per second and from 2 to 1 radians per second, respectively. In both recordings $A = 1$, $K_a = 0.1$, and $\zeta_p = 0.2$. From figure 9 the 95 percent tracking time is computed to be

$$T(1 \text{ to } 1.9) = \frac{2\omega_a}{A^2K_a} f\left(\frac{1}{2}\right) = \frac{(2)(2)}{(1)(0.1)} (0.34) = 13.6 \text{ seconds}$$

$$T(2 \text{ to } 1.05) = \frac{2\omega_a}{A^2K_a} f\left(\frac{2}{1}\right) = \frac{(2)(1)}{(1)(0.1)} (1.69) = 33.8 \text{ seconds}$$

These values are verified by the actual response. The ripple which is present on both runs is the second harmonic of the input frequency.

A linearized model of the frequency tracking system has been derived which hold for small changes in the frequency of the input signal. Assuming perturbations in the input and filter natural frequencies and neglecting products of perturbation leads to the linear variational equation.

$$\delta\dot{\omega}_{po} = \left.\frac{\partial\dot{\omega}_{po}}{\partial\omega_a}\right|_{\omega_a=\omega_{po}=\omega_o} \delta\omega_a + \left.\frac{\partial\dot{\omega}_{po}}{\partial\omega_{po}}\right|_{\omega_a=\omega_{po}=\omega_o} \delta\omega_{po}$$

For each of the nine combinations of demodulators and demodulator reference transfer functions, the linearized model is a first-order lag with unity static gain. Table 5 presents the time constants, which are functions of the equilibrium frequency ω_o. The response of the actual frequency tracking system is compared in figure 13 with the response of the linearized model, when its time constant is evaluated at the initial and final filter natural frequencies.

Harmonic Analysis.- The second harmonic of the input frequency is generated by the demodulator and represents a "jitter" of the tunable second-order filter's natural frequency. The effect of this jitter is to modulate control signals shaped by the adaptive tracking filter. An analysis was undertaken to determine the magnitude of the harmonics thus introduced into the control signals.

For steady-state conditions, the output can be expressed as a Fourier series with undetermined coefficients. After substituting this series into the time-varying system differential equation, a recursion formula is developed by equating the coefficients of terms having the same frequency. This relationship is written in band matrix form and solved on a digital computer.

The harmonics generated by the jitter at twice the frequency of the input is a special case of the more general problem which occurs when the input contains two frequency components. Details of the analysis of this multiple frequency input case are presented in Appendix A.

For a notch configuration employing the multiplier type of demodulator and the high-pass demodulator reference transfer function, the digital program was used to compute the magnitude of the first nine harmonics for various values of input and adaptive tracking filter parameters. The third harmonic is predominant, and the variation of its amplitude with the amplitude and frequency of the input, tracking gain, and damping ratio of the second-order filter pole, is shown in figures 14, 15, 16, and 17, respectively. From these and similar curves plotted for the other harmonics, the functional dependence of the various components of the output were determined graphically.

The general expression for the harmonics generated by the notch is:

$$\text{Peak Amplitude of } n^{th} \text{ harmonic in adaptive tracking notch output} = \begin{cases} \dfrac{c_1 A^5 K_a^2}{\omega_a^4 \zeta_p^2} & n = 1 \\[2ex] \dfrac{c_n A^n K_a^{\frac{n-1}{2}}}{\omega_a^{(n-1)} \zeta_p^{\frac{n-1}{2}}} & n = 3,5,7,\cdots \\[2ex] 0 & n = 0,2,4,\cdots \end{cases}$$

n	c_n
1	0.2906×10^{-2}
3	0.3095×10^{-1}
5	0.4963×10^{-3}
7	0.4926×10^{-5}
9	0.4009×10^{-7}

Multiple Frequency Input Analysis

This section presents the results of an analysis of the adaptive tracking filter for the case where the input contains two frequency components.

$$e_{in} = A \sin (\omega_a t + \theta_a) + B \sin (\omega_b t + \theta_b)$$

As in the single frequency input case, the assumption is made that the transient response of the second-order filter can be neglected.

Accuracy of Frequency Tracking System.- Static accuracy of the adaptive tracking filter has been determined by assuming steady-state conditions in the filter for an input containing two frequencies. The coordinate system shown in figure 18 is convenient for depicting the equilibrium location of the second-order filter's natural frequency relative to the two input frequencies. The horizontal center line represents $\omega_{po} = \omega_a$ and the vertical centerline $\omega_{po} = \omega_b$. The quadrants formed by these axes determine the relative size of ω_a, ω_b, and ω_{po} as given by the inequalities shown on the figure. With these coordinates, the diagonal lines with negative slopes are the loci of constant input frequency ratio ω_b/ω_a. Straight lines with slope k passing through the $(1,1)$ point represent a frequency tracking function of the form:

$$\omega_{po} = \left[\omega_a \omega_b^k\right]^{(1/k+1)}$$

The diagonal axis labeled (ω_b/ω_a), for example, is the geometric mean frequency,

$$\omega_{po} = \sqrt{\omega_a \omega_b}$$

The filter frequency is determined by setting the expression for the average demodulator output equal to zero. With a multiplier type demodulator, the average demodulator output can be determined by superposition, since all cross terms represent signals with zero average value. A high-pass demodulator reference results in the following sixth-order polynomial equation for ω_{po}:

$$\left(-A^2\omega_a^2 - B^2\omega_b^2\right)\omega_{po}^6 + \left(A^2\omega_a^4 + 2A^2\omega_a^2\omega_b^2 - 4A^2\zeta_p^2\omega_a^2\omega_b^2 + B^2\omega_b^4 + 2B^2\omega_a^2\omega_b^2 - 4B^2\zeta_p^2\omega_a^2\omega_b^2\right)\omega_{po}^4 + \left(-2A^2\omega_a^4\omega_b^2 + 4A^2\zeta_p^2\omega_a^4\omega_b^2 - A^2\omega_a^2\omega_b^4 - 2B^2\omega_a^2\omega_b^4 + 4B^2\zeta_p^2\omega_a^2\omega_b^4 - B^2\omega_a^4\omega_b^2\right)\omega_{po}^2 + \left(A^2\omega_a^4\omega_b^4 + B^2\omega_a^4\omega_b^4\right) = 0$$

Figure 19 is a plot of the positive real roots of this equation for an input having equal amplitude frequency components, and a filter pole damping ratio of 0.2. Only the first quadrant of figure 18 is shown. The intersection of a curve with the diagonal corresponding to the given input frequency ratio determines the filter frequency. For (ω_b/ω_a) less than 5.6, only one stable filter location exists independent of the initial frequency of the filter. The solution is near ω_b. When ω_b/ω_a is greater than 5.6, the filter will track toward ω_b or ω_a, depending on whether the initial filter frequency is above or below the dashed line shown. The arrows in the figure indicate the tracking path. It is possible to arrange the adaptive tracking filter to favor the lower frequency (ω_a) by use of the low-pass demodulator reference transfer function.

In figure 20, the filter pole damping ratio has been decreased to 0.05. The critical frequency ratio is 1.15 indicating considerable improvement in frequency discrimination.

No analytical solution has been found for the frequency tracking accuracy when demodulators other than the multiplier are used. Tests have been run, however, which indicate that the chopper type generally shows better frequency discrimination capability than the multiplier. It has also been noted that, with the chopper demodulator, the filter equilibrium frequency is dependent on the phase angle between the two frequency components of the input, when the input frequency ratio is an odd integer.

The order of magnitude of improvement is illustrated in figures 21 and 22. These are analog computer recordings comparing the tracking response of the chopper and multiplier demodulator configurations when the adaptive tracking filter frequency is initially high (figure 21) and low (figure 22). The recordings of the multiplier demodulator also verify figure 20.

Frequency Identification Time.- Tracking time for an input containing two frequencies can be determined using the same technique that was applied in the single frequency input case. For a multiplier type of demodulator, the average demodulator output, $e_{do} = \dot{\omega}_{po}/K_a$, can be obtained using superposition of the frequency errors produced by the two frequency components of the input applied separately. Figures 23 and 24 illustrate the frequency error functions obtained with inputs of the form:

$$e_{in} = A(\sin \omega_a t + \sin 2\omega_a t) \quad \text{and} \quad e_{in} = A(\sin \omega_a t + \sin 3\omega_a t)$$

The amplitudes and frequencies of both components of the input were normalized, and the high-pass demodulator reference was assumed for these figures. Zero crossings correspond to the equilibrium filter natural frequencies given in figure 19. Similar frequency error characteristics for the chopper and double chopper demodulators must be obtained using either digital or analog simulation, since superposition does not apply.

Effective identification time is obtained using:

$$t_2 - t_1 = \int_{\omega_p(t_1)}^{\omega_p(t_2)} \frac{1}{\dot{\omega}_p} d\omega_p \approx \int_{\omega_{po}(t_1)}^{\omega_{po}(t_2)} \frac{1}{\dot{\omega}_{po}} d\omega_{po}$$

The time required for the adaptive tracking filter to track to 95 percent of its final value has been computed for the error characteristics given in figure 23 and is plotted in figure 25 for $\zeta_p = 0.2$ and in figure 26 for $\zeta_p = 0.1$. Given the ratio of the initial filter natural frequency to the lower input frequency $(\omega_p/\omega_a) = X$ the tracking time is computed by multiplying the value of the function $f(X)$, given in figure 25 or 26, by (ω_a/A^2K_a).

Harmonic Analysis.- With two frequencies present in the input to the adaptive tracking filter, the output of a multiplier type of demodulator contains the sum, difference, and second harmonics of both input frequencies. This "jitter" creates a complex modulation of the control signals shaped by the tunable second-order filter. The difference term is likely to be predominant due to the gain characteristic of the integrator in the frequency tracking system.

An analysis was undertaken to evaluate the effect of the tracking jitter on the transmission of the filter. Details of this study are presented in Appendix A. The result of the analysis is a digital computer program which computes the magnitude of the various harmonics and subharmonics in the filter output. Test cases have been run for equal amplitude frequency components, and preliminary results are summarized in table 6.

APPLICATION TO THE S-IB-201 BENDING STABILIZATION PROBLEM

Application studies were performed to demonstrate the ability of two adaptive tracking filters to both gain- and phase-stabilize the first two bending modes of the S-IB-201 launch vehicle. To meet this objective, two control systems using first and second mode tracking filters were designed and evaluated.

The vehicle model used for the application studies is the S-IB-201 configuration pictured in figure 27. The vehicle equations and data for the S-IB-201 vehicle were supplied by Marshall Space Flight Center and are summarized in Appendix B.

Fixed-point simulation and analytical studies were conducted at launch, maximum dynamic pressure, burnout, and points of control system gain change. The flight times corresponding to these trajectory points are summarized in table 7 along with the dominant structural modes at each time. Propellant slosh effects were not included during initial point studies, although later studies were based on a vehicle model which included the SIV-B Lox tank mode.

A real-time launch trajectory simulation study was conducted in addition to the fixed-point studies. The vehicle model used for this study included the first three bending modes, the fourth and fifth cluster modes, and the SIV-B Lox tank slosh mode.

Design Philosophy

The objective of any flight control system design, whether conventional or adaptive, is to provide good rigid body response while providing acceptable stability margins with respect to parameter uncertainties and variations. Structural mode stabilization must be considered from the point of view of meeting this overall objective. The design philosophy adopted during the application studies reflects this point of view.

Control Sensor Location.- The control sensors of the S-IB-201 configuration are located in the Instrument Unit as shown in figure 27. As reported in NASA memo no. R-ASTR-F-65-6, this location was selected as a compromise based on practical considerations. At this location, the phase of the first two bending signals detected by the attitude and attitude rate sensors is destabilizing. This situation is further aggravated by the large magnitude of the first and second bending mode slopes. The adaptive tracking filter application studies were based on this control sensor location.

Bending Mode Stabilization.- Two approaches to the bending mode stabilization problem are gain and phase stabilization. A gain stabilization approach requires that the control system provide enough attenuation at the bending mode frequencies to ensure system stability regardless of the bending mode phase. A phase stabilization approach, on the other hand, is aimed at actively controlling the bending mode. To accomplish this, the control system must provide both the proper gain and phase characteristics at the bending mode frequency to obtain a closed loop damping of the mode greater than its open loop damping.

Both gain and phase stabilization approaches were used in the application studies. Two adaptive tracking filter configurations were established: one for gain stabilization of the first two bending modes; the second for phase stabilization of these modes. A gain stabilization approach was adopted for higher bending and cluster modes.

Ground Rules.- In view of the overall control system design objectives, the following ground rules were established for the application studies:

- Maintain rigid body performance levels achieved by the conventional control system used in the S-IB-201 vehicle.
- Establish first and second mode tracking filter configurations for both gain and phase stabilization of the first two bending modes.
- Provide gain stabilization of bending and cluster modes not being actively controlled.

System Design

A control system was designed on the basis of the design philosophy outlined previously in this report. Both point trajectory simulation and analytical studies were conducted as part of the design effort. These studies were performed at the critical flight times and included the structural modes indicated in table 7.

System Description.- The S-IB-201 control system utilizing first and second bending mode adaptive tracking filters is shown in figure 28. Consistent with the objective of maintaining rigid body performance levels obtained with the conventional S-IB-201 system, attitude and attitude rate gain schedules reported in NASA memo no. R-ASTR-F-57 are retained, as well as the accelerometer channel gain and compensation networks required for aerodynamic load relief. The actuation system transfer function is a third-order approximation of the S-IB-201 engine dynamics.

The two adaptive tracking filter configurations used for gain and phase stabilization are also shown on figure 28. For phase stabilization, two second-order lag-lead networks are employed. The frequency response characteristics of both first and second mode filters are shown in figures 29 and 30, respectively. For gain stabilization, the adaptive tracking filters are configured as notch filters having the frequency response characteristics shown in figure 31.

Analytical Design.- Bending compensation requirements were first established from stability analyses in which no bending compensation was employed in the attitude and attitude rate channel. At this time it was verified that the bending detected by the accelerometer in the load alleviation loop was so heavily attenuated by the accelerometer filters that it could be ignored in subsequent stability analyses. Propellant slosh was not considered initially, although it was recognized that the system gain should be held as low as possible in the slosh mode frequency range.

Compensation Requirements: The requirements for bending mode compensation can be seen from the gain-phase plot of figure 32. This plot was made at the forty second flight time and illustrates the requirement for gain stabilization of the fifth cluster mode shown peaking at 22.09 radians per second. A 4-radian per second first-order lag network was selected to provide this compensation. The gain-phase plot of figure 33 shows the effect of this fixed compensation network. Note that not only is the fifth cluster mode gain-stabilized, but the previously unstable first and second bending modes have been stabilized. This is a direct consequence of the forward location of the control sensors. Note in figure 32 that although both the first and second bending modes are unstable, their peaks are offset from 180 degrees. This offset occurs at all flight times and is produced by the actuation system lag at 17 radians per second.

In view of the increased uncertainties in the higher frequency structural mode parameters, a design objective of maintaining at least 15 dB of gain margin at these frequencies was established. The addition of the fixed 4-radian lag network in addition to the 17-radian actuator lag, provides a 12 dB per octave roll-off above 17 radians per second and permits this objective to be met. Thus the control system bandwidth is restricted to the frequencies being actively controlled, i.e., the first two bending modes.

Phase Stabilization Configuration: Several possible adaptive tracking filter compensator configurations were studied as candidates for phase stabilization of the first two bending modes. These included offset notch and all-pass configurations as well as the lag-lead configuration shown in figure 28. As the result of the actuation system and fixed compensation lags previously noted, use of either offset notch or all-pass filter characteristics required that the filter center frequencies be offset above the open loop bending mode frequencies from 30 to 40 percent. The lag-lead characteristic, on the other hand, is able to provide almost the exact phase shift required to achieve maximum closed-loop damping of the mode without this frequency offset. In addition to this desirable phase characteristic, a total of 8 dB of attenuation is produced above the second mode bending frequency by the lag-lead compensators.

Gain-phase plots illustrating phase stabilization of the first two structural modes of the S-IB-201 at the flight times listed in table 7 are presented in figures 34 - 38. (The dashed portions of these curves are interpolated.) A review of these plots reveals that although the first and second modes are indeed phase-stabilized, the gain of the second mode is so low that only a nominal improvement in second mode damping is obtained. This illustrates a significant point. Consider, for example, the zero-second plot (figure 34). Note that the fifth cluster mode peaks near 180 degrees. The gain margin at 20 radians is 20 dB. Any attempt to increase the gain at the second mode frequency at 16 radians would be reflected in a tradeoff in fifth cluster mode gain margin.

The results of the phase stabilization analytical design were verified by fixed-point simulation studies at the critical flight times. The same vehicle model used for the simulation was also used for the analytical design. Closed loop damping ratios obtained with the lag-lead configurations are summarized in figure 39. It should be noted that an open loop structural damping of 0.01 was assumed for all modes.

Interaction between the first and second mode filters and tolerance to frequency offset were also investigated. For a ±20 percent frequency offset, negligible interaction between the first and second mode tracking filters was observed. The effect of filter offset on the damping ratio of the mode being controlled is shown in figure 40 for the 80-second flight time.

Gain Stabilization Configuration: The results of gain stabilization with the notch filter configuration of figure 28 are presented in the gain-phase plots of figures 41 - 45. Note that at the 140-second flight time (figure 45), the third bending mode peaks at 180 degrees with 14 dB of gain margin. Assume that the fixed compensation lag is removed. The result would be to shift the third mode peak about 80 degrees to the right (phase-lead) with a gain increase of about 20 dB resulting in a 40-radian per second instability. This third mode problem at burnout was the dominant reason for including the fixed compensation network in the gain stabilization system configuration.

As was done for phase stabilization, the analytical design results were verified by a fixed-point simulation study. The effect of tracking filter interaction was investigated as well as the system tolerance to ±20 percent frequency offsets. As was noted in the discussion of phase stabilization, interaction in terms of the frequency offset of one filter affecting the other was slight. However, offset of the first mode filter below the first bending mode rapidly drives the system unstable near the first bending mode frequency as shown in figure 46. This destabilizing tendency results from the phase-lead introduced by the notch filter above the notch frequency, and demonstrates the requirement for precisely tracking the bending mode frequency.

Slosh Mode Effects: The effect of propellant slosh on system stability was investigated by adding the dominant S-IB-201 propellant slosh mode (SIV-B Lox tank) to the vehicle model used in the initial design studies. The results are presented for both phase and gain stabilization in figures 47 through 56. These plots verify the assumption that the primary effect of propellant sloshing is a slight reduction in the rigid body gain margin. A secondary effect of the SIV-B Lox mode is an increase in the bending mode frequencies and a reduction in the bending mode gain caused by inertial coupling through the slosh mode. This results in a slight reduction in the closed loop bending mode damping from the values indicated in figure 39.

Trajectory Simulation

A real-time trajectory simulation was conducted to evaluate the performance of the control system configurations for both phase and gain stabilization. The simulation was from launch to burnout and included the first three bending modes, the fourth and fifth cluster modes, and the SIV-B Lox tank slosh mode. The equations used in this simulation were simplified by eliminating nonessential coupling terms, and are summarized in Appendix B. A standard NASA 12-kilometer wind profile (memo no. ASTR-F-65-6) with a sharp-edged gust at 75 seconds was also simulated.

Multiplier type demodulators were used for both first and second bending mode adaptive tracking filters. Limiters were also employed to restrict the frequency tracking ranges to reasonable values. The frequency ranges established by these limits are 6 to 14 radians per second for the first mode filter; 16 to 24 radians per second for the second. The tracking filter frequencies were nominally centered within these ranges at 10 and 20 radians per second respectively.

A difficulty was encountered during the trajectory simulation study of the phase stabilization configuration. As a result of insufficient bending mode excitation and improved bending mode damping, the dominant oscillatory mode occurring in the system was the propellant slosh mode. Consequently, the first mode filter tended to track the slosh mode frequency. This tendency was minimized by incorporating additional high-pass filtering in both inputs to the demodulators of the adaptive tracking filters. The additional filters are defined by the following transfer functions:

First mode demodulator filters:

$$G(s) = \frac{S^2}{\frac{S^2}{10^2} + 2\,\frac{(0.1)}{10}\,S + 1}$$

Second mode demodulator filters:

$$G(s) = \frac{S^2}{\frac{S^2}{20^2} + 2\,\frac{(0.1)}{20}\,S + 1}$$

These filters were retained in the adaptive tracking filters used for gain stabilization, although subsequent analysis of the gain stabilization results indicate that they were probably not necessary.

Phase Stabilization.- Figure 57 illustrates the ability of the adaptive tracking filters in a phase stabilization configuration to simultaneously track and improve the damping of the first two bending modes. In this figure the bending modes are excited by a pulsed thrust angle deflection at the 80-second flight time. The trajectory was fixed at this point, and to clarify the resulting transient responses, propellant slosh was not included. Both first and second mode filters are initialized well below the bending frequencies. With this frequency offset, the closed loop damping of both modes is approximately equal to their open loop damping of 0.01. As the filters track to the bending frequencies, the damping improves, as indicated by the almost linear decrement of the first bending mode transient. Note also, that the frequencies to which the filters tracked very nearly coincide with the open loop frequencies of the first two bending modes.

Trajectory recordings are presented in figures 58 through 68 for nominal and off-nominal bending mode parameters. Runs were made with the adaptive tracking filters not tracking and tracking to demonstrate any improvement obtained by tracking the bending mode frequencies. As an additional aid in interpreting the trajectory recordings, gain-phase plots are presented in figures 69 through 72.

Trajectory runs made with nominal bending mode parameters are shown in figures 58 and 69. Although, when excited at 75 seconds, the first mode adaptive tracking filter tracked from an initial frequency of 10 radians per second to 9 radians per second, no significant improvement is noted. This is substantiated by the gain-phase plots of figure 69 which approximates the situation just prior to and following excitation by the sharp-edged gust at 75 seconds. The plots illustrate that when the filter tracked to 9 radians per second it centered the first bending mode peak, but the closed loop damping of the mode did not change significantly.

Trajectory runs made with the first bending mode frequency reduced 20 percent are presented in figures 60 and 61. The trajectories reflect the same observations noted in the previous paragraph, and are substantiated by the gain-phase plots of figure 70. It is interesting to note that the first mode tracking filter did not track down to the open loop frequency of 7.35 radians per second. If it had, the filter phase characteristic would have centered the mode.

Trajectory runs made with the first mode frequency increased are presented in figures 62 and 63.

Figure 64 is a trajectory run with the first mode bending slope increased 6 decibels. This run illustrates an interesting sequence of events which can be described with the aid of the gain-phase plots of figures 71 and 72. Note that at 80 seconds the first mode tracking filter initially tracks to about 8 radians per second. As can be seen in the gain-phase plots of figure 71, when the first mode filter tracks to this frequency, the first mode phase margin (10 radians per second) is increased. Referring again to the trajectory recording, as the first mode damps out, the predominant remaining oscillation is that of the SIV-B Lox tank slosh mode. The filter then attempts to track down to the slosh mode frequency and drives into the 6-radian per second limit, where it remains until the first bending mode is again excited near 100 seconds. The first mode filter detects this oscillation and tracks to about 8 radians per second, again damping the mode. As at 80 seconds, once the bending mode has been damped, the slosh mode oscillation attracts the first mode filter, which subsequently drives into the lower frequency limit. The first mode filter remains at this limit for the rest of the trajectory, since at the higher flight times, the mode is inherently gain-stabilized. The situation at T = 100 seconds is illustrated by the gain-phase plots in figure 72. The dashed curve shows the situation with the first mode tracking filter at its lower limit. As a result of the filter having tracked this frequency, it no longer provides the lag necessary to keep the first mode frequency centered at zero degrees, thus causing a reduction in phase margin at 9.2 radians per second. Consequently, a closed loop peaking occurs near this crossover frequency to which the first mode filter tracks. When the filter tracks to 8 radians per second, the first bending mode is again centered.

The tracking performance of the second mode adaptive tracking filter for off-nominal second bending mode parameters is illustrated in figures 65, 66, and 67.

Gain Stabilization.- Gain stabilization trajectory recordings are presented in figures 73 through 83 for nominal and off-nominal first and second bending mode parameters. Trajectory runs are presented with the adaptive tracking filters both tracking and not tracking. Gain-phase plots are also provided in figures 84 through 87, as an aid in interpreting the trajectory runs. The same frequency tracking limits used for the phase stabilization system were used in the gain stabilization study.

Figures 73 and 74 are trajectory runs made with nominal bending mode parameters. Note in figure 74 that when excited by the gust at 75 seconds, the first mode filter tracks down and then back up to about 9.6 radians per second. This sequence is explained by the gain-phase plots in figures 84 and 85. Figure 84 illustrates the situations prior to the disturbance and after the first mode filter has tracked to 9.6 radians per second. Note that initially, the first mode was phase-stabilized as a result of initializing the first mode filter frequency above the open loop bending mode frequency. After the filter tracks to 9.6 radians per second, the mode is gain-stabilized. Figure 85 is a gain-phase plot illustrating the situation when the first mode filter is located at 8.4 radians per second, the frequency to which it tracks before settling out at 9.6 radians per second. What apparently occurs, is that when the system is excited by the sharp-edged gust, the first mode filter tends to track down to this frequency. However, as the filter center frequency is offset below the bending mode frequency, the phase lead introduced at the bending mode frequency destabilizes the mode, thus forcing the tracking filter back to the bending mode frequency and gain-stabilizing the mode.

Figures 75, 76 and 77 are trajectory recordings made with the first bending mode frequency reduced 20 percent. The trajectory run of figure 75 was made with the first mode slope at its nominal value. The situation of the system with and without tracking is illustrated at 80 seconds in the gain-phase plots of figure 86. Note that as a result of the first bending mode being initially phase stabilized, the first mode notch filter tracked to the closed loop frequency of the phase-stabilized system and tended to center the mode near zero degrees. Gain stabilization is never actually achieved in this case. The trajectory runs of figures 76 and 77 were made with the first mode slope increased 6 decibels. In neither case was stabilization achieved, although in figure 77 propellant sloshing caused the first mode filter to track to the low frequency limit. The gain-phase plots of figure 87 show that when the filter tracks below the first bending mode frequency, the first mode is destabilized.

Figures 78 and 79 are trajectory runs made with the first mode frequency increased 20 percent and the first mode slope increased 12 decibels. These two recordings demonstrate the ability of the first mode adaptive tracking filter to gain-stabilize a first bending mode instability.

Figure 80 is a trajectory run made with the first bending mode frequency nominal and the first mode slope increased 9 decibels.

Figures 81, 82, and 83 are trajectory runs made for off-nominal second bending mode parameters.

CONCLUSIONS AND RECOMMENDATIONS

Analytical and computer studies were conducted to define the operating characteristics of the adaptive tracking filter. Three variables which were analyzed in detail and are used to describe the filter characteristics are:

- Tracking error
- Identification time
- Harmonics in output signal

These variables are dependent on the type of frequency discrimination filter utilized in the tracking loop, the loop gain, the type of demodulator employed, and the characteristics of the input signal.

No tracking error exists if the input signal contains only one frequency component. If the input signal is comprised of two frequencies, the tracking error can be computed knowing the relative amplitude and frequency separation of the two input components and the damping ratio of the second-order filter pole. Under certain conditions it is also required to know the initial natural frequency of the filter. The error is dependent (to a small extent) on the type of demodulator utilized. Results from computer studies show that a small improvement in tracking accuracy can be achieved with the chopper or double chopper type demodulators as compared to the multiplier type demodulator. However, due to the complexity of the equations, only the multiplier type was analyzed in detail.

Three different frequency discrimination filters are available in the adaptive tracking filter configuration. The output of one of the three filters is the reference input to the demodulator. The three filters have characteristics of high-pass, low-pass, and all-pass filters. Selection of a particular filter is determined by the application. For the S-IB-201 control system application, the high-pass filter was utilized because it was necessary to filter out the rigid body and propellant slosh signal frequencies as much as possible.

The adaptive tracking filter utilizes one second-order filter to accomplish both frequency identification and control (shaping). Because of this dual function, the damping ratio of the filter poles must be selected as a compromise between tracking error and desirable gain and phase characteristics for the shaping network.

If a large damping ratio is used (favoring the control function), then it is possible, under certain conditions, for the filter to track to other frequencies present in the input signal. This occurence can destabilize the overall system. As a consequence of the above, it was concluded that two separate filters should be employed to accomplish the two required functions independently. The two filters would be frequency slaved.

The dynamics of the tracking loop (which are related to the identification time) are those of a first-order system. The time constant is dependent on the specific type of demodulator being used. For the multiplier type demodulator, the time constant is proportional to the product of the initial filter frequency and the damping ratio squared divided by the square of the input signal amplitude. With the chopper demodulator, the time constant is proportional to the same system parameters, although the damping ratio and input signal amplitude appear as the first power in lieu of the second power. The time constant of the double chopper demodulator system is the same as that of the chopper demodulator except it is independent of the input signal amplitude. The criteria for an acceptable identification time that was used in the launch vehicle simulation studies was that identification take place within five cycles of the particular body bending mode being identified. This criteria was satisfied in practically all cases. The cases where identification required longer than five cycles were when the bending mode amplitudes decreased rapidly because of large closed loop damping.

The harmonics present in the filter output result from the demodulation and multiplication processes. The amplitude of the harmonics are proportional to the loop gain of the tracking system and inversely proportional to the input signal frequency. The computer studies of the S-IB-201 model vehicle showed that the harmonics were of negligible magnitude (based on the criteria of a five cycle identification period) and could be neglected for purposes of linear stability analyses of the vehicle.

Two adaptive control systems were designed for the S-IB-201 launch vehicle using adaptive tracking filters. In both systems, tracking filters were designed to track the first and second bending mode frequencies. Both the attitude and rate gyro were located at the instrument unit. The first system gain stabilized the first and second bending modes from launch to first stage burnout. For ±20 percent variations in the bending mode frequencies, the first bending mode slope margin was 5 dB with the first mode frequency 20 percent low, and 12 dB with the first mode frequency 20 percent high. The second system phase stabilized the first two bending modes from launch to first stage burnout. For ±20 percent variations in the bending mode frequencies, the first bending mode slope margin was 2 dB with the first mode frequency 20 percent low and 12 dB with the first mode frequency 20 percent high. For both the gain and phase stabilization systems, the second bending mode slope margin was greater than 12 dB for all cases.

In both the gain and phase stabilization control systems, the overall stability, when subjected to first mode frequency and slope variations, was determined by the "high frequency rigid body" going unstable and not by the stability of the first bending mode. Because the rigid body mode frequency was outside the designed operating range of the first mode tracking filter, the adaptive phase stabilization system has basically the same first mode slope margin as the MSFC conventional system.

Based on the results of this study, the adaptive tracking filter system offers certain potential advantage as a control system for large flexible launch vehicles and should be considered for possible future applications. In order to further improve the capability and performance of the tracking filter system, it is recommended that work in the following areas be performed:

- Analyze and evaluate a tracking filter system using two frequency-slaved second-order filters.
- Analyze the filter characteristics using chopper and double chopper type demodulators.
- Design the tracking filter to operate over the frequency interval covering the high frequency rigid body mode as well as the first bending mode range.
- Investigate the use of separate adaptive filters in the attitude, rate, and load alleviation loops.
- Study the utilization of an adaptive tracking filter control system to eliminate the redesign effort for vehicle changes and payload modifications.

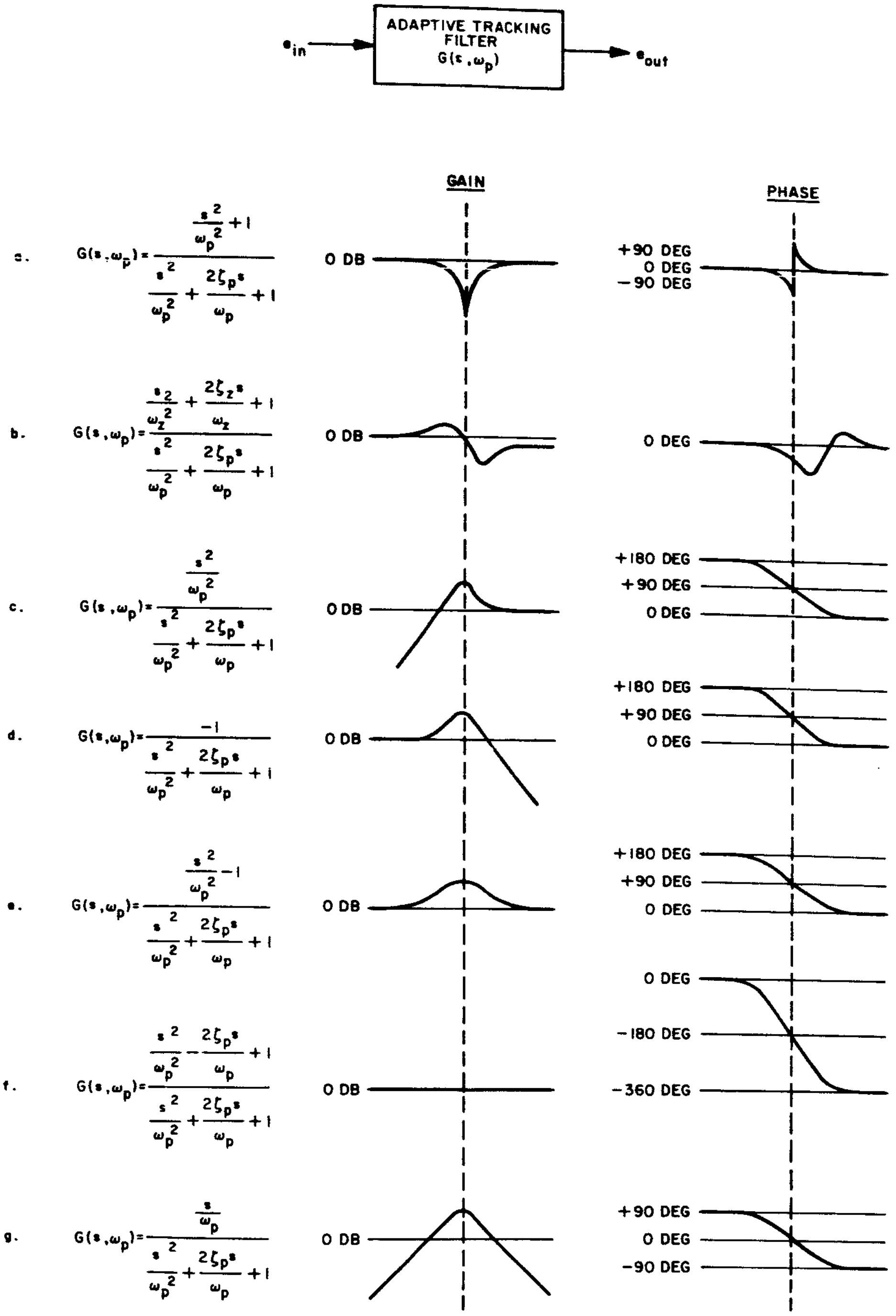

Figure 1. Typical Transfer Functions Obtainable with the Adaptive Tracking Filter

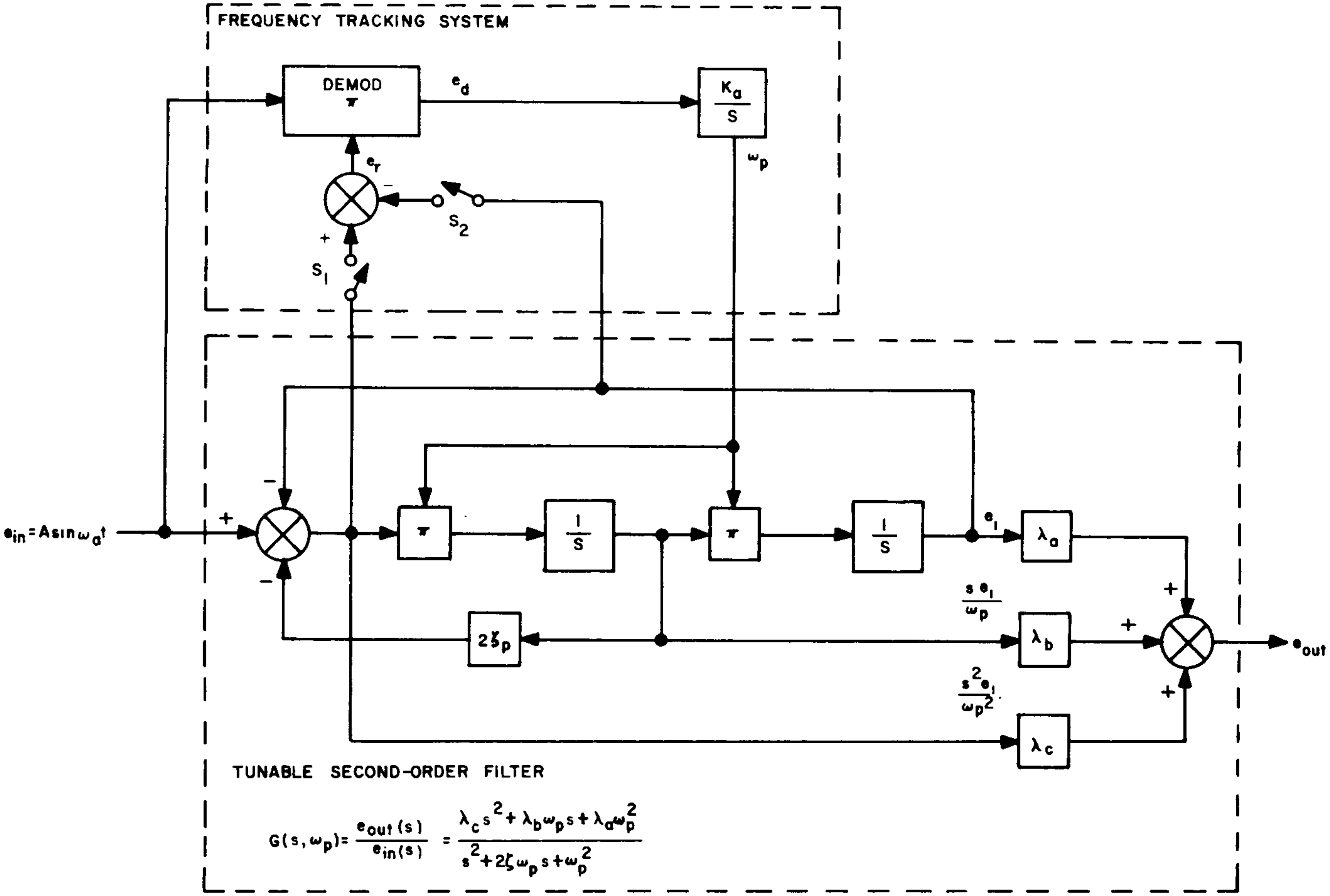

Figure 2. Block Diagram of Adaptive Tracking Filter

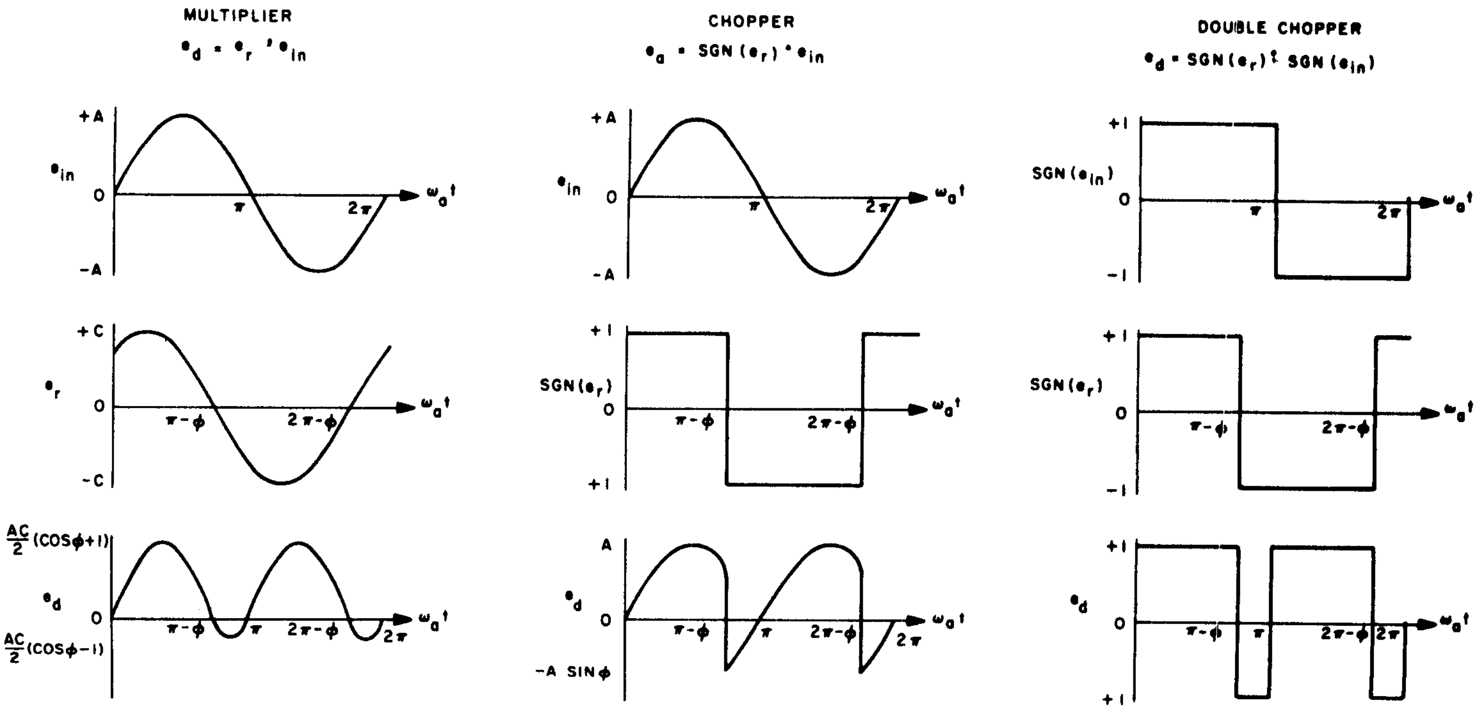

$e_{in} = A \sin(\omega_a t)$

$e_r = C \sin(\omega_a t + \phi)$

ADAPTIVE TRACKING FILTER FREQUENCY BELOW INPUT FREQUENCY $(0 < \phi < \frac{\pi}{2})$

Figure 3. Operation of Various Types of Demodulators

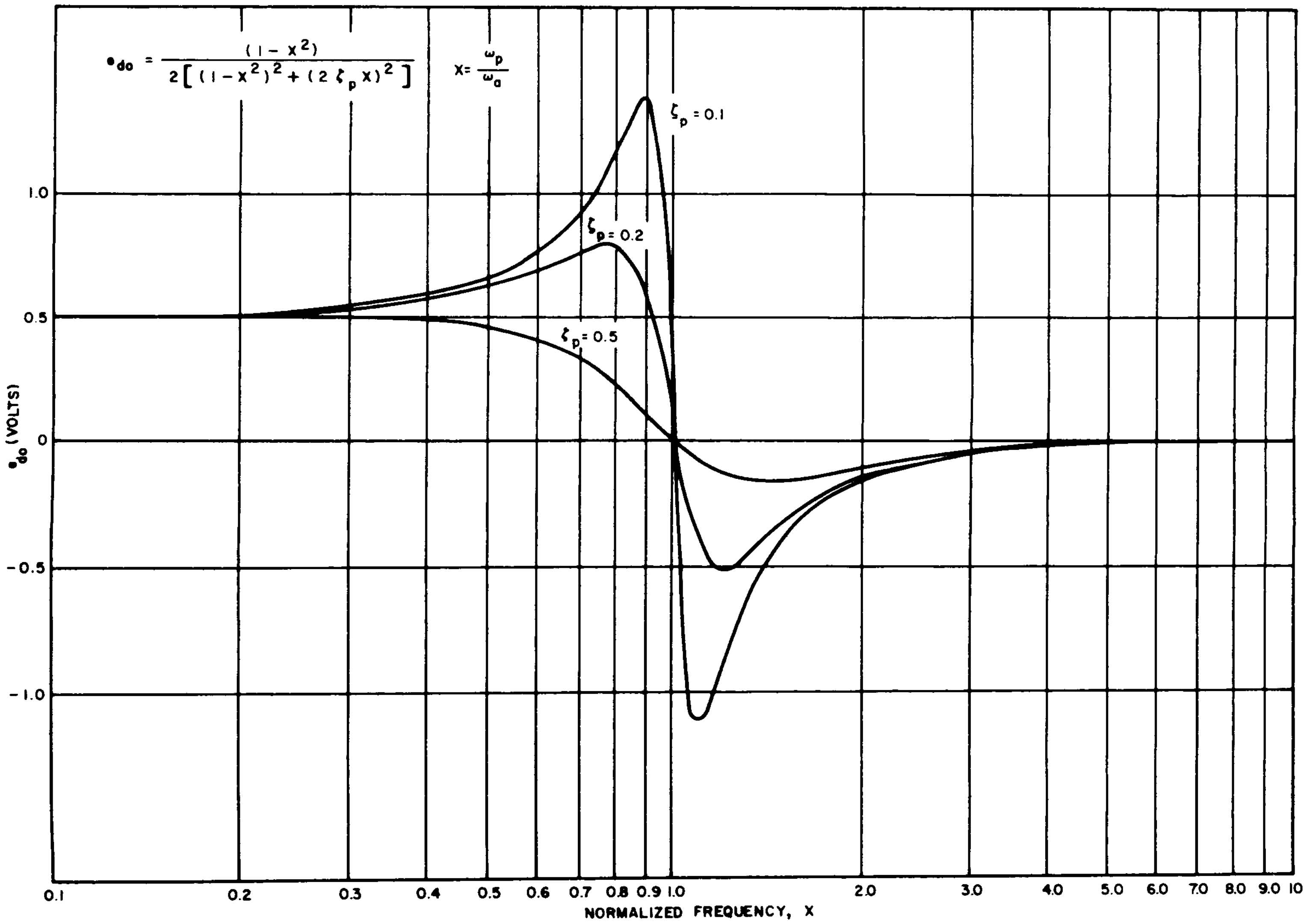

Figure 4. Amplitude of DC Component of Demodulator Output, Multiplier Type Demodulator, High-Pass Reference, $e_{in} = \sin \omega_a t$

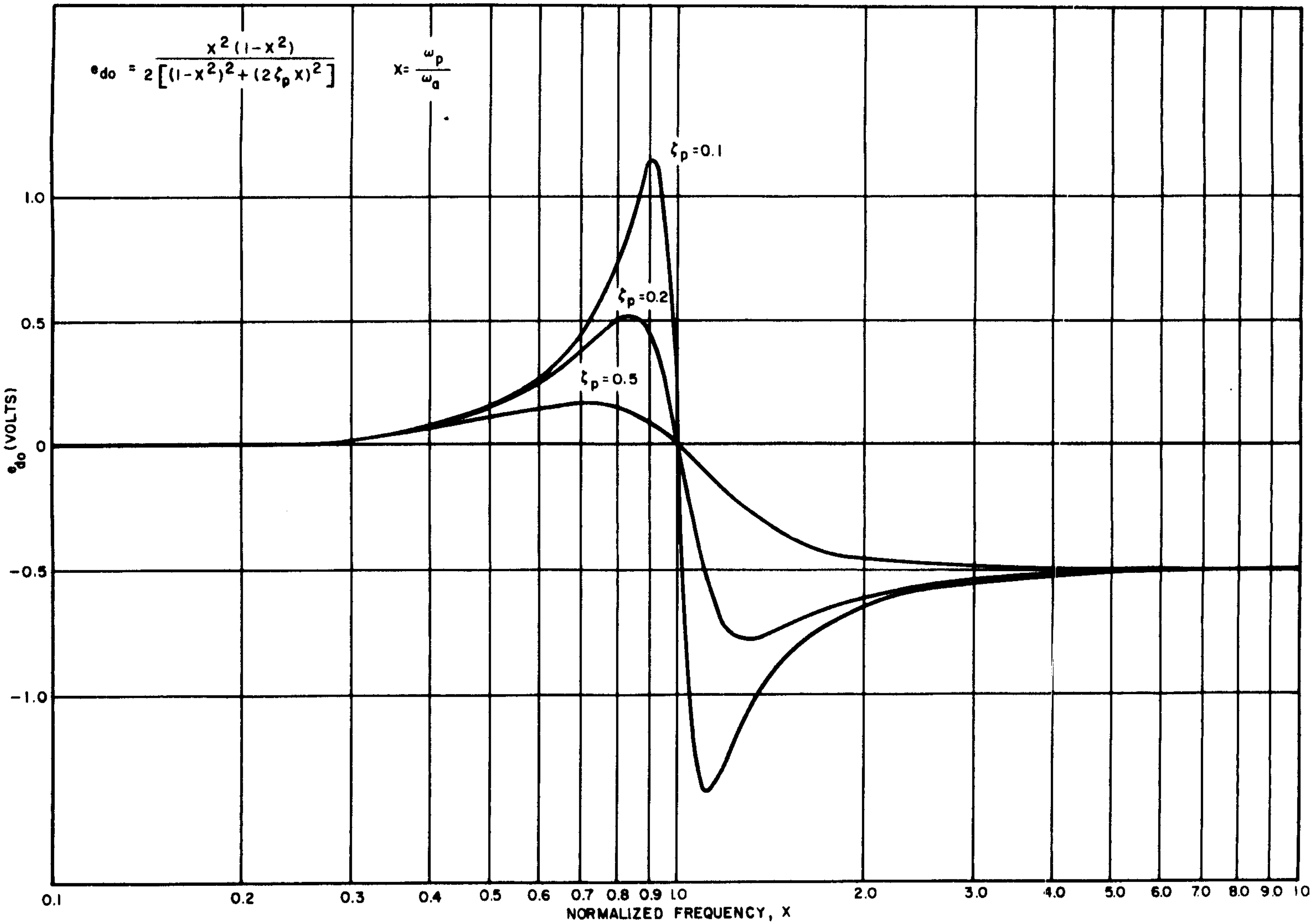

Figure 5. Amplitude of DC Component of Demodulator Output, Multiplier Type Demodulator, Low-Pass Reference, $e_{in} = \sin \omega_a t$

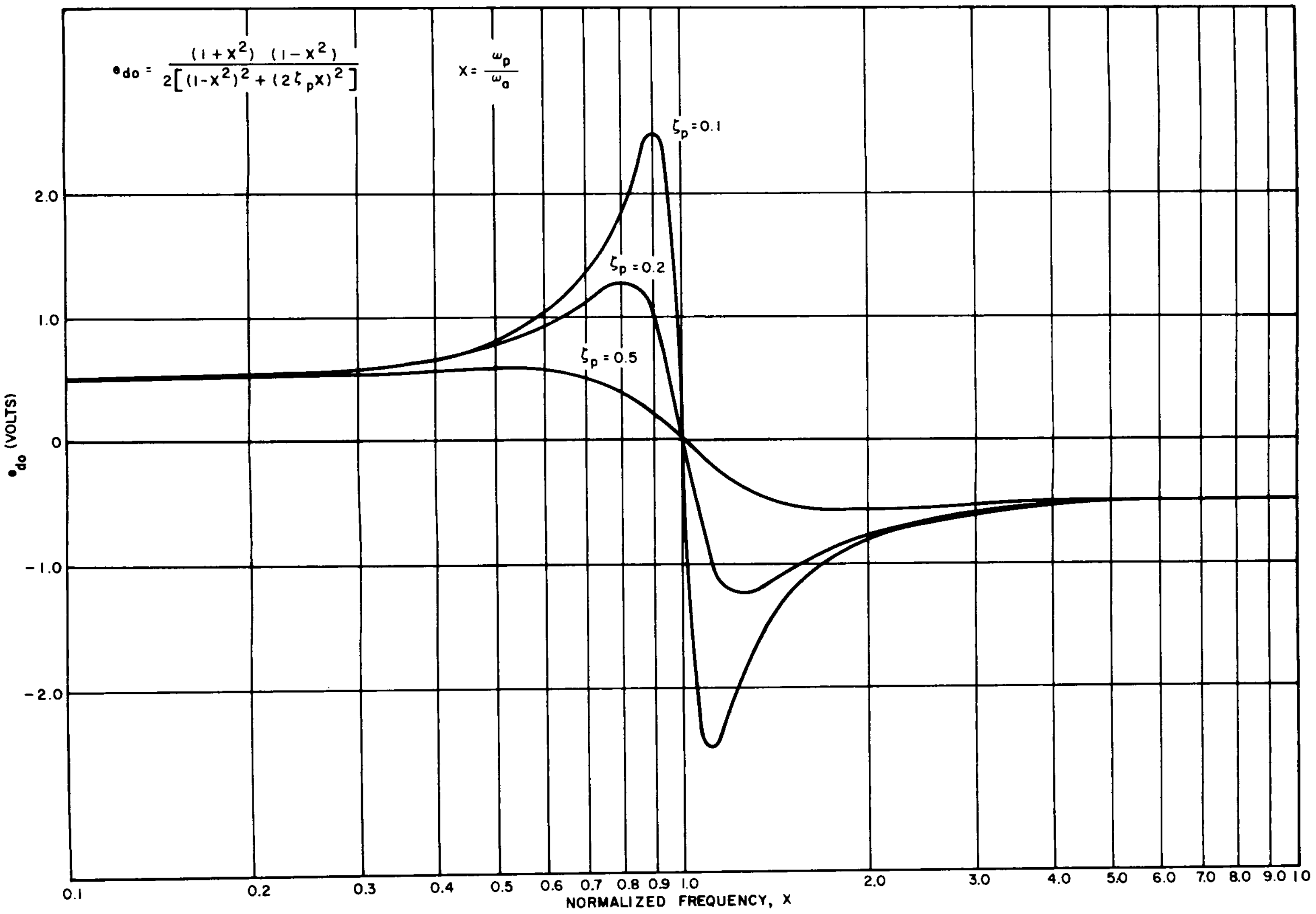

Figure 6. Amplitude of DC Component of Demodulator Output, Multiplier Type Demodulator, All-Pass Reference, $e_{in} = \sin \omega_a t$

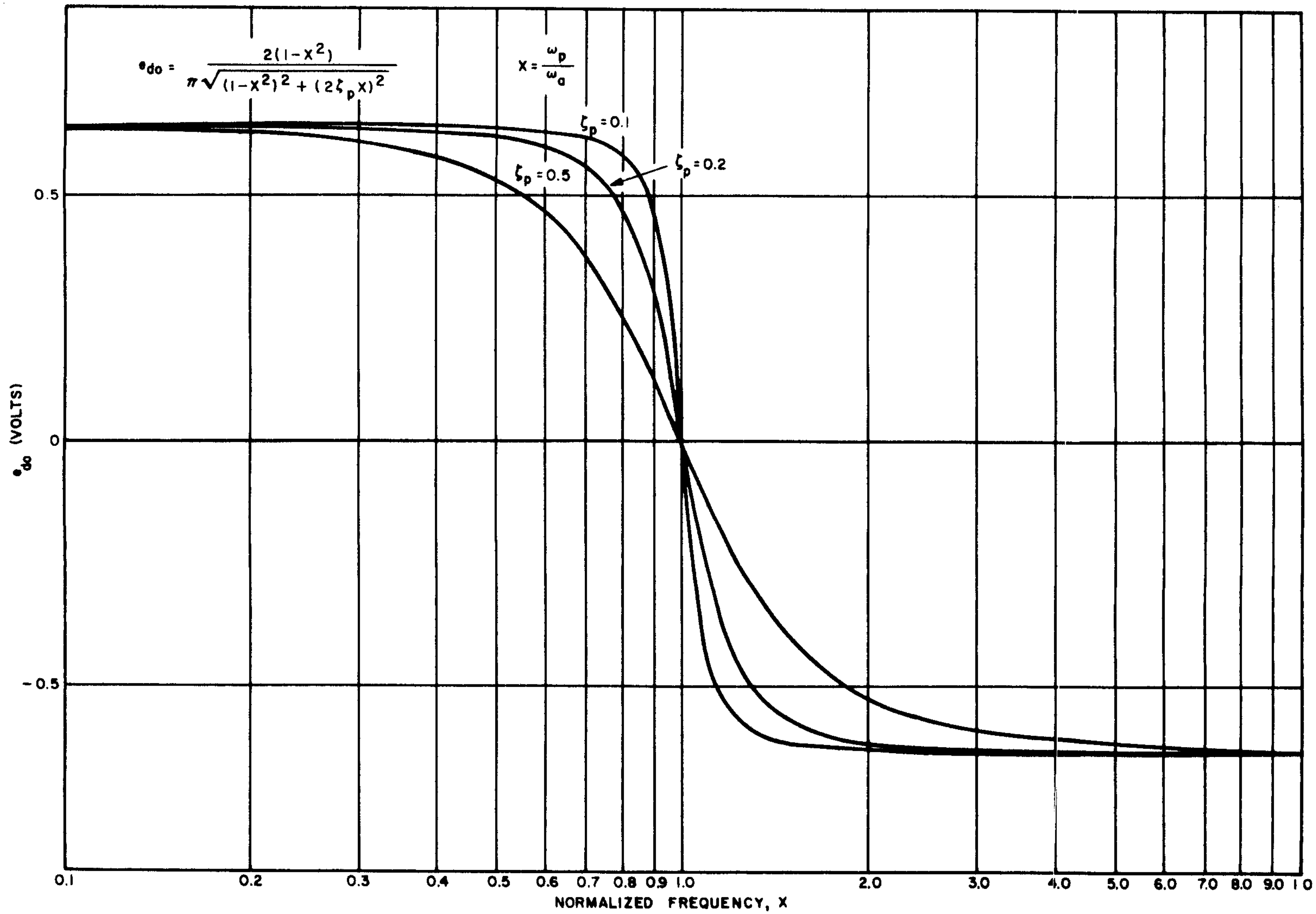

Figure 7. Amplitude of DC Component of Demodulator Output, Chopper Type Demodulator, $e_{in} = \sin \omega_a t$

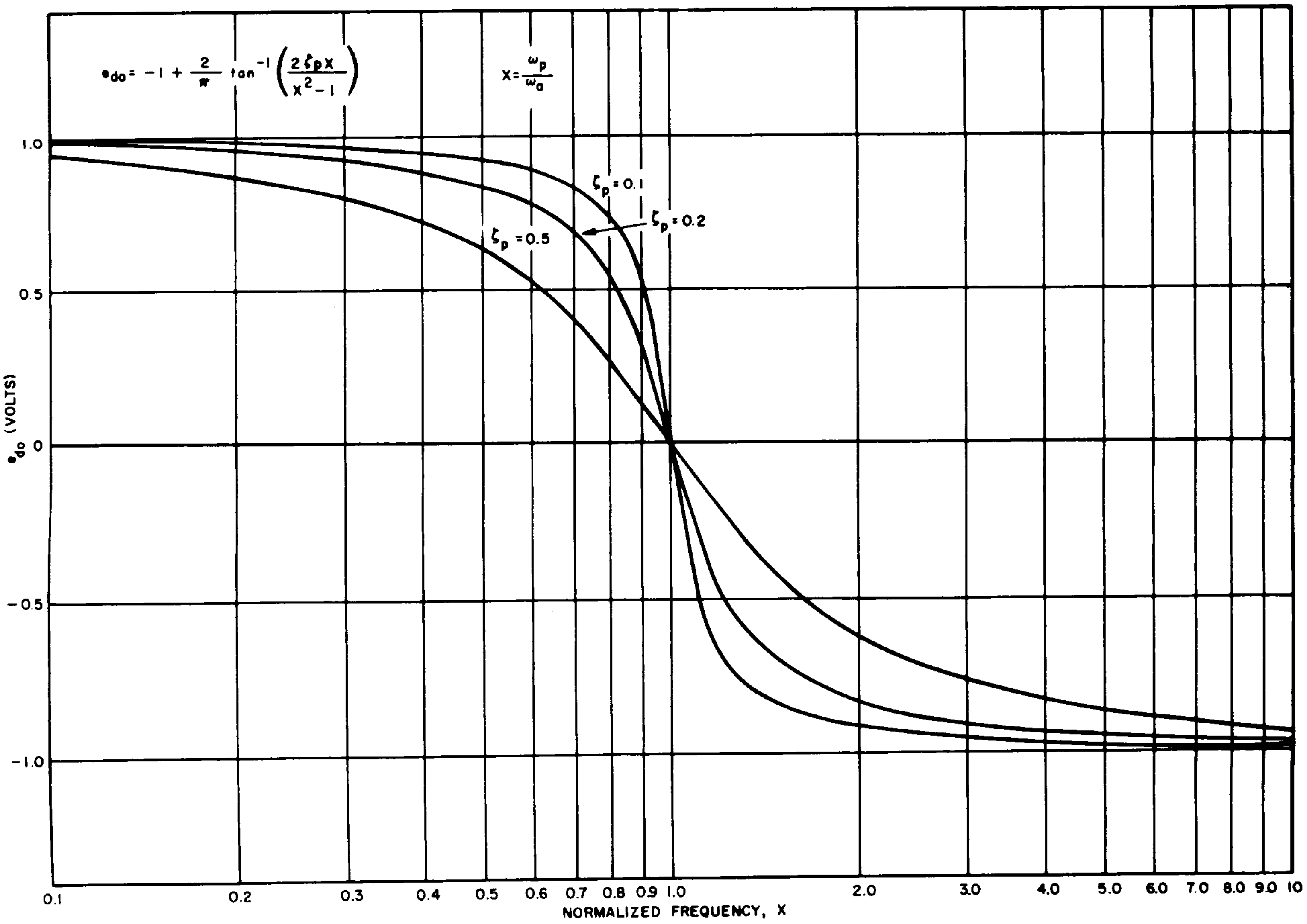

Figure 8. Amplitude of DC Component of Demodulator Output, Double Chopper Type Demodulator, $e_{in} = \sin \omega_a t$

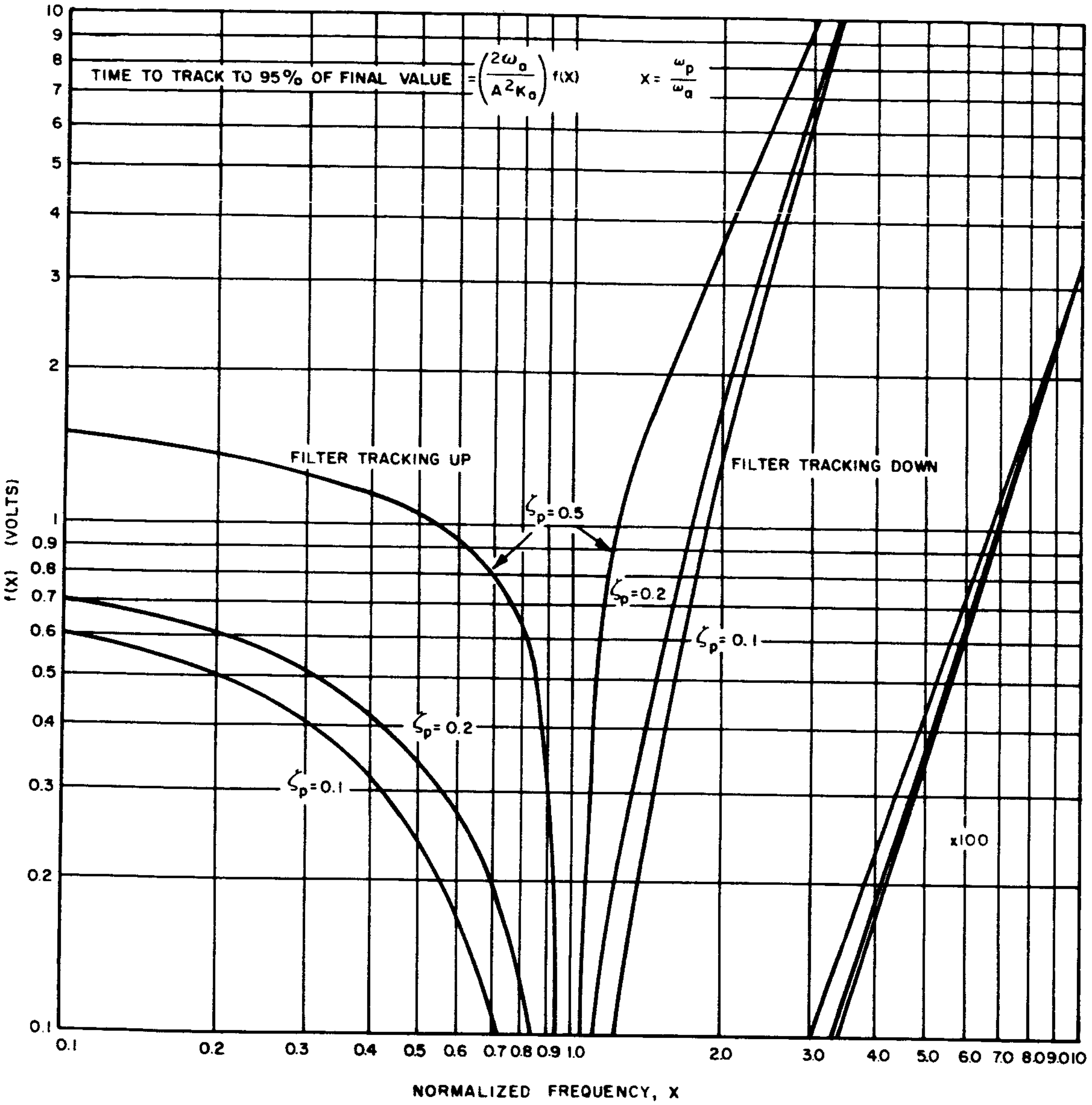

Figure 9. Tracking Time of Adaptive Tracking Filter, Multiplier Type Demodulator, High-Pass Reference

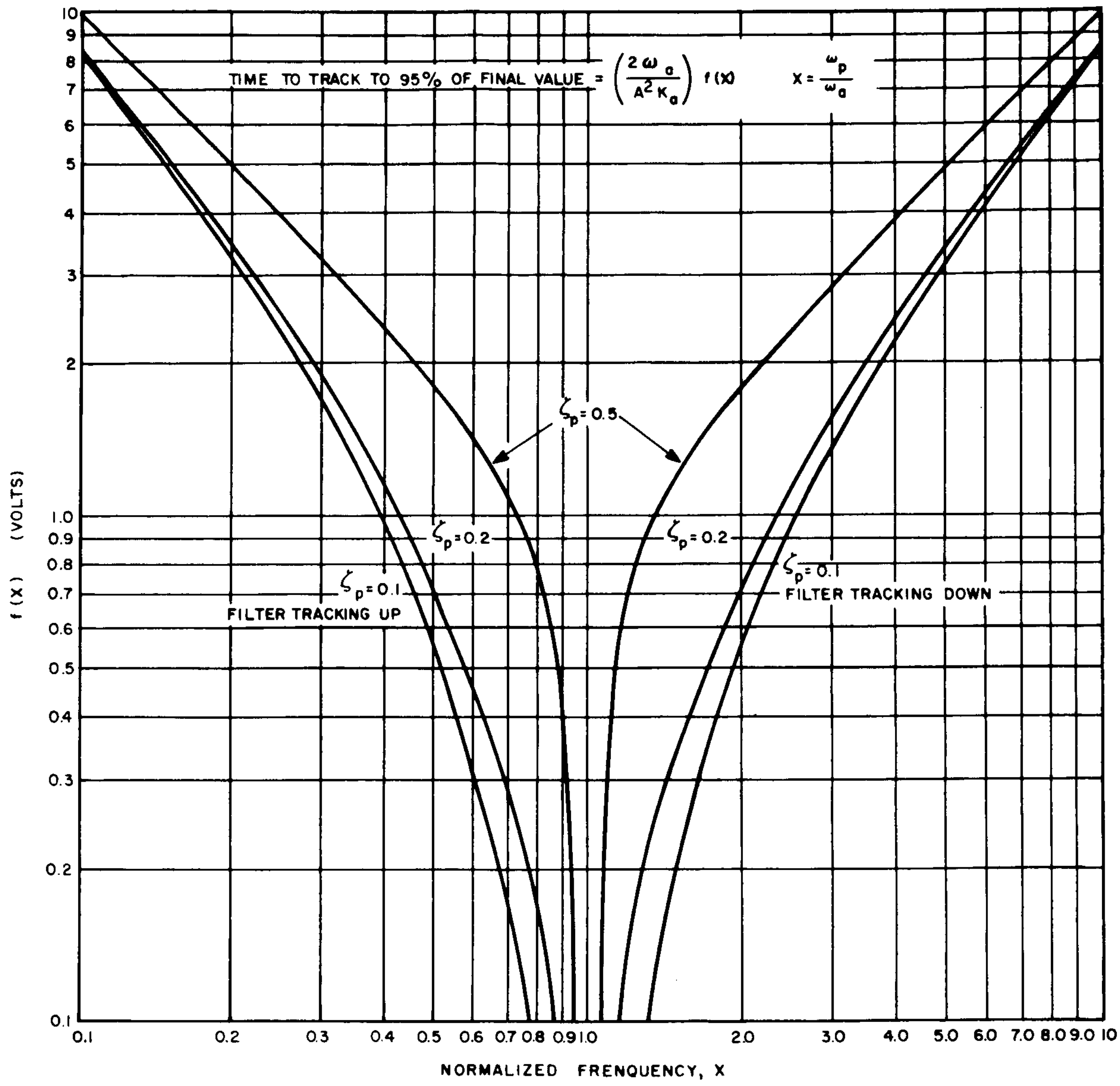

Figure 10. Tracking Time of Adaptive Tracking Filter, Multiplier Type Demodulator, Low-Pass Reference

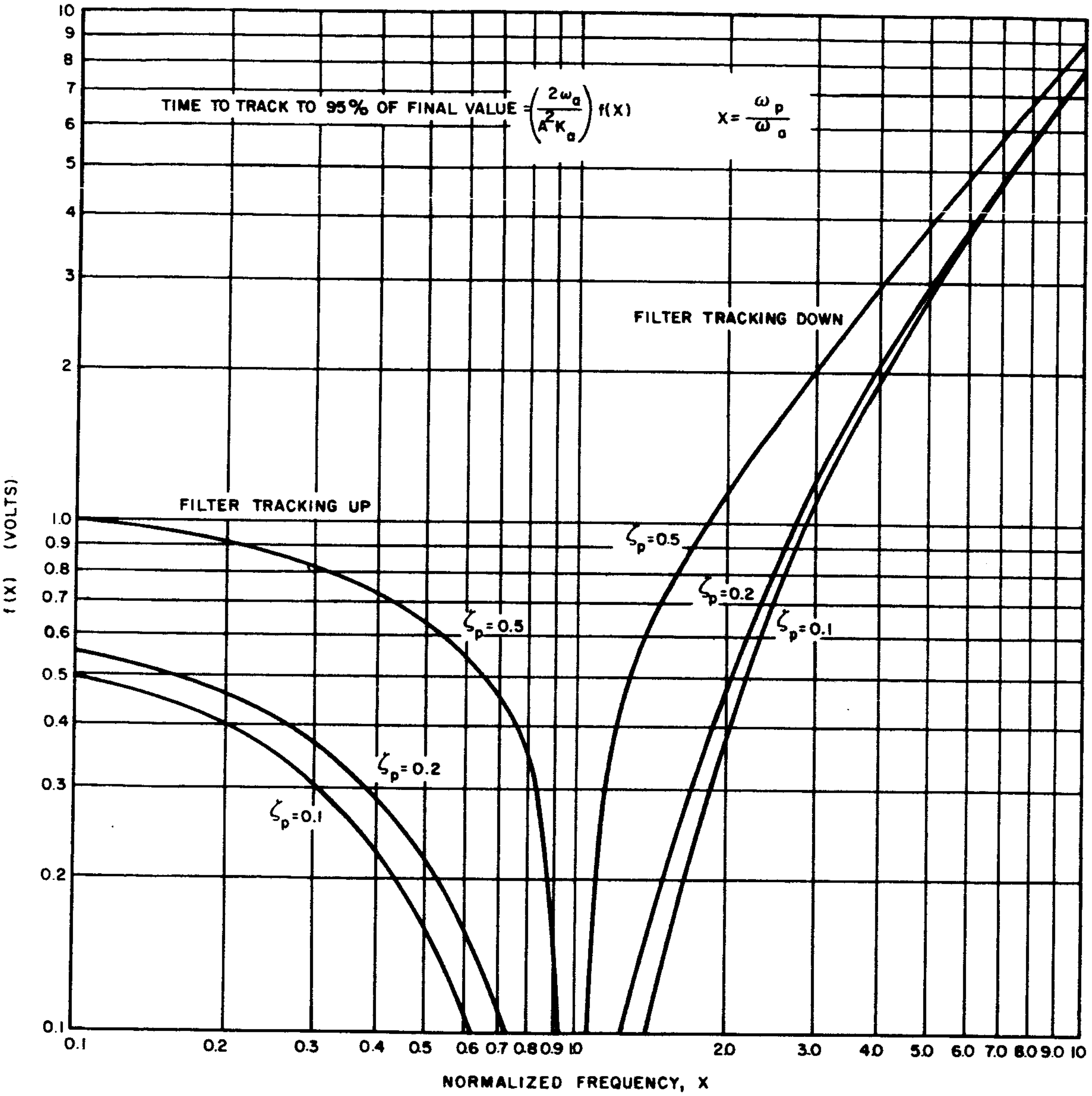

Figure 11. Tracking Time of Adaptive Tracking Filter, Multiplier Type Demodulator, All-Pass Reference

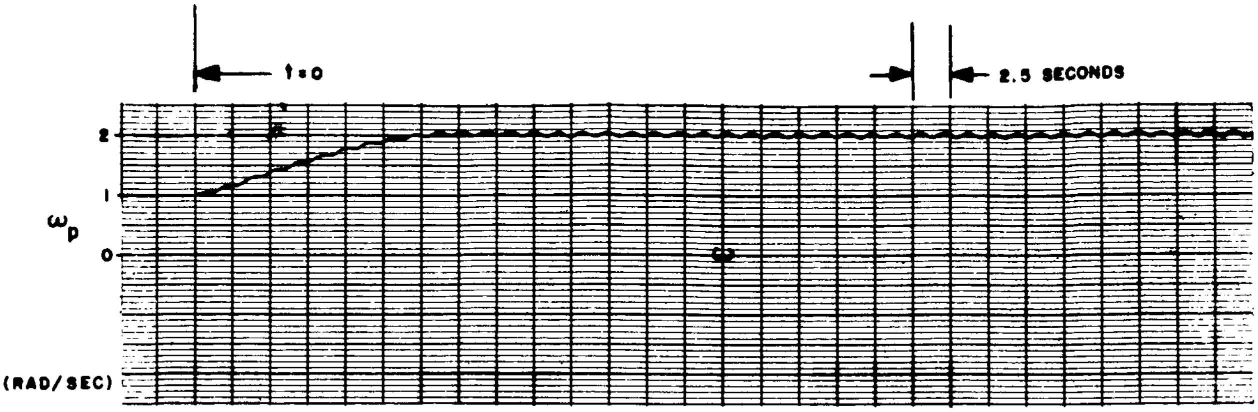

(a) $e_{in} = \sin[1+1(t)]t$

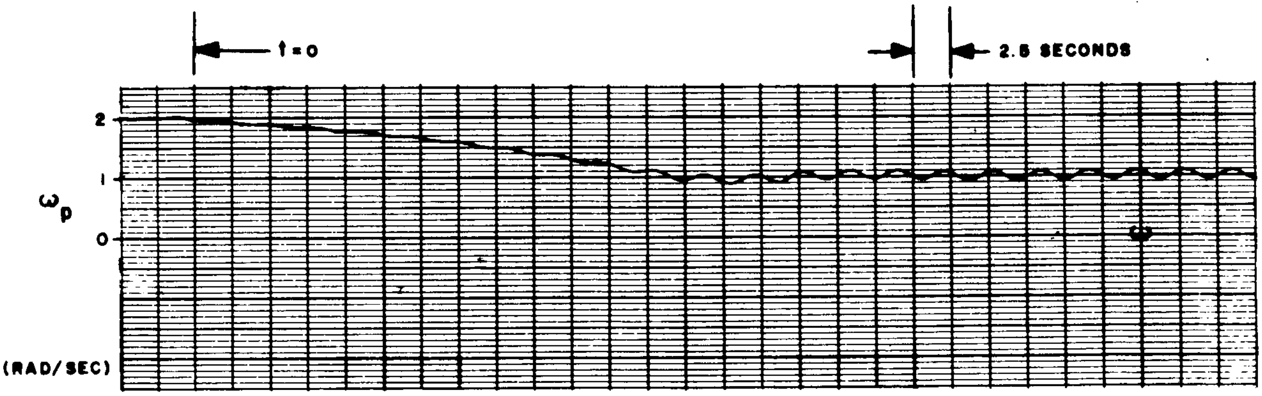

(b) $e_{in} = \sin[2-1(t)]t$

NOTE: $1(t) \triangleq \begin{matrix} 0, t<0 \\ 1, t>0 \end{matrix}$

Figure 12. Time Response of Frequency Tracking System

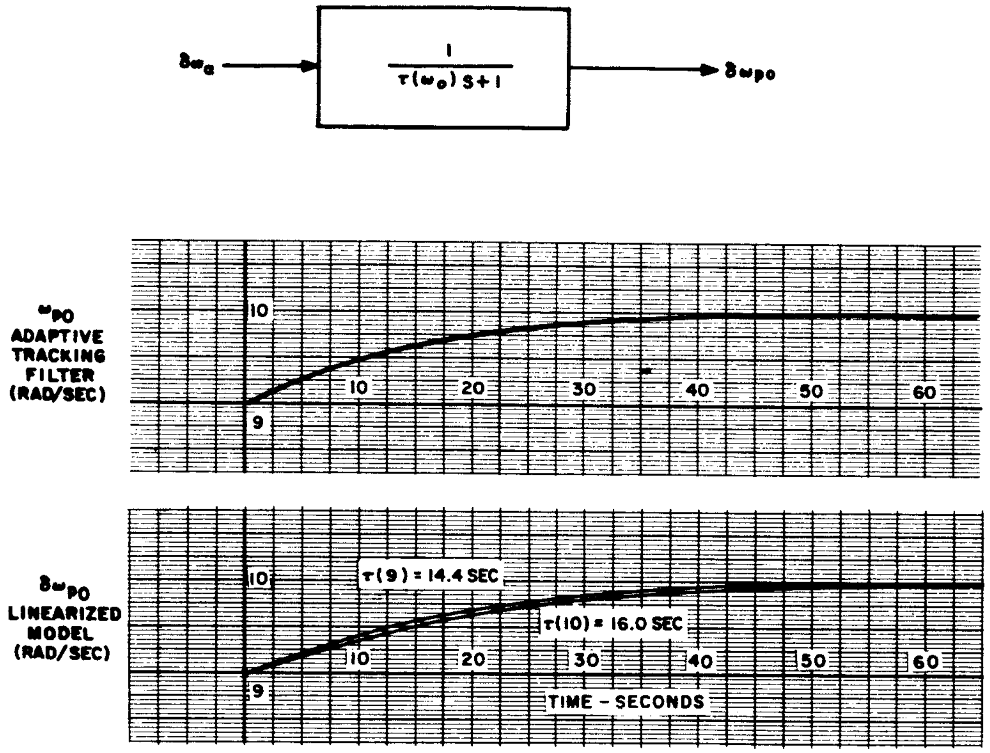

NOTE: $1(t) \triangleq 0, t<0$

$1, t>0$

DEMODULATOR TYPE: $e_d = e_r \cdot e_{in}$

DEMODULATOR REFERENCE

TRANSFER FUNCTION:

$$\frac{\frac{s^2}{\omega_p^2}}{\frac{s^2}{\omega_p^2} + \frac{2\zeta_p s}{\omega_p} + 1}$$

$K_a = 0.1, \zeta_p = 0.2$

Figure 13. Time Response to a Step Change in Frequency, Adaptive Tracking Filter and Linearized Model of Frequency Tracking System, $e_{in} = \sin[9 + 1(t)]\, t$

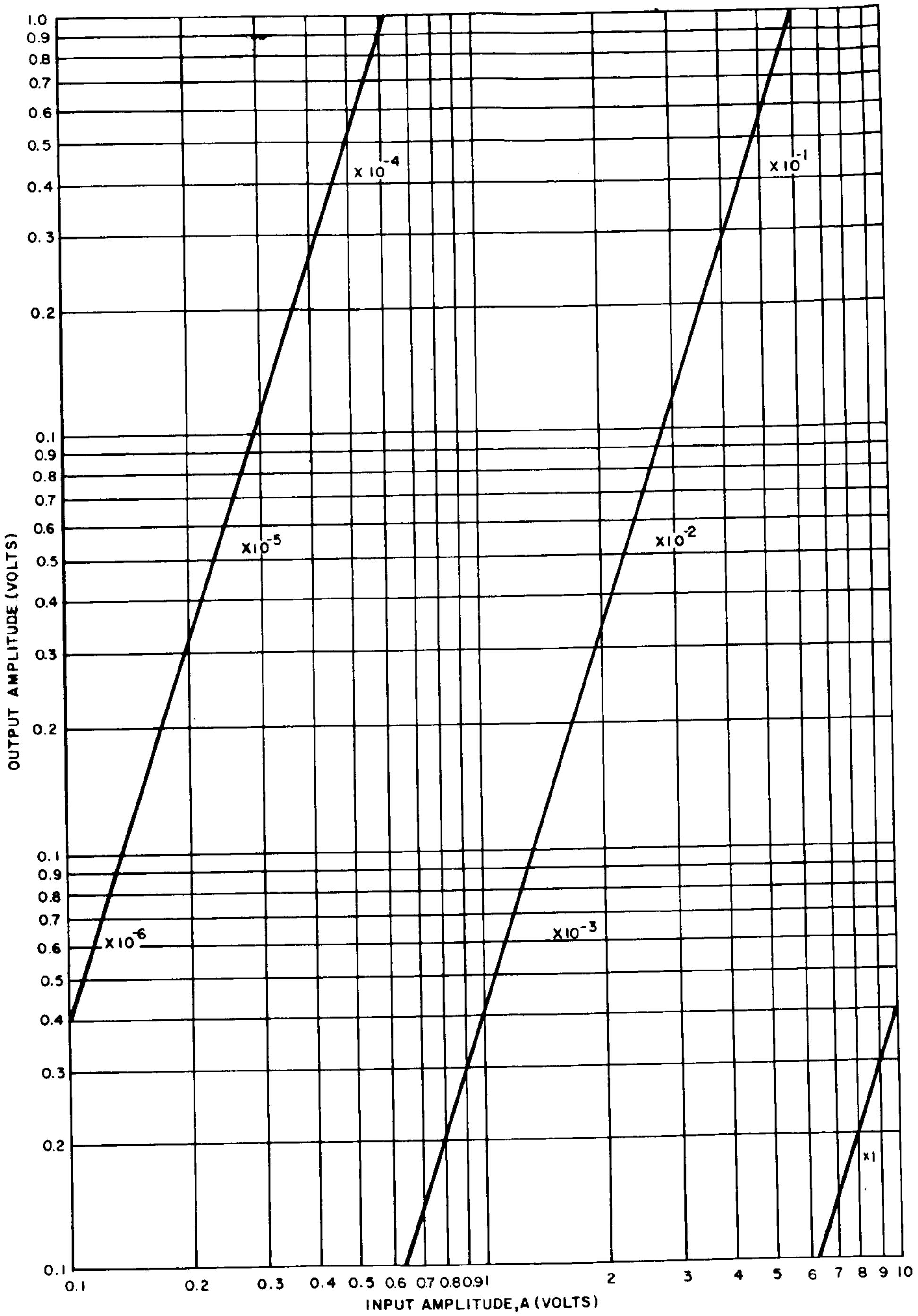

Figure 14. Amplitude of Third Harmonic Component of Adaptive Tracking Filter Output versus Input Signal Amplitude, $\omega_a = 20$, $K_a = 1$, $\zeta_p = 0.2$, $\zeta_z = 0$

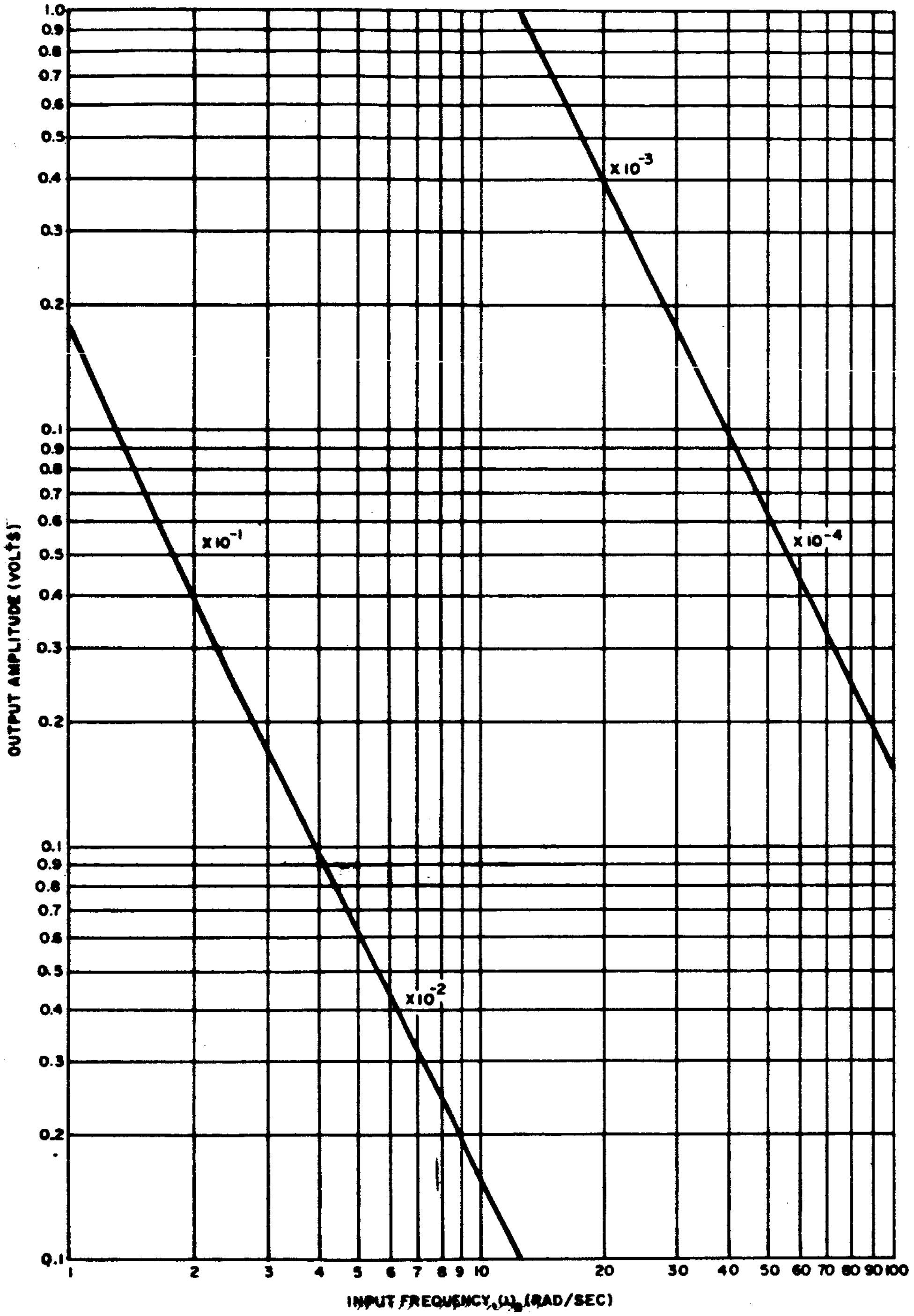

Figure 15. Amplitude of Third Harmonic Component of Adaptive Tracking Filter Output versus Input Signal Frequency, $A = 1$, $K_a = 1$, $\zeta_p = 0.2$, $\zeta_z = 0$

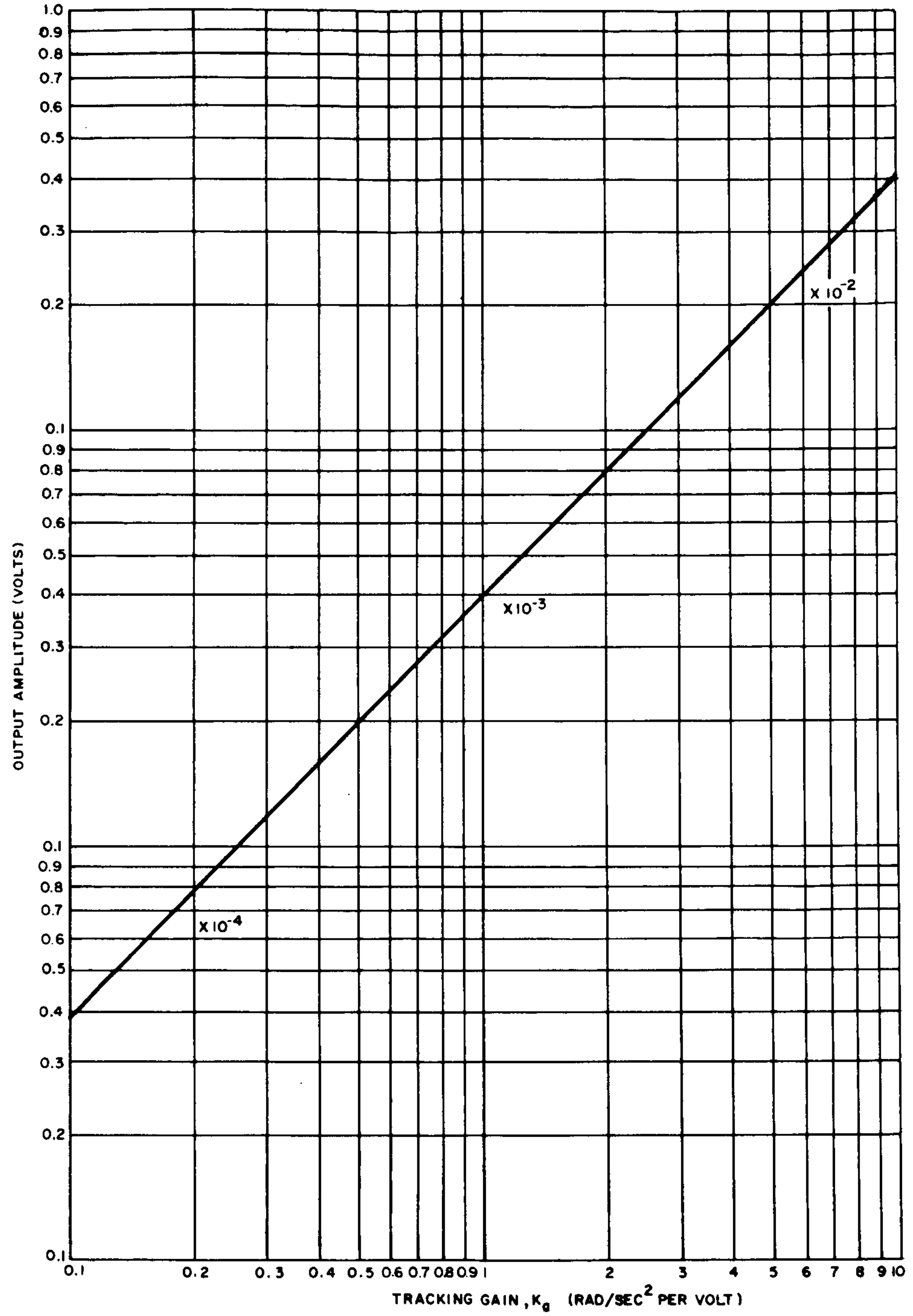

Figure 16. Amplitude of Third Harmonic Component of Adaptive Tracking Filter Output versus Tracking Gain, $A = 1$, $\omega_a = 20$, $\zeta_p = 0.2$, $\zeta_z = 0$

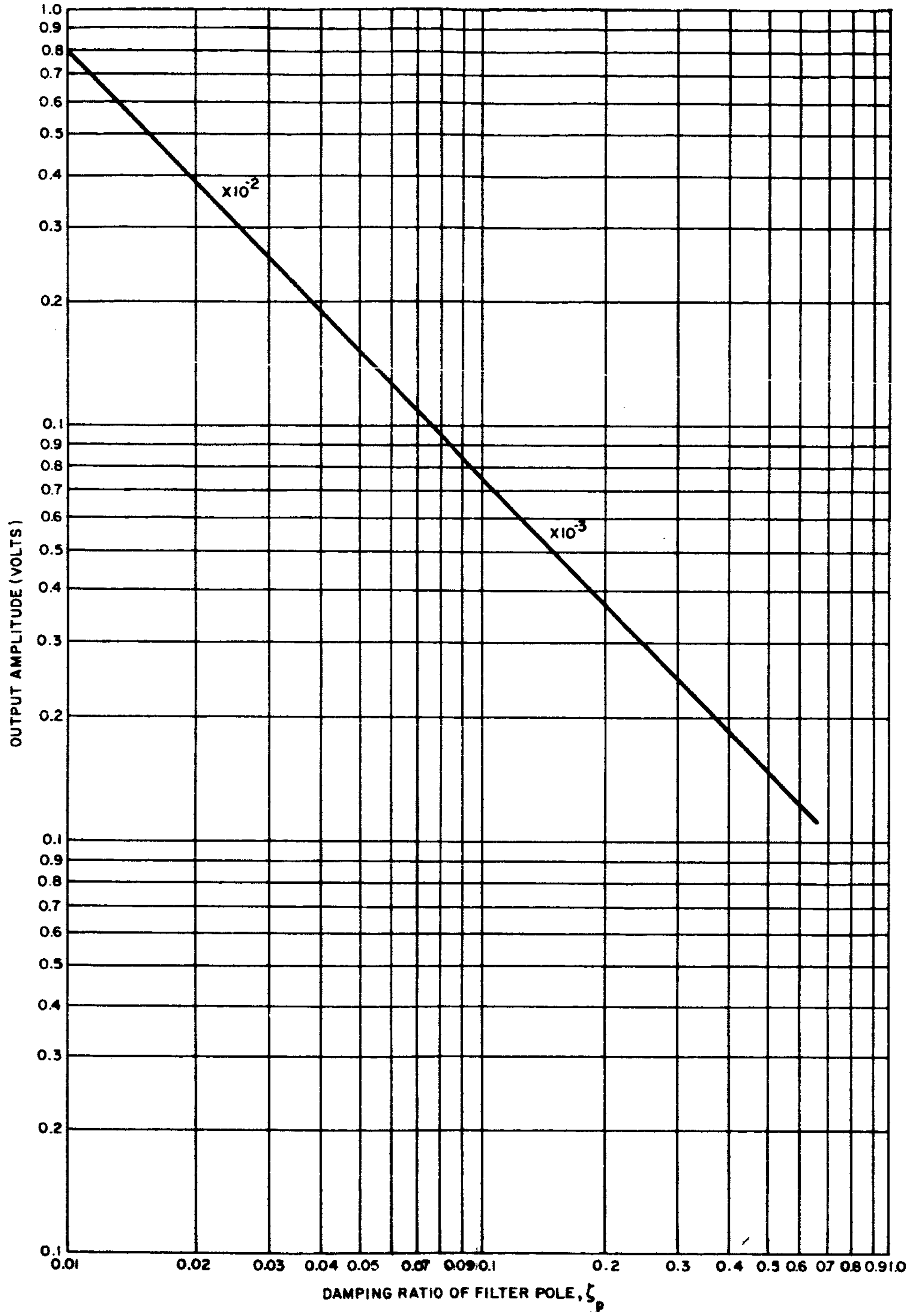

Figure 17. Amplitude of Third Harmonic Component of Adaptive Tracking Filter Output versus Damping Ratio of Second-Order Filter Pole, $A = 1$, $\omega_a = 20$, $K_a = 1$, $\zeta_z = 0$

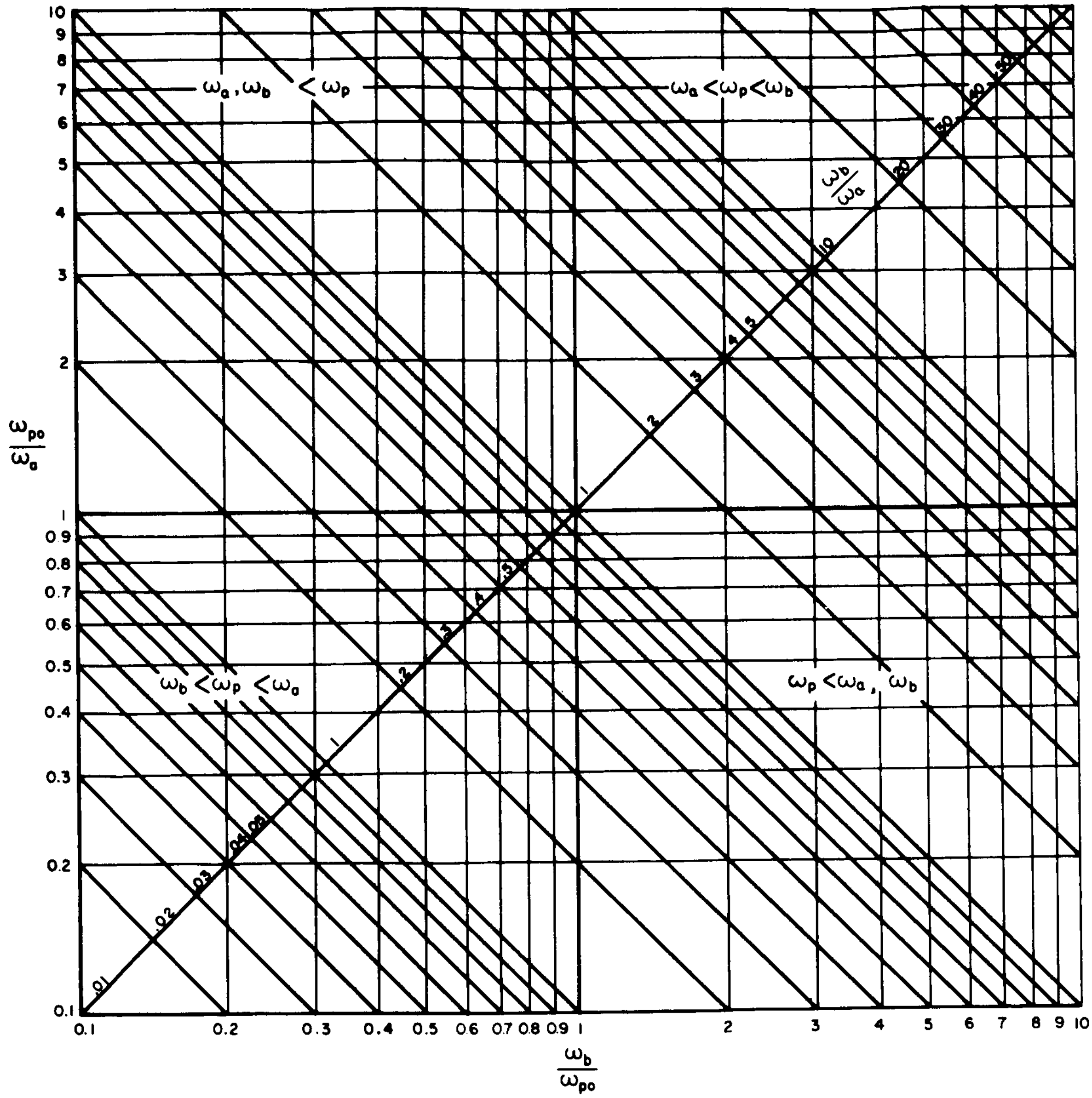

Figure 18. Coordinate System Used to Define Tracking Accuracy

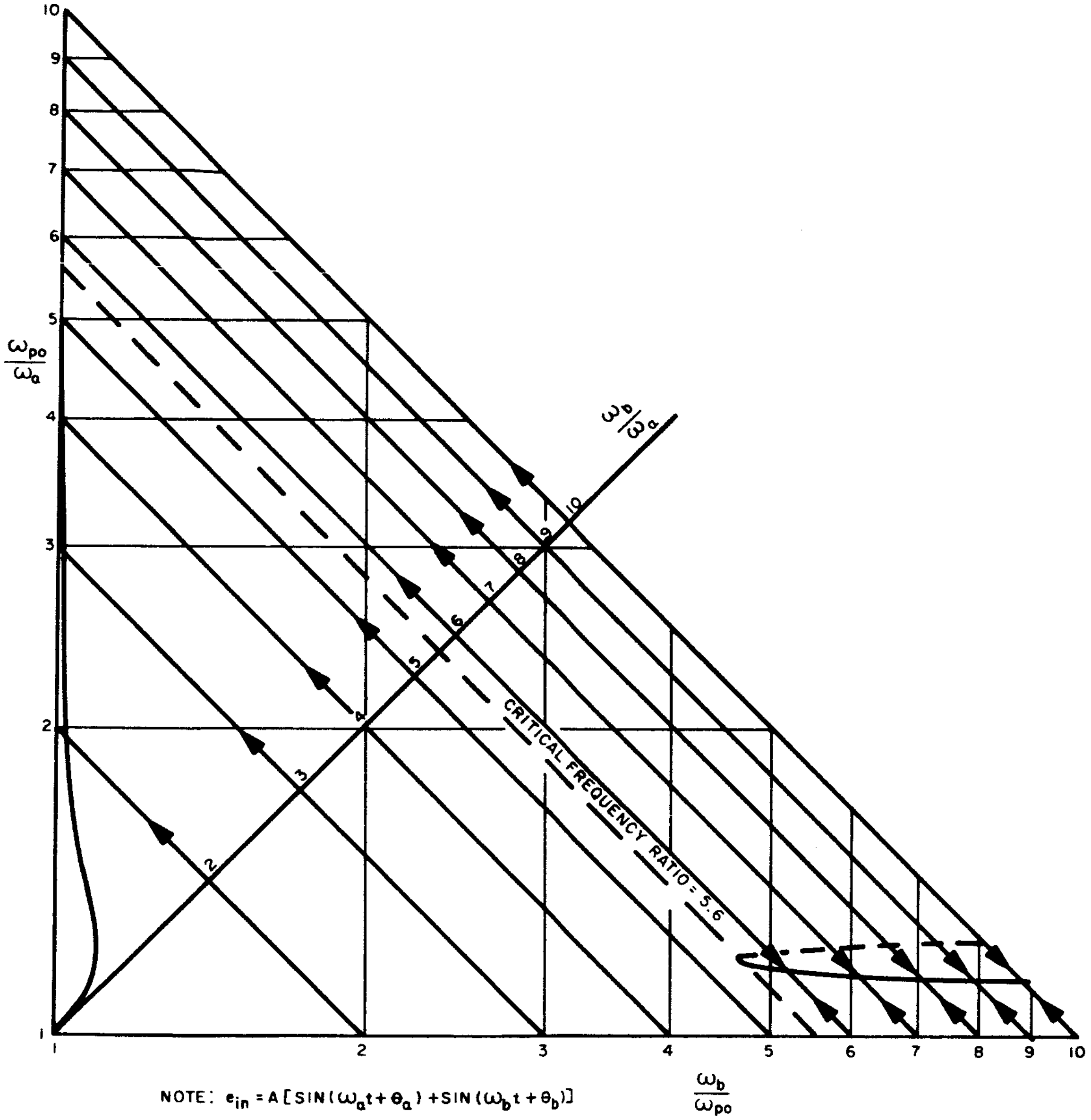

NOTE: $e_{in} = A[\sin(\omega_a t+\theta_a) + \sin(\omega_b t+\theta_b)]$

DEMODULATOR TYPE: $e_d = e_r \cdot e_{in}$

DEMODULATOR REFERENCE TRANSFER FUNCTION: $G(S,\omega_p) = \dfrac{\dfrac{S^2}{\omega_p^2}}{\dfrac{S^2}{\omega_p^2} + \dfrac{2\zeta_p S}{\omega_p} + 1}$

Figure 19. Tracking Accuracy of Adaptive Tracking Filter, $\zeta_p = 0.2$

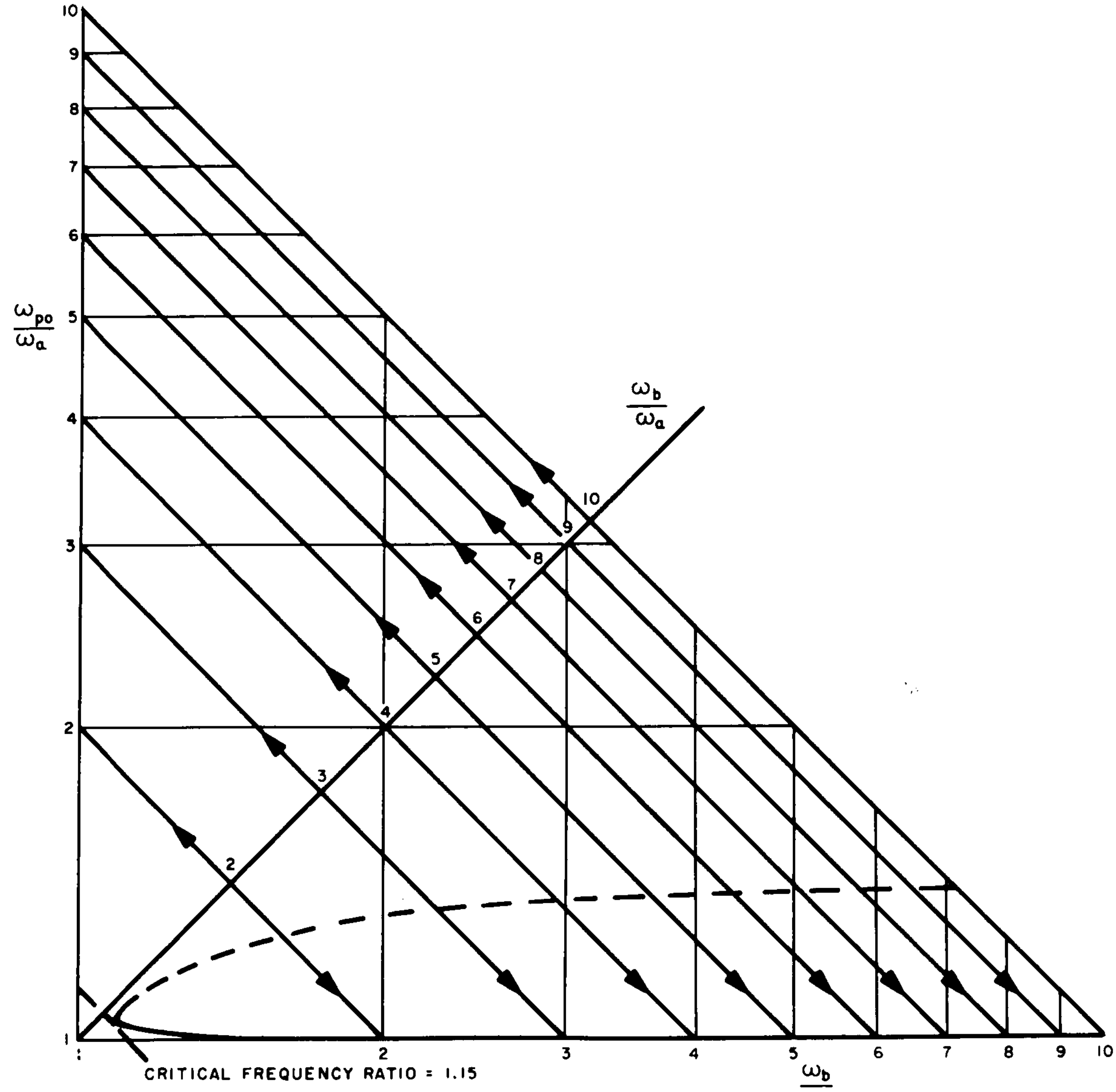

NOTE: $e_{in} = A[\sin(\omega_a t + \theta_a) + \sin(\omega_b t + \theta_b)]$

DEMODULATOR TYPE: $e_d = e_r \cdot e_{in}$

DEMODULATOR REFERENCE TRANSFER FUNCTION: $G(S,\omega_p) = \dfrac{\dfrac{S^2}{\omega_p^2}}{\dfrac{S^2}{\omega_p^2} + \dfrac{2\zeta_p S}{\omega_p} + 1}$

Figure 20. Tracking Accuracy of Adaptive Tracking Filter, $\zeta_p = 0.05$

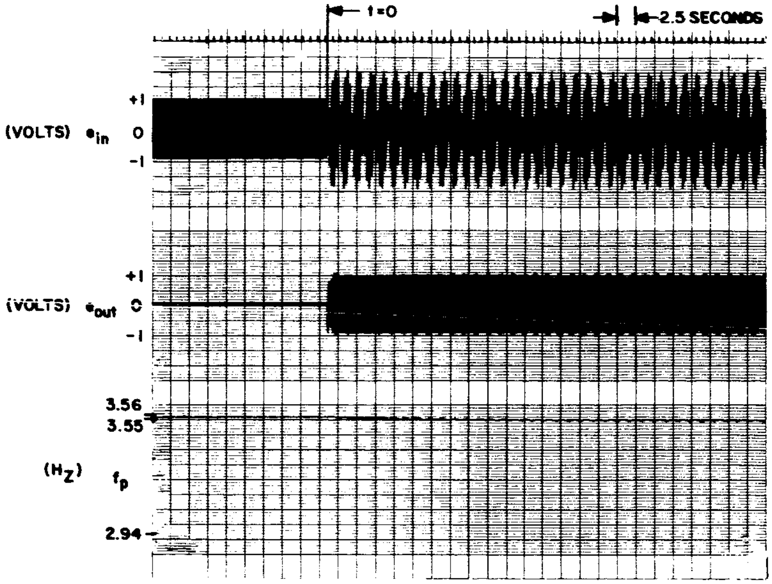

CHOPPER TYPE DEMODULATOR

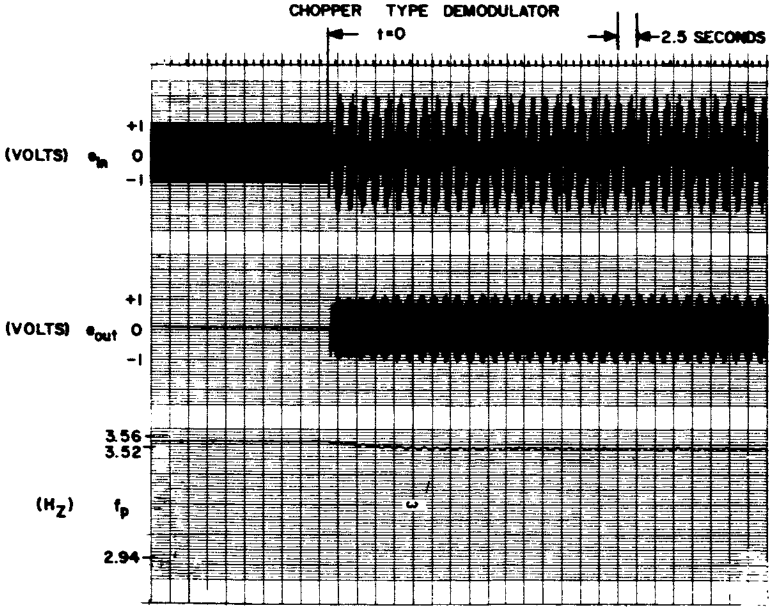

MULTIPLIER TYPE DEMODULATOR

HIGH PASS REFERENCE, $\zeta_p = 0.05$

$$e_{in} = \begin{cases} \mathrm{SIN}\ (2\pi\ 3.56t), & t<0 \\ \mathrm{SIN}\ (2\pi\ 3.56\ t) + \mathrm{SIN}\ (2\pi 2.94\ t), & t>0 \end{cases}$$

Figure 21. Comparison of Tracking Accuracy of Chopper and Multiplier Type Demodulators, Filters Initially Tracking Higher Frequency

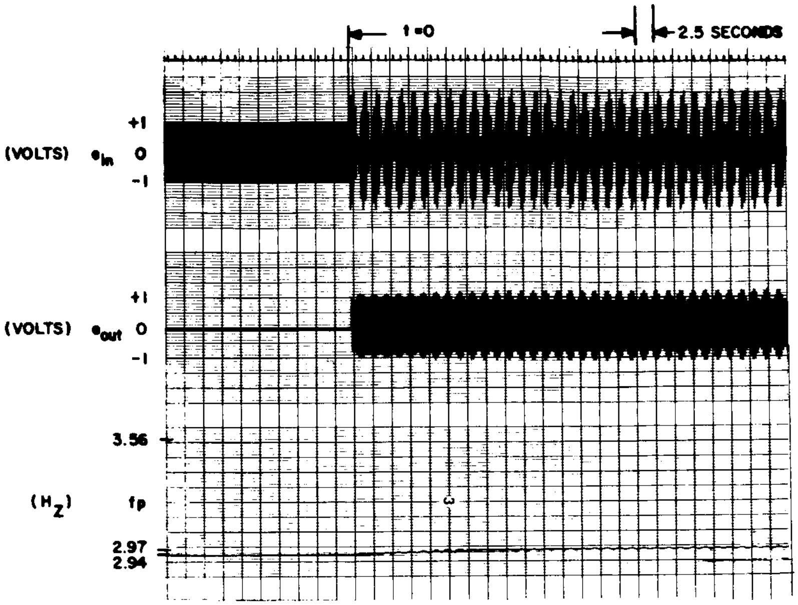

CHOPPER TYPE DEMODULATOR

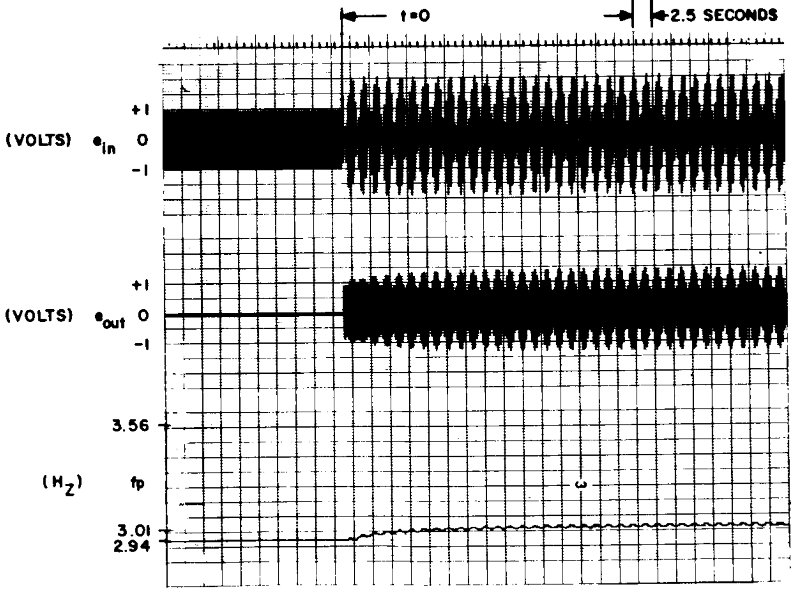

MULTIPLIER TYPE DEMODULATOR

HIGH PASS REFERENCE, $\zeta_p = 0.05$

$$e_{in} = \begin{cases} \mathrm{SIN}(2\pi\, 2.94\, t), & t < 0 \\ \mathrm{SIN}(2\pi\, 2.94\, t) + \mathrm{SIN}(2\pi 3.56\, t), & t > 0 \end{cases}$$

Figure 22. Comparison of Tracking Accuracy of Chopper and Multiplier Type Demodulators, Filters Initially Tracking Lower Frequency

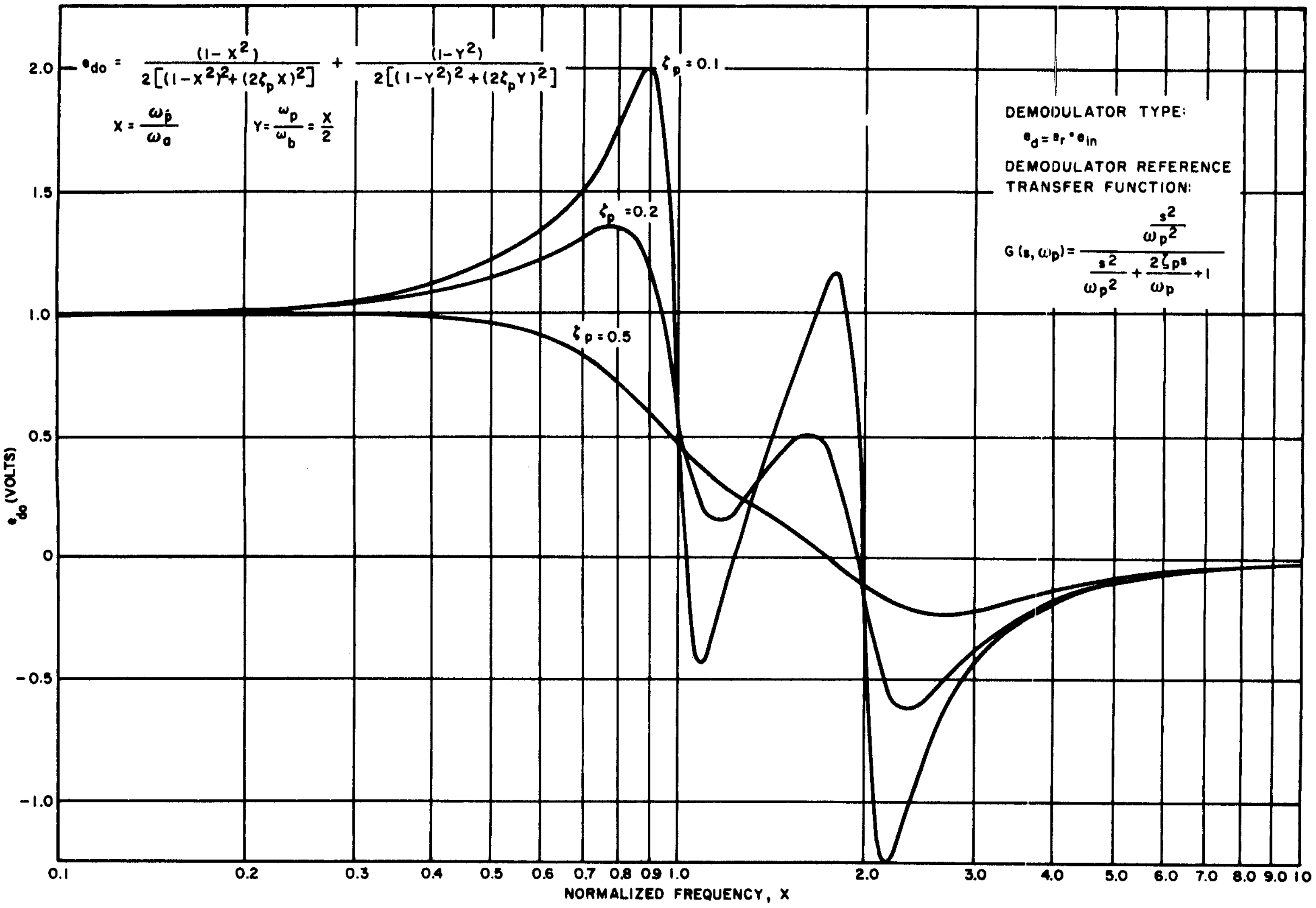

Figure 23. Amplitude of DC Component of Demodulator Output, $e_{in} = \sin \omega_a t + \sin 2\omega_a t$

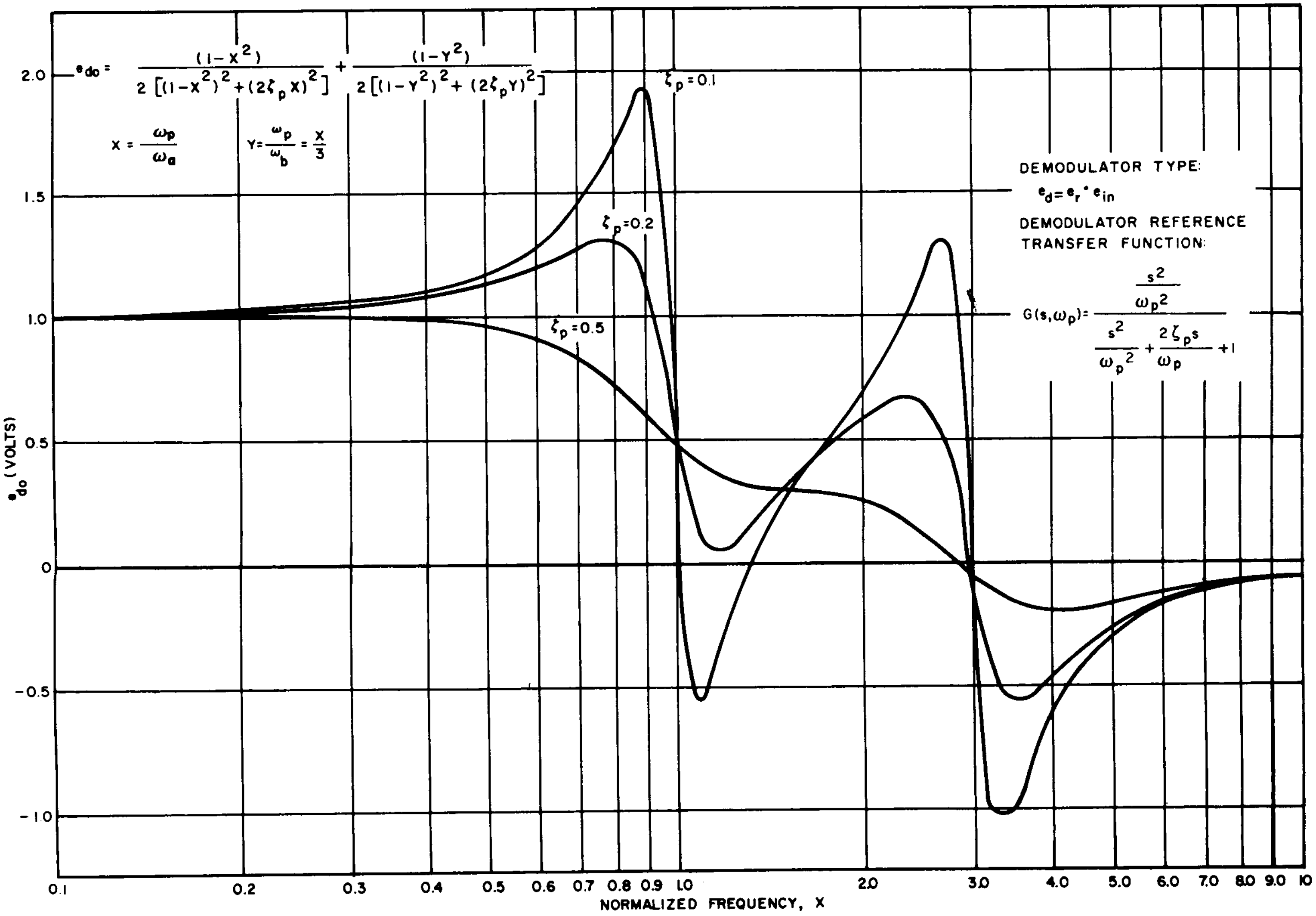

Figure 24. Amplitude of DC Component of Demodulator Output, $e_{in} = \sin \omega_a t + \sin 3\omega_a t$

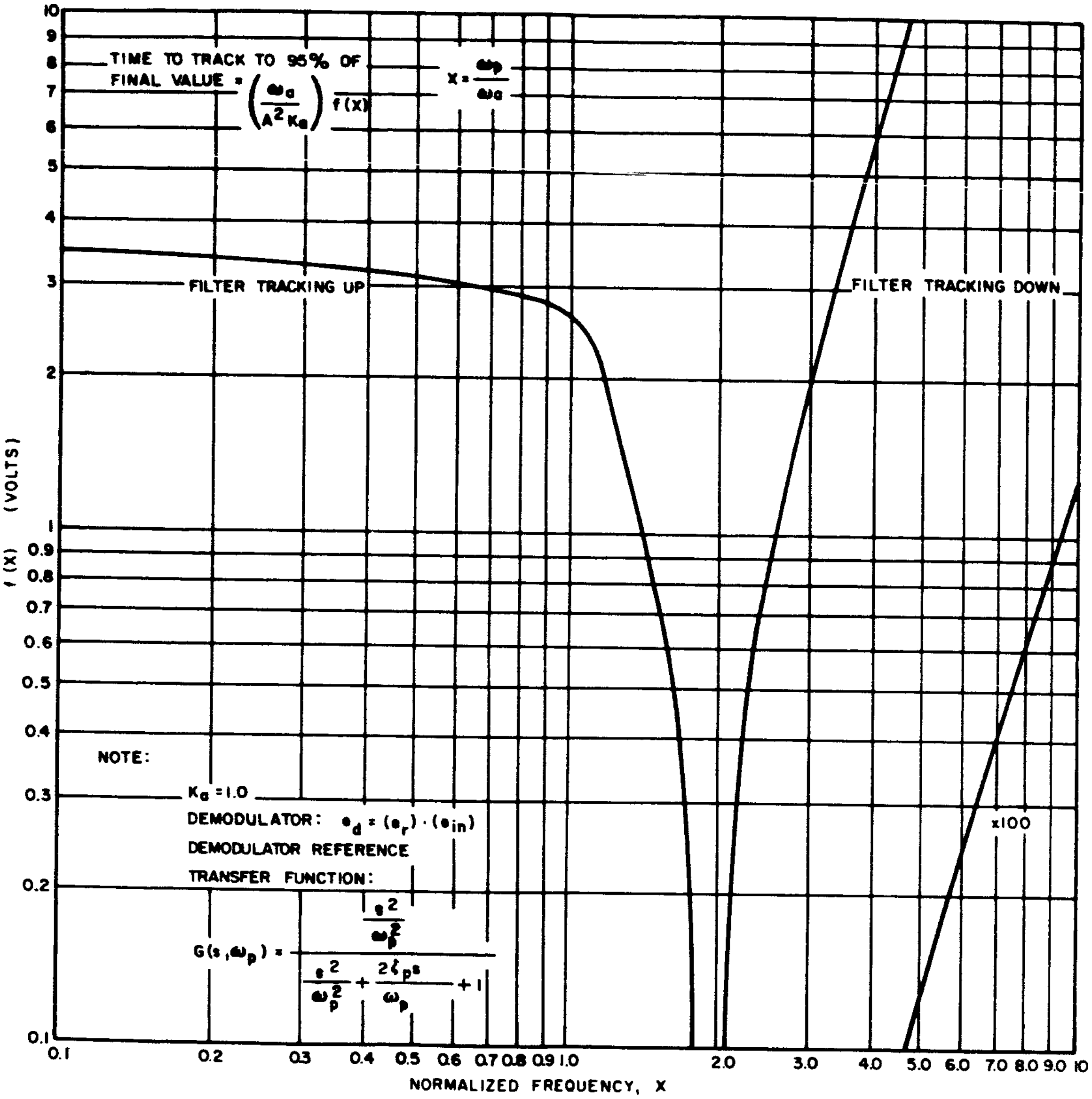

Figure 25. Tracking Time of Adaptive Tracking Filter, $e_{in} = A\ (\sin \omega_a t + \sin 2\omega_a t)$, $\zeta_p = 0.2$

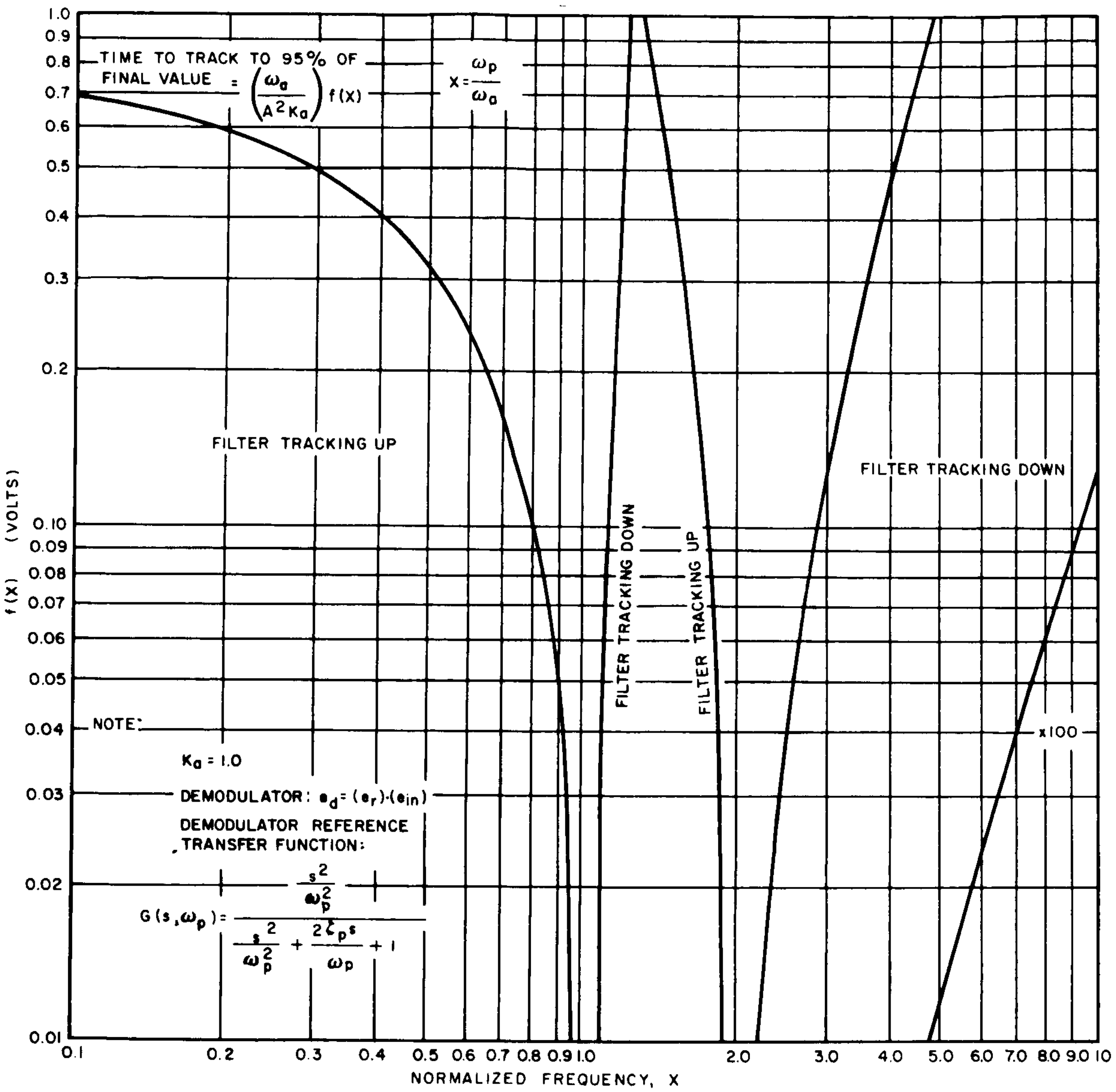

Figure 26. Tracking Time of Adaptive Tracking Filter, $e_{in} = A\ (\sin \omega_a t + \sin 2\omega_a t)$, $\zeta_p = 0.1$

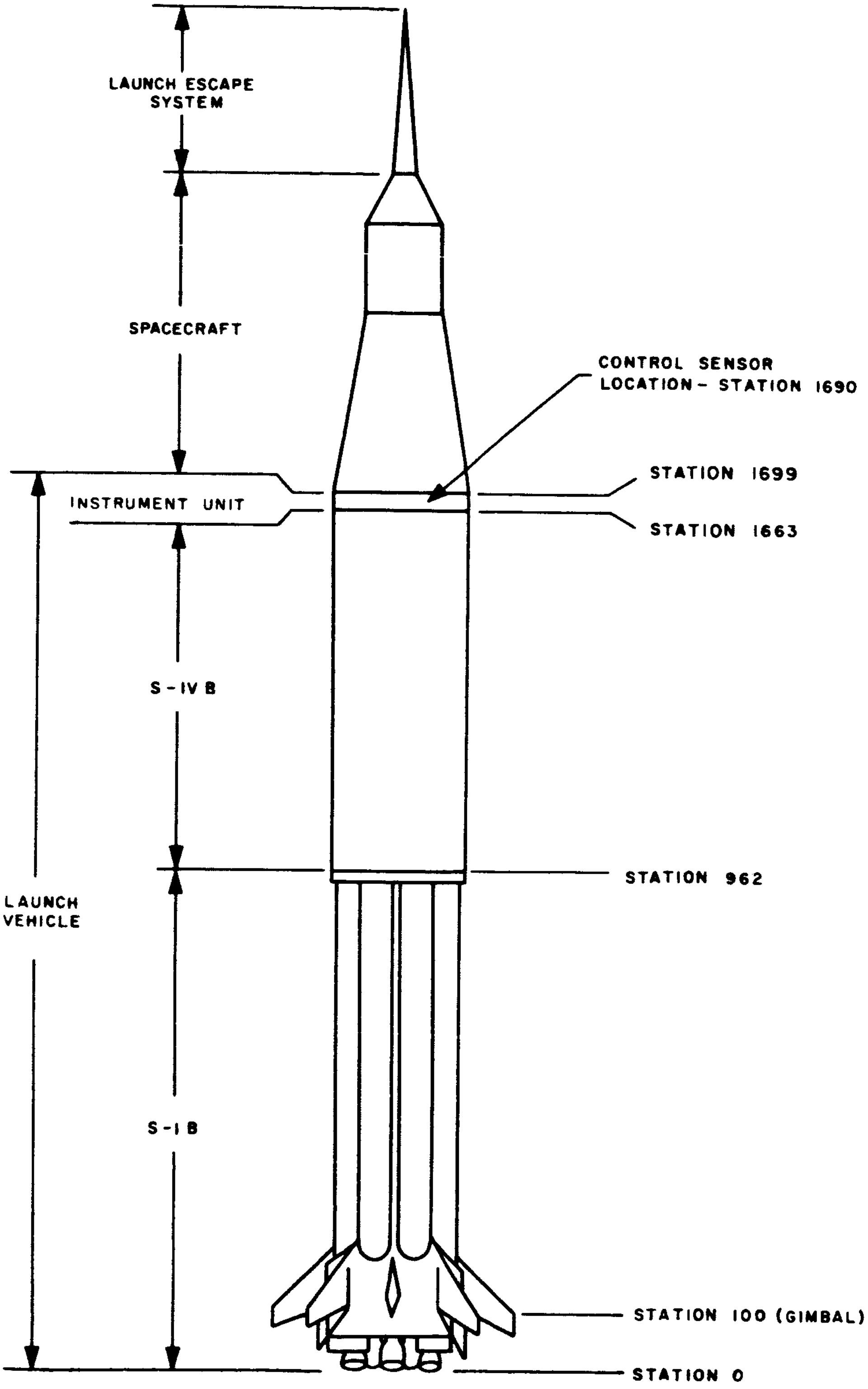

Figure 27. S-IB-201 Configuration

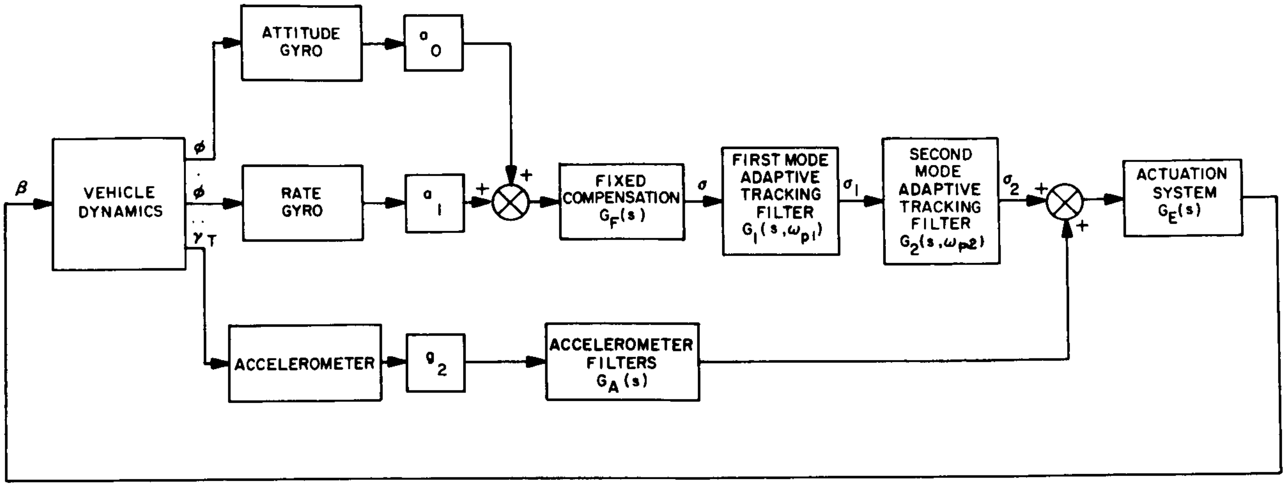

CONTROL SYSTEM PARAMETERS

FIXED ELEMENTS

$$G_F(s) = \frac{1}{\frac{s}{4} + 1}$$

$$G_A(s) = \frac{1}{(\frac{s}{0.2} + 1)(s + 1)}$$

$$G_E(s) = \frac{1}{(\frac{s}{17} + 1)(\frac{s^2}{46.7^2} + \frac{2(0.15)s}{46.7} + 1)}$$

SYSTEM GAINS

GAIN CONSTANTS	FLIGHT TIME - SECONDS							
	0	20	40	60	80	100	120	140
a_0	1.5	1.5	1.5	1.5	1.5	1.167	0.5	0.5
a_1	2.3	2.3	2.3	2.3	2.3	1.8	0.8	0.8
g_2	0	0	1.83	5.5	5.5	3.67	0	0

ADAPTIVE TRACKING FILTERS
GAIN STABILIZATION

$$G_1(s,\omega_{p1}) = \frac{\frac{s^2}{\omega_{p1}^2} + 1}{\frac{s^2}{\omega_{p1}^2} + \frac{2(0.2)s}{\omega_{p1}} + 1}$$

$$G_2(s,\omega_{p2}) = \frac{\frac{s^2}{\omega_{p2}^2} + 1}{\frac{s^2}{\omega_{p2}^2} + \frac{2(0.2)s}{\omega_{p2}} + 1}$$

ADAPTIVE TRACKING FILTERS
PHASE STABILIZATION

$$G_1(s,\omega_{p1}) = \frac{\frac{s^2}{(1.25\,\omega_{p1})^2} + \frac{2(0.1)s}{1.25\omega_{p1}} + 1}{\frac{s^2}{\omega_{p1}^2} + \frac{2(0.2)s}{\omega_{p1}} + 1}$$

$$G_2(s,\omega_{p2}) = \frac{\frac{s^2}{(1.25\,\omega_{p2})^2} + \frac{2(0.2)s}{1.25\omega_{p2}} + 1}{\frac{s^2}{\omega_{p2}^2} + \frac{2(0.1)s}{\omega_{p2}} + 1}$$

Figure 28. S-IB-201 Control System Utilizing First and Second Bending Mode Adaptive Tracking Filters

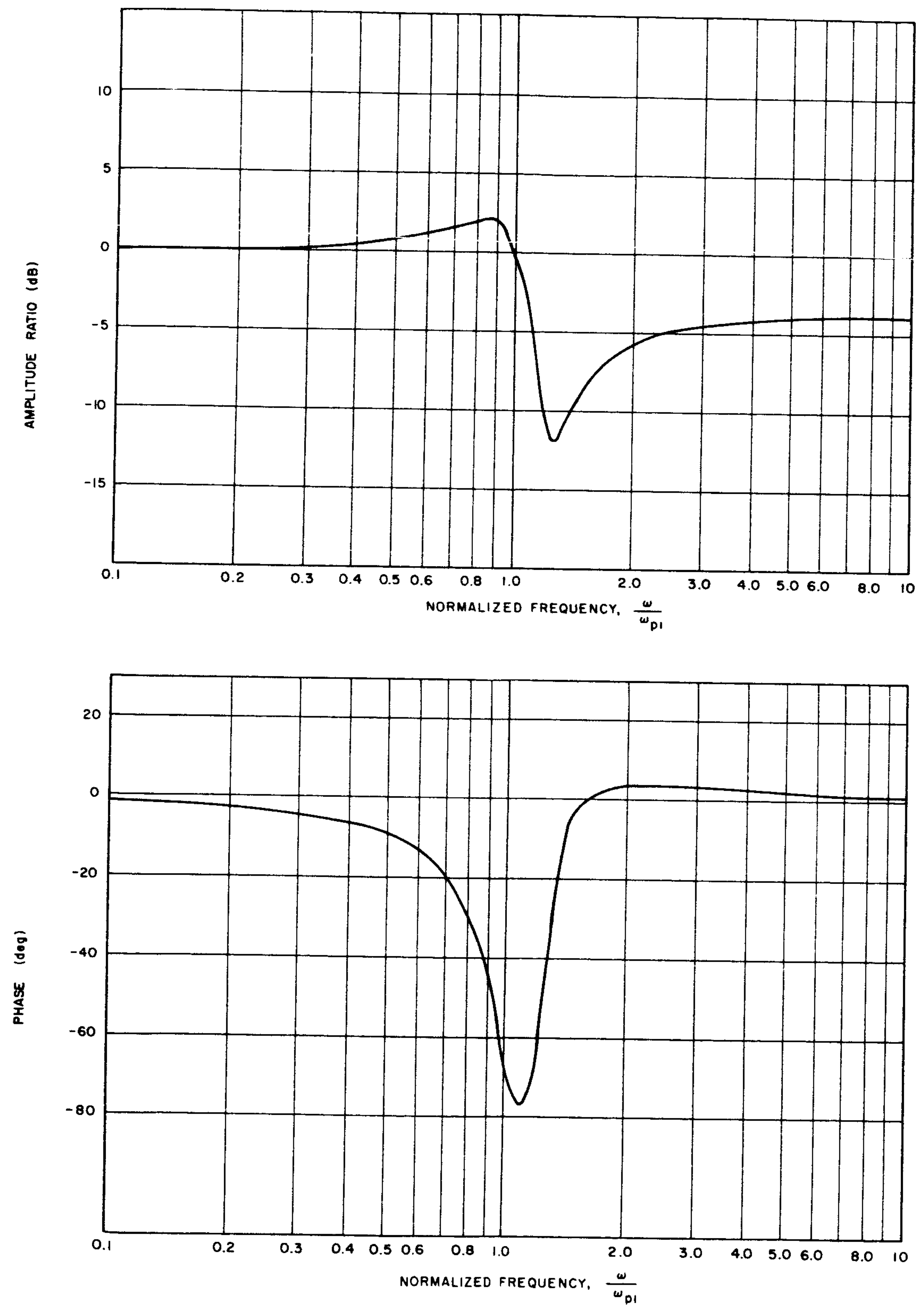

Figure 29. Frequency Response of First Mode Adaptive Tracking Filter for Phase Stabilization

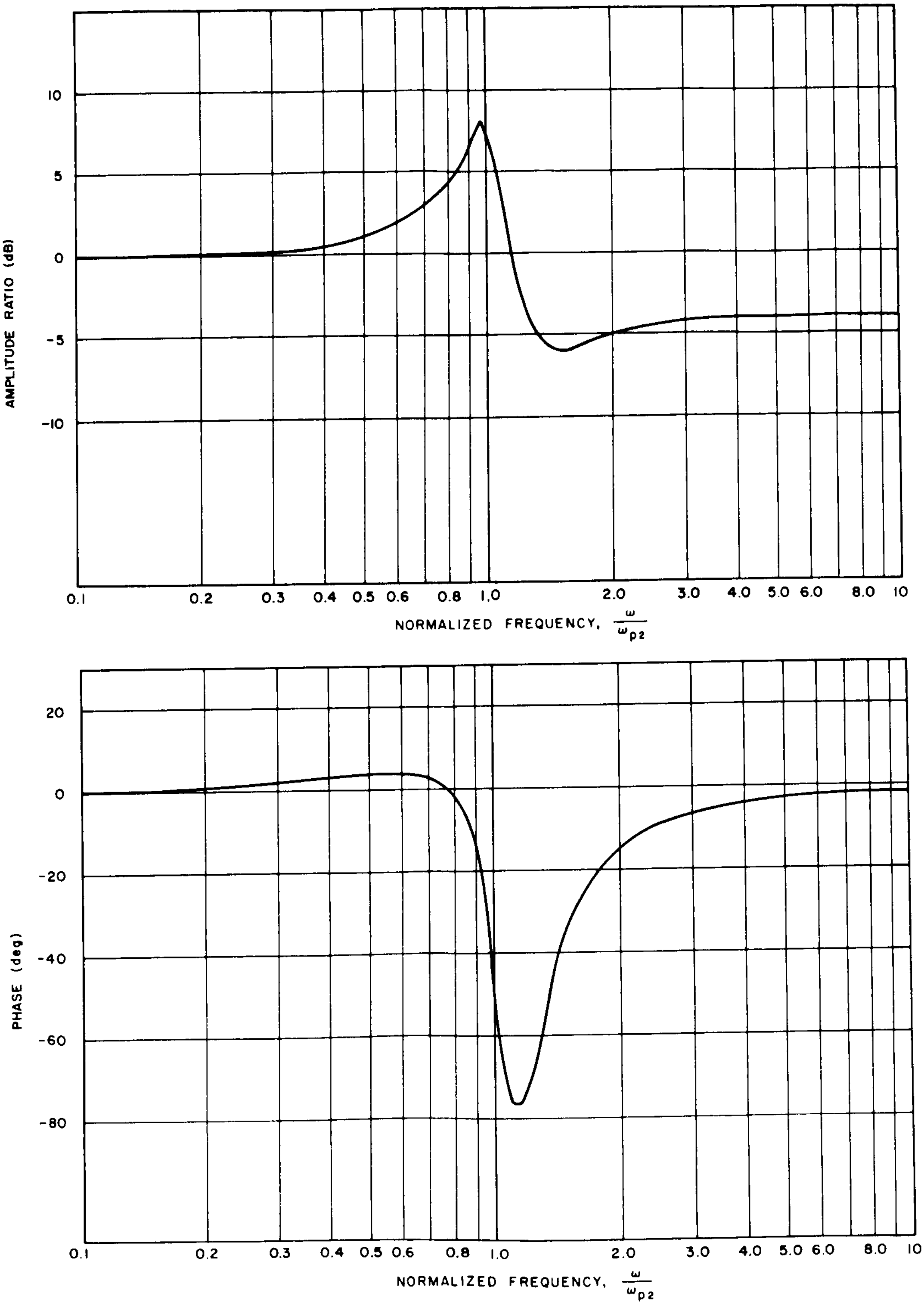

Figure 30. Frequency Response of Second Mode Adaptive Tracking Filter for Phase Stabilization

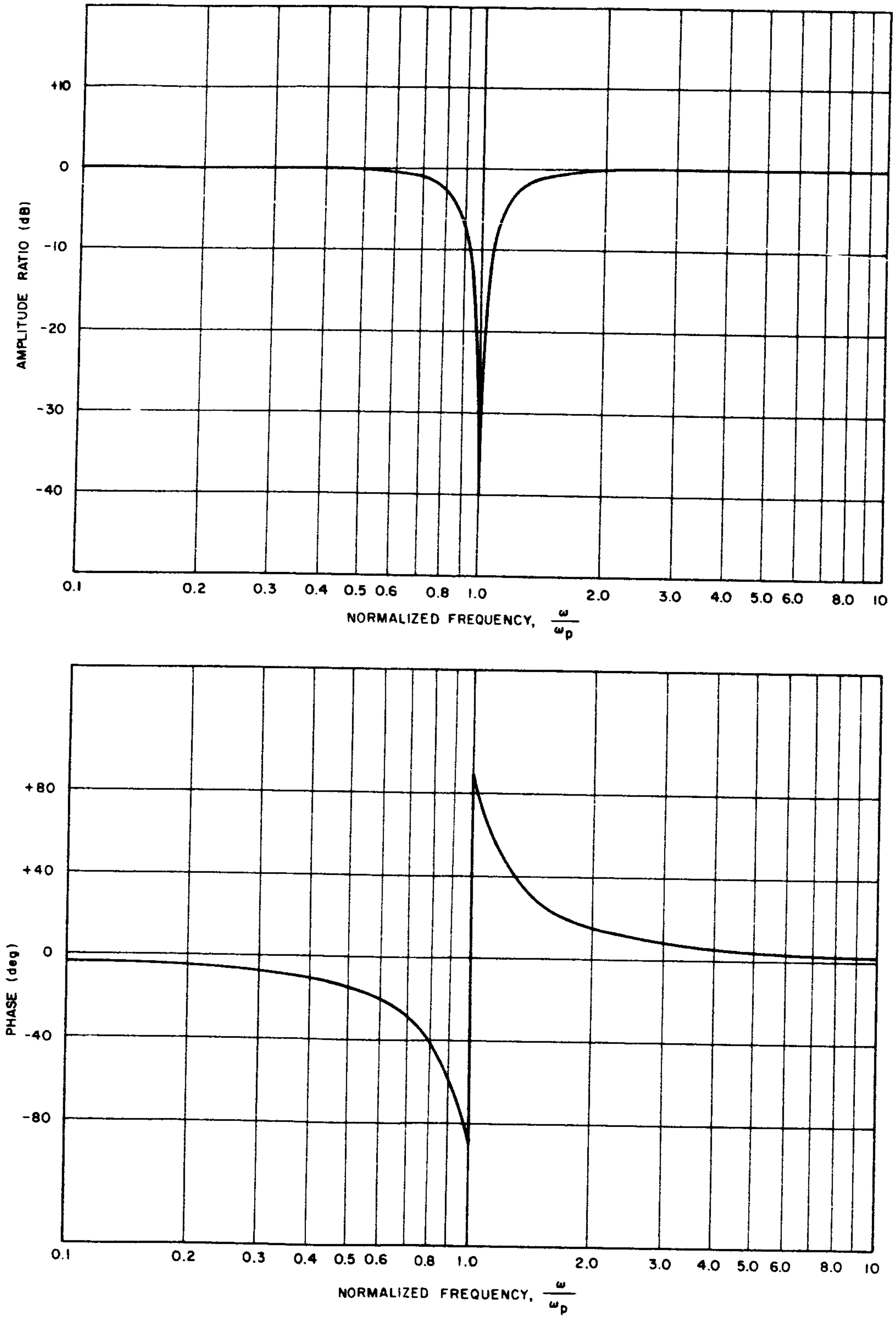

Figure 31. Frequency Response of Both Adaptive Tracking Filters Configured for Gain Stabilization

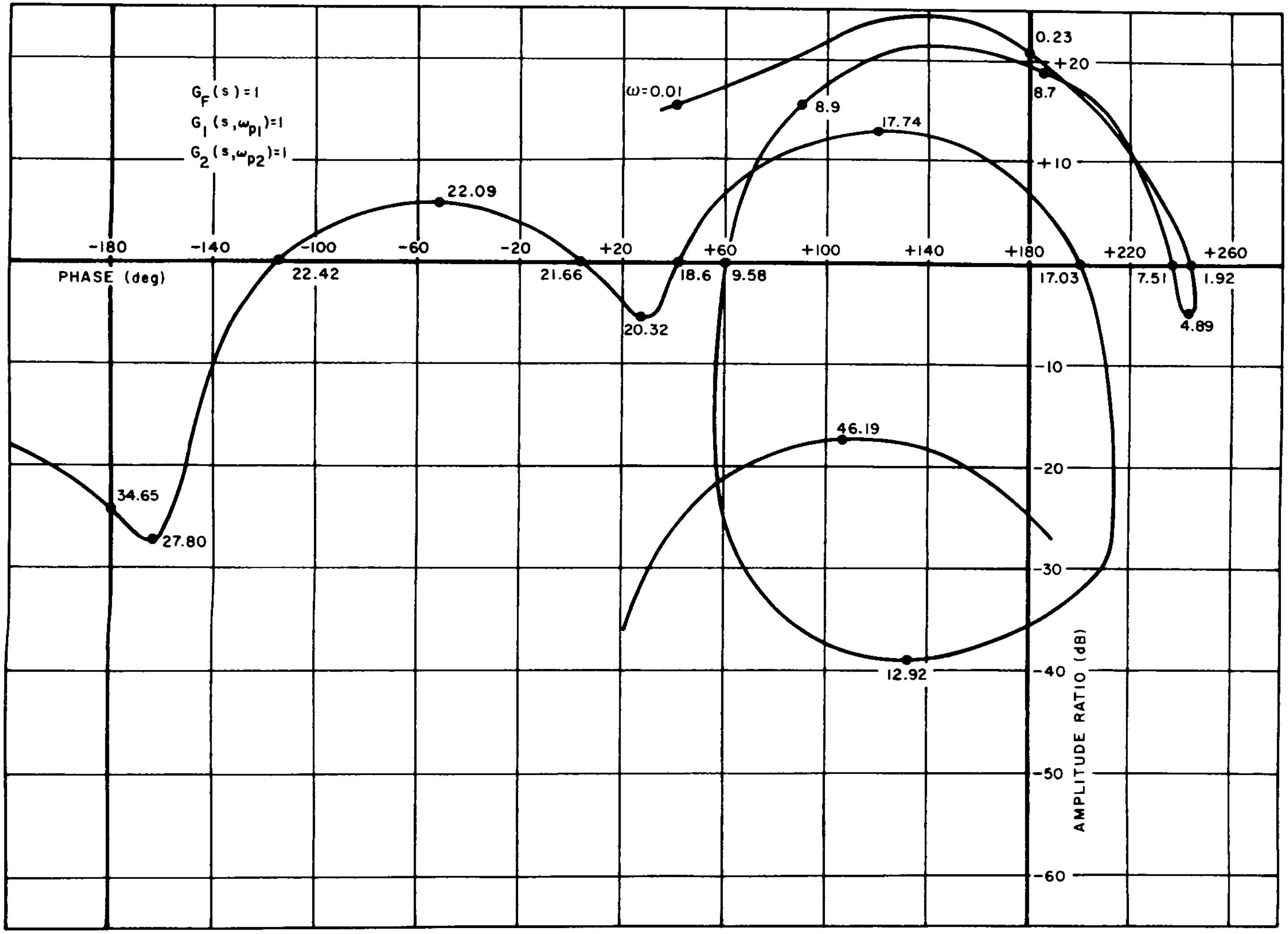

Figure 32. Gain-Phase Plot, No Bending Compensation in Attitude or Attitude Rate Channels, T = 40 Seconds

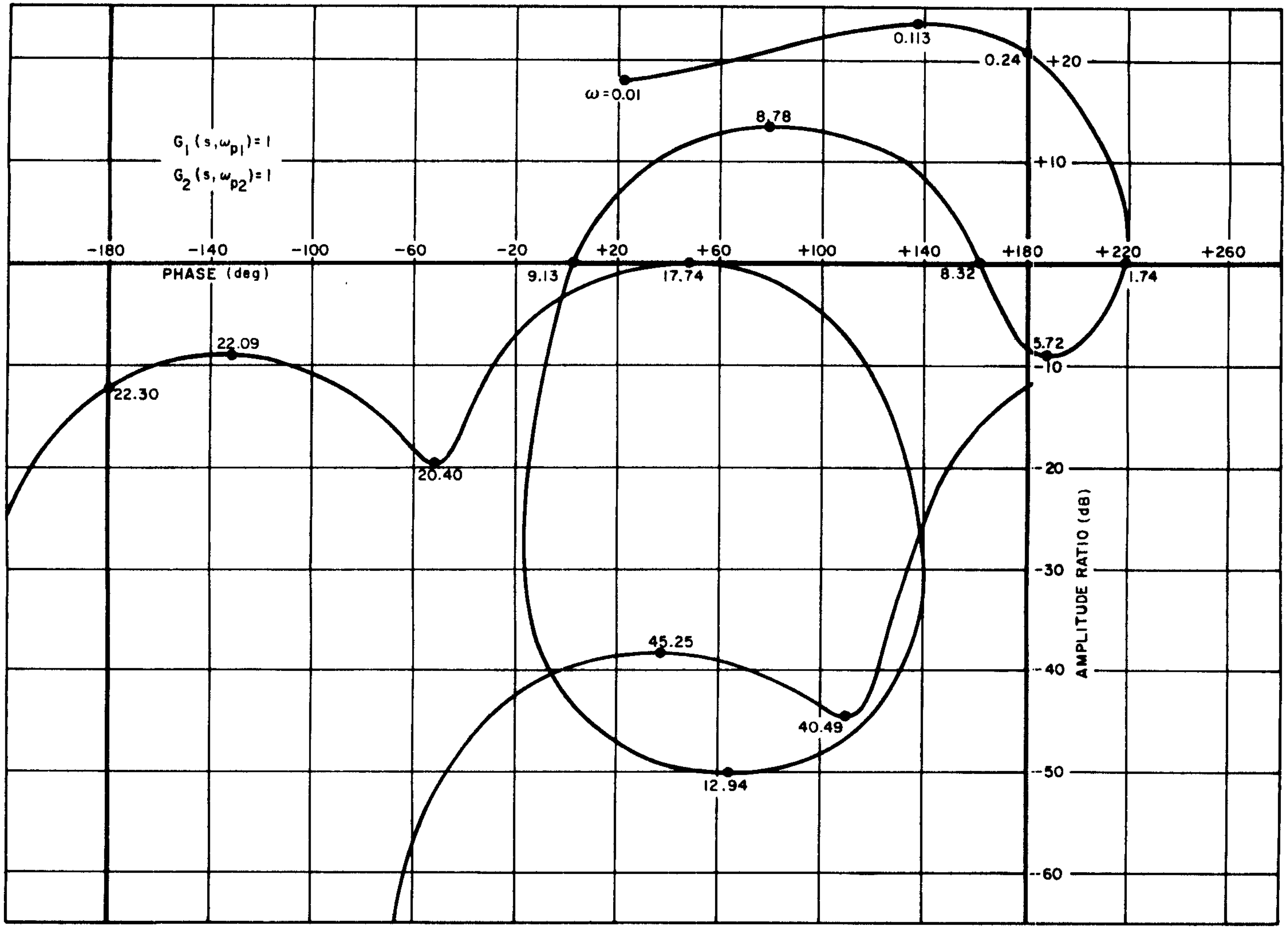

Figure 33. Gain-Phase Plot, Fixed Compensation Only in Attitude and Attitude Rate Channels, T = 40 Seconds

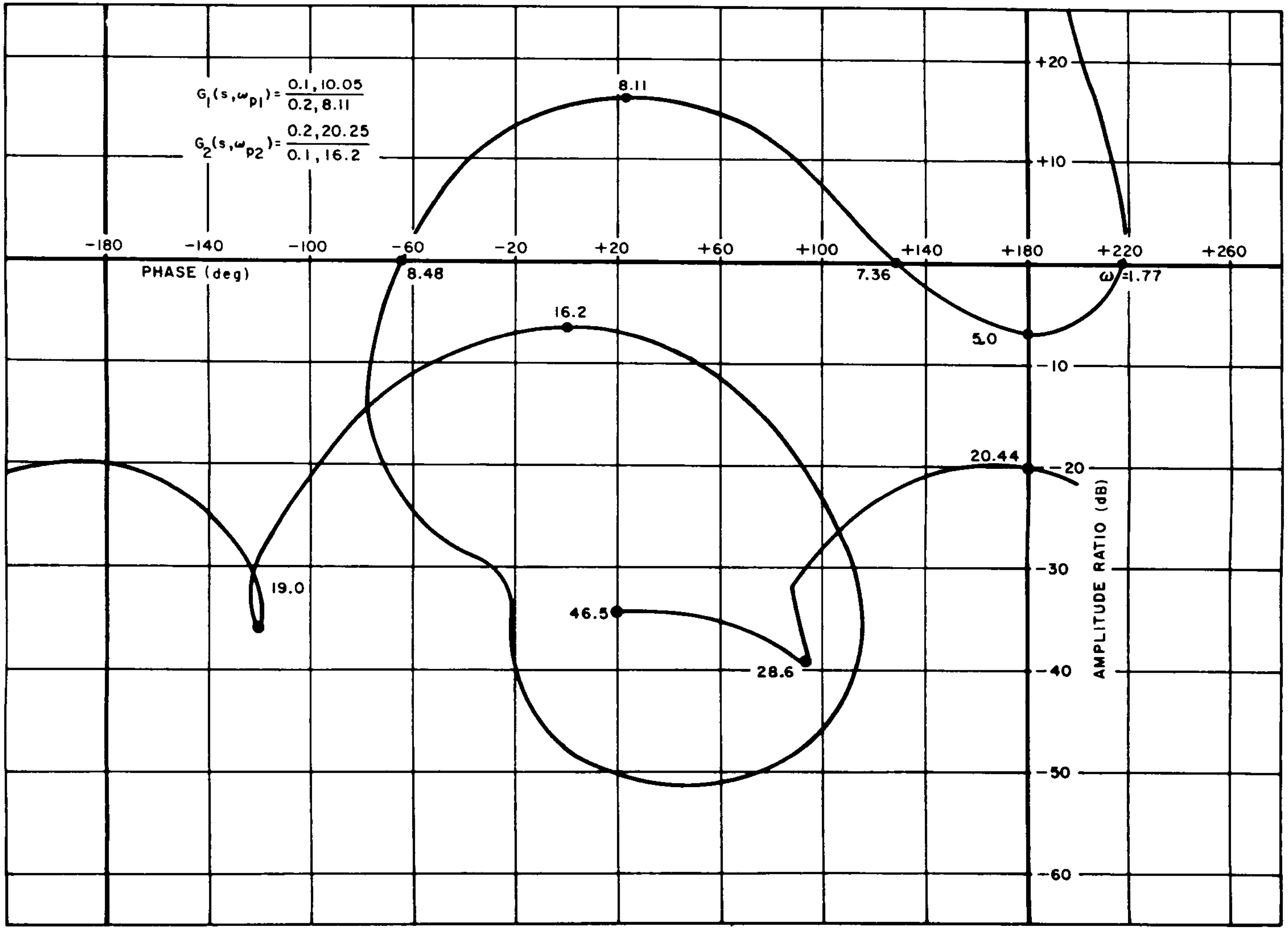

Figure 34. Gain-Phase Plot, Phase Stabilization, Propellant Slosh Not Included, T = 0 Seconds

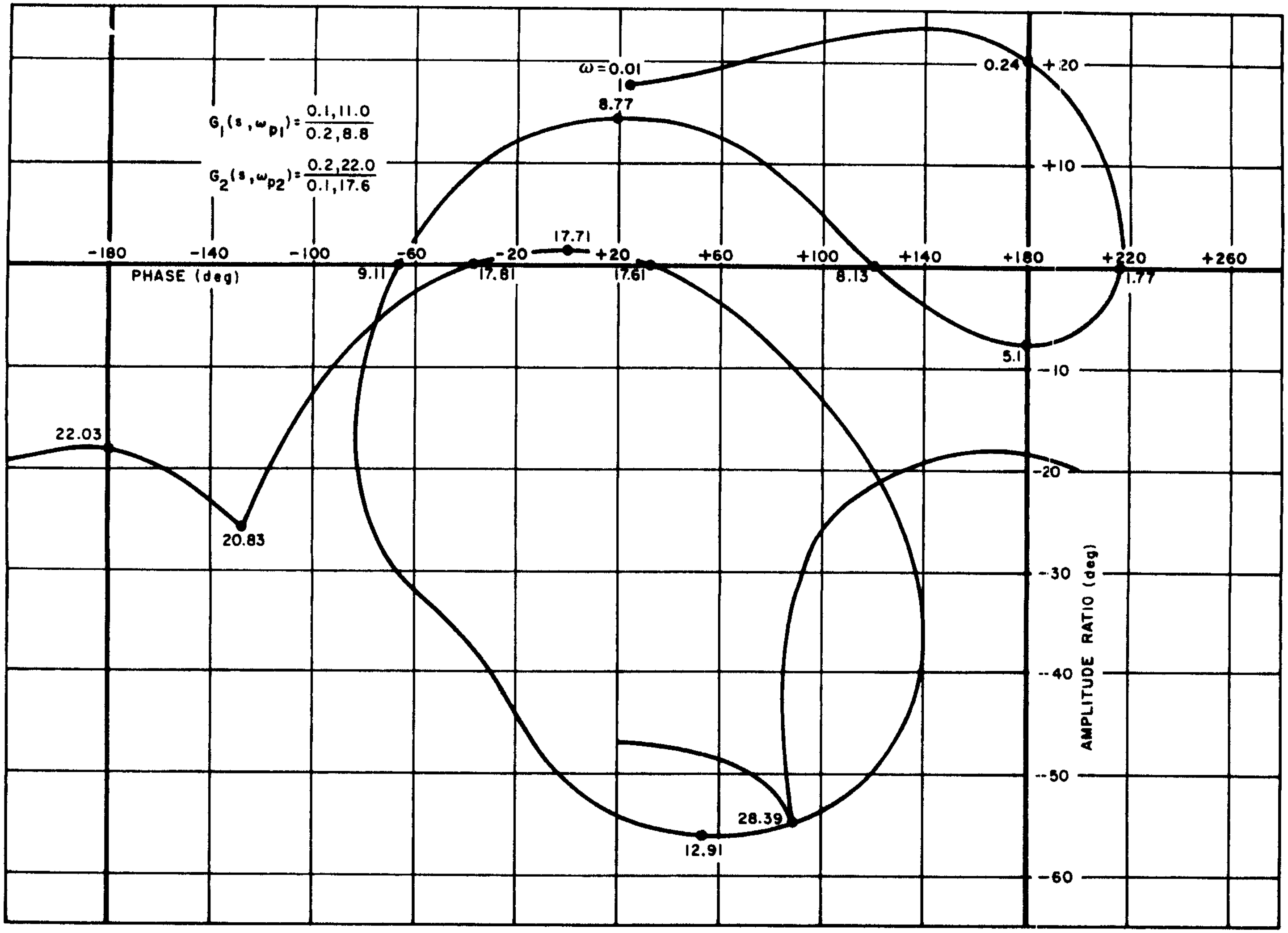

Figure 35. Gain-Phase Plot, Phase Stabilization, Propellant Slosh Not Included, T = 40 Seconds

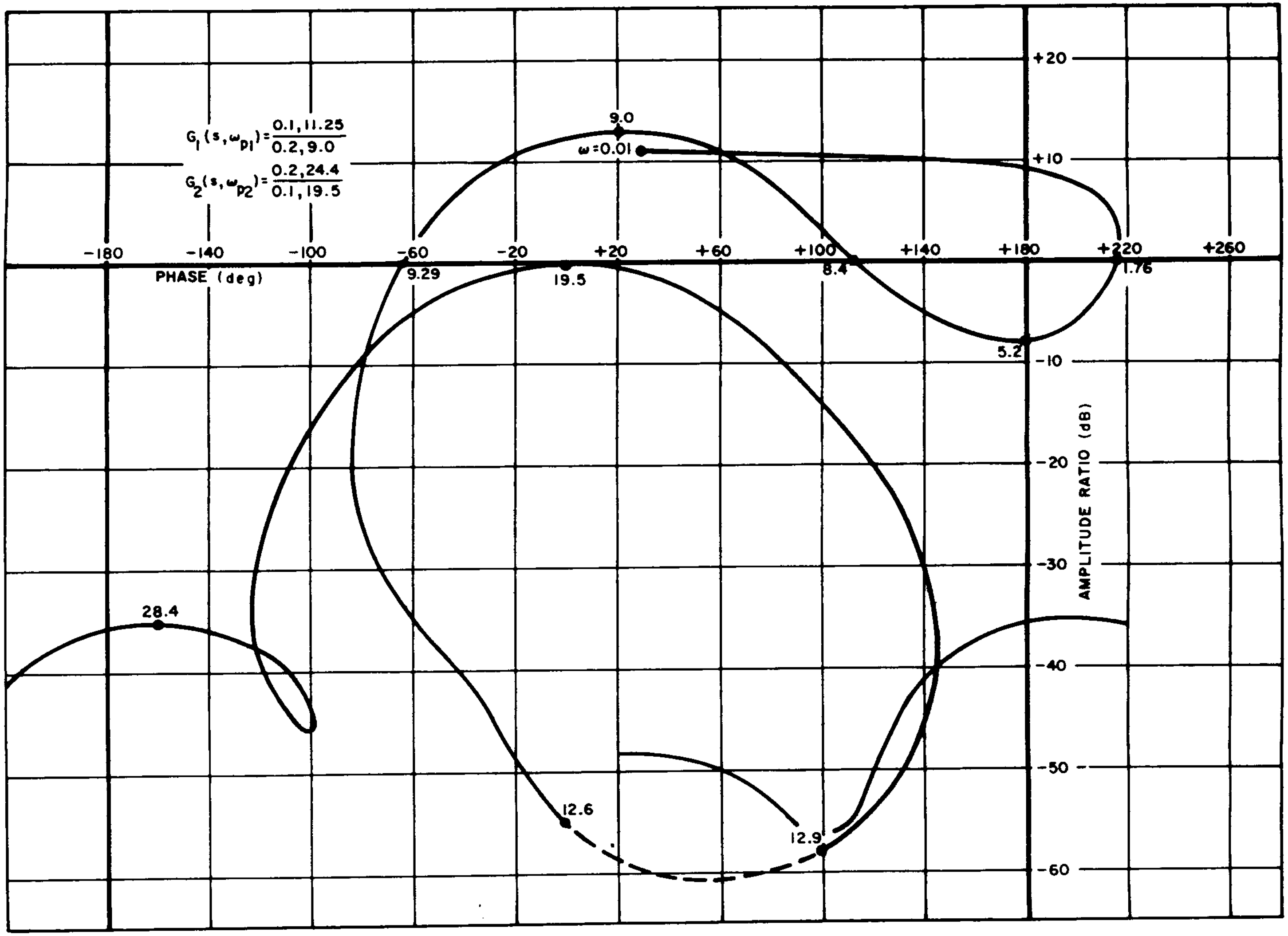

Figure 36. Gain-Phase Plot, Phase Stabilization, Propellant Slosh Not Included, T = 80 Seconds

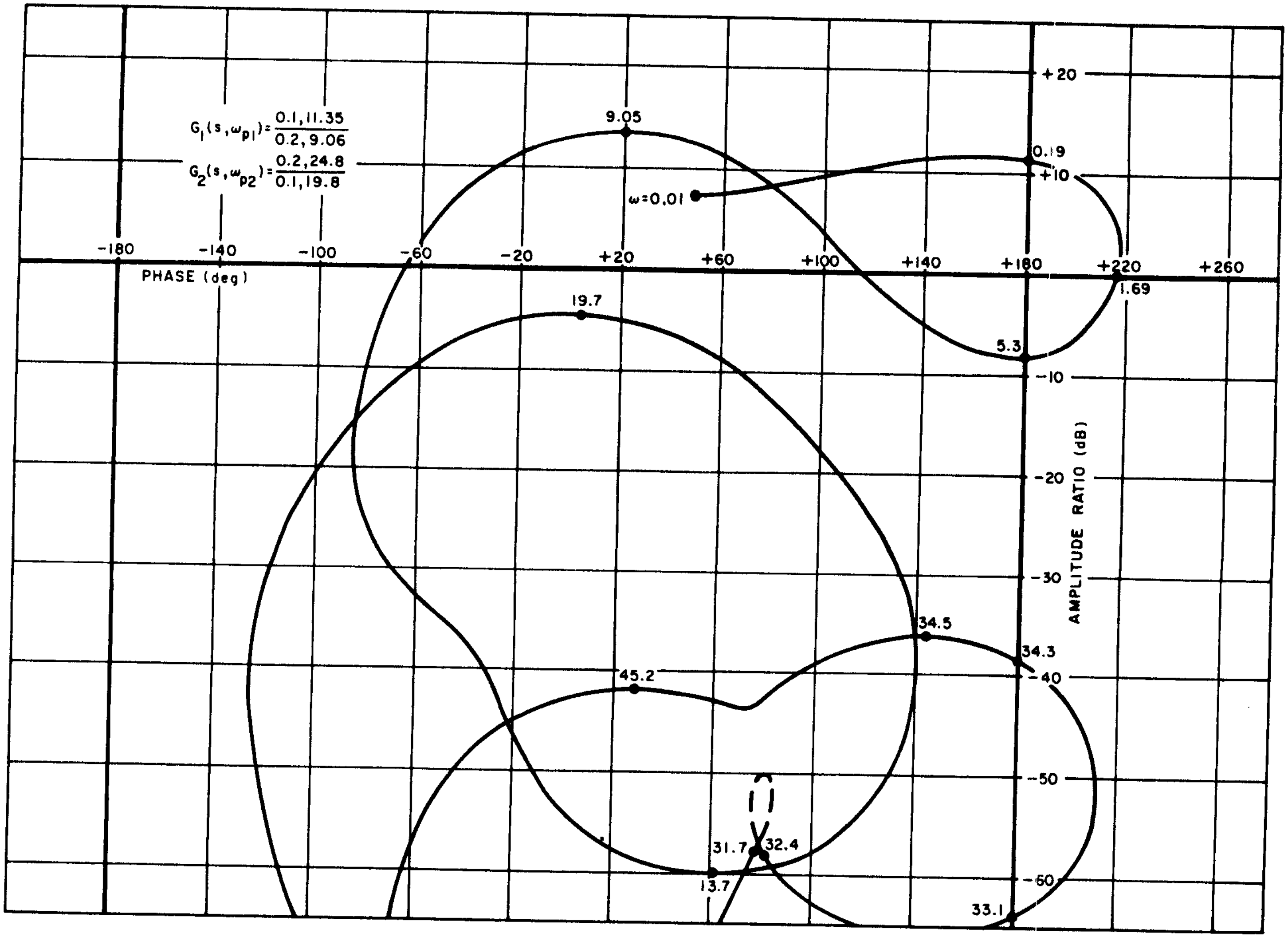

Figure 37. Gain-Phase Plot, Phase Stabilization, Propellant Slosh Not Included, T = 100 Seconds

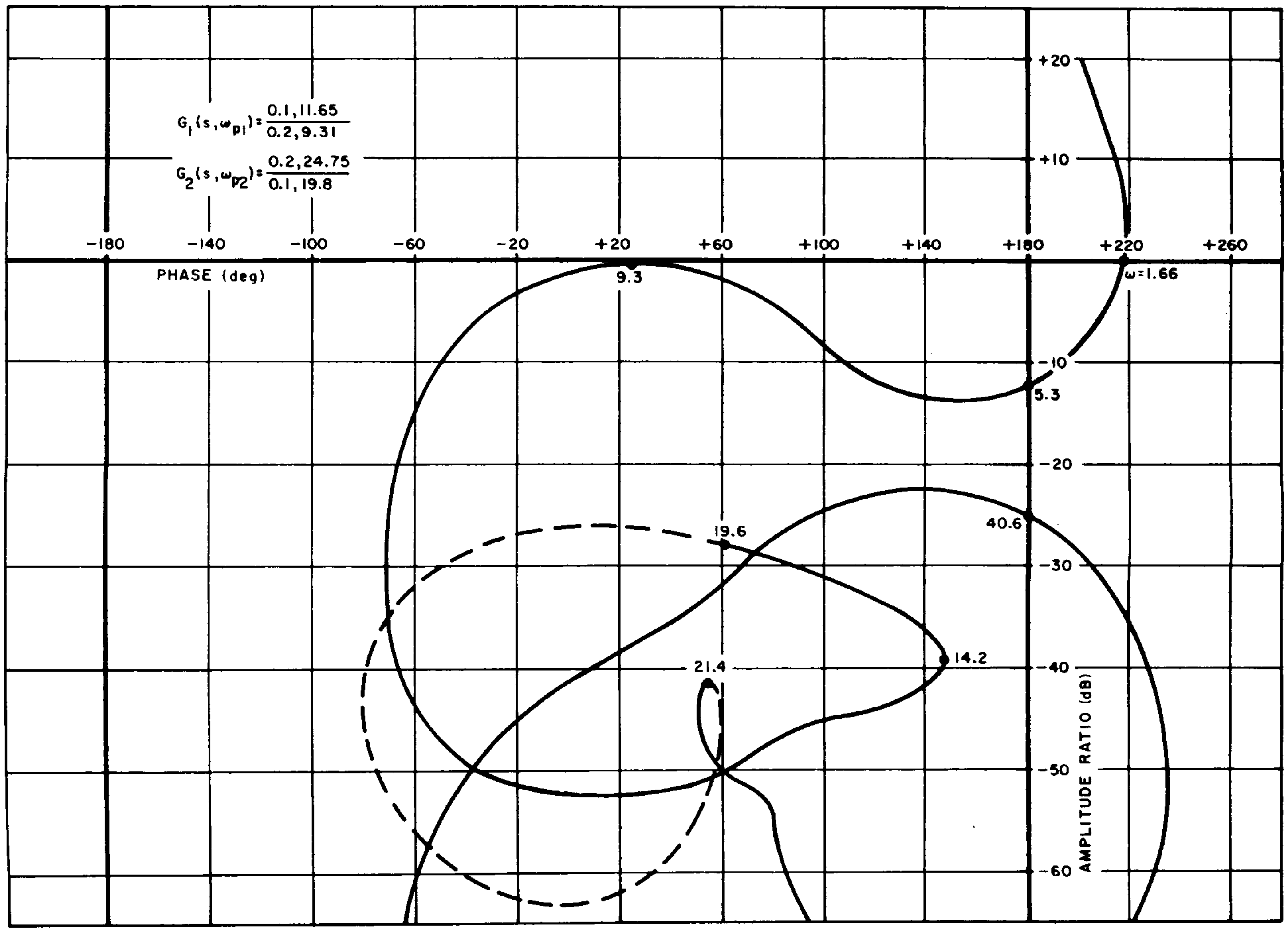

Figure 38. Gain-Phase Plot, Phase Stabilization, Propellant Slosh Not Included, T = 140 Seconds

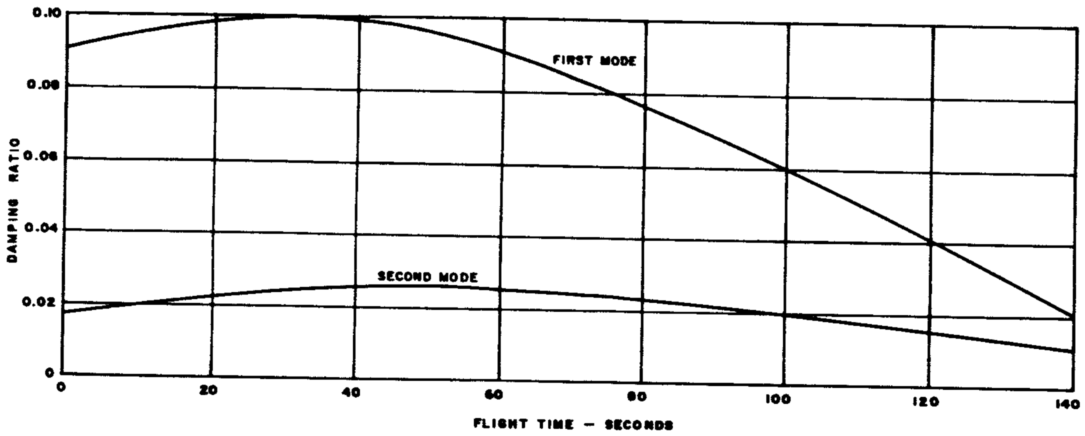

Figure 39. Closed Loop First and Second Mode Damping Ratios as a Function of Flight Time, Phase Stabilization

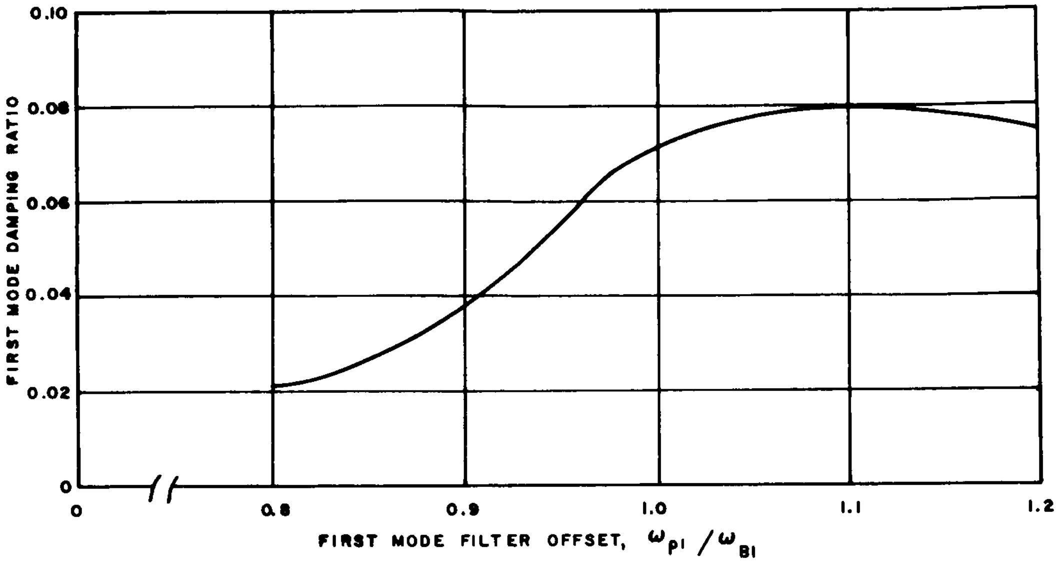

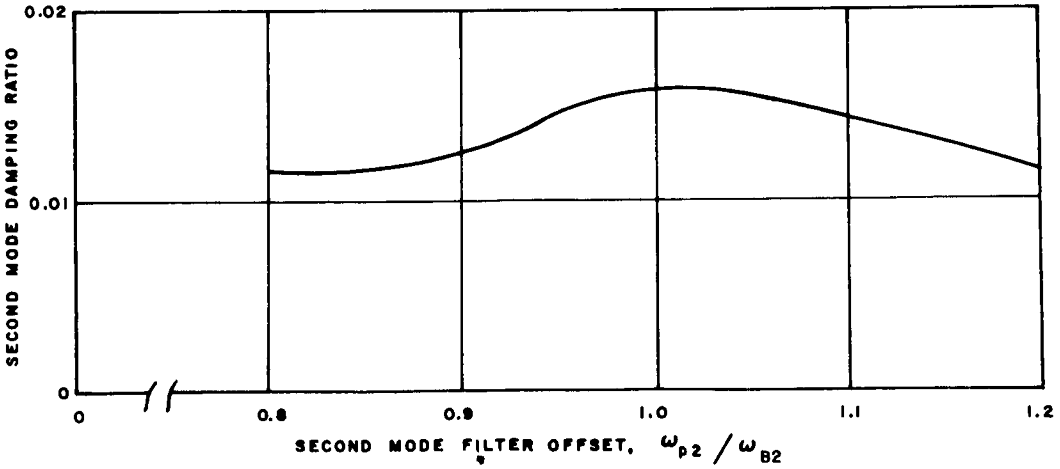

Figure 40. First and Second Mode Closed Loop Damping Ratios as a Function of Adaptive Tracking Filter Frequency Offset, Phase Stabilization, T = 80 Seconds

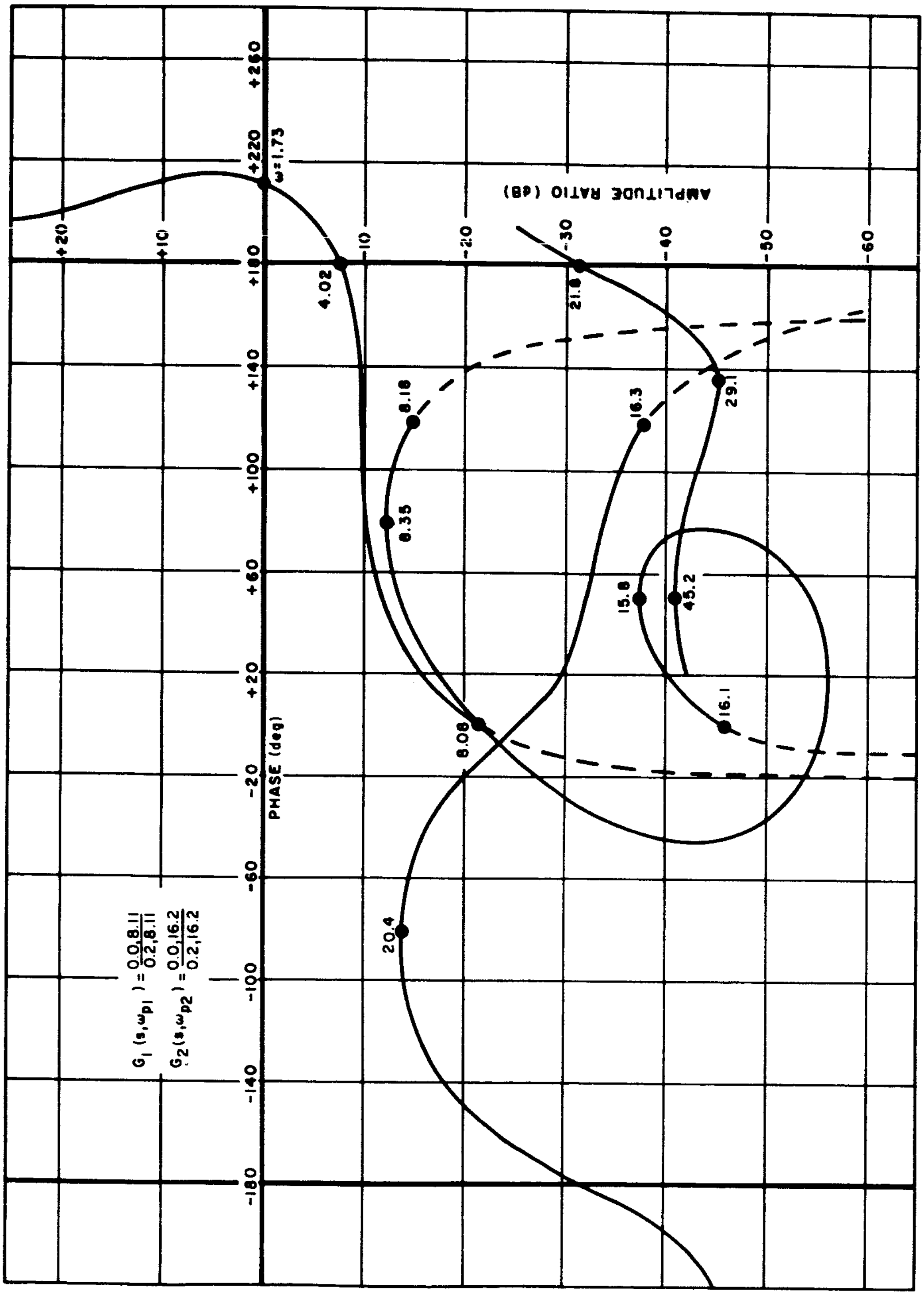

Figure 41. Gain-Phase Plot, Gain Stabilization, Propellant Slosh Not Included, T = 0 Seconds

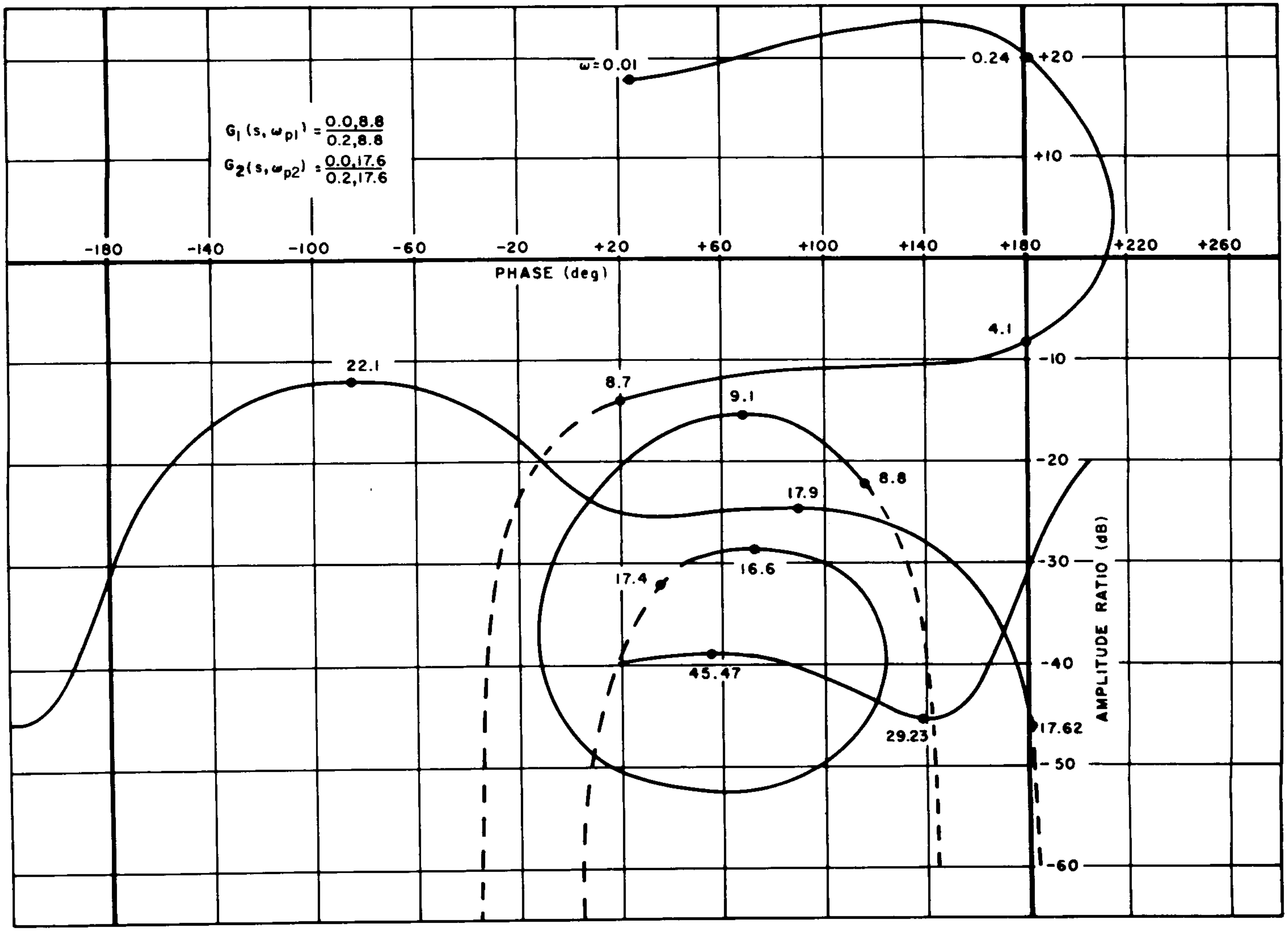

Figure 42. Gain-Phase Plot, Gain Stabilization, Propellant Slosh Not Included, T = 40 Seconds

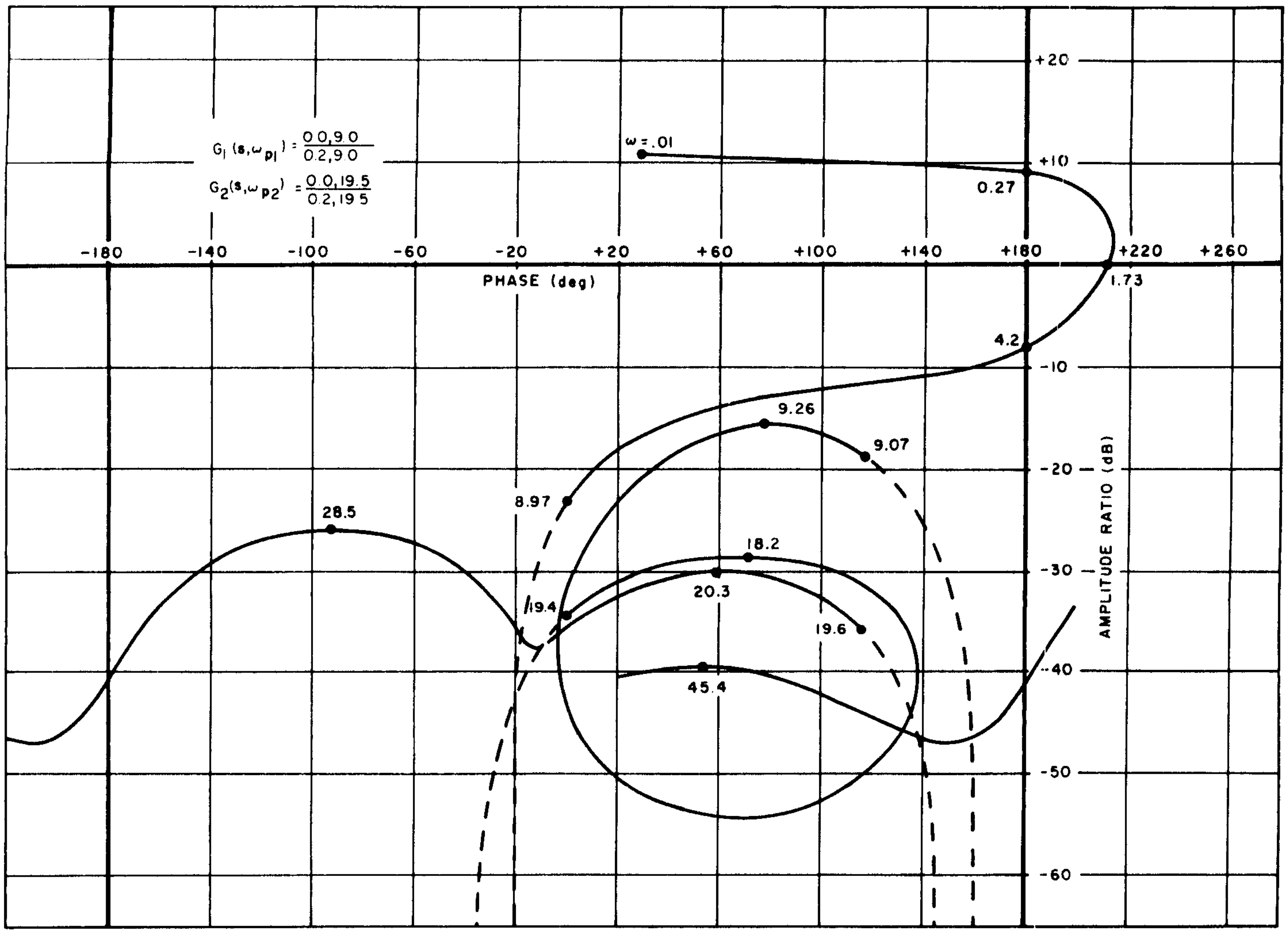

Figure 43. Gain-Phase Plot, Gain Stabilization, Propellant Slosh Not Included, T = 80 Seconds

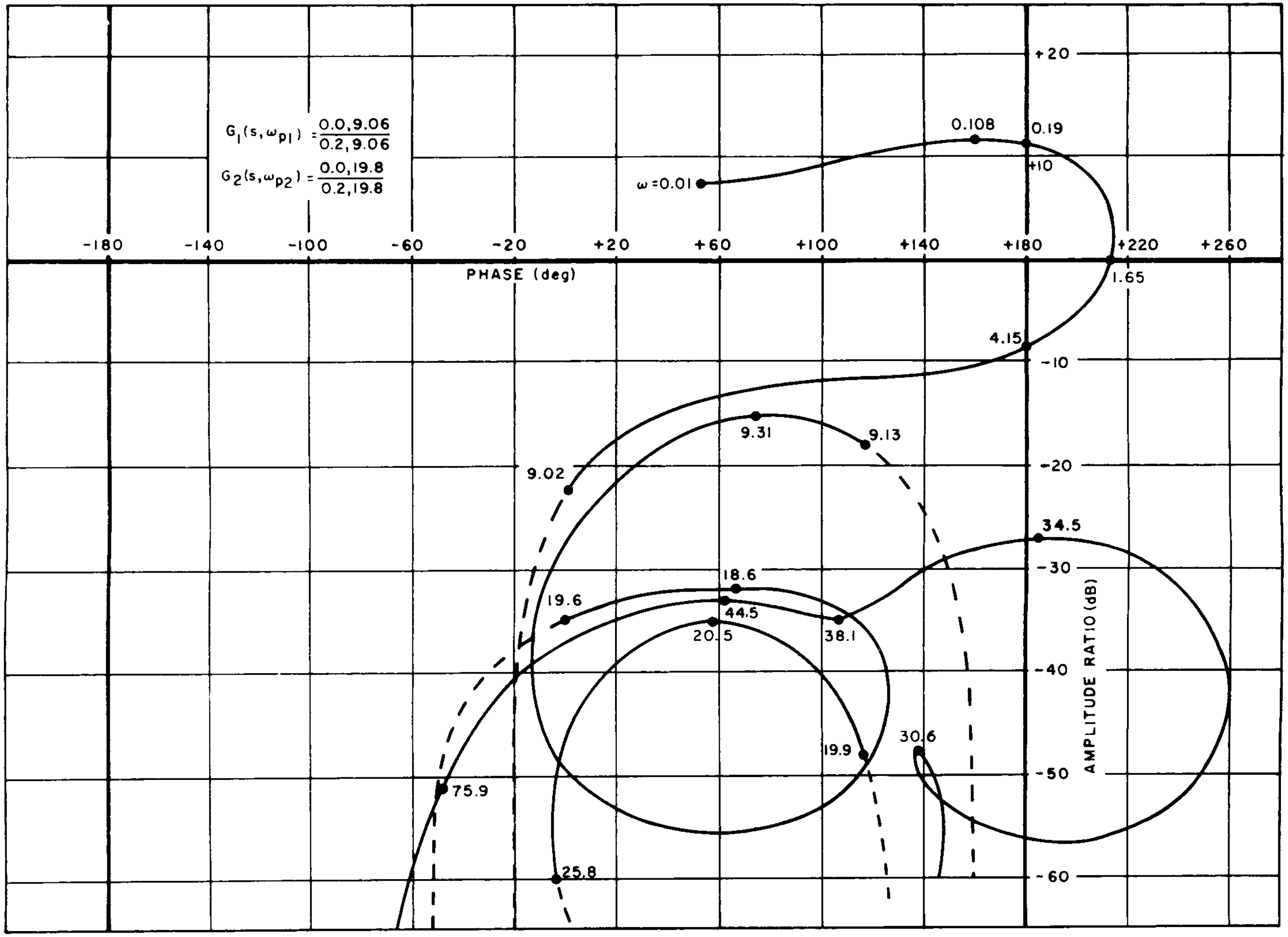

Figure 44. Gain-Phase Plot, Gain Stabilization, Propellant Slosh Not Included, T = 100 Seconds

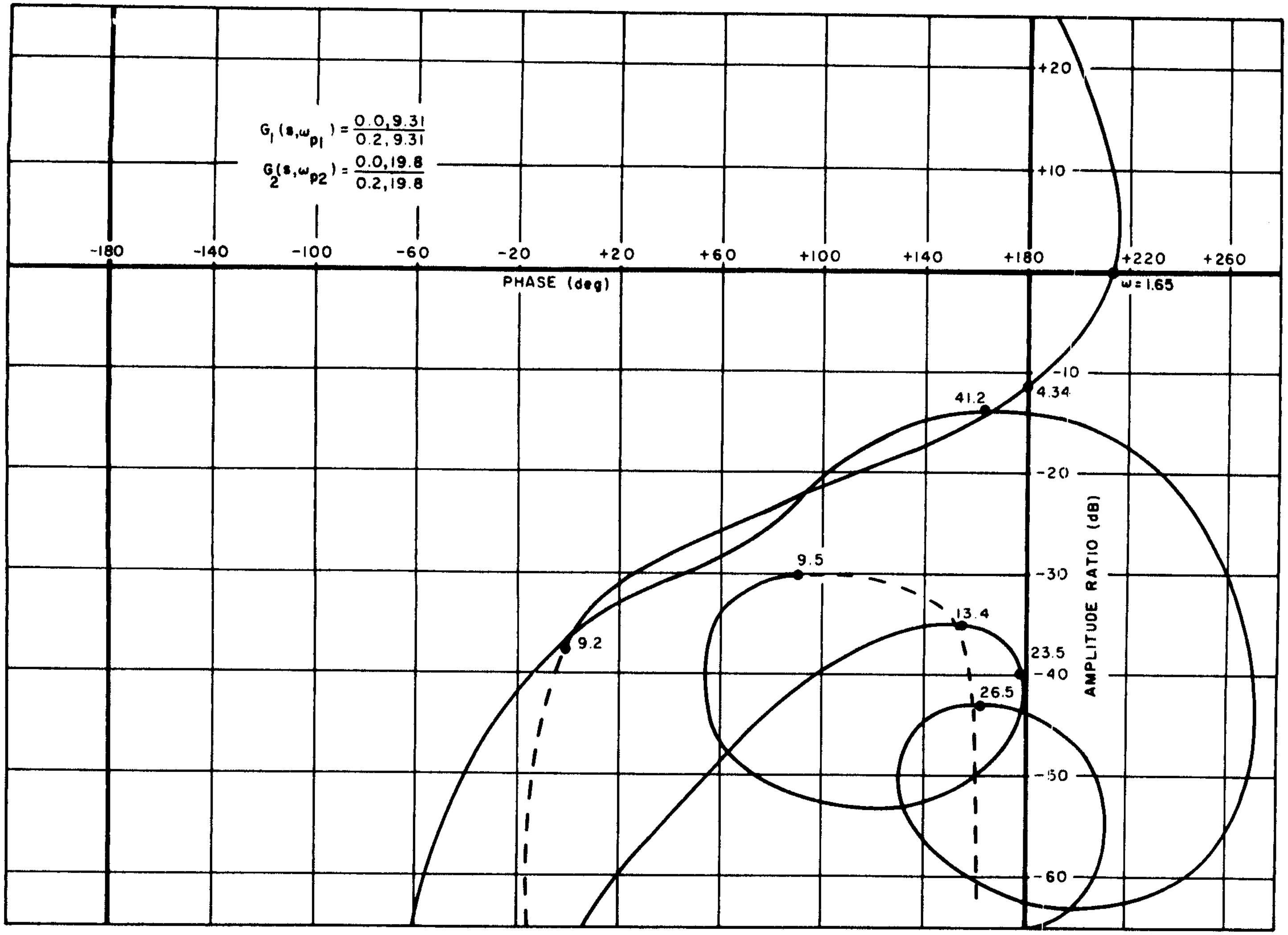

Figure 45. Gain-Phase Plot, Gain Stabilization, Propellant Slosh Not Included, T = 140 Seconds

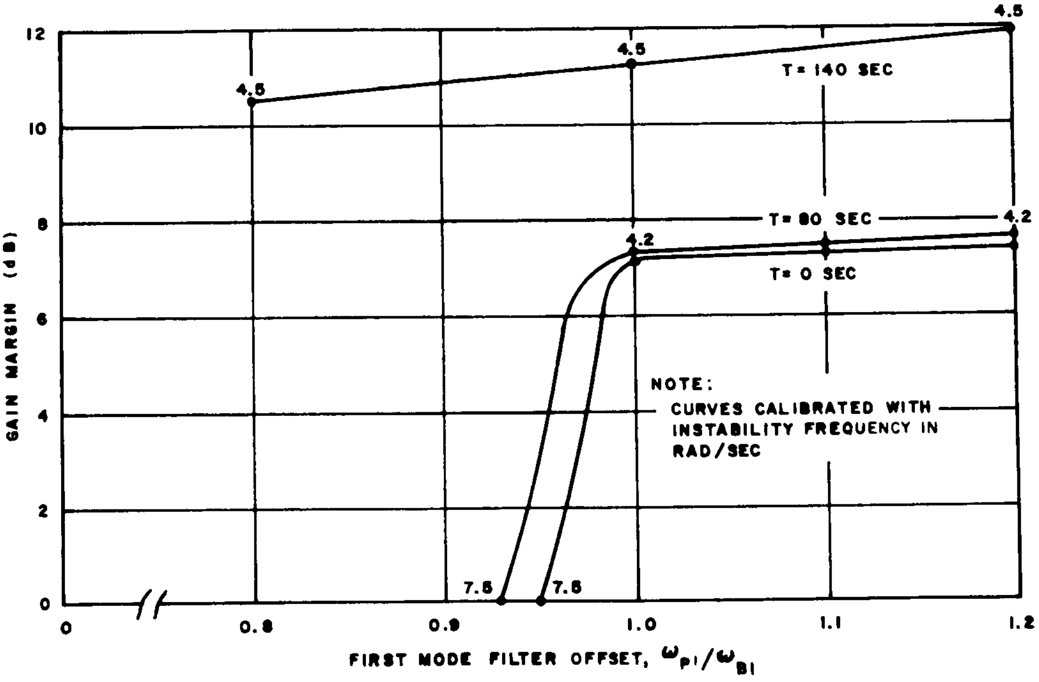

Figure 46. Effect of First Mode Adaptive Tracking Filter Frequency Offset, Gain Stabilization

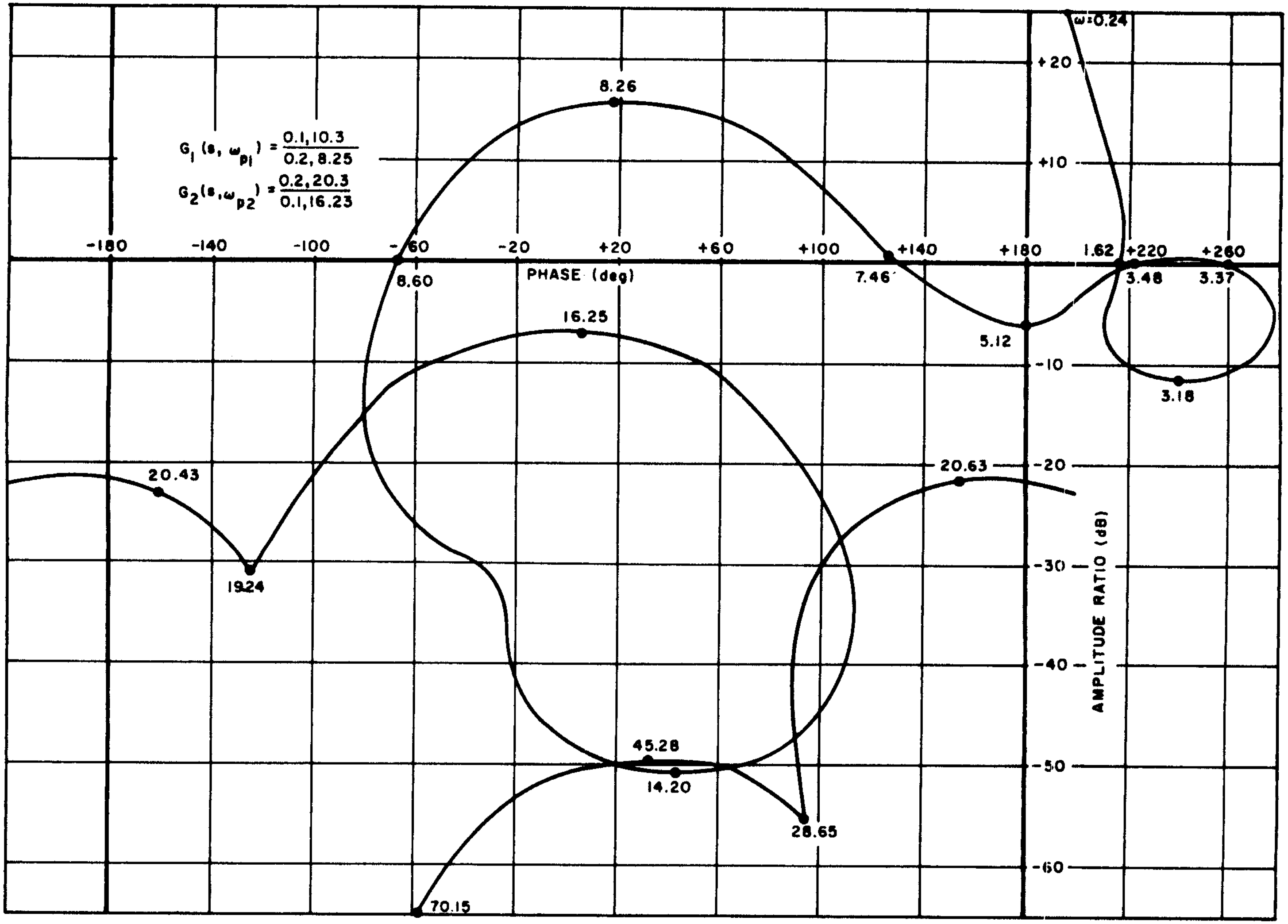

Figure 47. Gain-Phase Plot, Phase Stabilization, Propellant Slosh Included, T = 0 Seconds

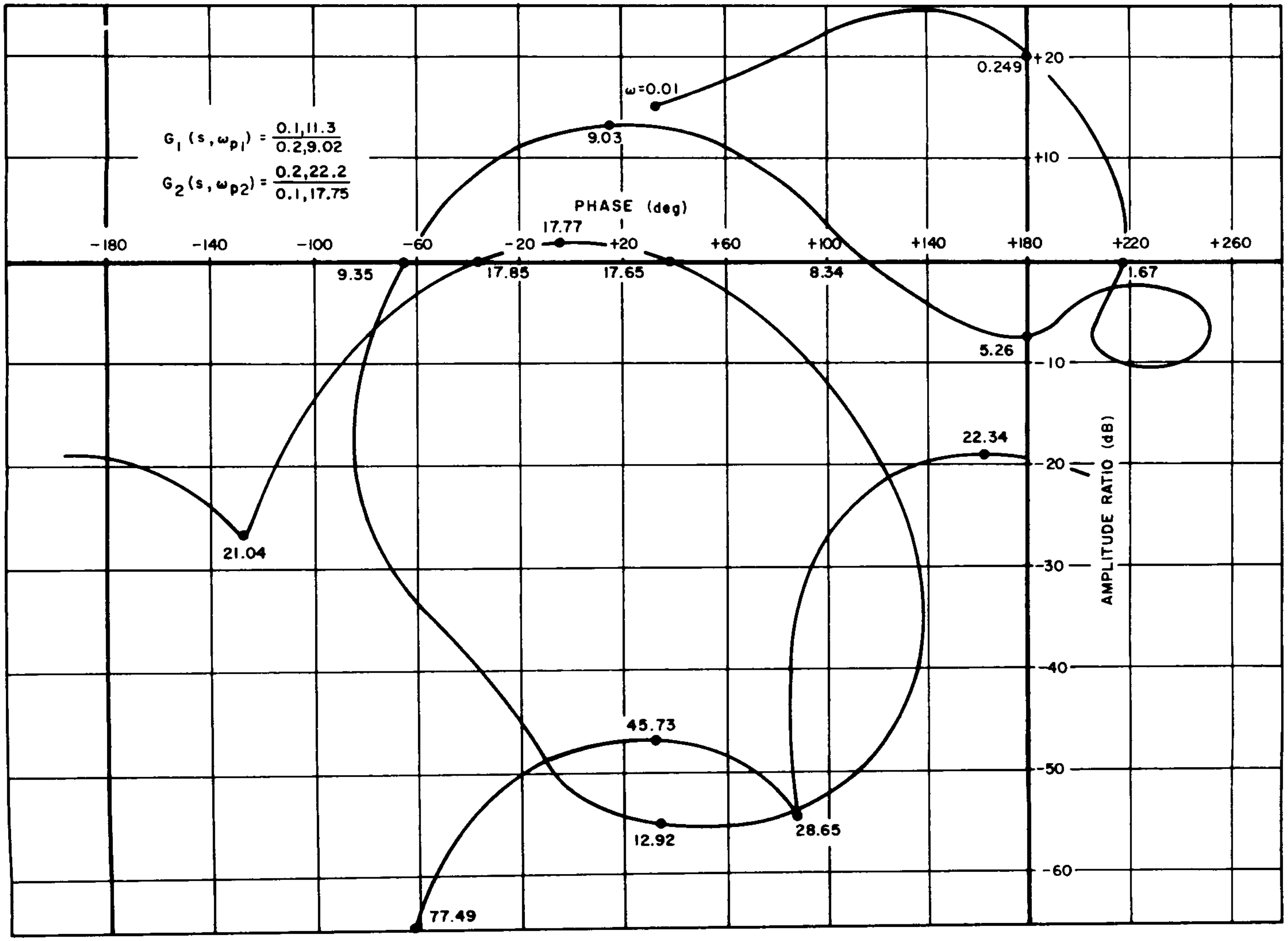

Figure 48. Gain-Phase Plot, Phase Stabilization Propellant Slosh Included, T = 40 Seconds

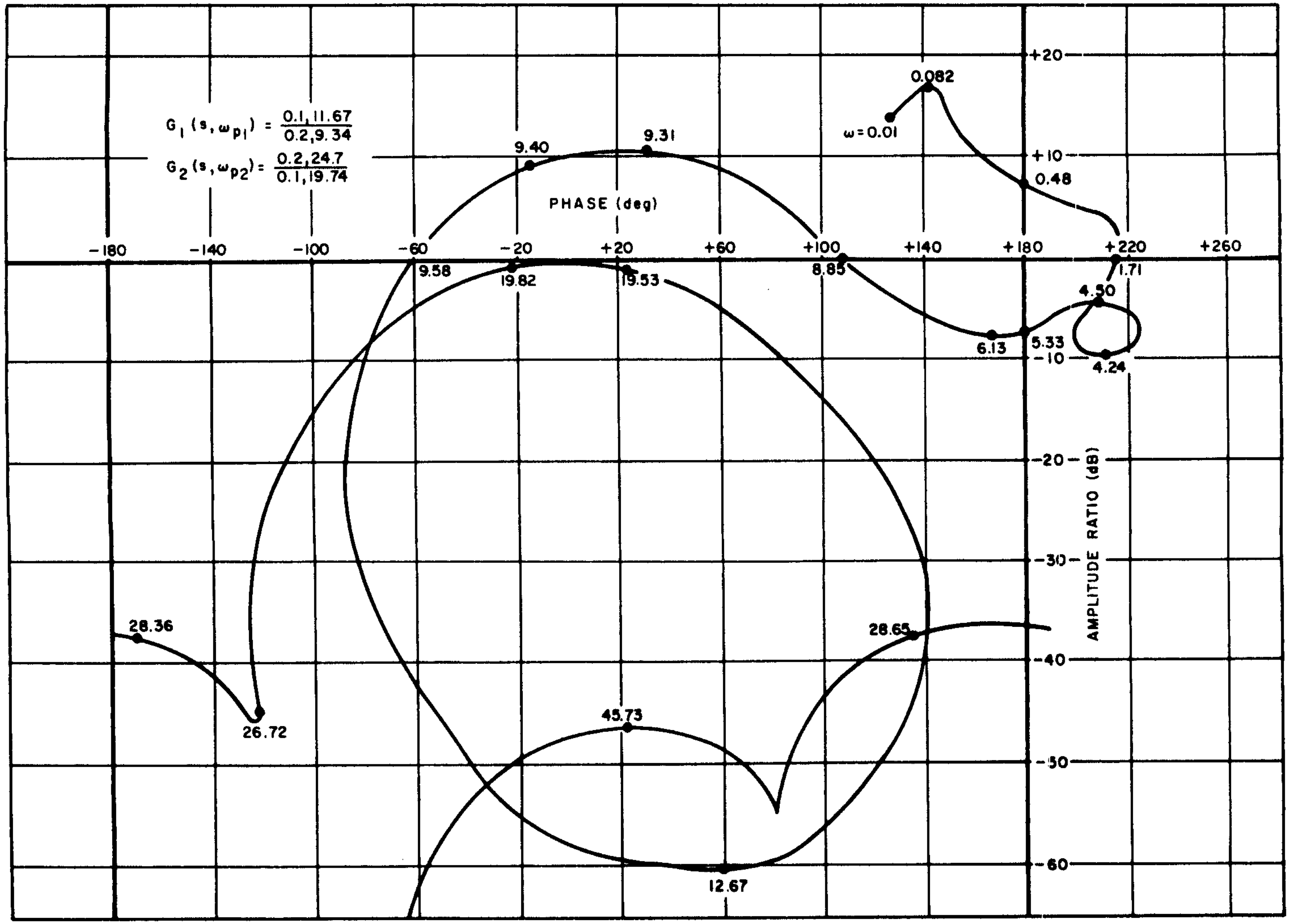

Figure 49. Gain-Phase Plot, Phase Stabilization, Propellant Slosh Included, T = 80 Seconds

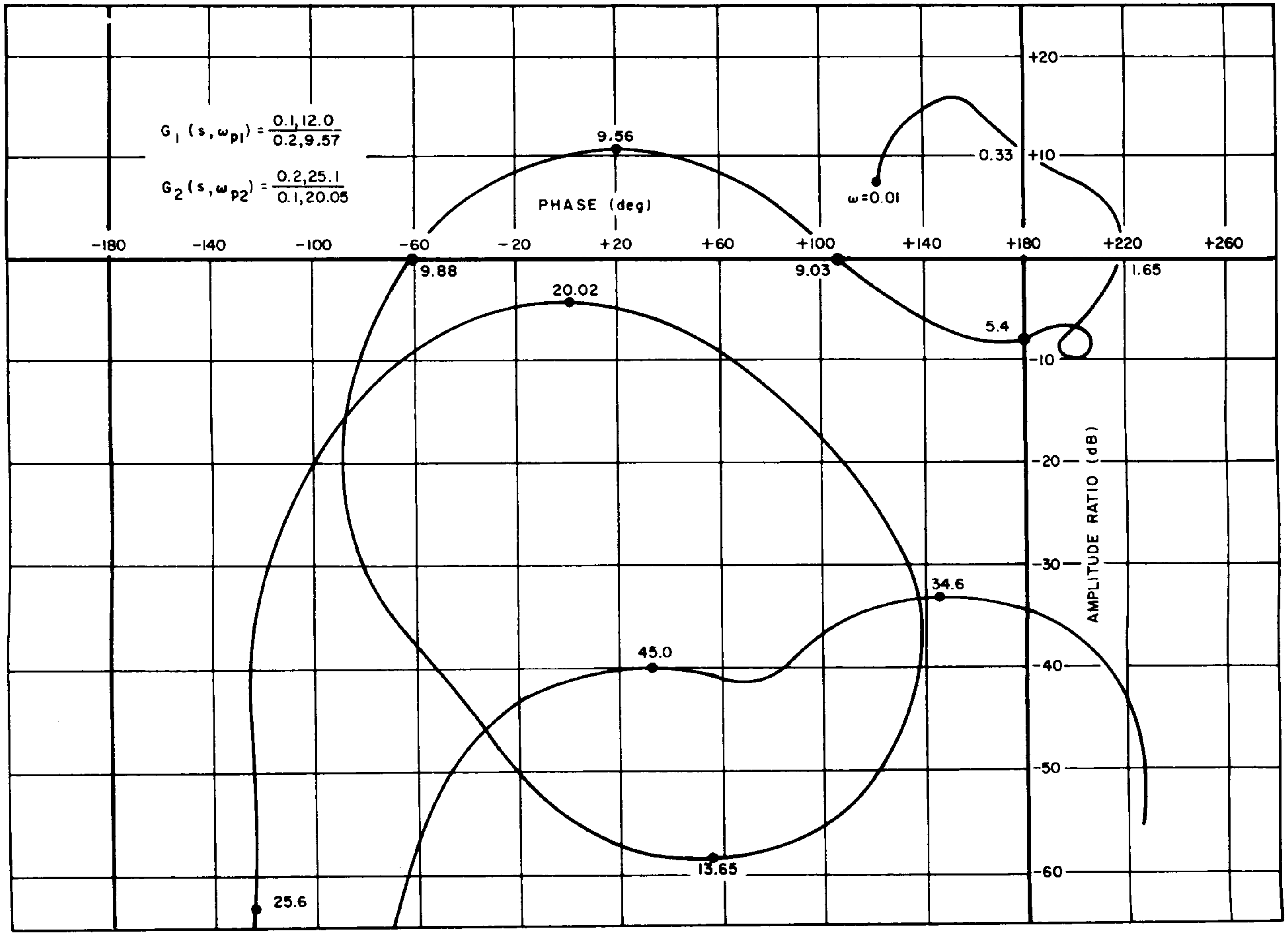

Figure 50. Gain-Phase Plot, Phase Stabilization, Propellant Slosh Included, T = 100 Seconds

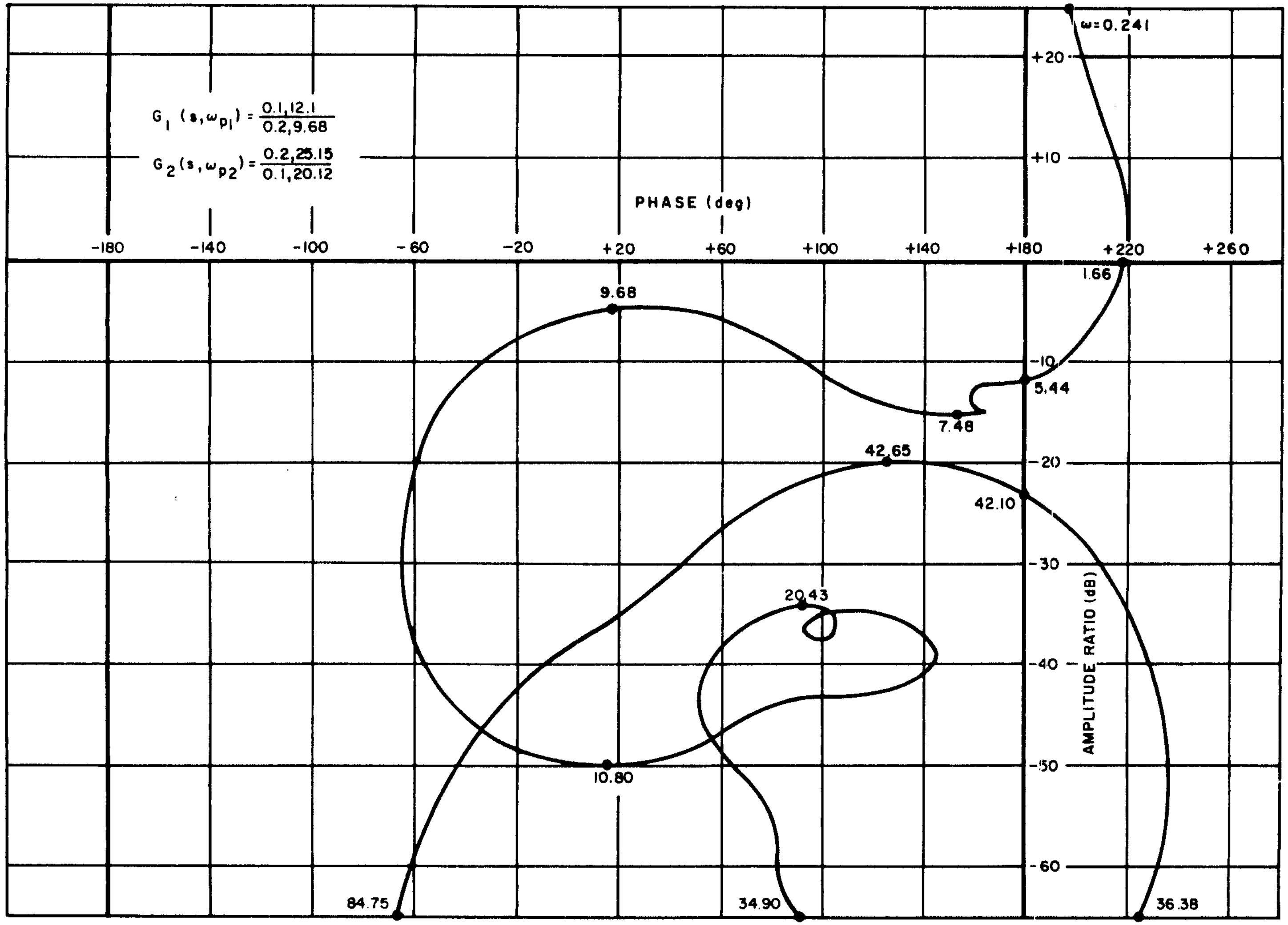

Figure 51. Gain-Phase Plot, Phase Stabilization, Propellant Slosh Included, T = 140 Seconds

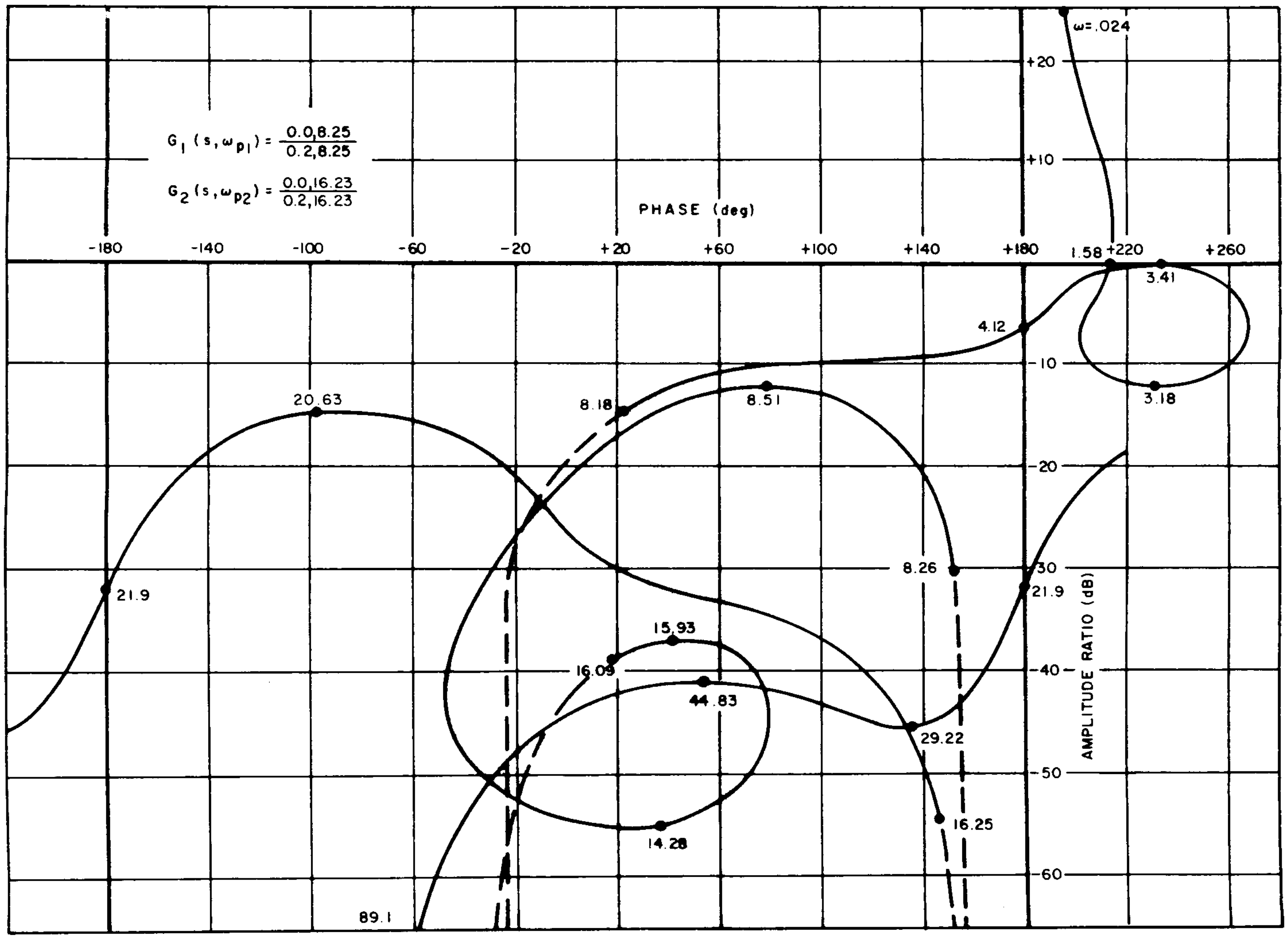

Figure 52. Gain-Phase Plot, Gain Stabilization, Propellant Slosh Included, T = 0 Seconds

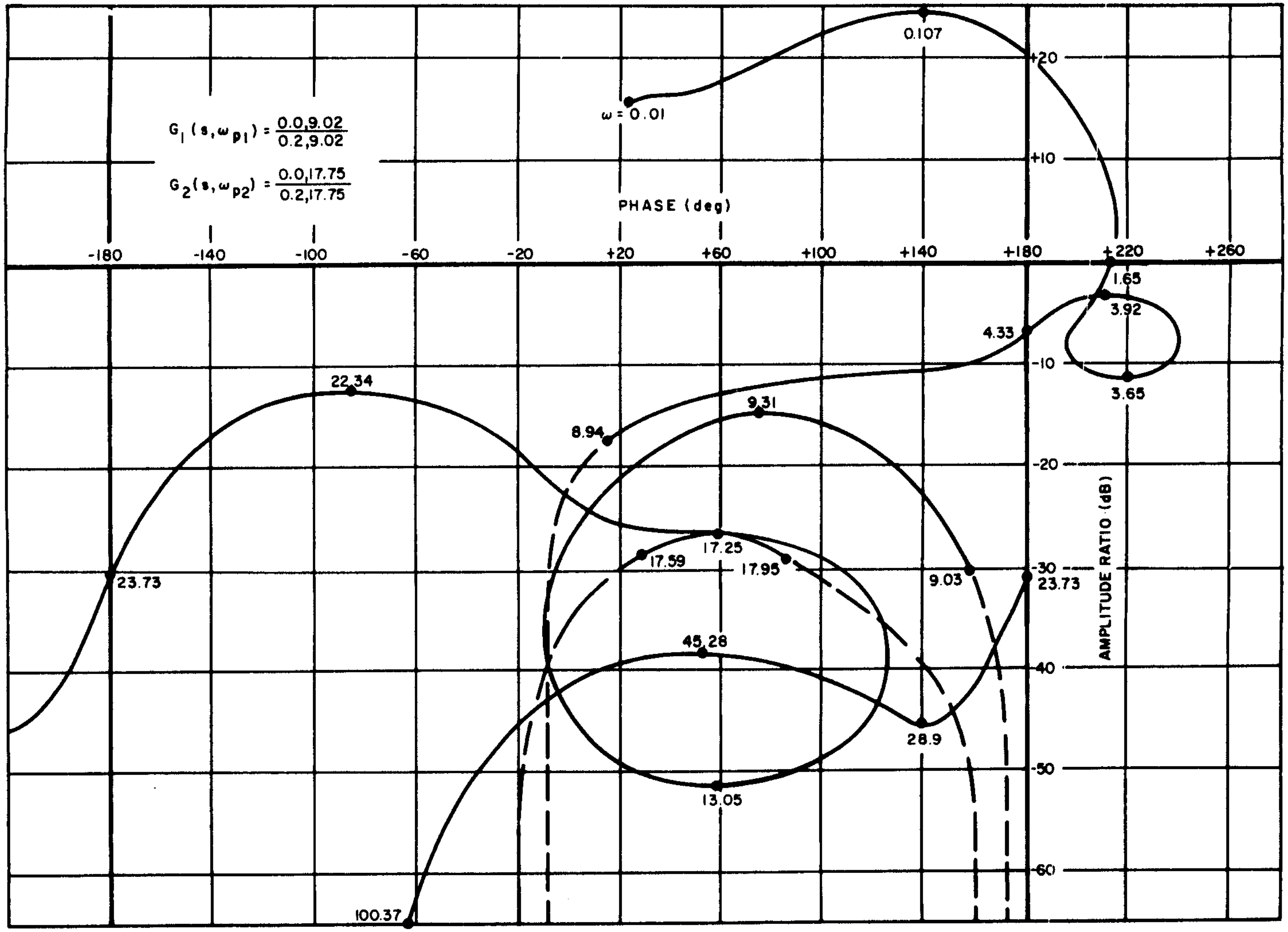

Figure 53. Gain-Phase Plot, Gain Stabilization, Propellant Slosh Included, T = 40 Seconds

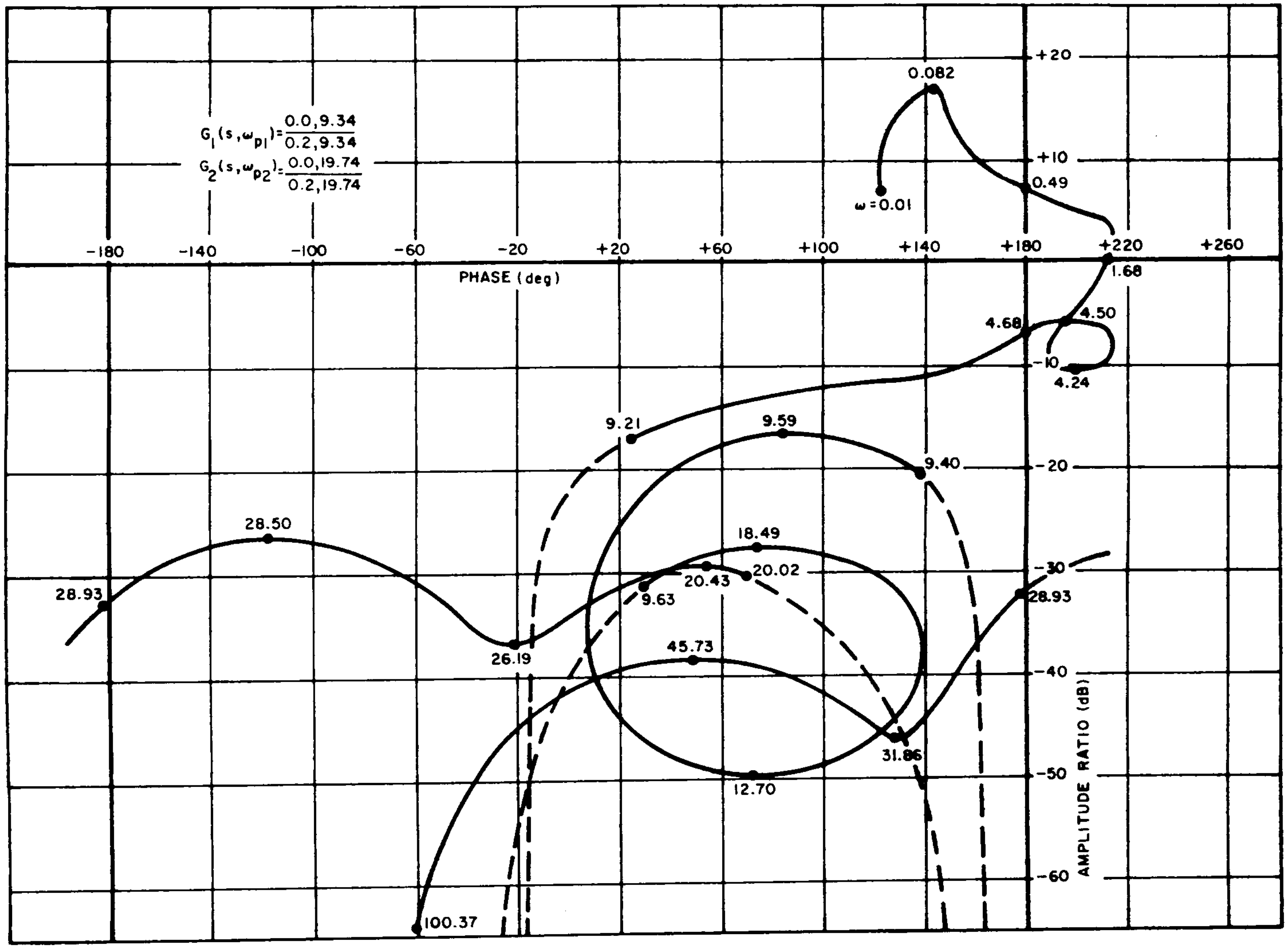

Figure 54. Gain-Phase Plot, Gain Stabilization, Propellant Slosh Included, T = 80 Seconds

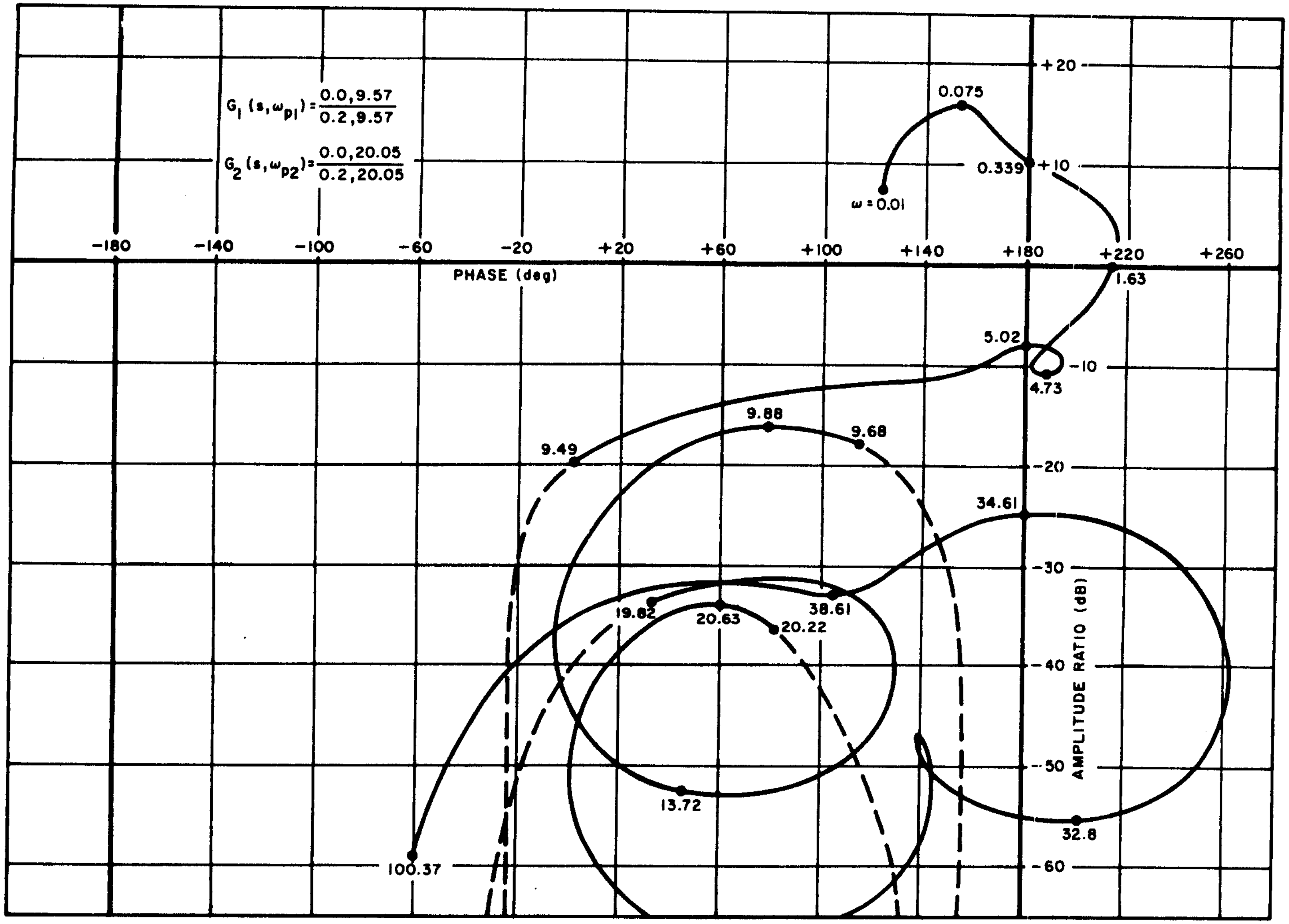

Figure 55. Gain-Phase Plot, Gain Stabilization, Propellant Slosh Included, T = 100 Seconds

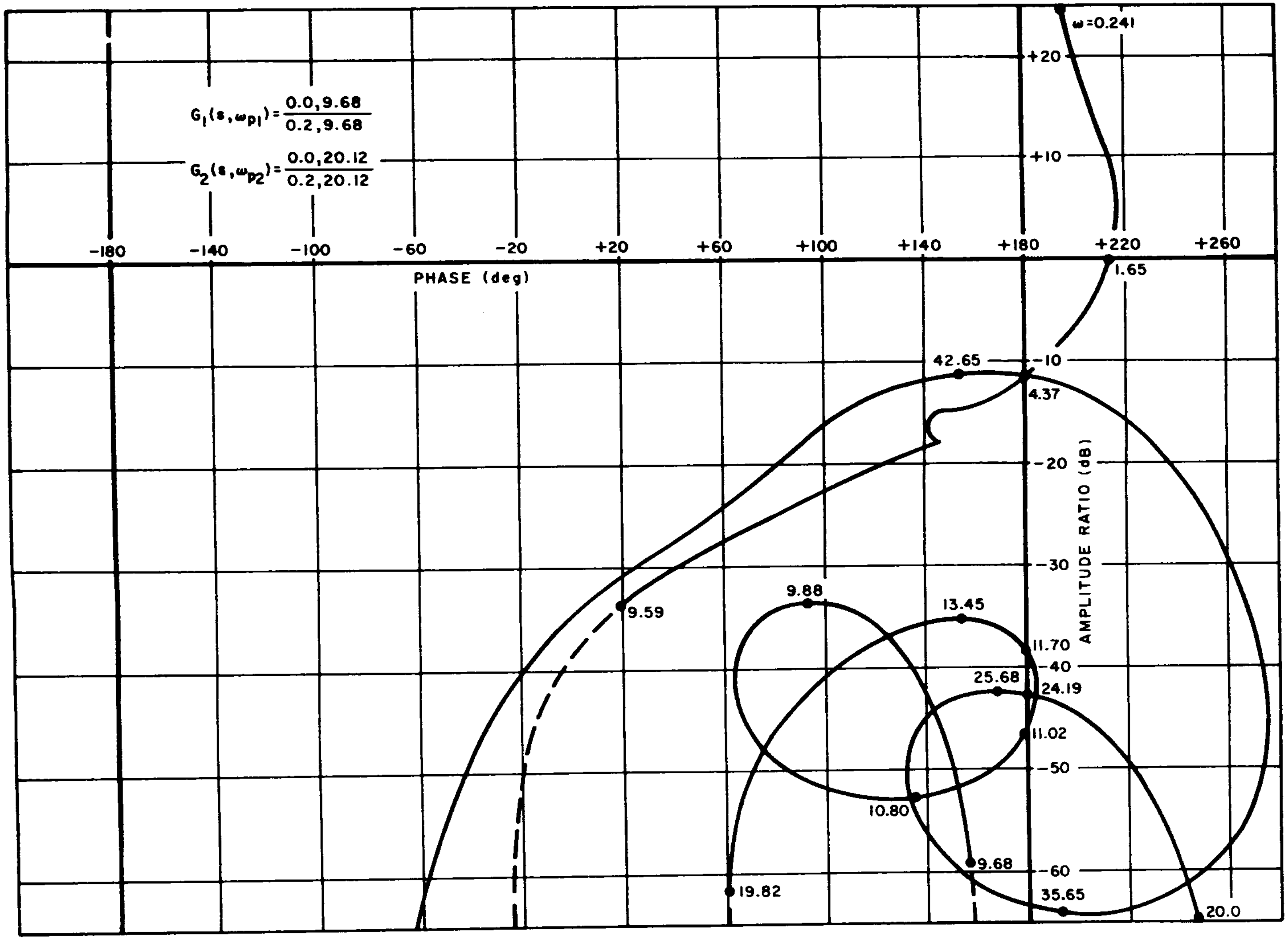

Figure 56. Gain-Phase Plot, Gain Stabilization, Propellant Slosh Included, T = 140 Seconds

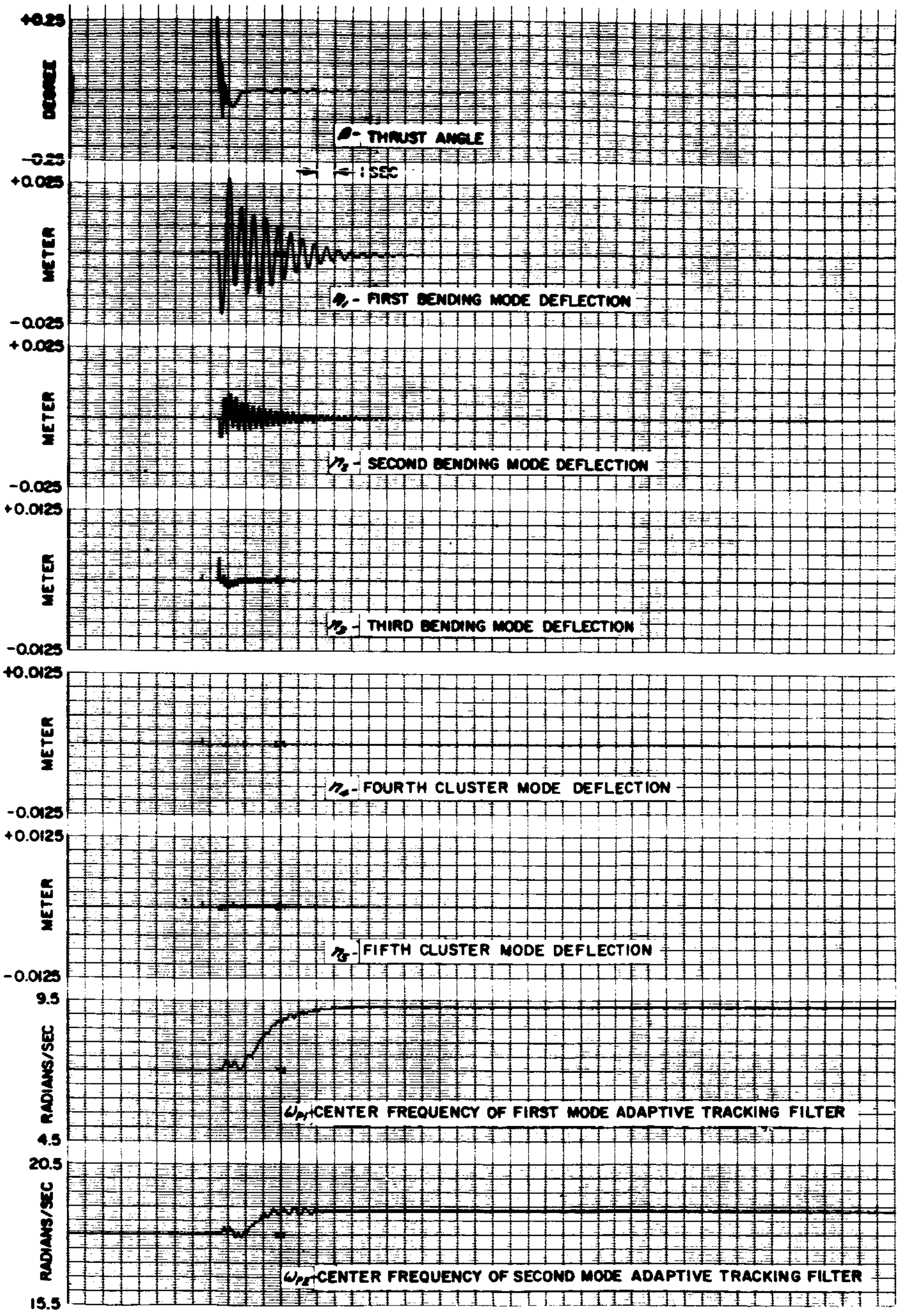

Figure 57. S-IB-201 Bending Mode Response to Actuator Pulse Disturbance, First and Second Mode Adaptive Tracking Filters in Phase Stabilization Configuration, T = 80 Seconds

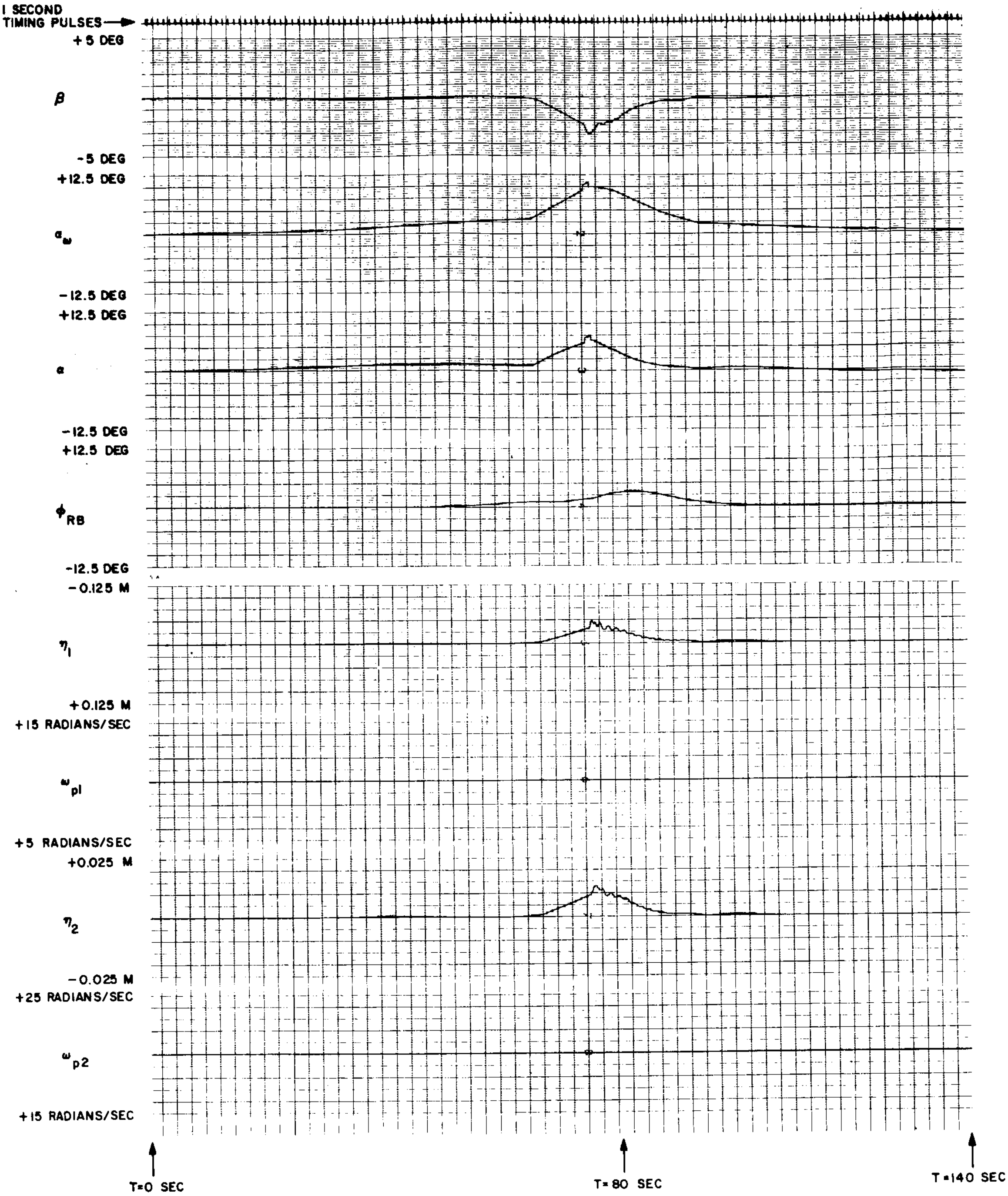

Figure 58A. S-IB-201 Launch Trajectory, Phase Stabilization, Nominal Bending Parameters, Filters Not Tracking

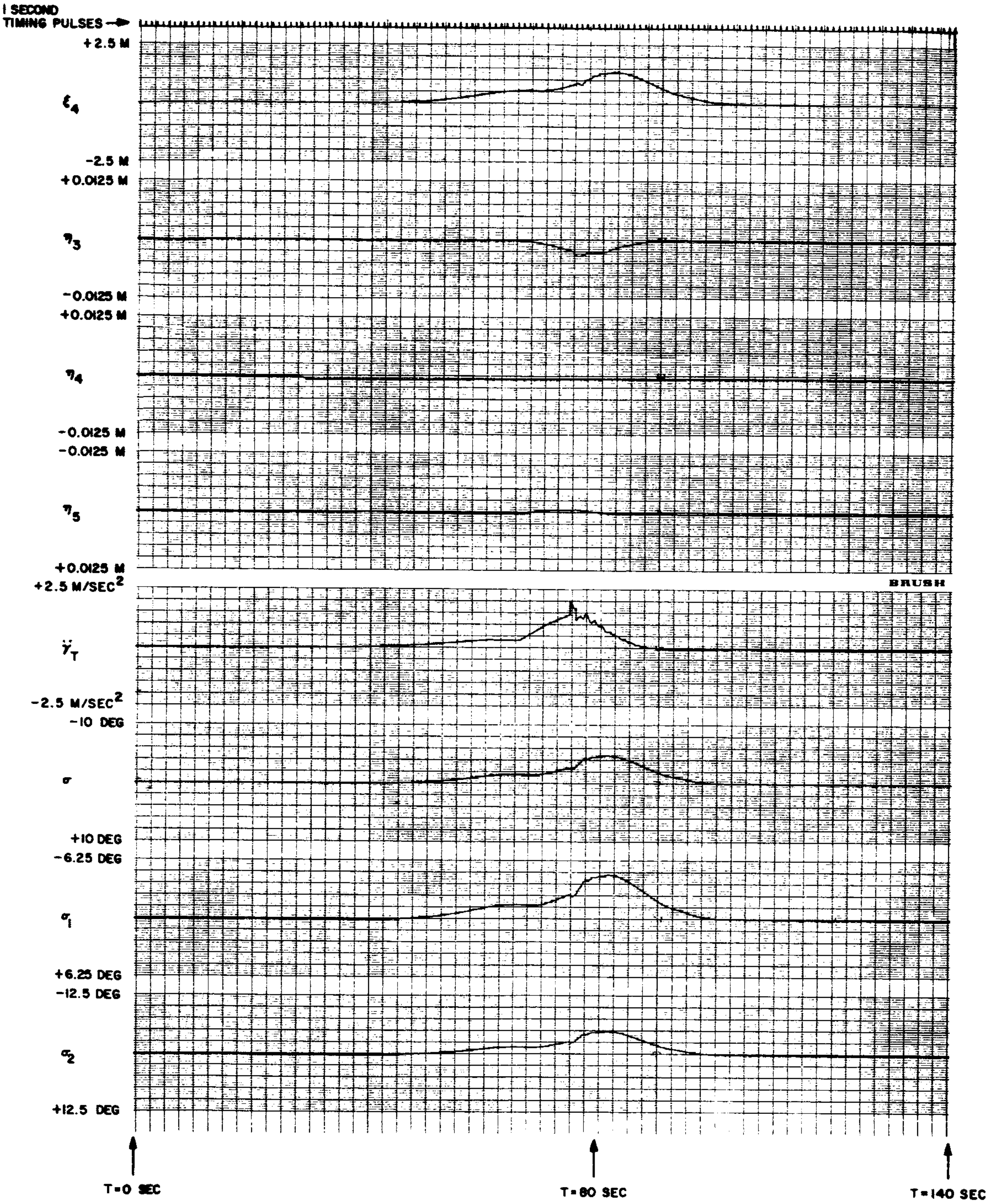

Figure 58B. S-IB-201 Launch Trajectory, Phase Stabilization, Nominal Bending Parameters, Filters Not Tracking

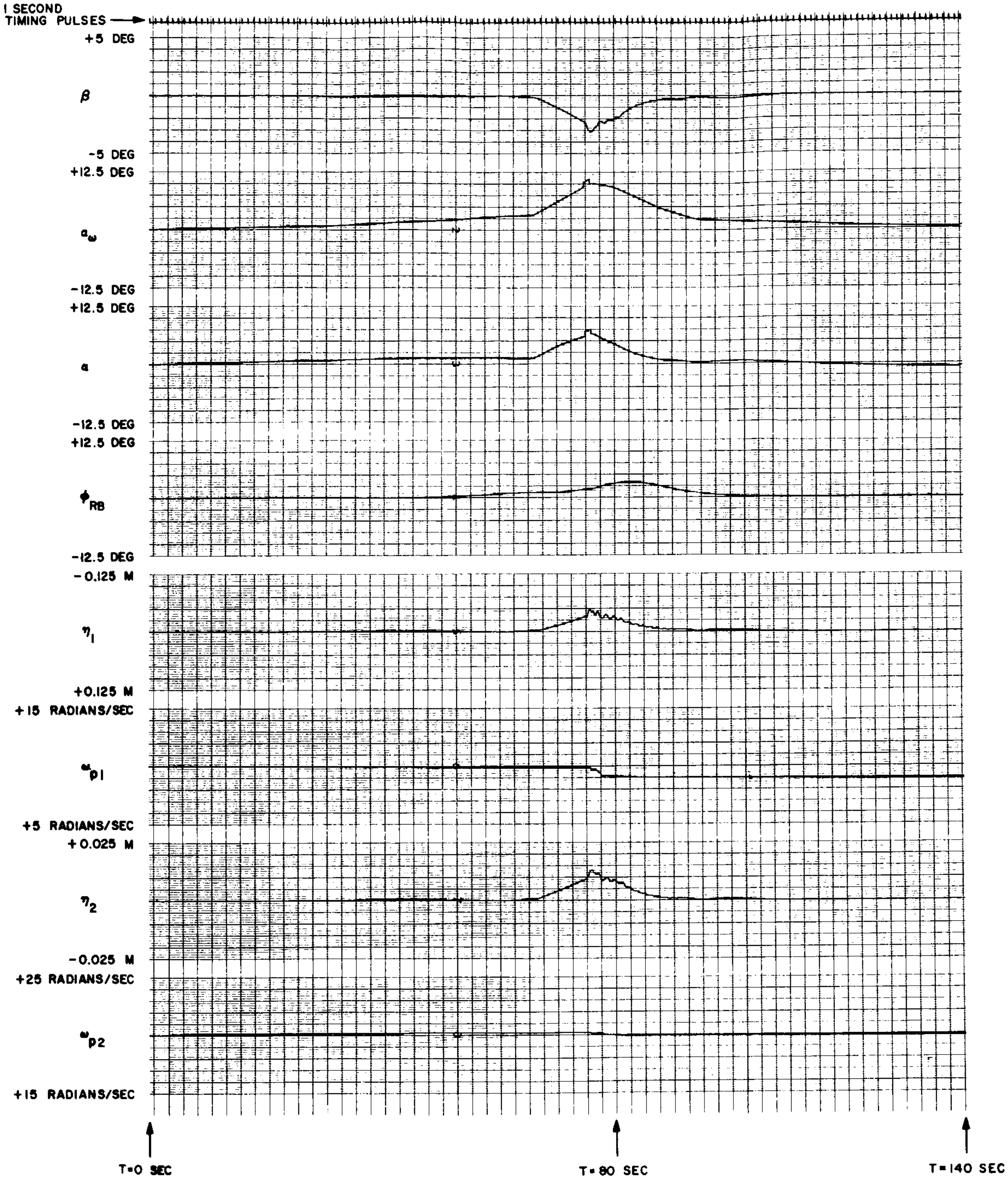

Figure 59A. S-IB-201 Launch Trajectory, Phase Stabilization, Nominal Bending Parameters, Filters Tracking

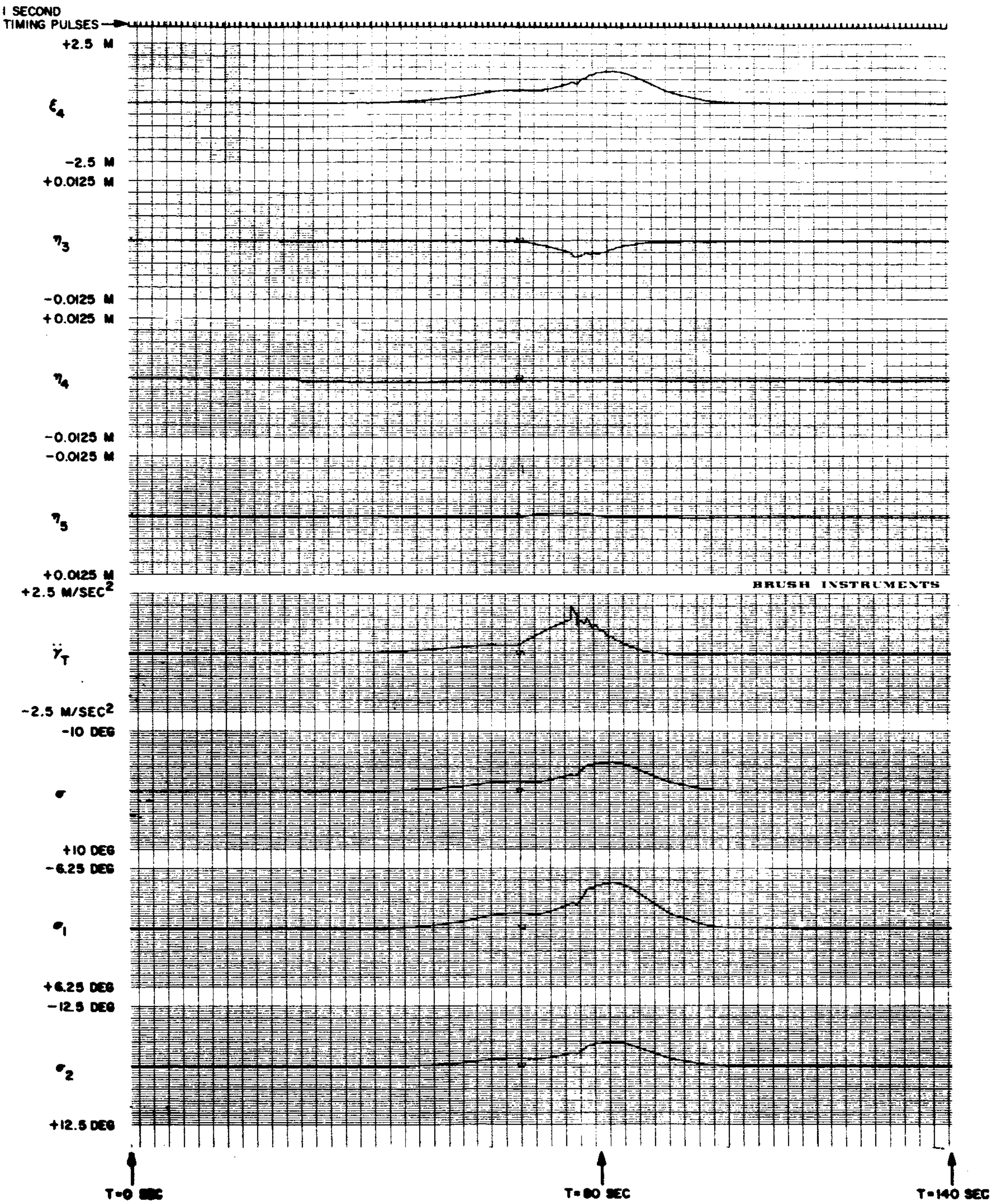

Figure 59B. S-IB-201 Launch Trajectory, Phase Stabilization, Nominal Bending Parameters, Filters Tracking

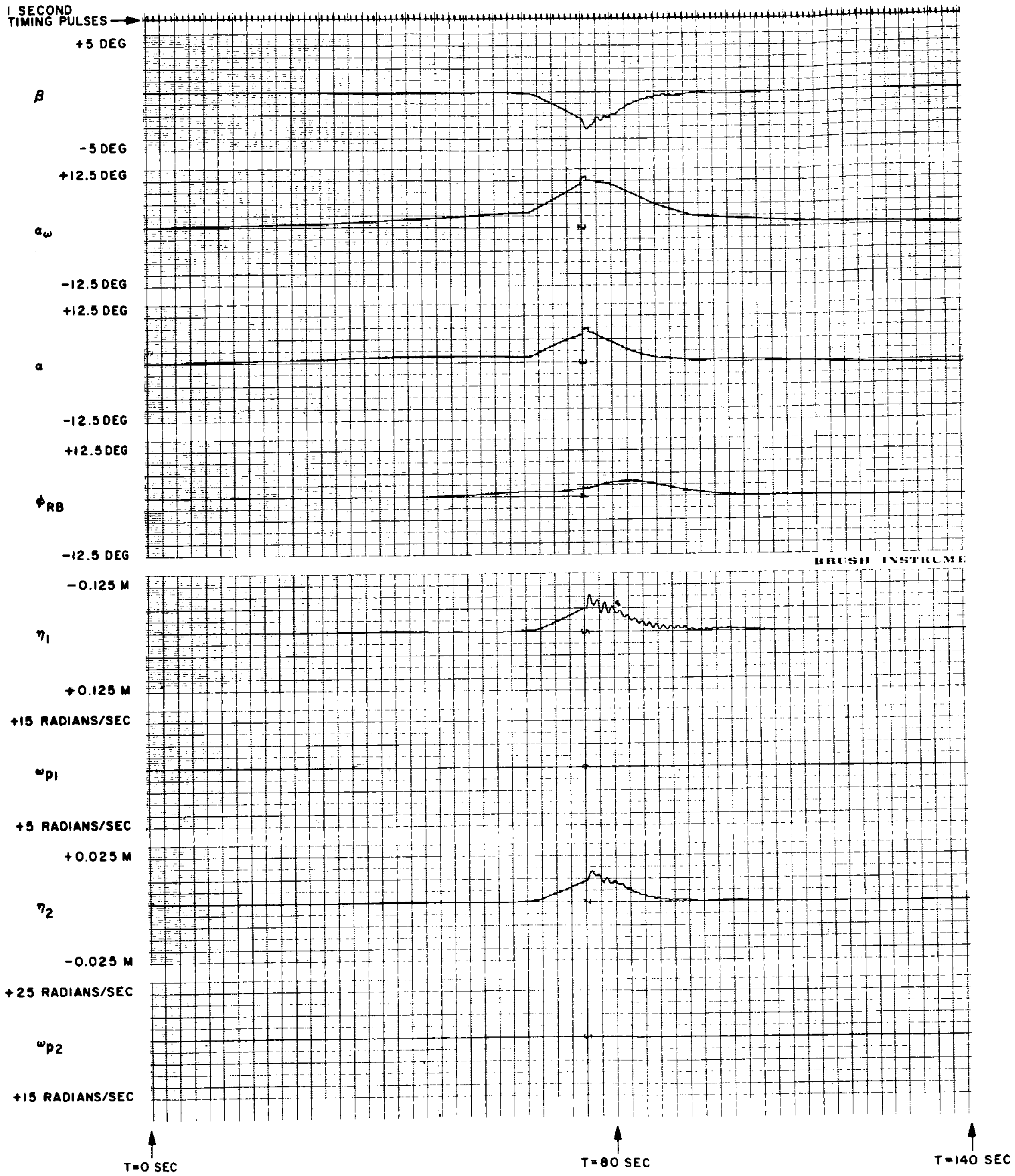

Figure 60A. S-IB-201 Launch Trajectory, Phase Stabilization, First Mode Frequency Reduced 20 Percent, Filters Not Tracking

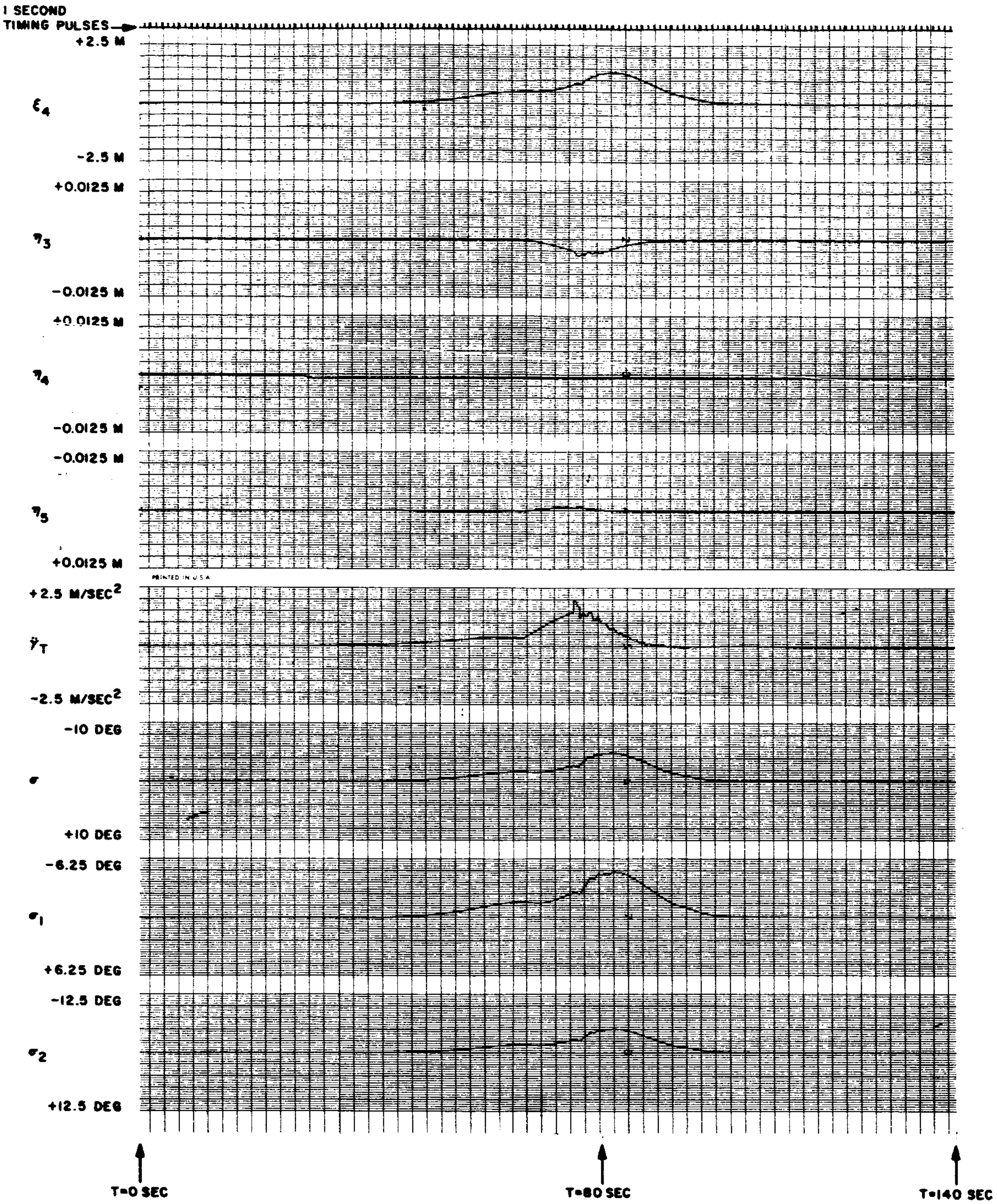

Figure 60B. S-IB-201 Launch Trajectory, Phase Stabilization, First Mode Frequency Reduced 20 Percent, Filters Not Tracking

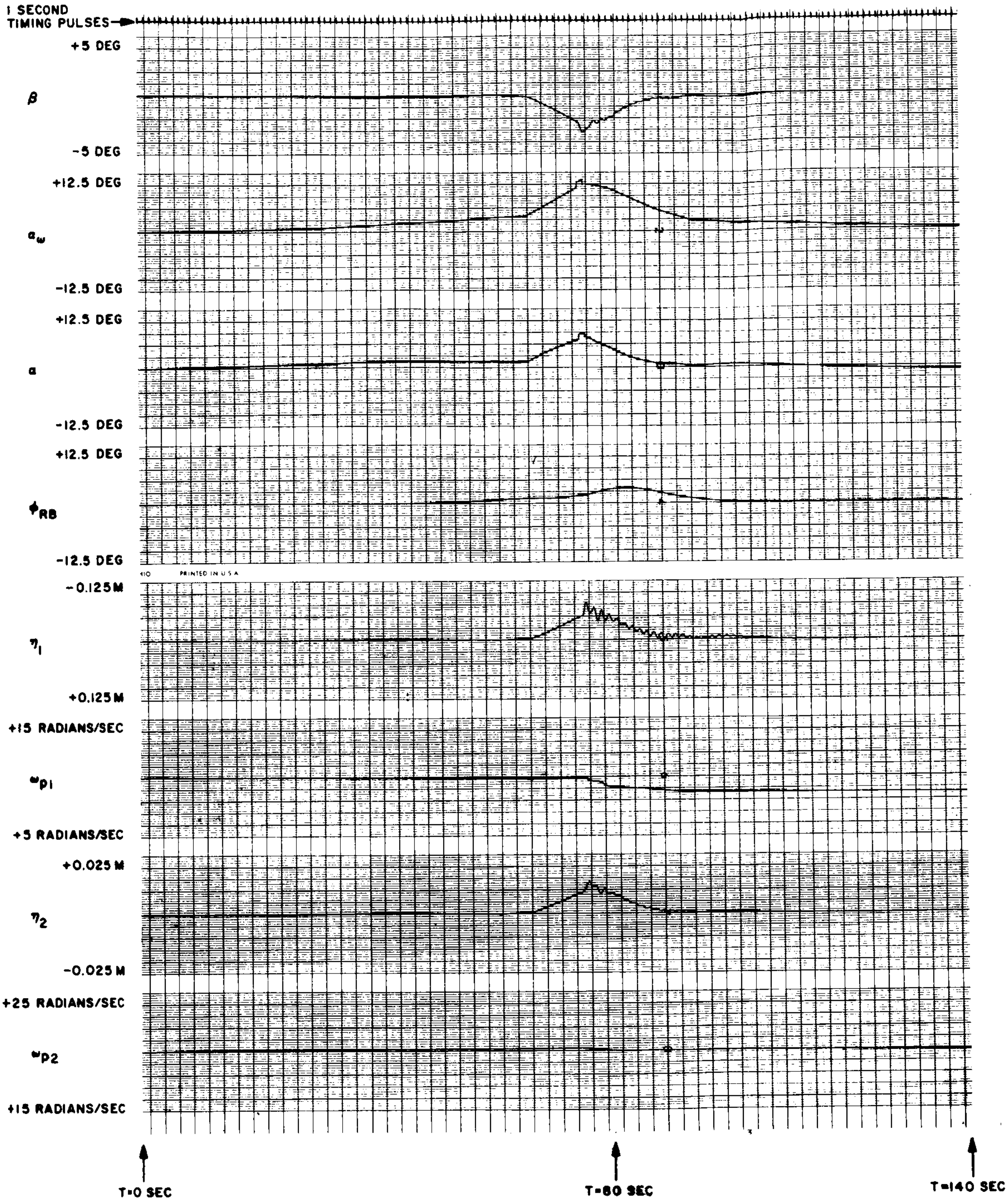

Figure 61A. S-IB-201 Launch Trajectory, Phase Stabilization, First Mode Frequency Reduced 20 Percent, Filters Tracking

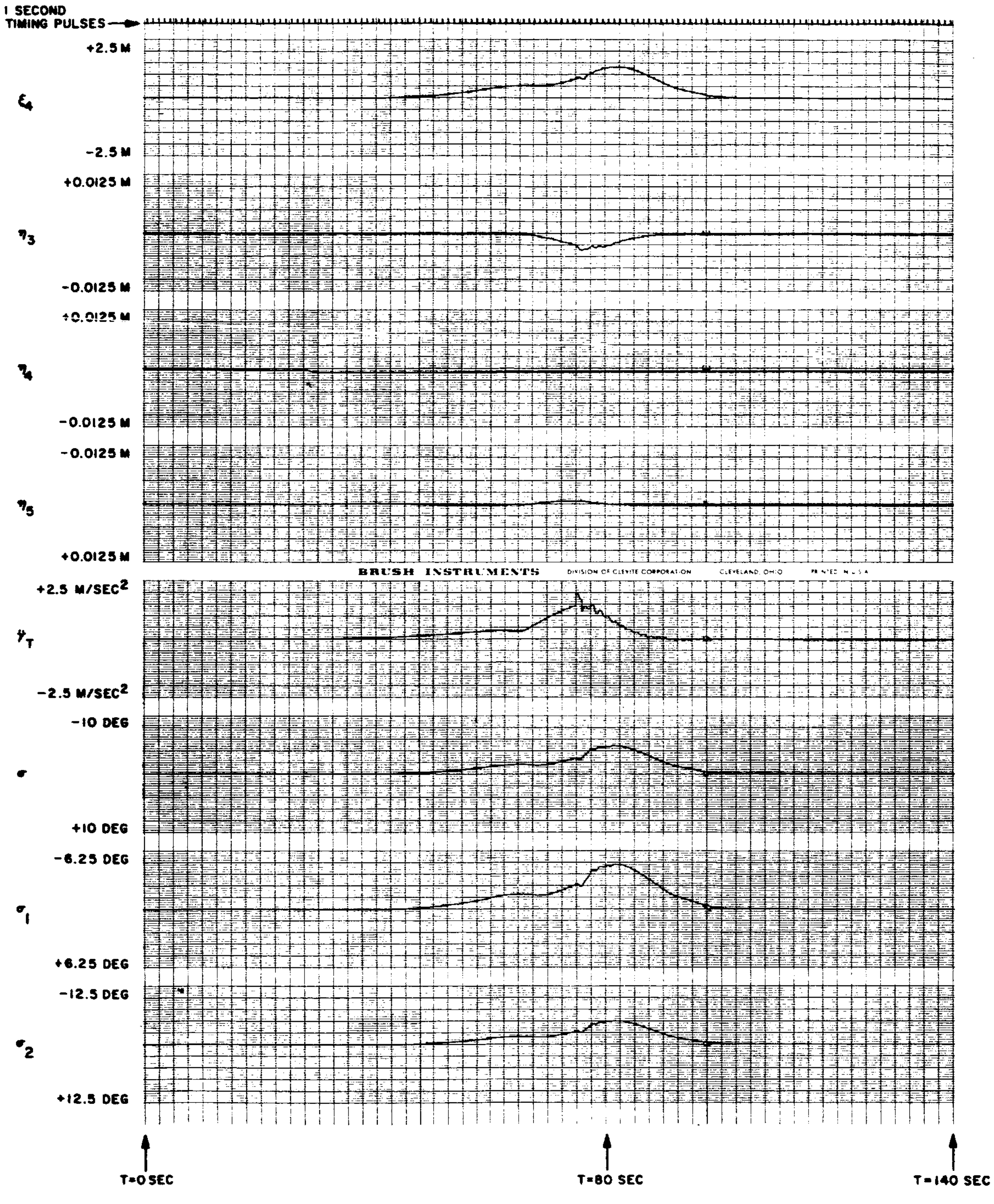

Figure 61B. S-IB-201 Launch Trajectory, Phase Stabilization, First Mode Frequency Reduced 20 Percent, Filters Tracking

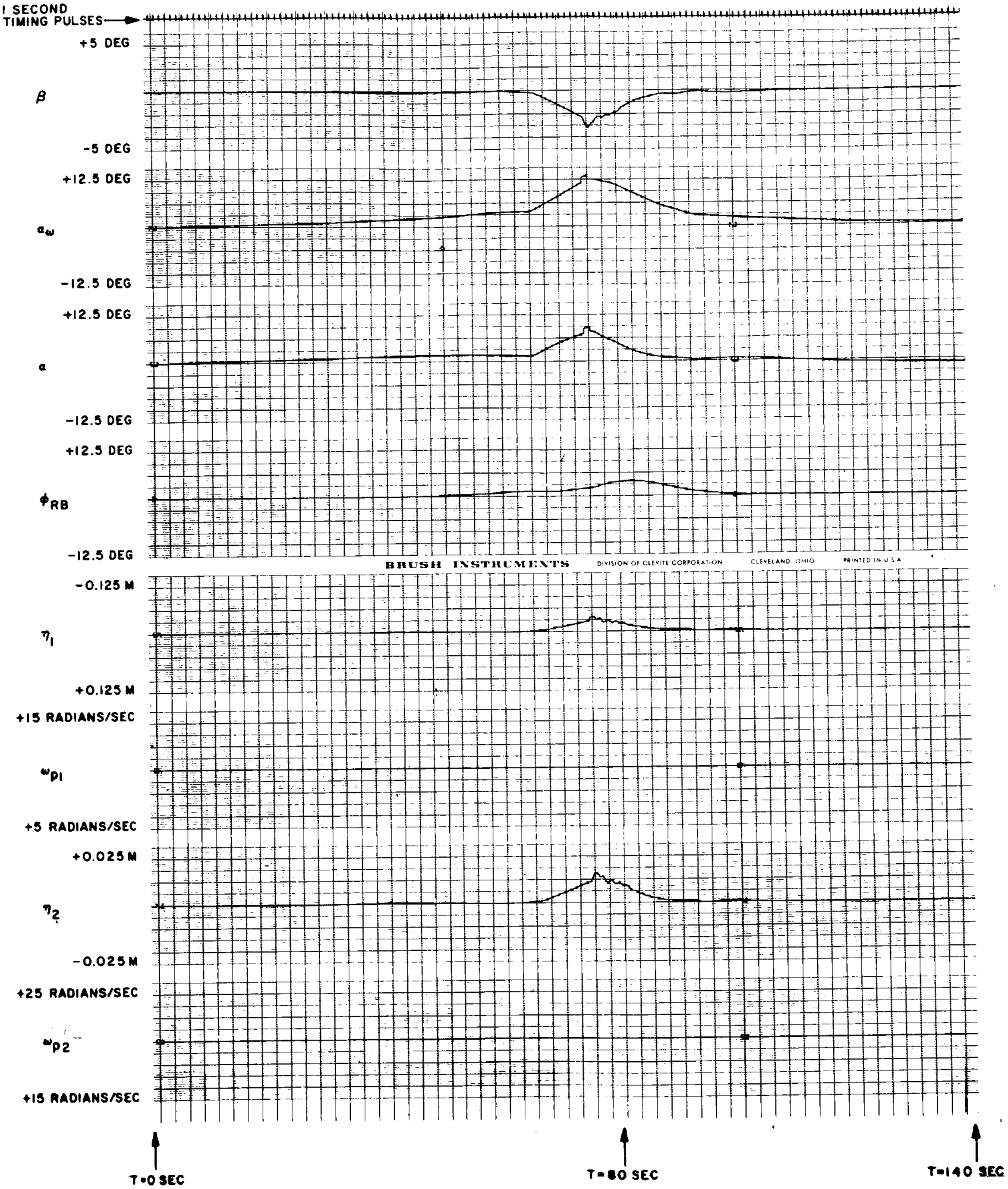

Figure 62A. S-IB-201 Launch Trajectory, Phase Stabilization, First Mode Frequency Increased 20 Percent, Filters Not Tracking

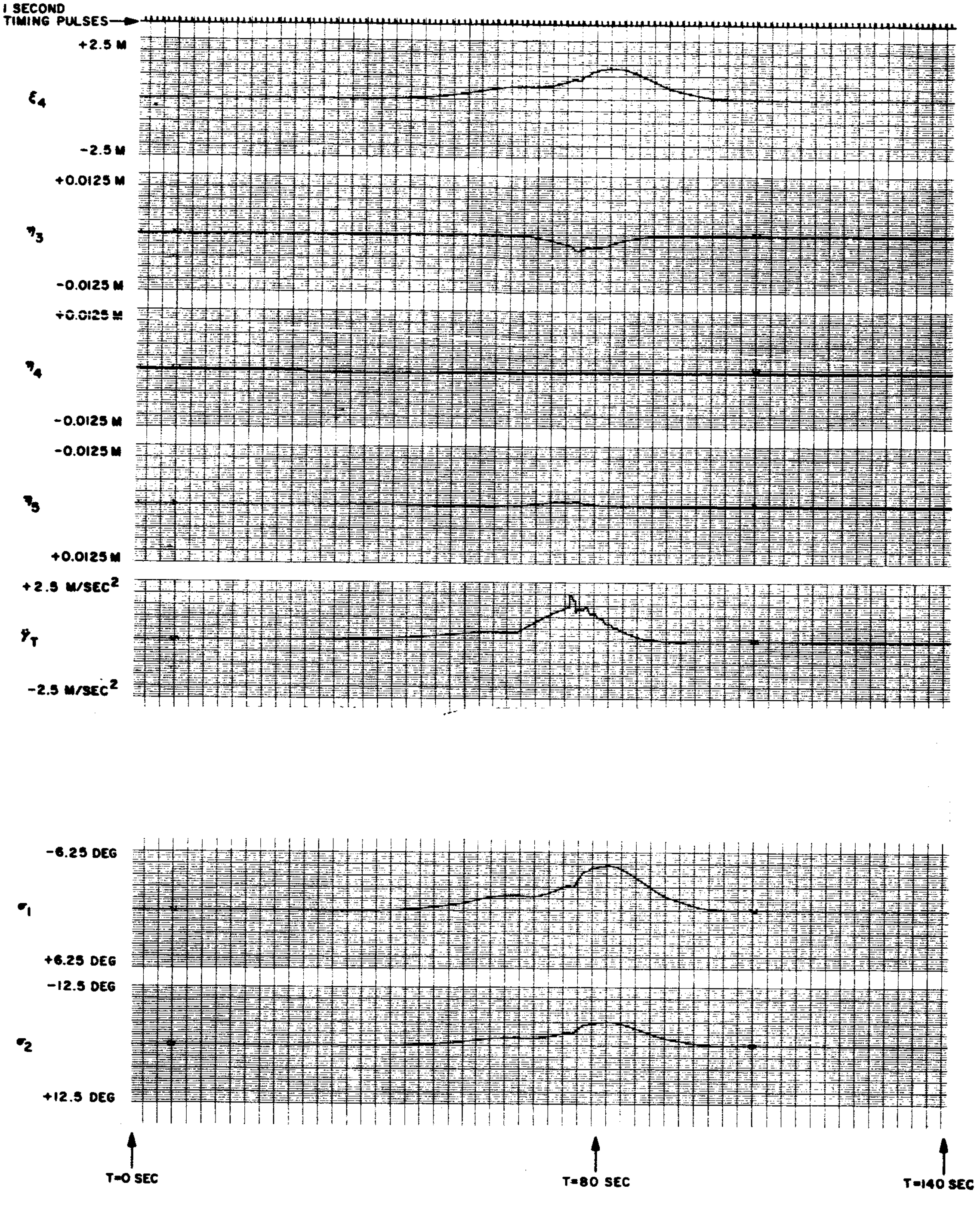

Figure 62B. S-IB-201 Launch Trajectory, Phase Stabilization, First Mode Frequency Increased 20 Percent, Filters Not Tracking

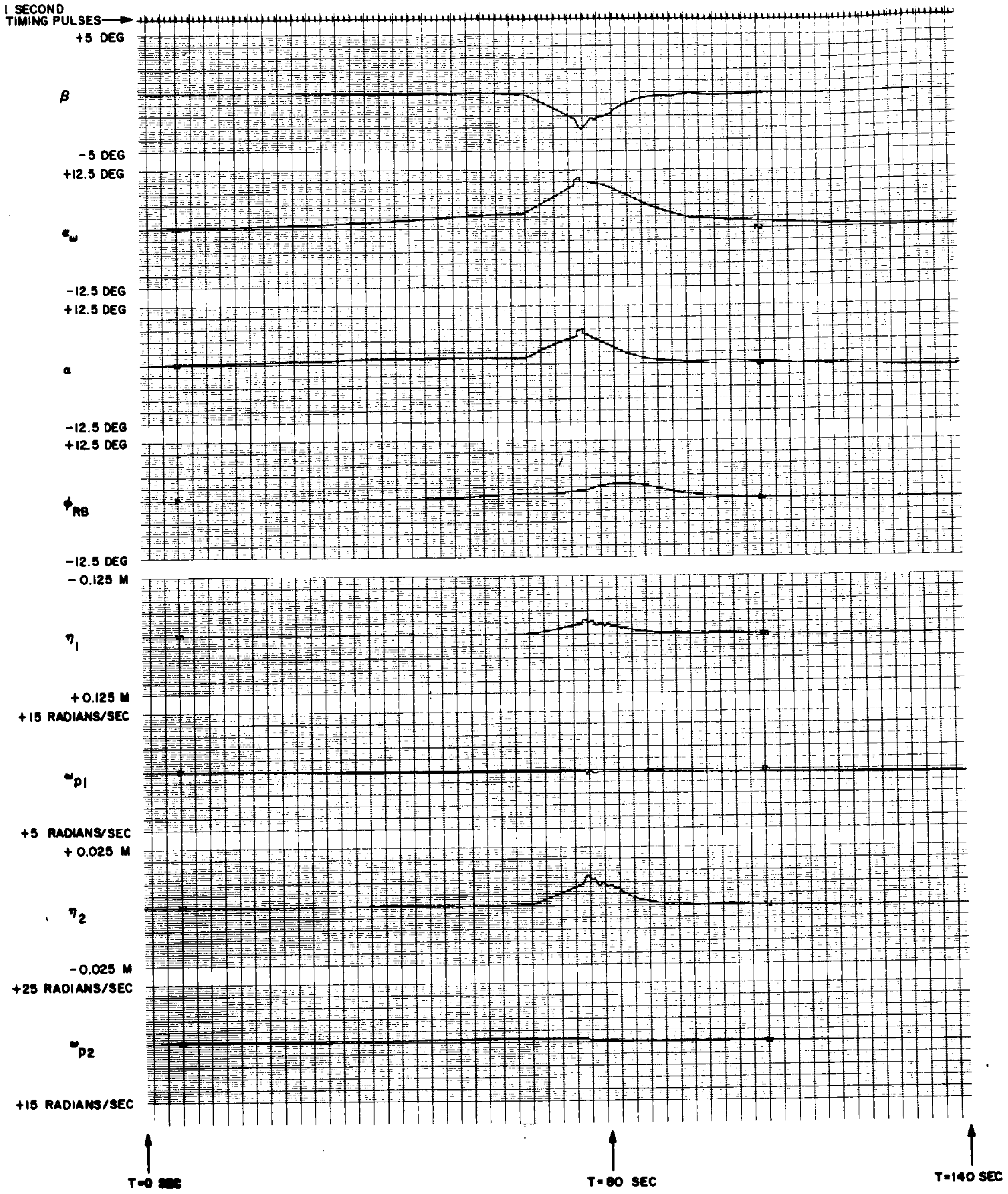

Figure 63A. S-IB-201 Launch Trajectory, Phase Stabilization, First Mode Frequency Increased 20 Percent, Filters Tracking

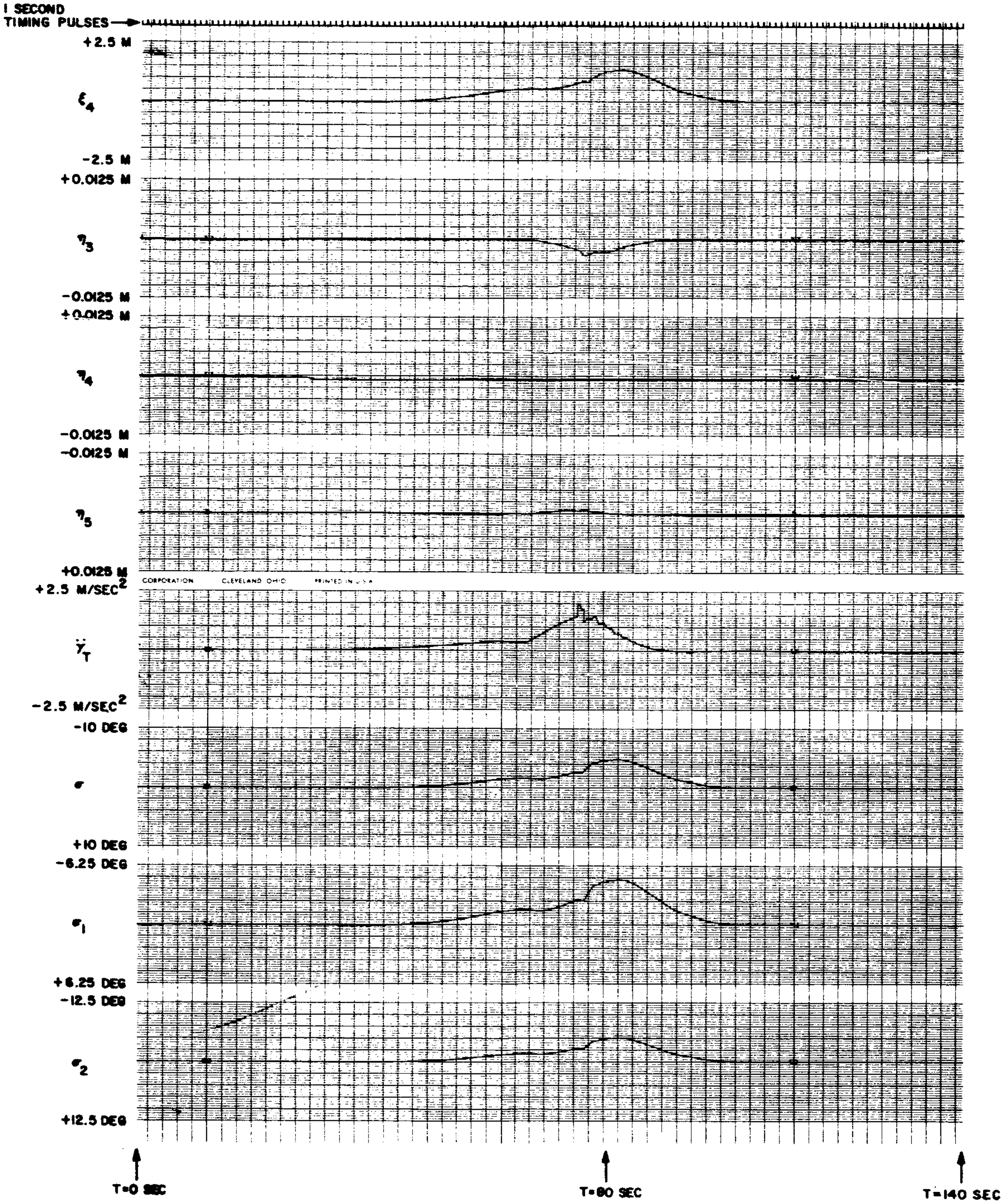

Figure 63B. S-IB-201 Launch Trajectory, Phase Stabilization, First Mode Frequency Increased 20 Percent, Filters Tracking

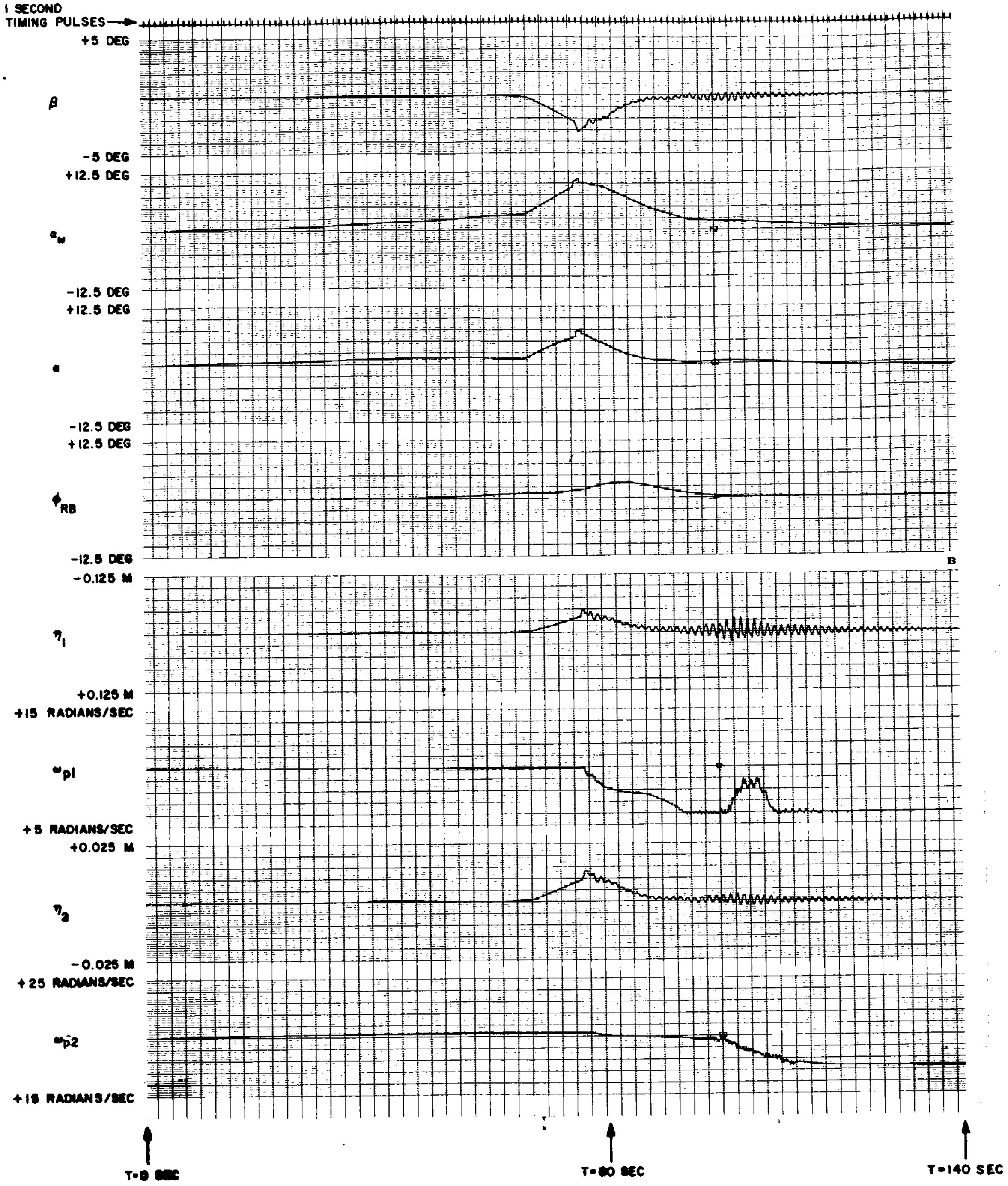

Figure 64A. S-IB-201 Launch Trajectory, Phase Stabilization, First Mode Slope Increased 6 dB, Filters Tracking

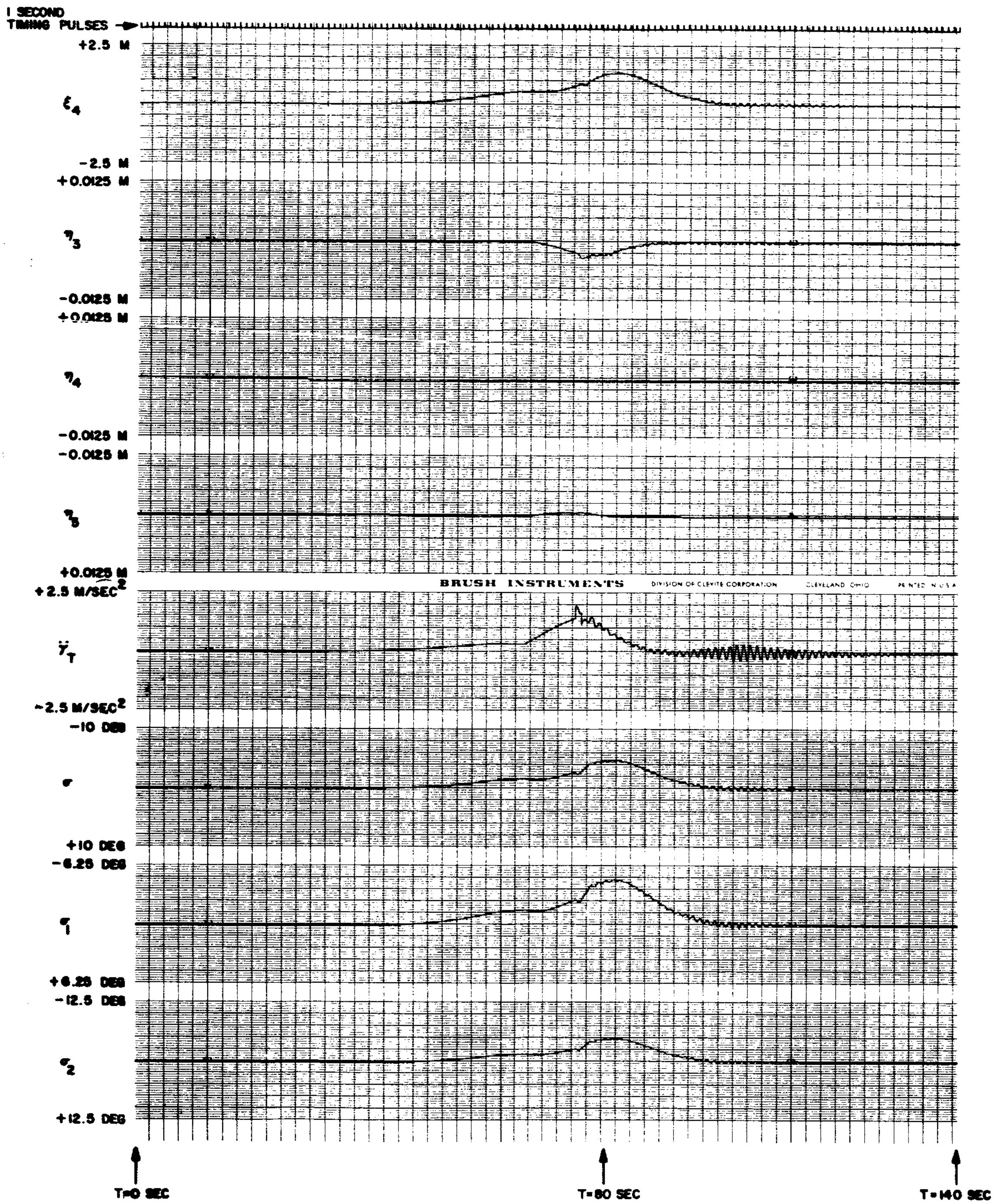

Figure 64B. S-IB-201 Launch Trajectory, Phase Stabilization, First Mode Slope Increased 6 dB, Filters Tracking

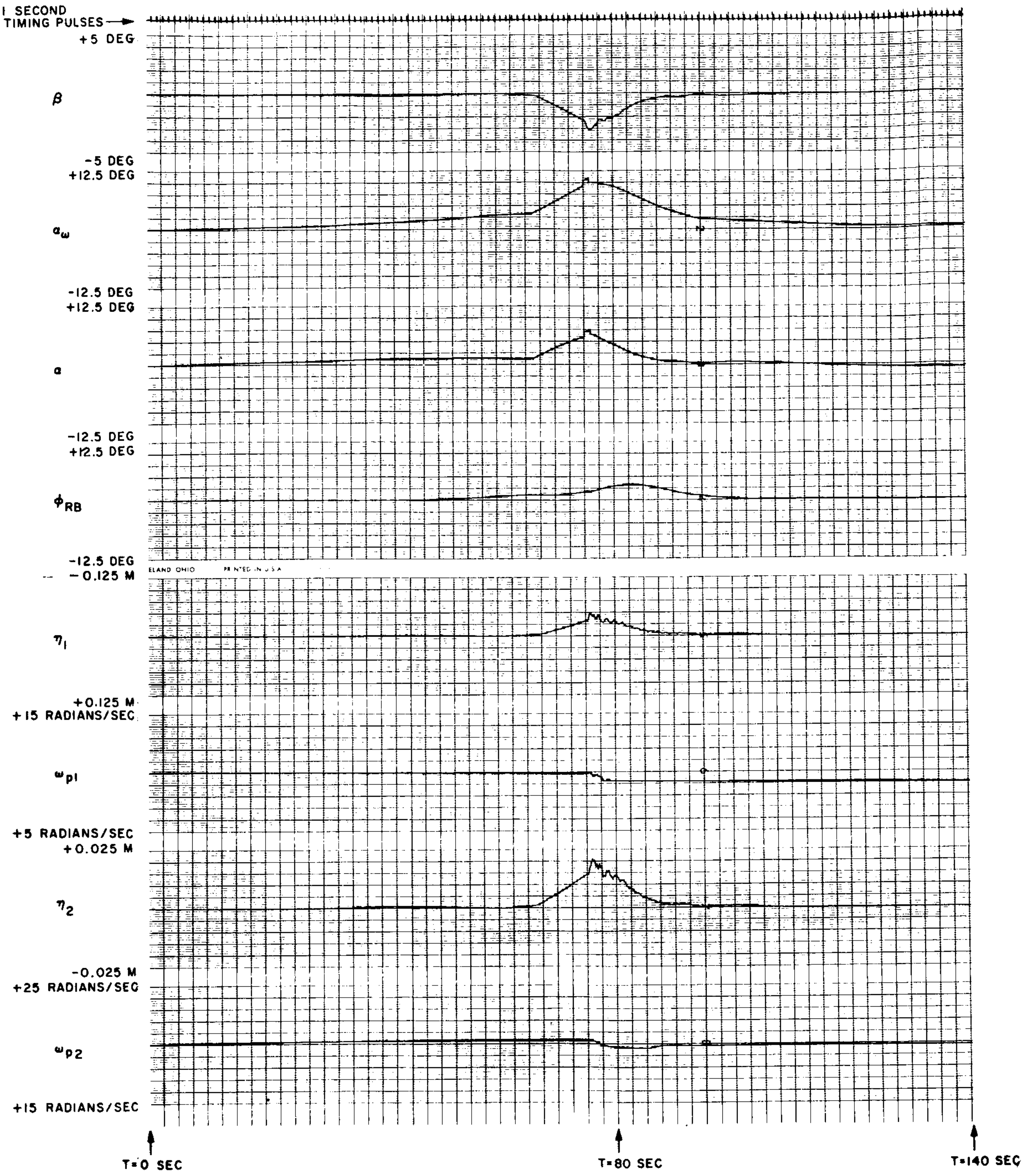

Figure 65A. S-IB-201 Launch Trajectory, Phase Stabilization, Second Mode Frequency Reduced 20 Percent, Filters Tracking

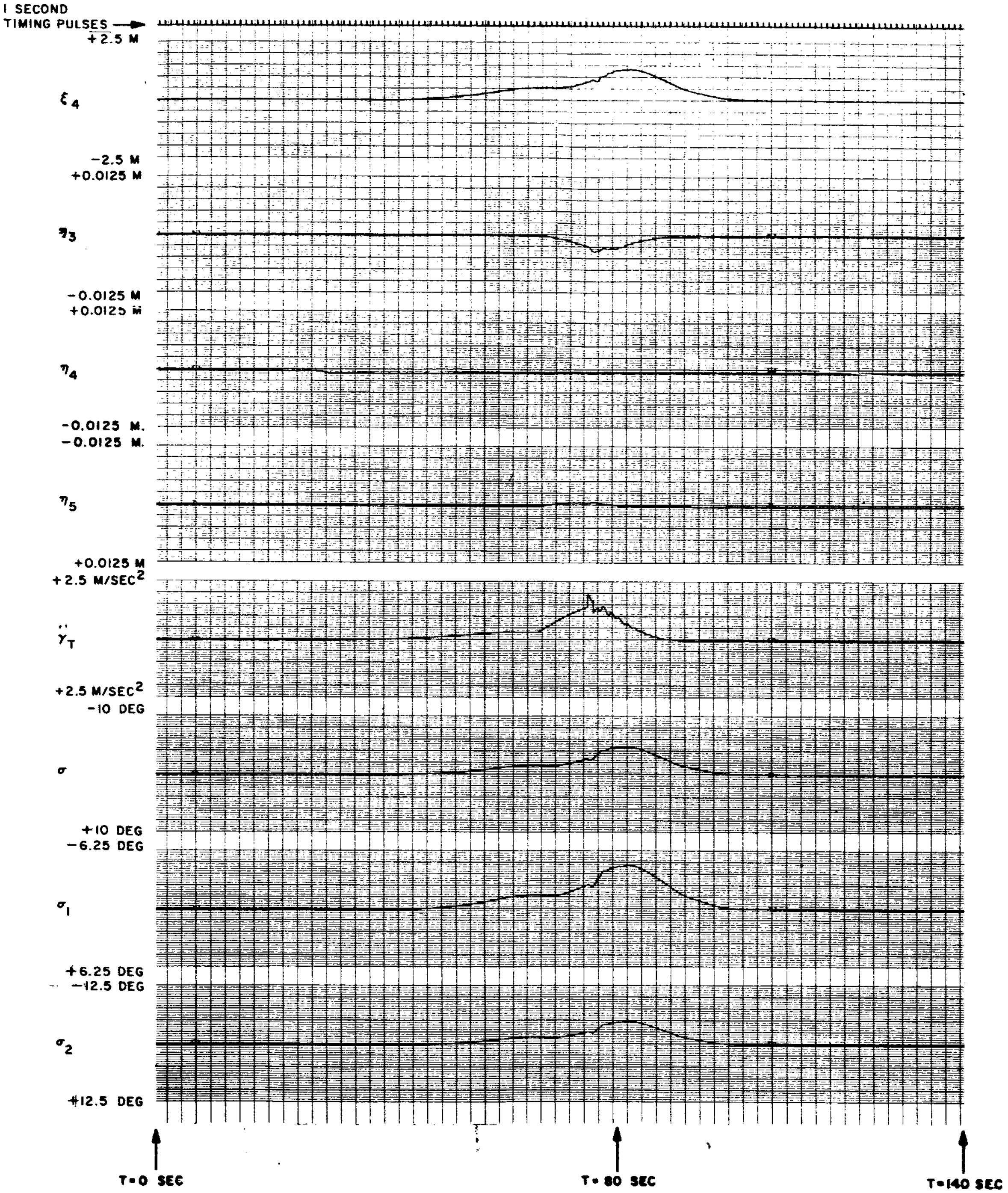

Figure 65B. S-IB-201 Launch Trajectory, Phase Stabilization, Second Mode Frequency Reduced 20 Percent, Filters Tracking

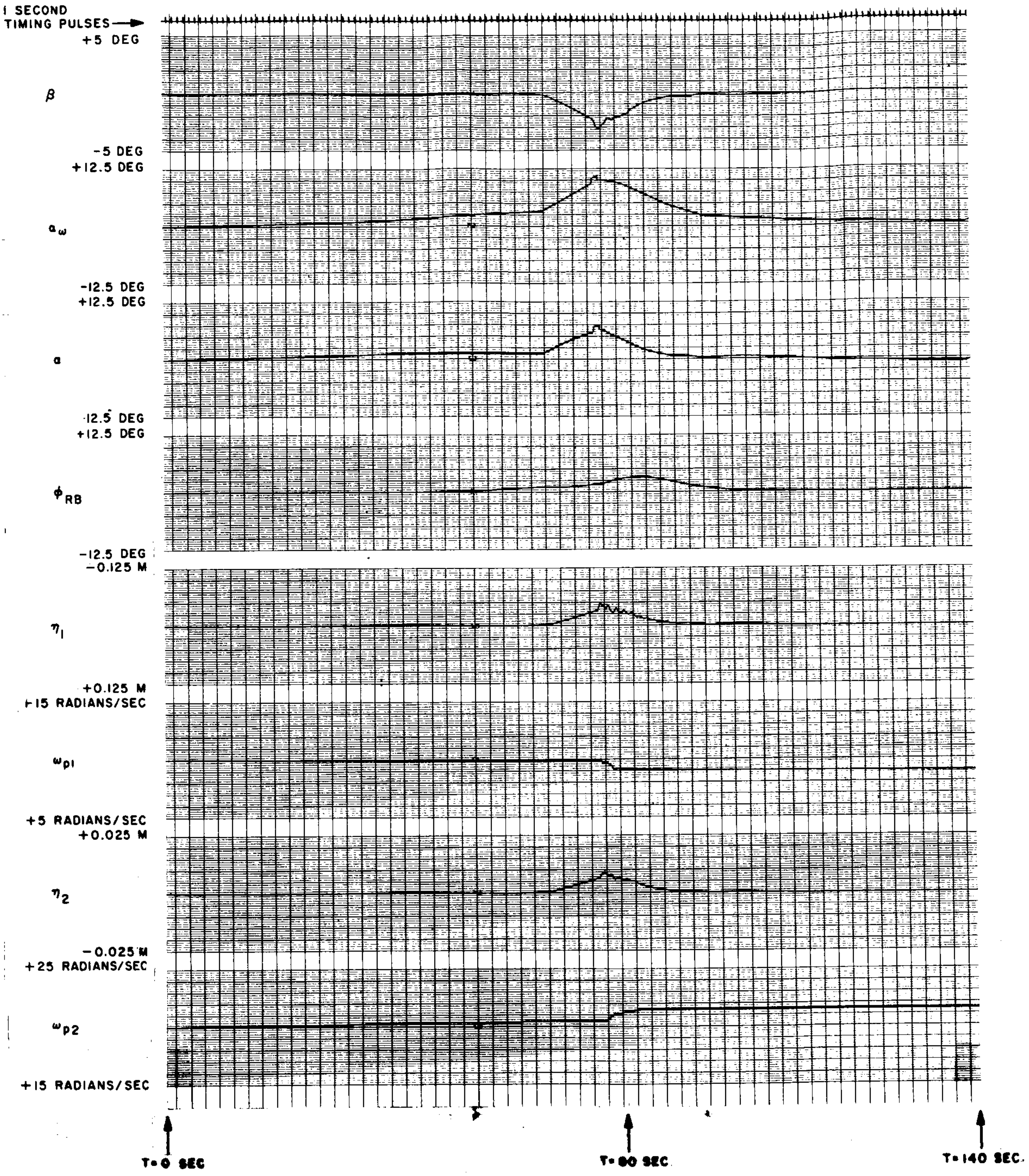

Figure 66A. S-IB-201 Launch Trajectory, Phase Stabilization, Second Mode Frequency Increased 20 Percent, Filters Tracking

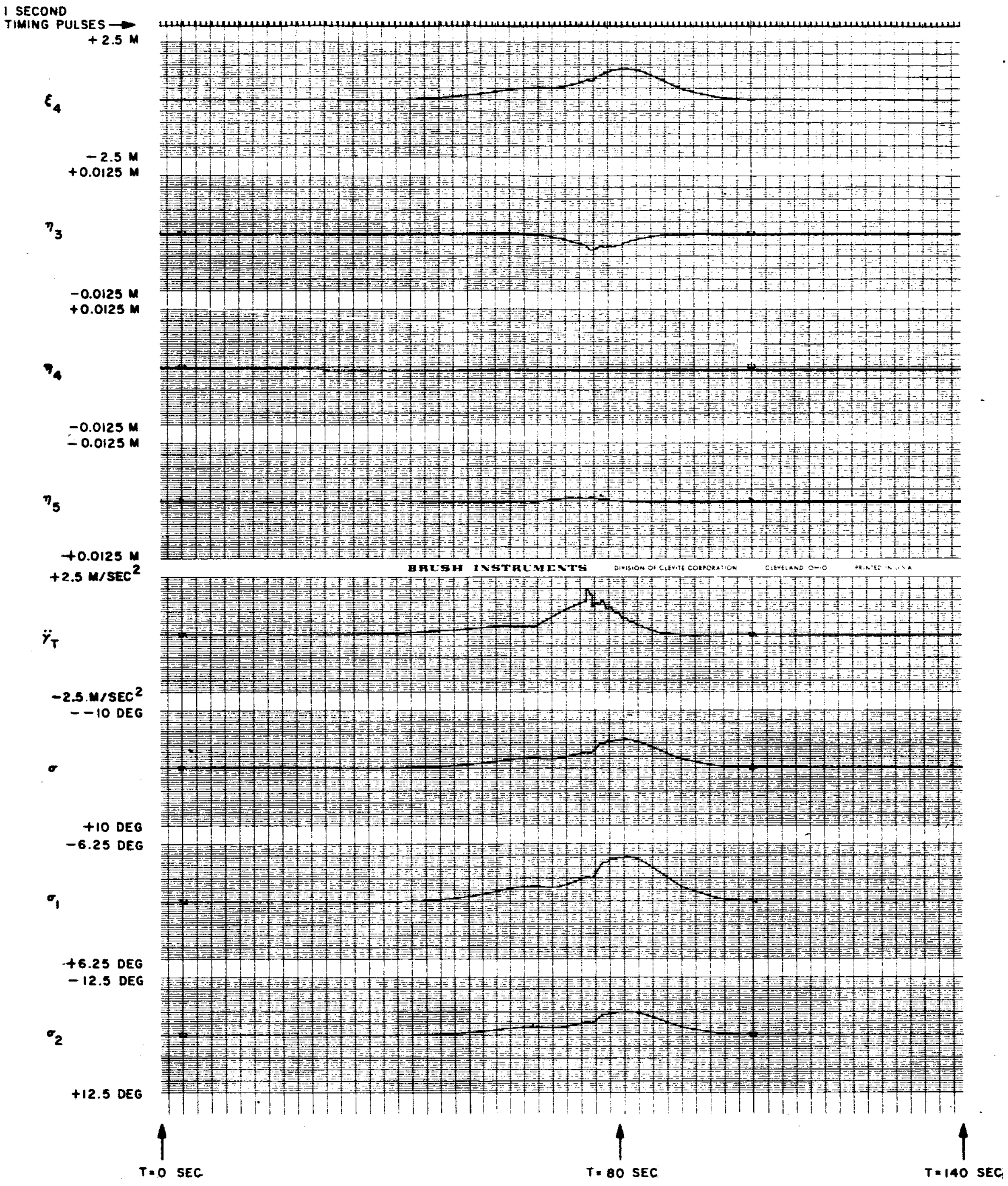

Figure 66B. S-IB-201 Launch Trajectory, Phase Stabilization, Second Mode Frequency Increased 20 Percent, Filters Tracking

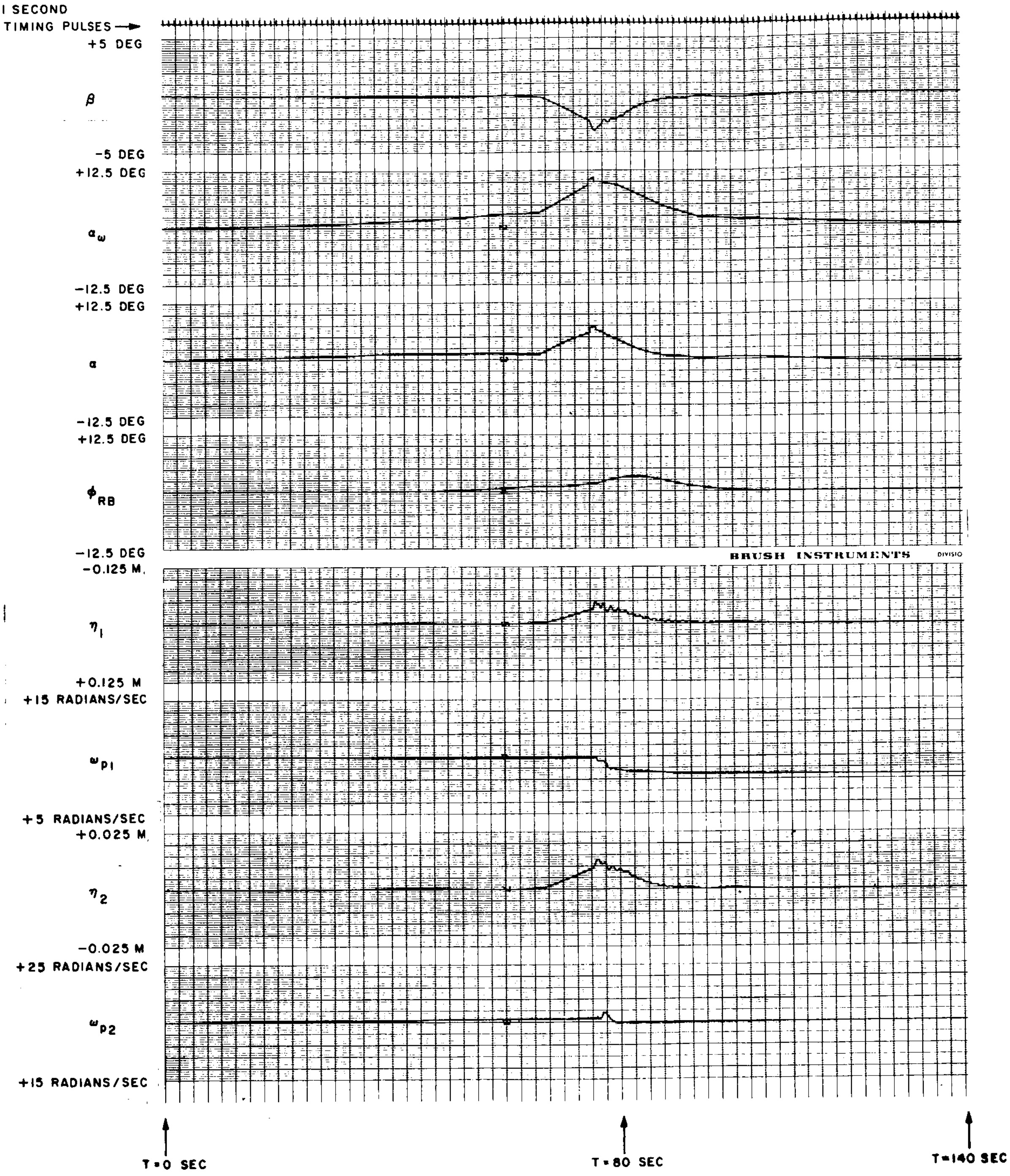

Figure 67A. S-IB-201 Launch Trajectory, Phase Stabilization, Second Mode Slope Increased 12 dB, Filters Tracking

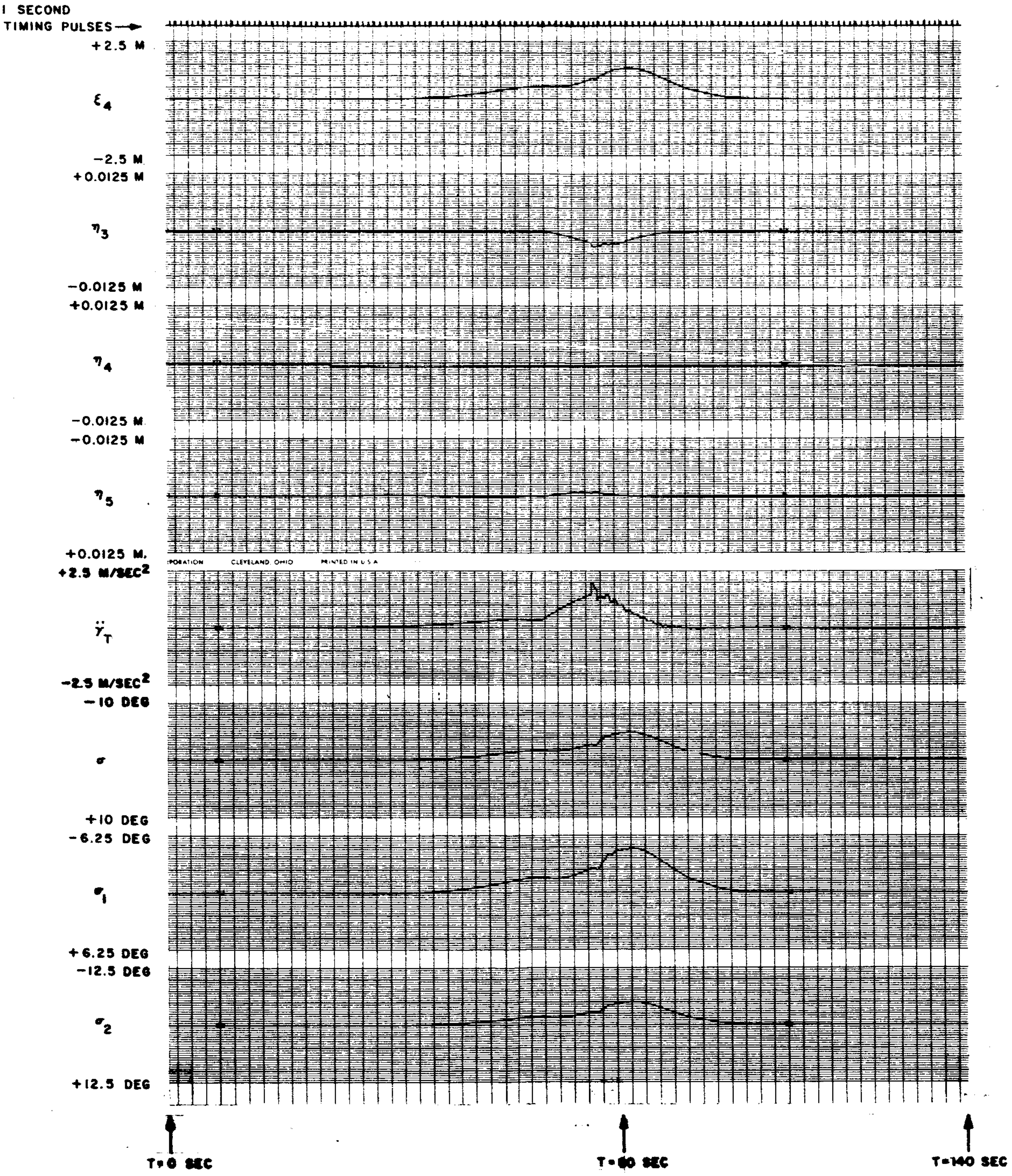

Figure 67B. S-IB-201 Launch Trajectory, Phase Stabilization, Second Mode Slope Increased 12 dB, Filters Tracking

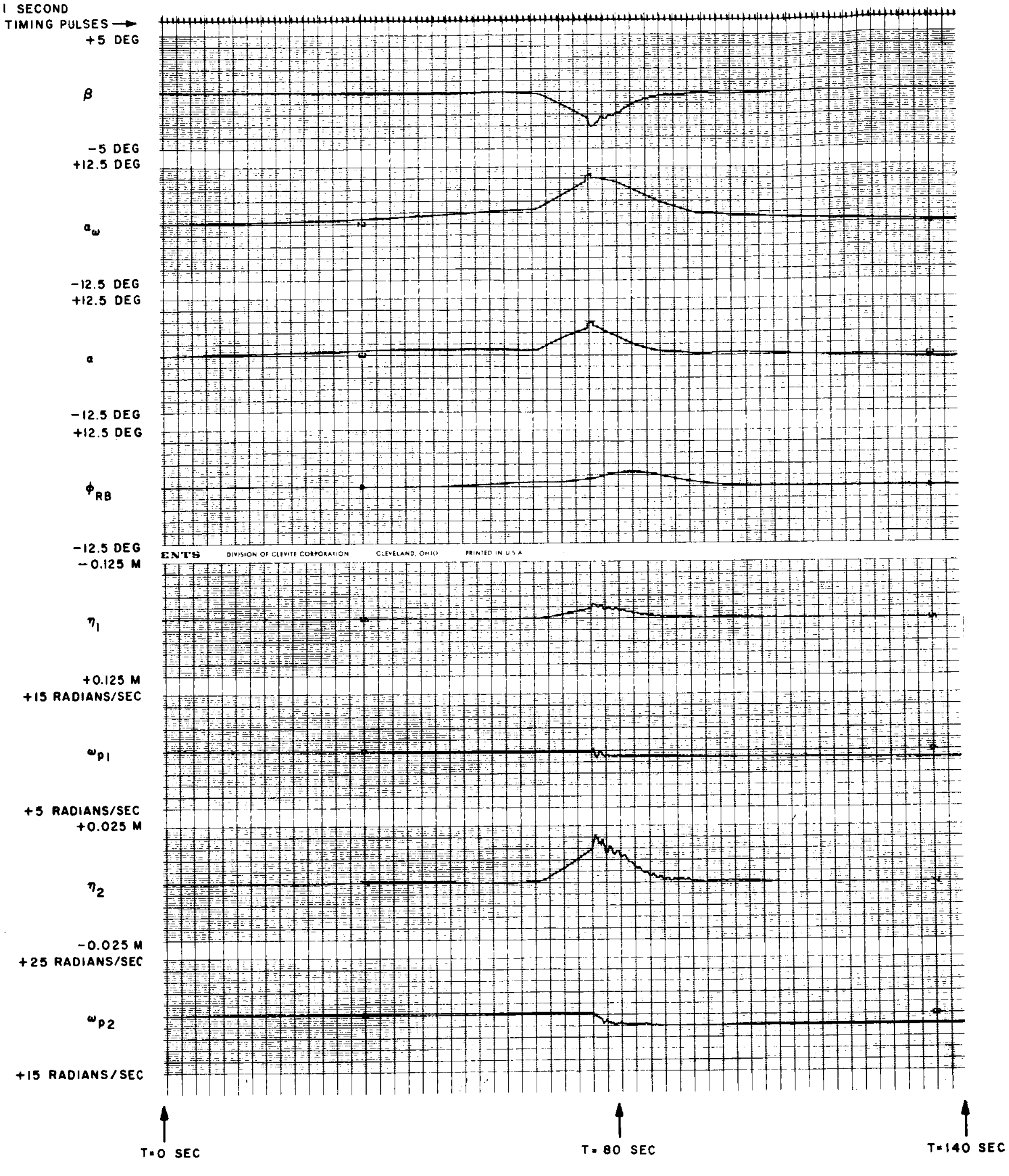

Figure 68A. S-IB-201 Launch Trajectory, Phase Stabilization, First Mode Frequency Increased 20 Percent, Second Mode Frequency Decreased 20 Percent, First and Second Mode Slopes Increased 6 dB, Filters Tracking

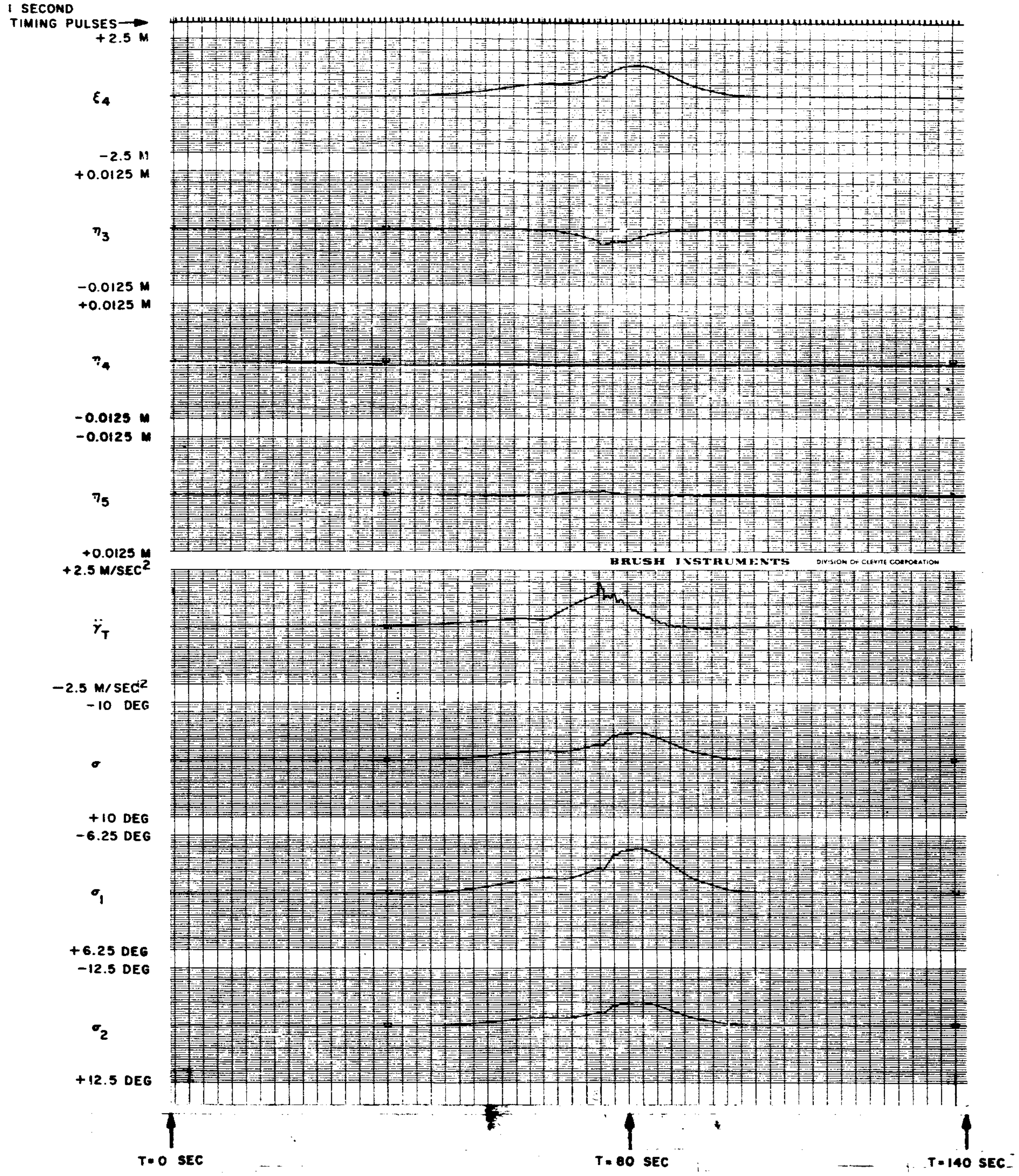

Figure 68B. S-IB-201 Launch Trajectory, Phase Stabilization, First Mode Frequency Increased 20 Percent, Second Mode Frequency Decreased 20 Percent, First and Second Mode Slopes Increased 6 dB, Filters Tracking

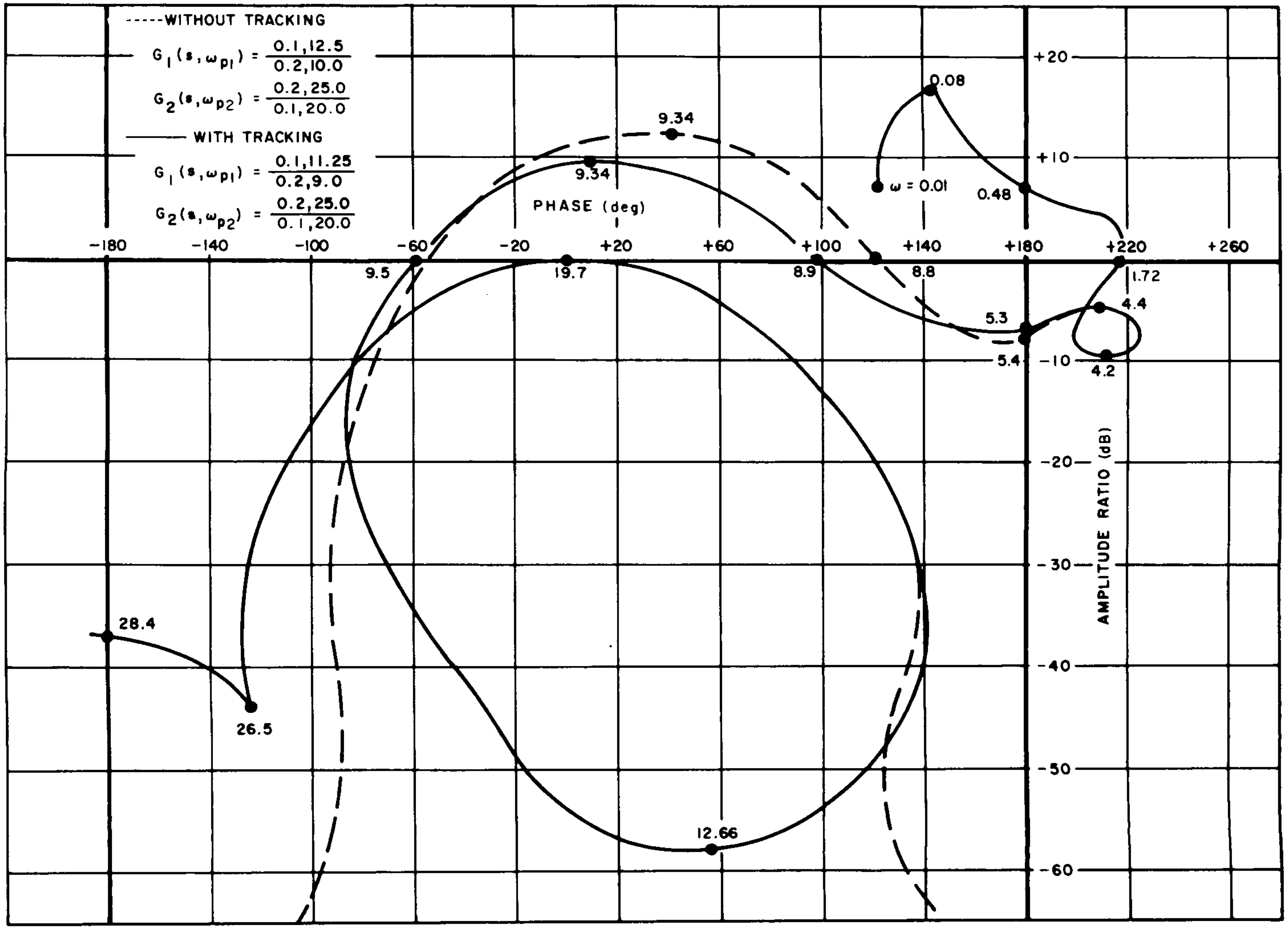

Figure 69. Gain-Phase Plot, Phase Stabilization, With and Without Tracking, Nominal Bending Parameters, T = 80 Seconds

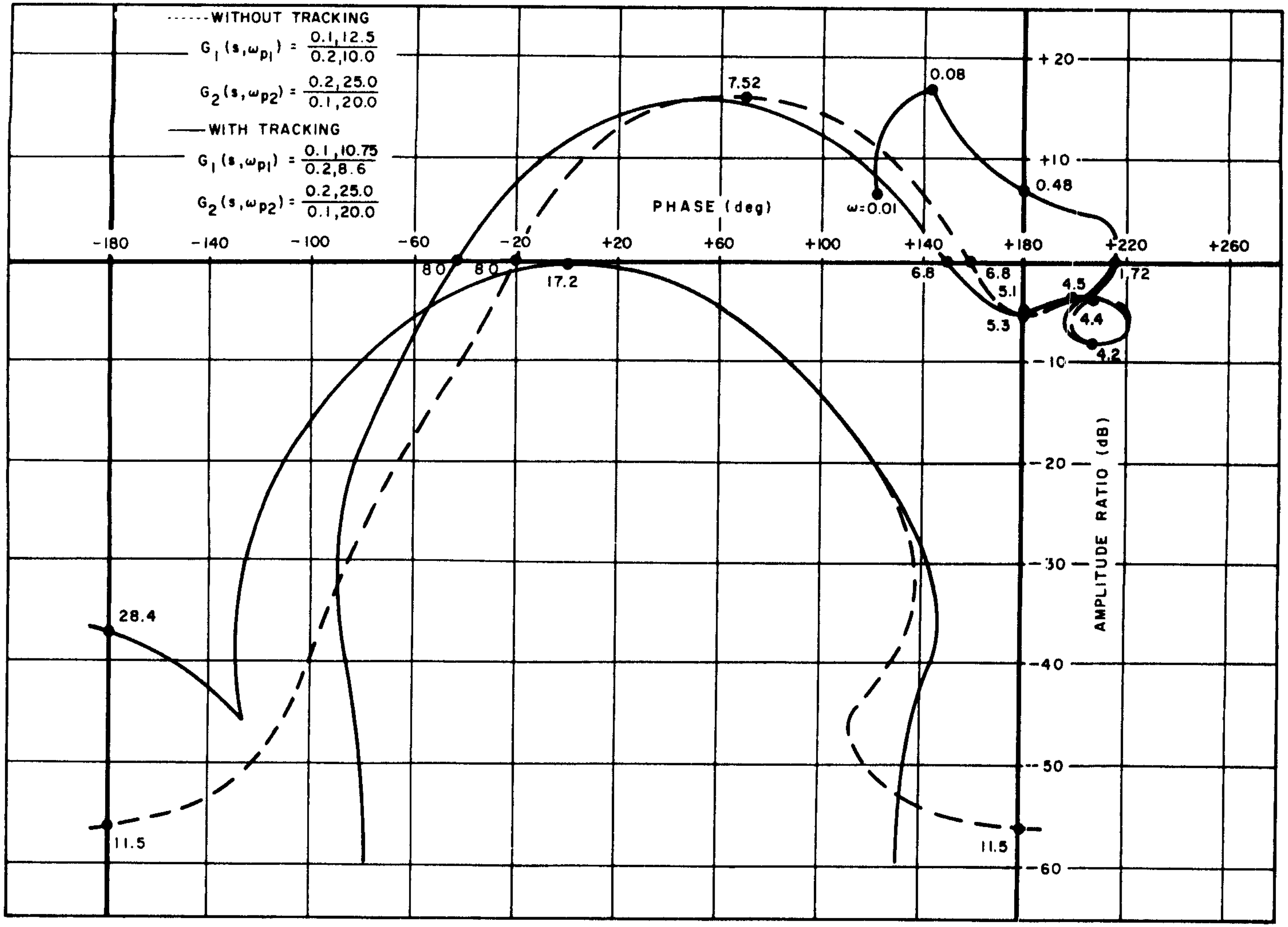

Figure 70. Gain-Phase Plot, Phase Stabilization, With and Without Tracking, First Bending Mode Frequency Reduced 20 Percent, T = 80 Seconds

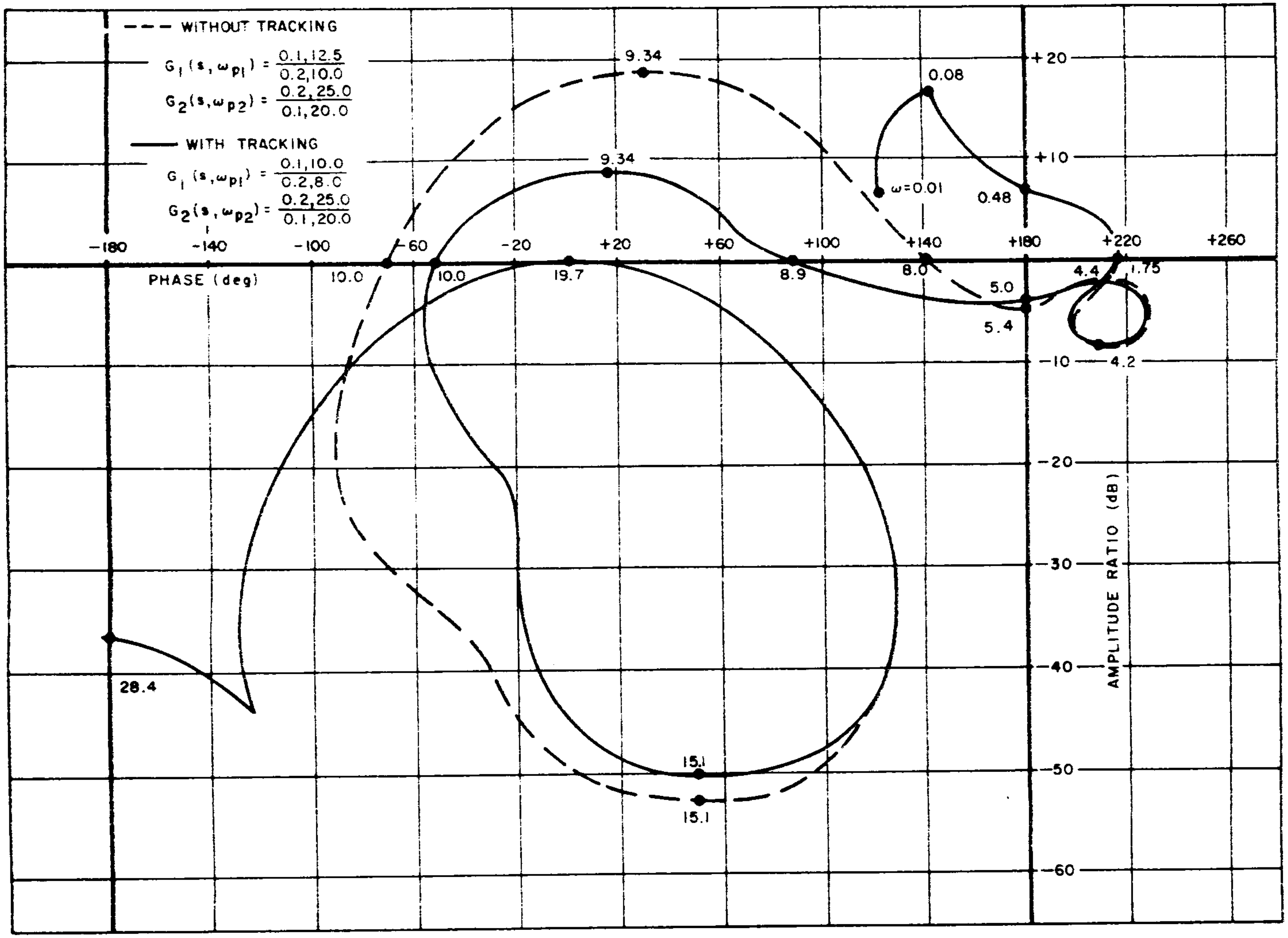

Figure 71. Gain-Phase Plot, Phase Stabilization, With and Without Tracking, First Mode Slope Increased 6 dB, T = 80 Seconds

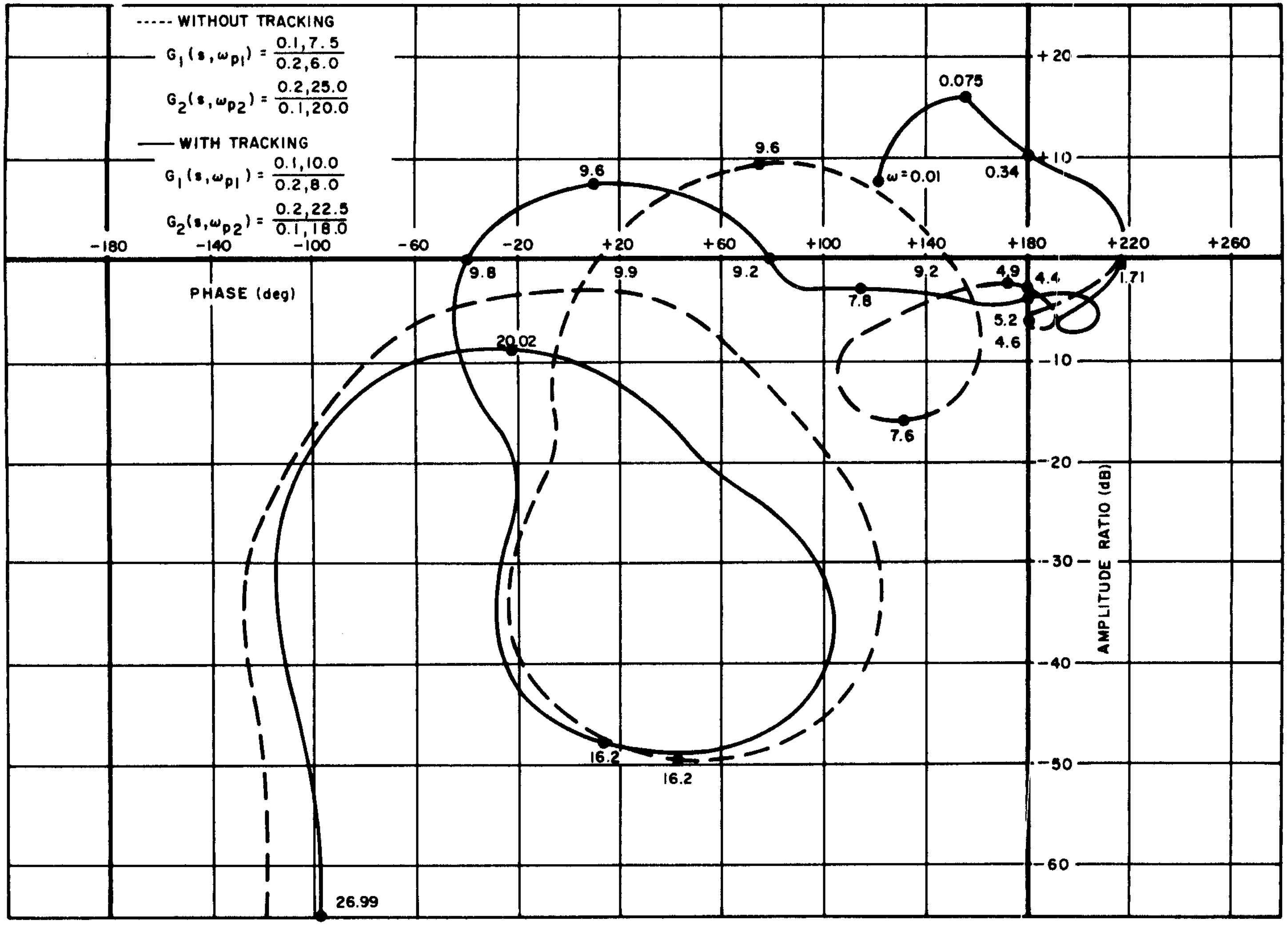

Figure 72. Gain-Phase Plot, Phase Stabilization, With and Without Tracking, First Mode Slope Increased 6 dB, T = 100 Seconds

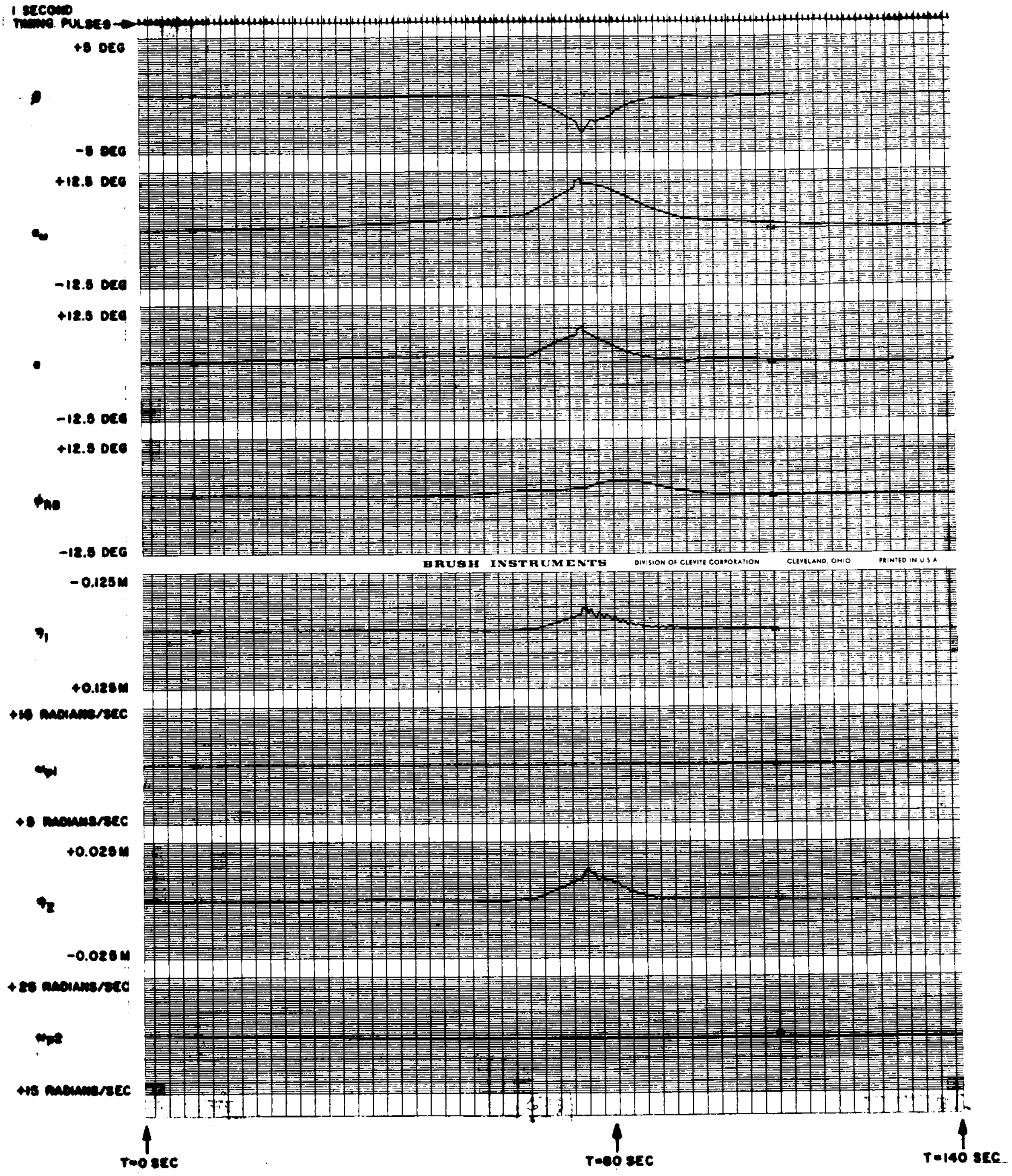

Figure 73A. S-IB-201 Launch Trajectory, Gain Stabilization, Nominal Bending Parameters, Filters Not Tracking

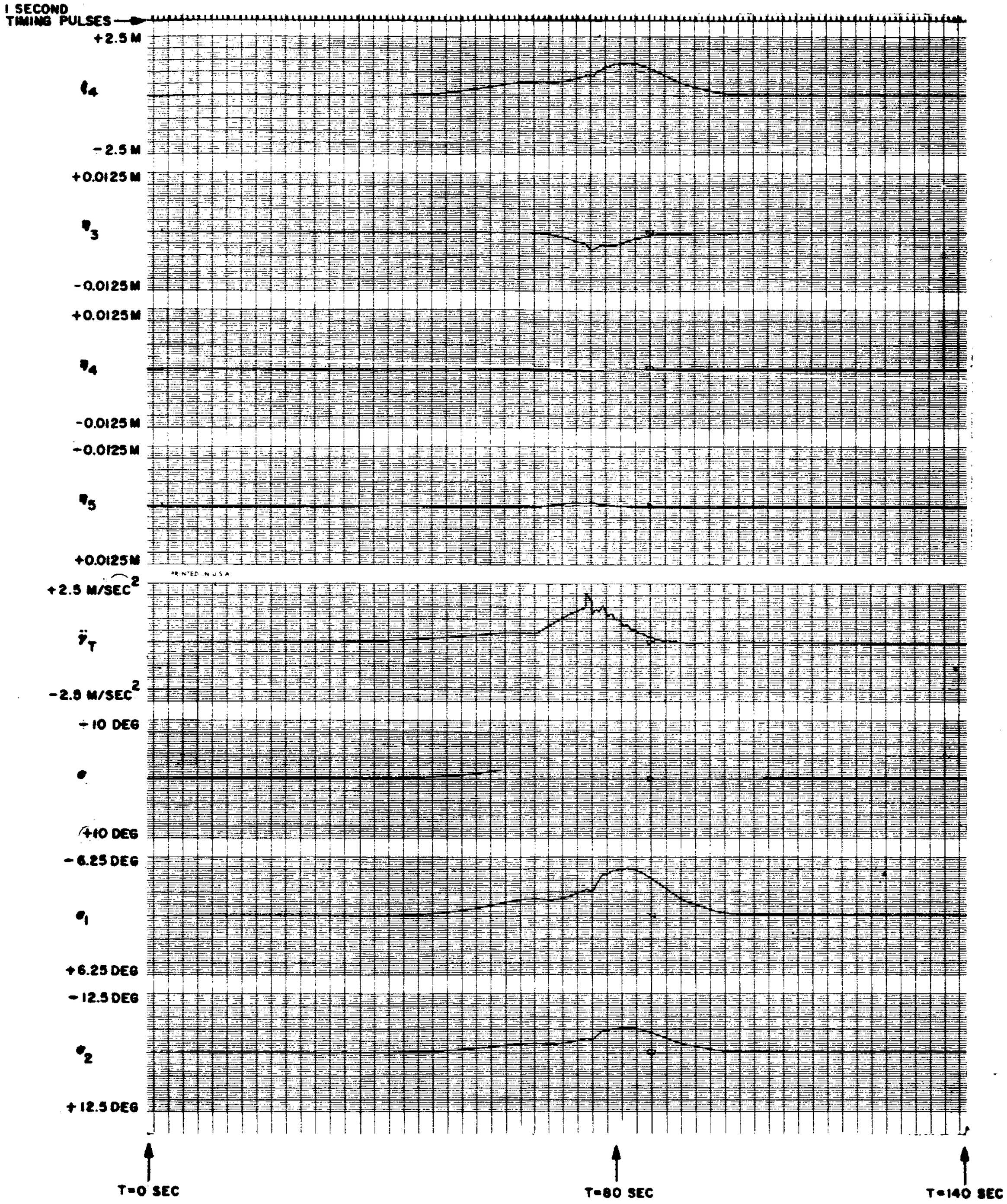

Figure 73B. S-IB-201 Launch Trajectory, Gain Stabilization, Nominal Bending Parameters, Filters Not Tracking

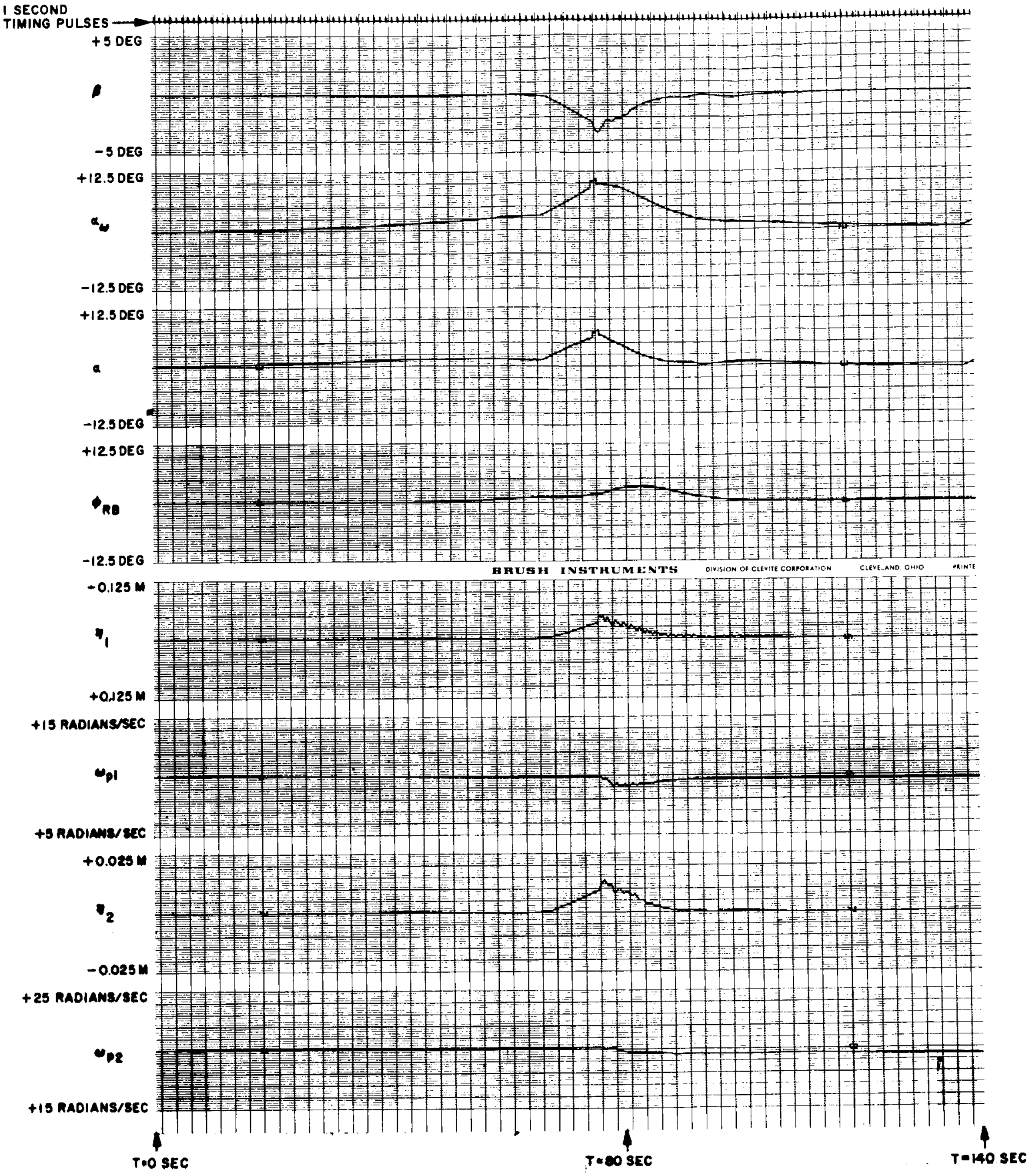

Figure 74A. S-IB-201 Launch Trajectory, Gain Stabilization, Nominal Bending Parameters, Filters Tracking

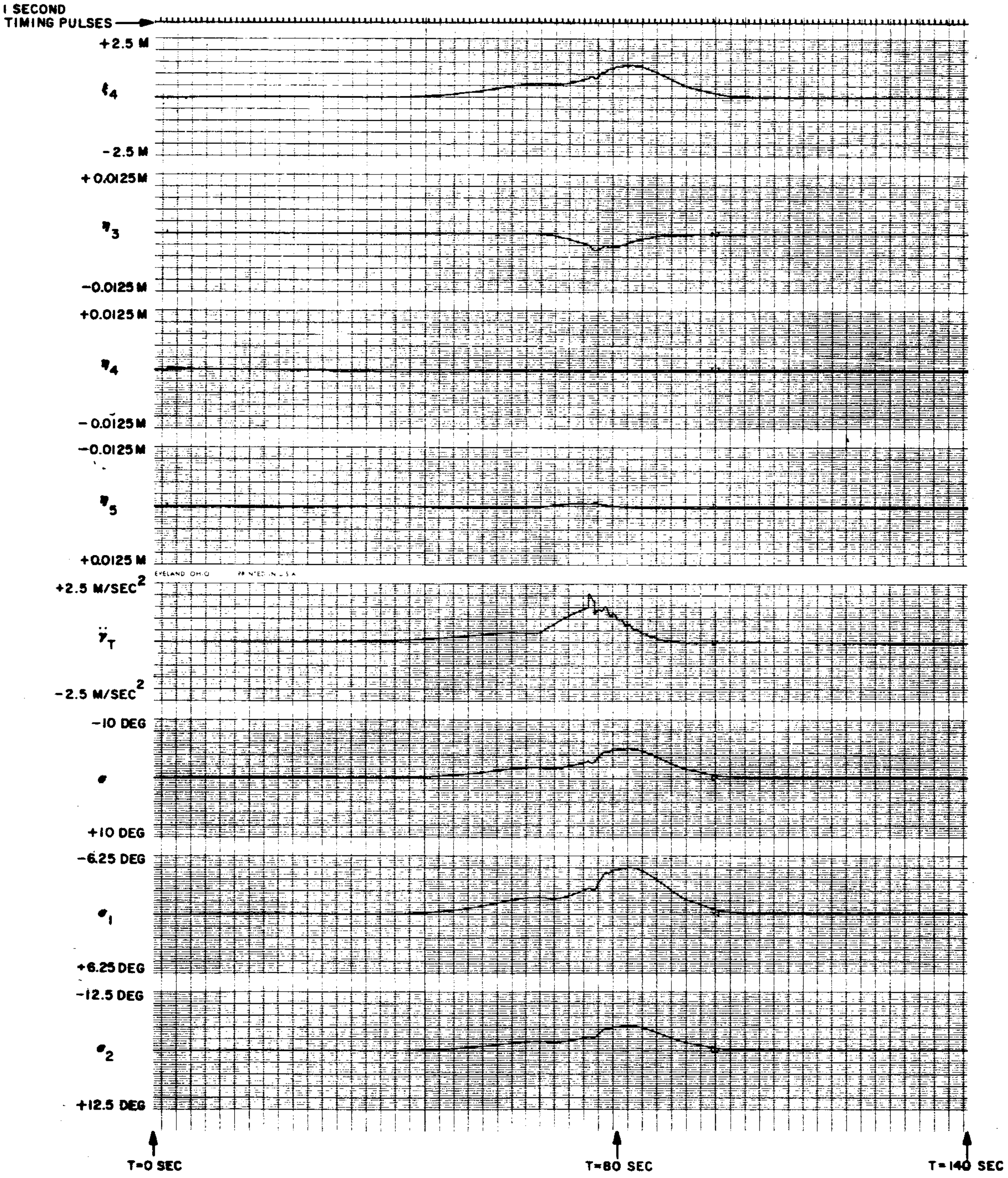

Figure 74B. S-IB-201 Launch Trajectory, Gain Stabilization, Nominal Bending Parameters, Filters Tracking

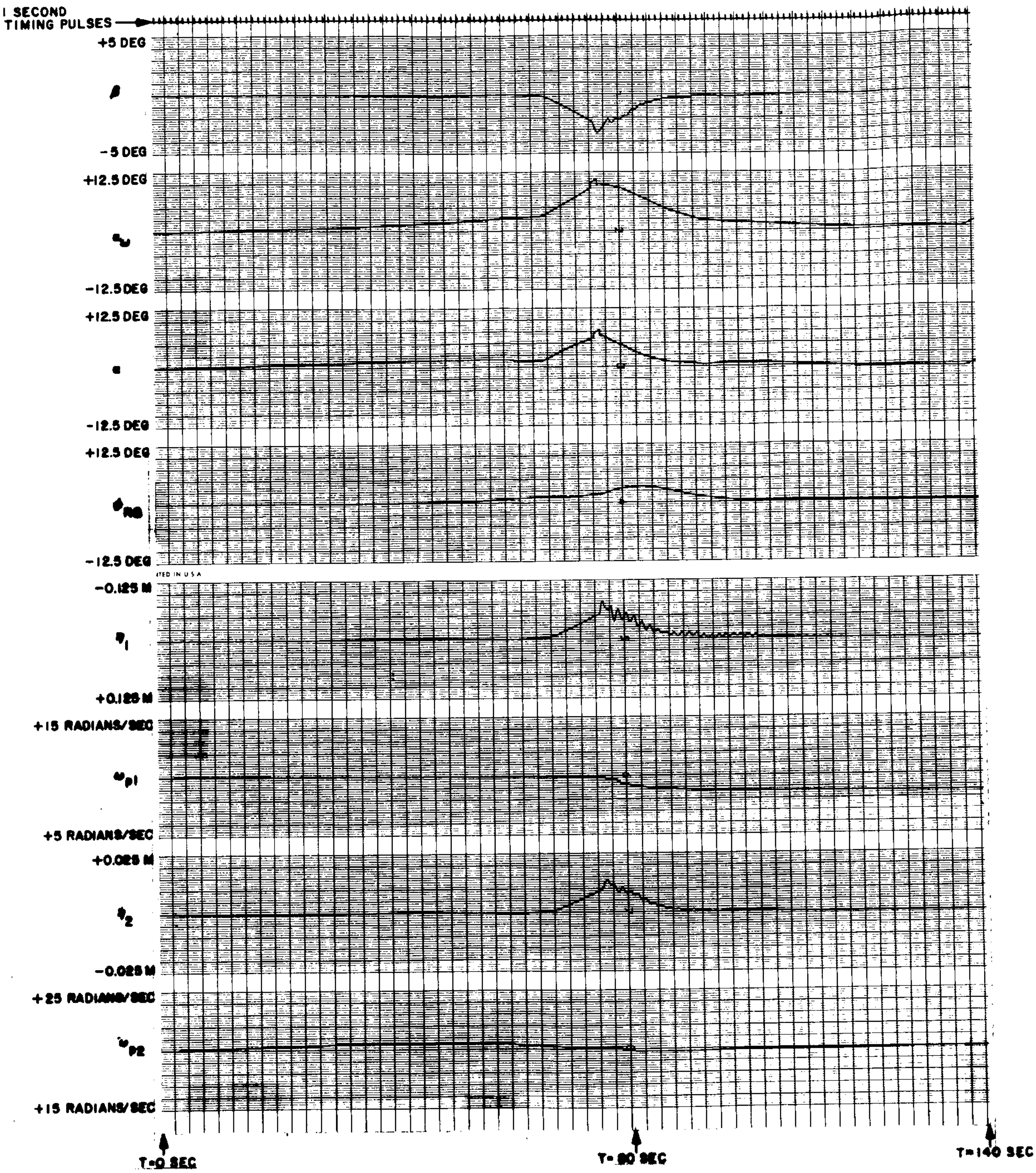

Figure 75A. S-IB-201 Launch Trajectory, Gain Stabilization, First Mode Frequency Reduced 20 Percent, First Mode Slope Nominal, Filters Tracking

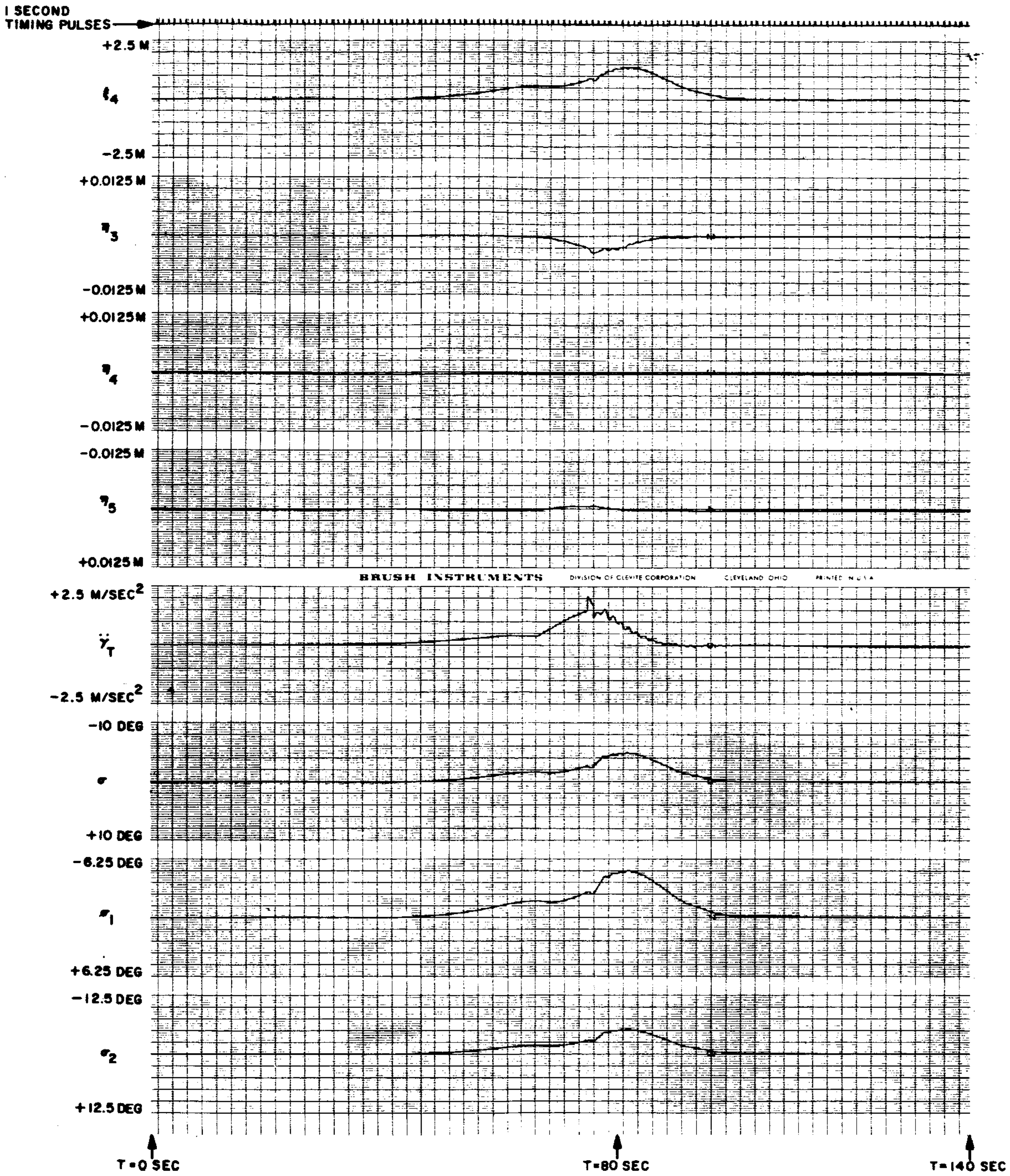

Figure 75B. S-IB-201 Launch Trajectory, Gain Stabilization, First Mode Frequency Reduced 20 Percent, First Mode Slope Nominal, Filters Tracking

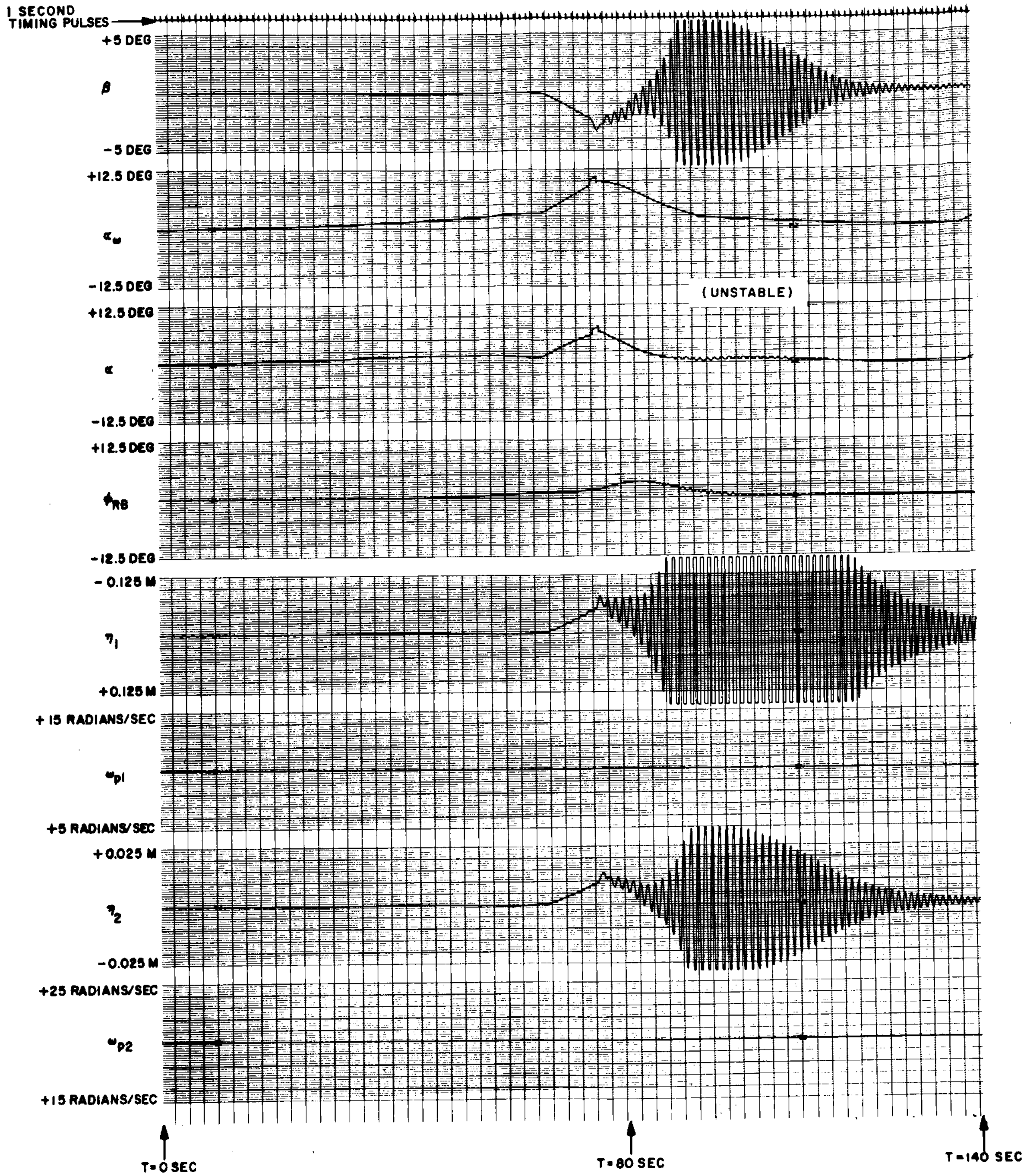

Figure 76A. S-IB-201 Launch Trajectory, Gain Stabilization, First Mode Frequency Reduced 20 Percent, First Mode Slope Increased 6 dB, Filters Not Tracking

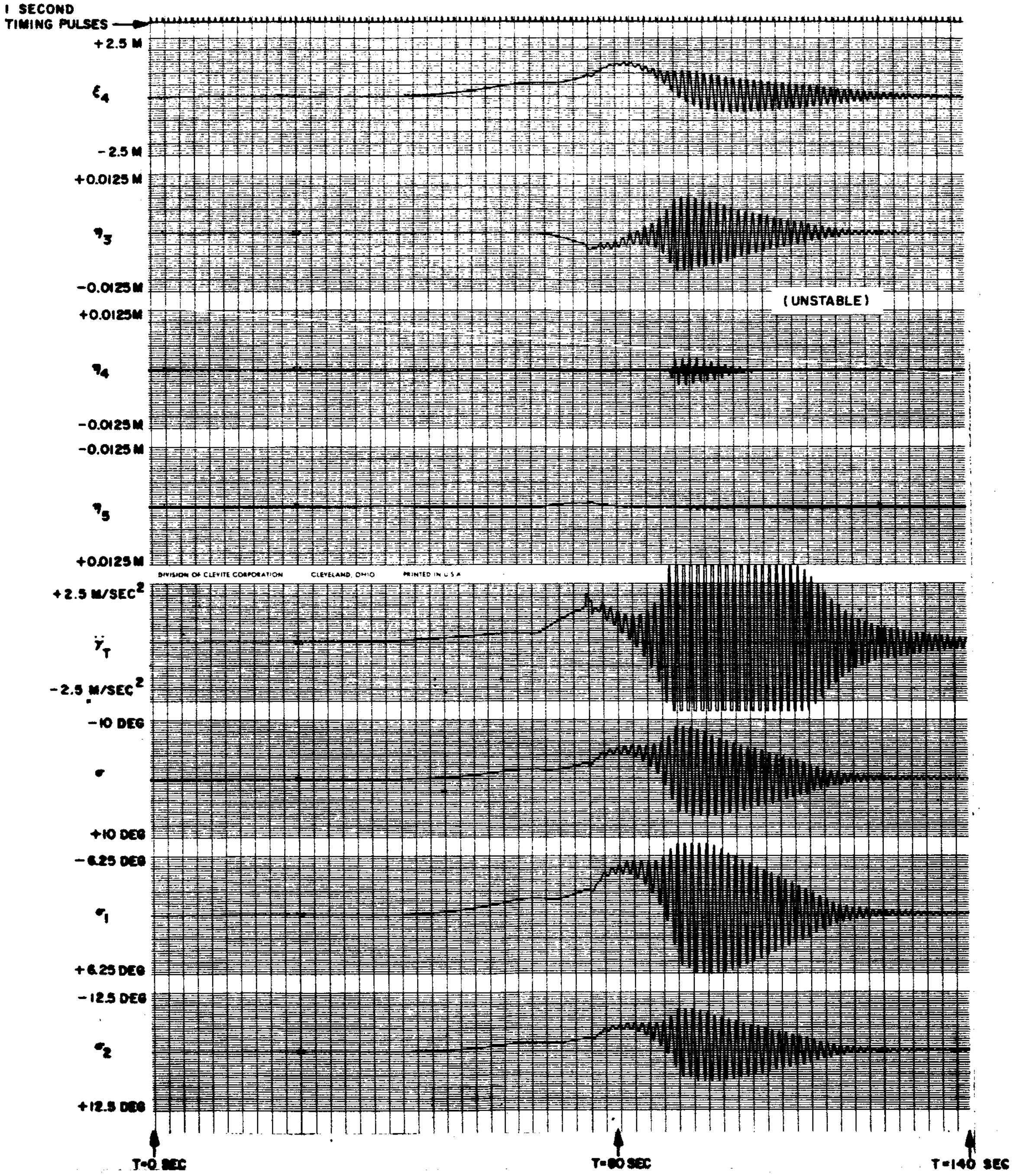

Figure 76B. S-IB-201 Launch Trajectory, Gain Stabilization, First Mode Frequency Reduced 20 Percent, First Mode Slope Increased 6 dB, Filters Not Tracking

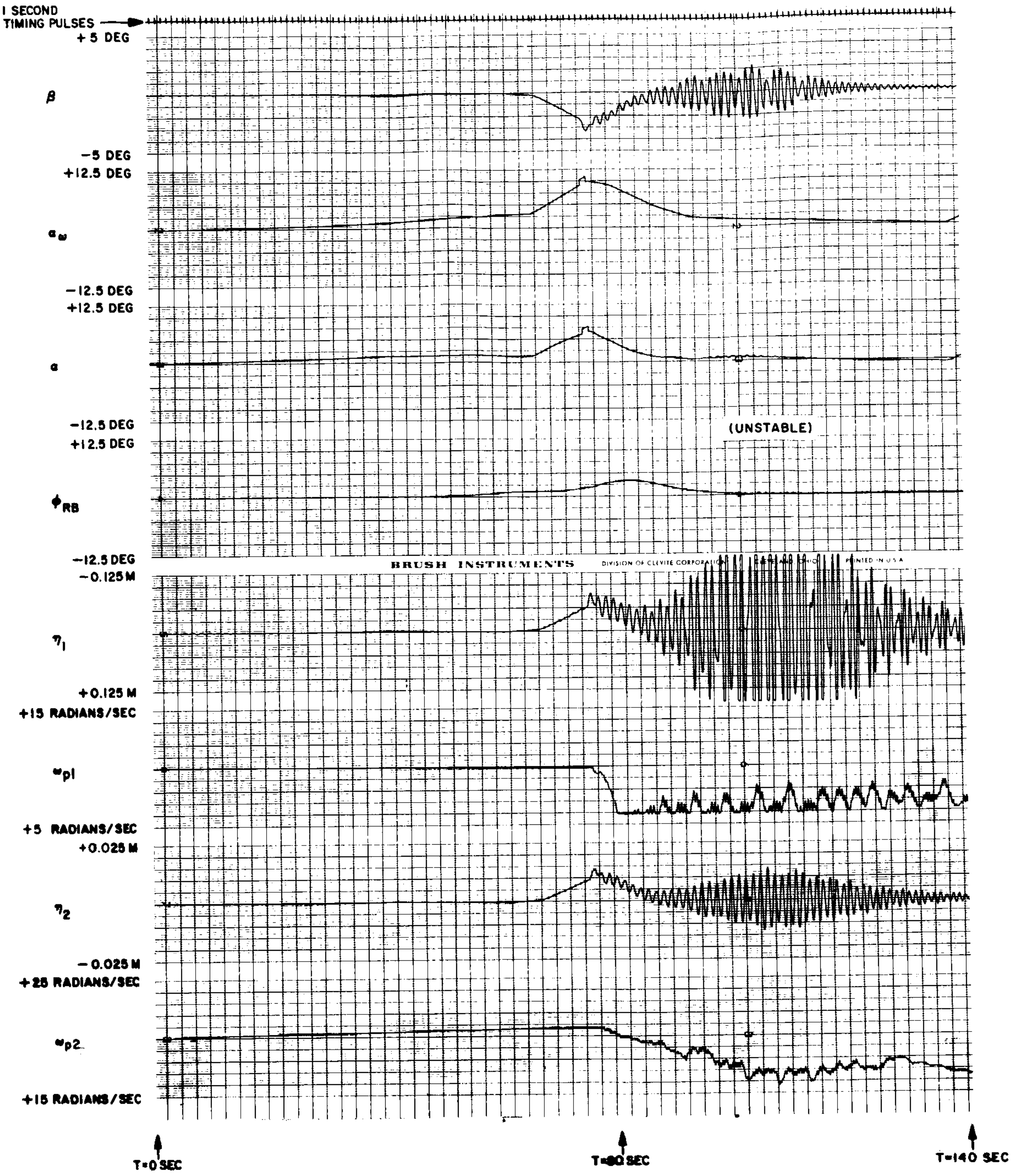

Figure 77A. S-IB-201 Launch Trajectory, Gain Stabilization, First Mode Frequency Reduced 20 Percent, First Mode Slope Increased 6 dB, Filters Tracking

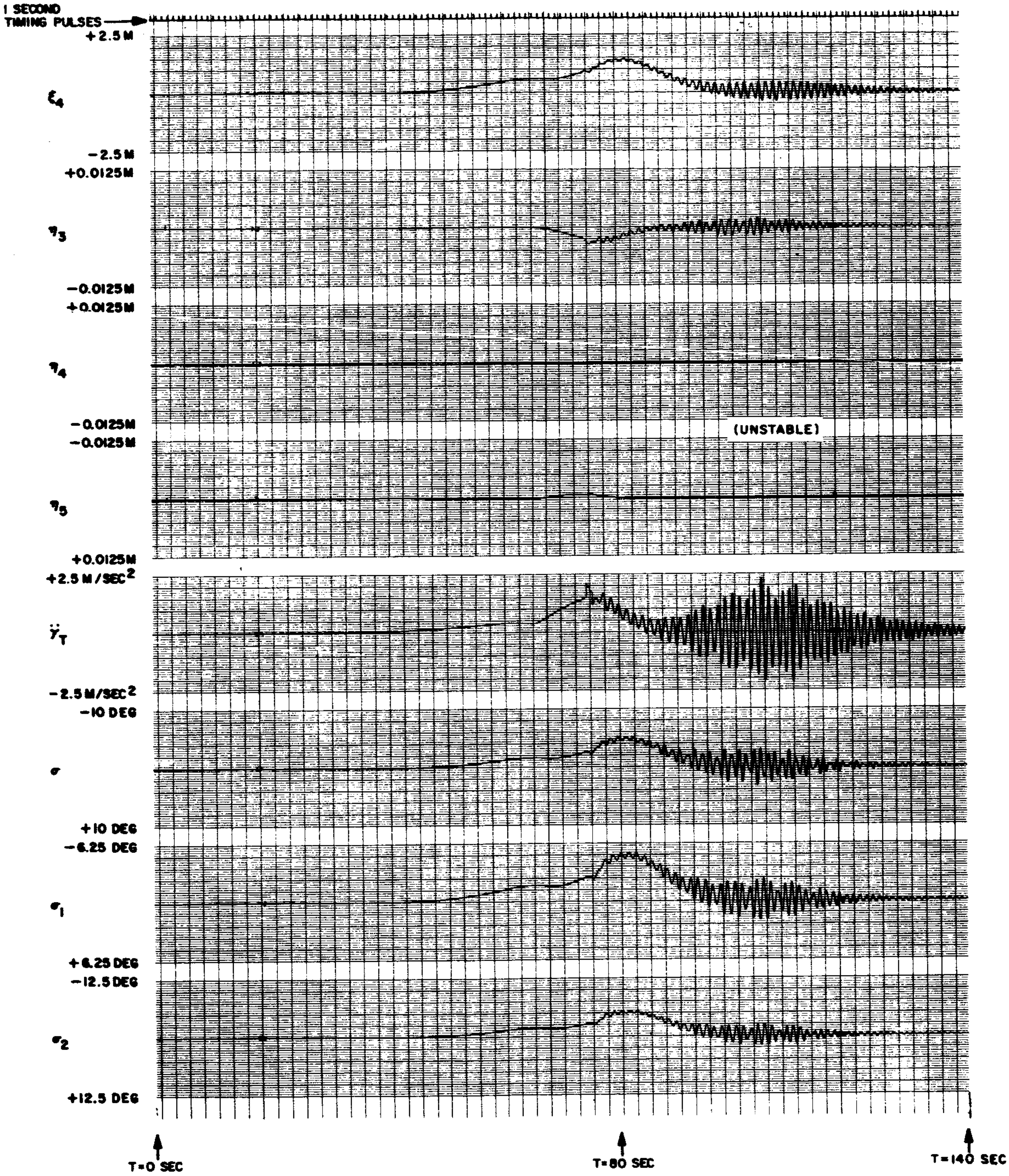

Figure 77B. S-IB-201 Launch Trajectory, Gain Stabilization First Mode Frequency Reduced 20 Percent, First Mode Slope Increased 6 dB, Filters Tracking

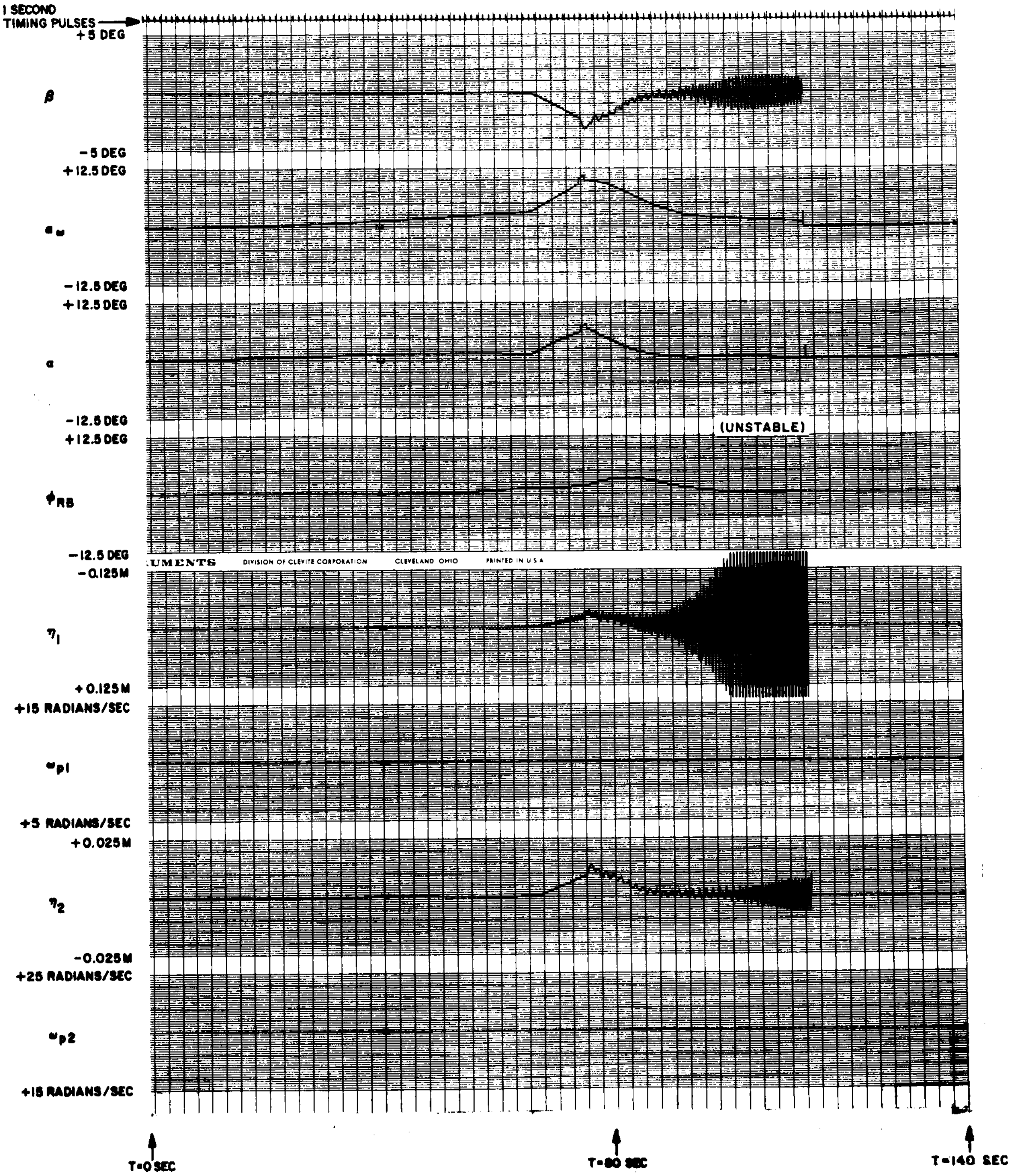

Figure 78A. S-IB-201 Launch Trajectory, Gain Stabilization, First Mode Frequency Increased 20 Percent, First Mode Slope Increased 12 dB, Filters Not Tracking

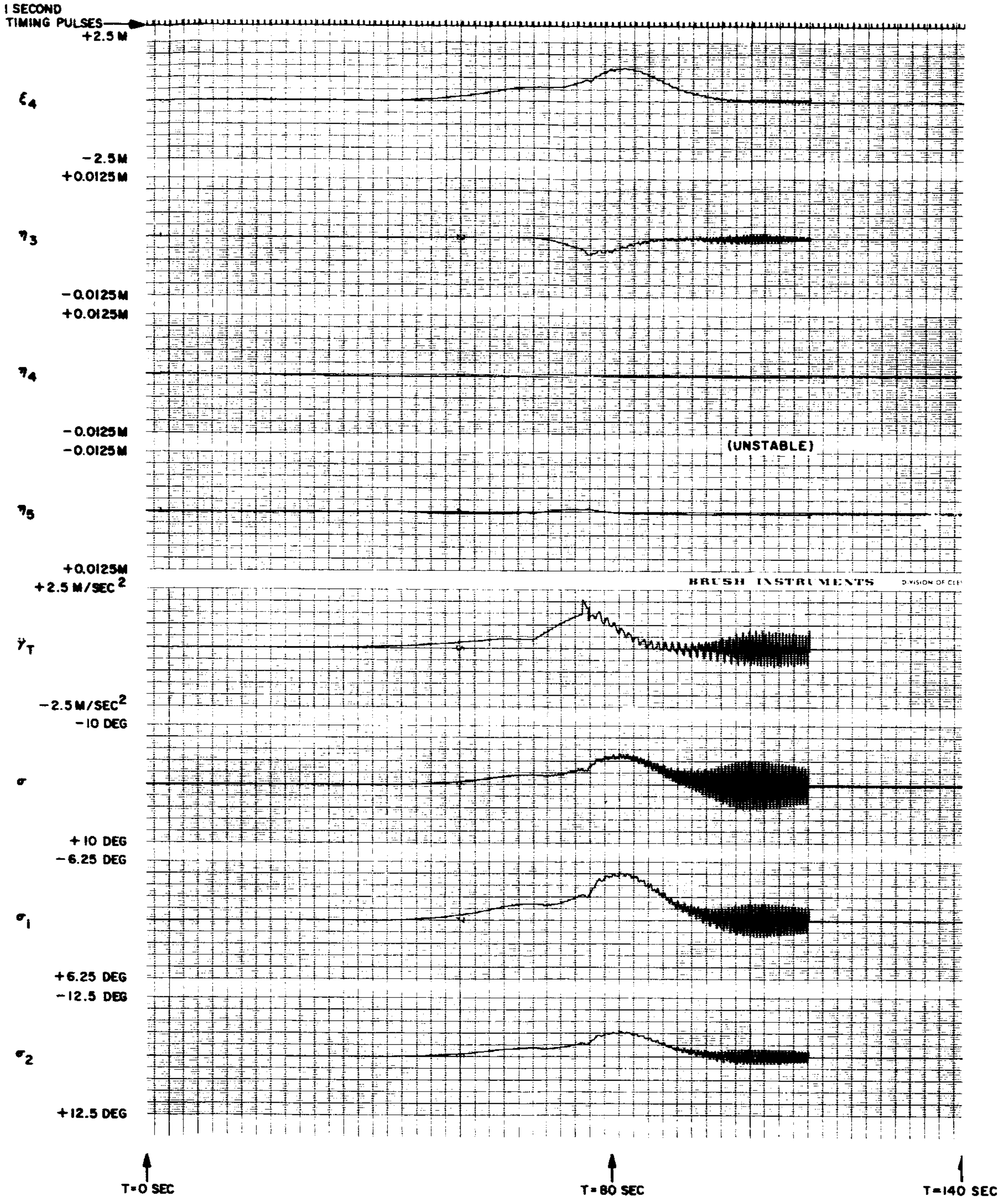

Figure 78B. S-IB-201 Launch Trajectory, Gain Stabilization, First Mode Frequency Increased 20 percent, First Mode Slope Increased 12 dB, Filters Not Tracking

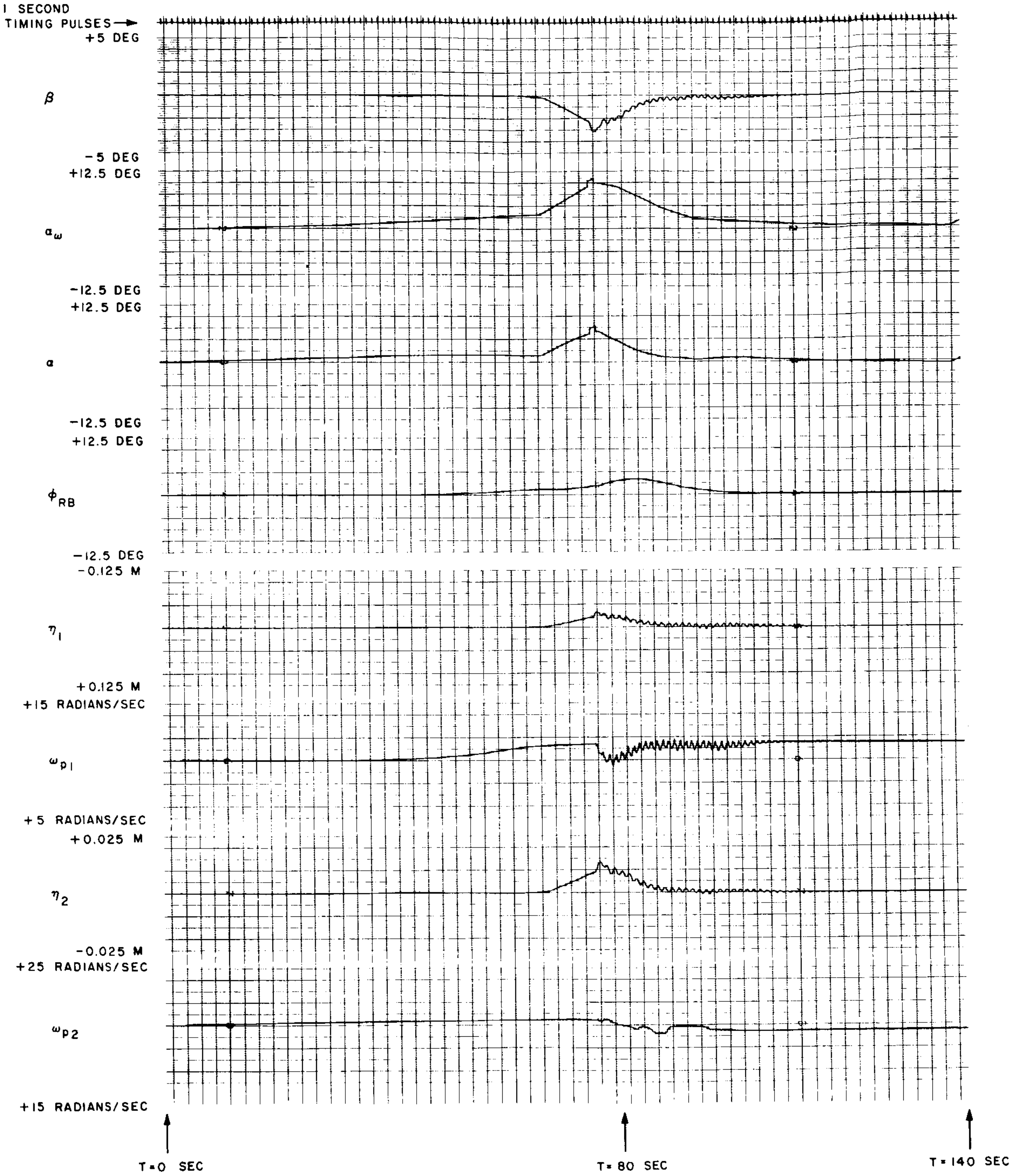

Figure 79A. S-IB-201 Launch Trajectory, Gain Stabilization, First Mode Frequency Increased 20 Percent, First Mode Slope Increased 12 dB, Filters Tracking

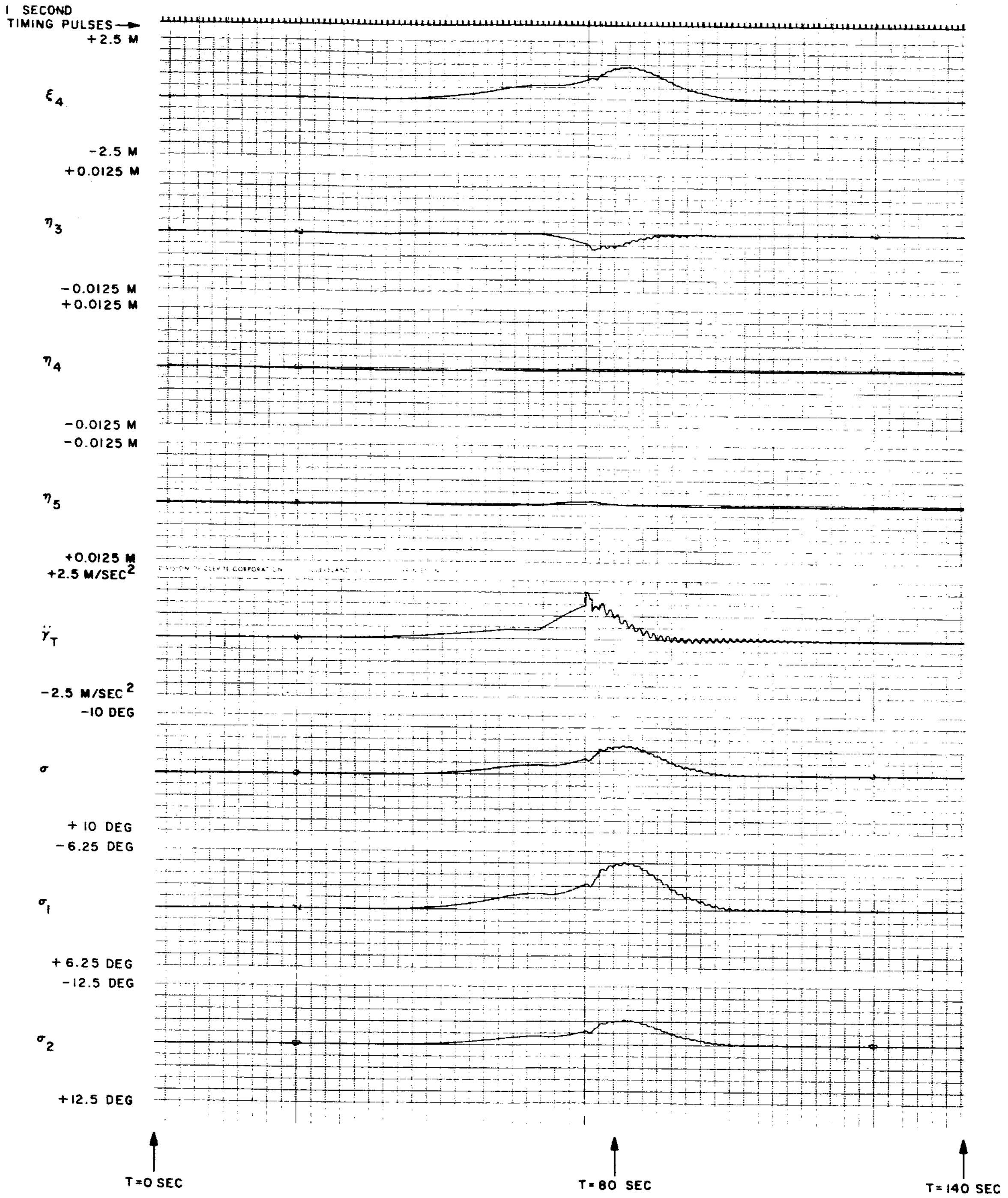

Figure 79B. S-IB-201 Launch Trajectory, Gain Stabilization, First Mode Frequency Increased 20 Percent, First Mode Slope Increased 12 dB, Filters Tracking

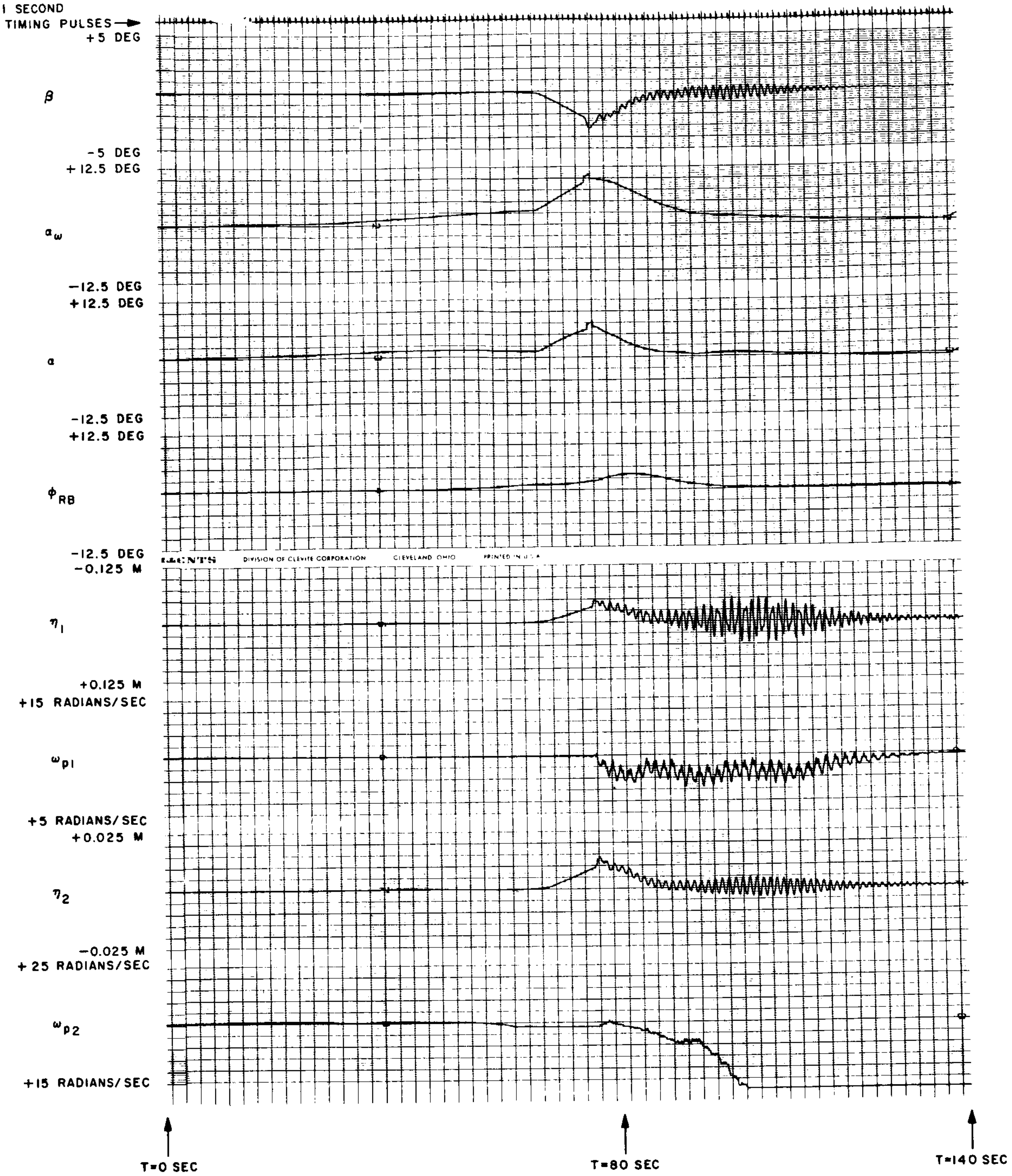

Figure 80A. S-IB-201 Launch Trajectory, Gain Stabilization, First Mode Slope Increased 9 dB, Filters Tracking

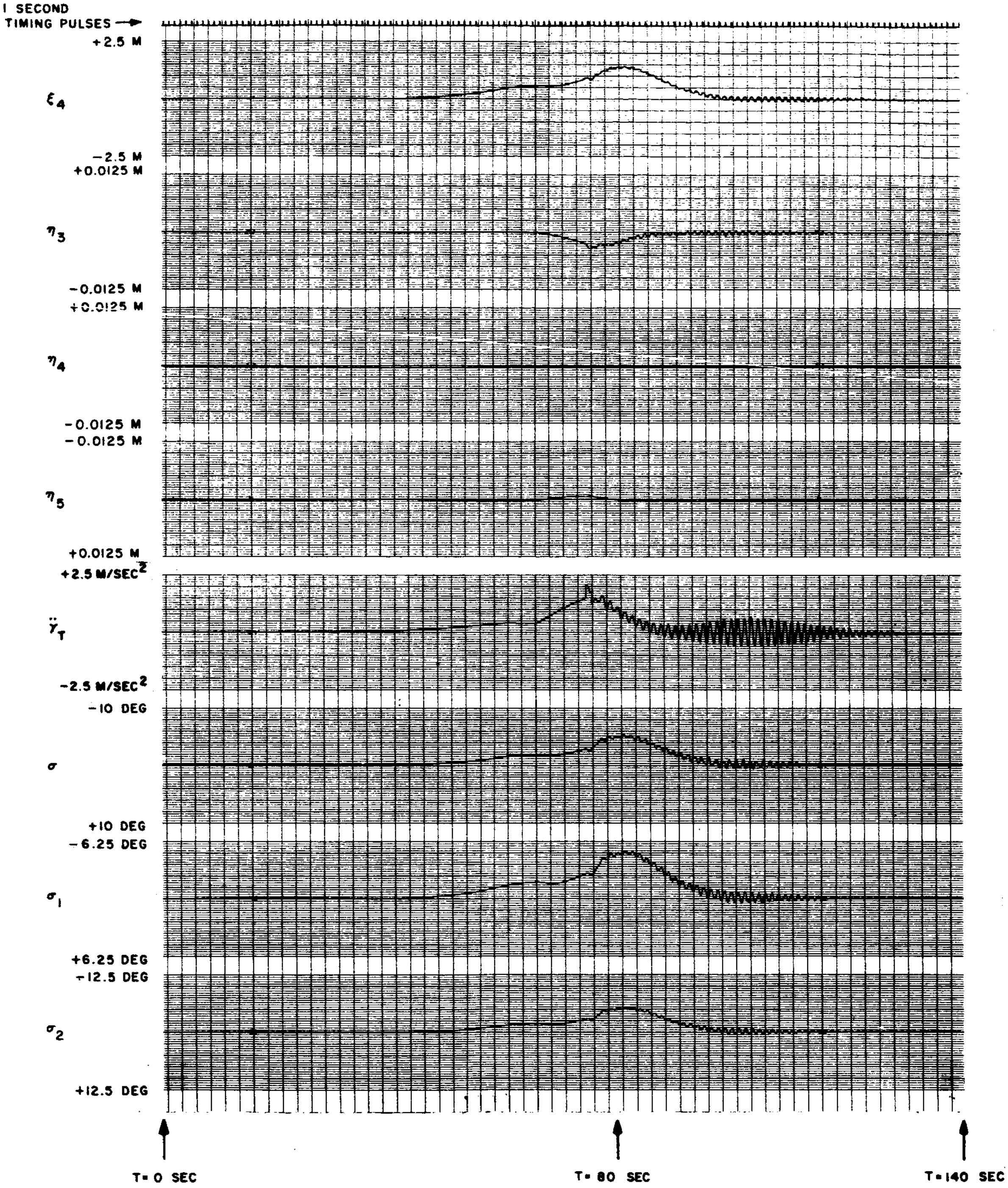

Figure 80B. S-IB-201 Launch Trajectory, Gain Stabilization, First Mode Slope Increased 9 dB, Filters Tracking

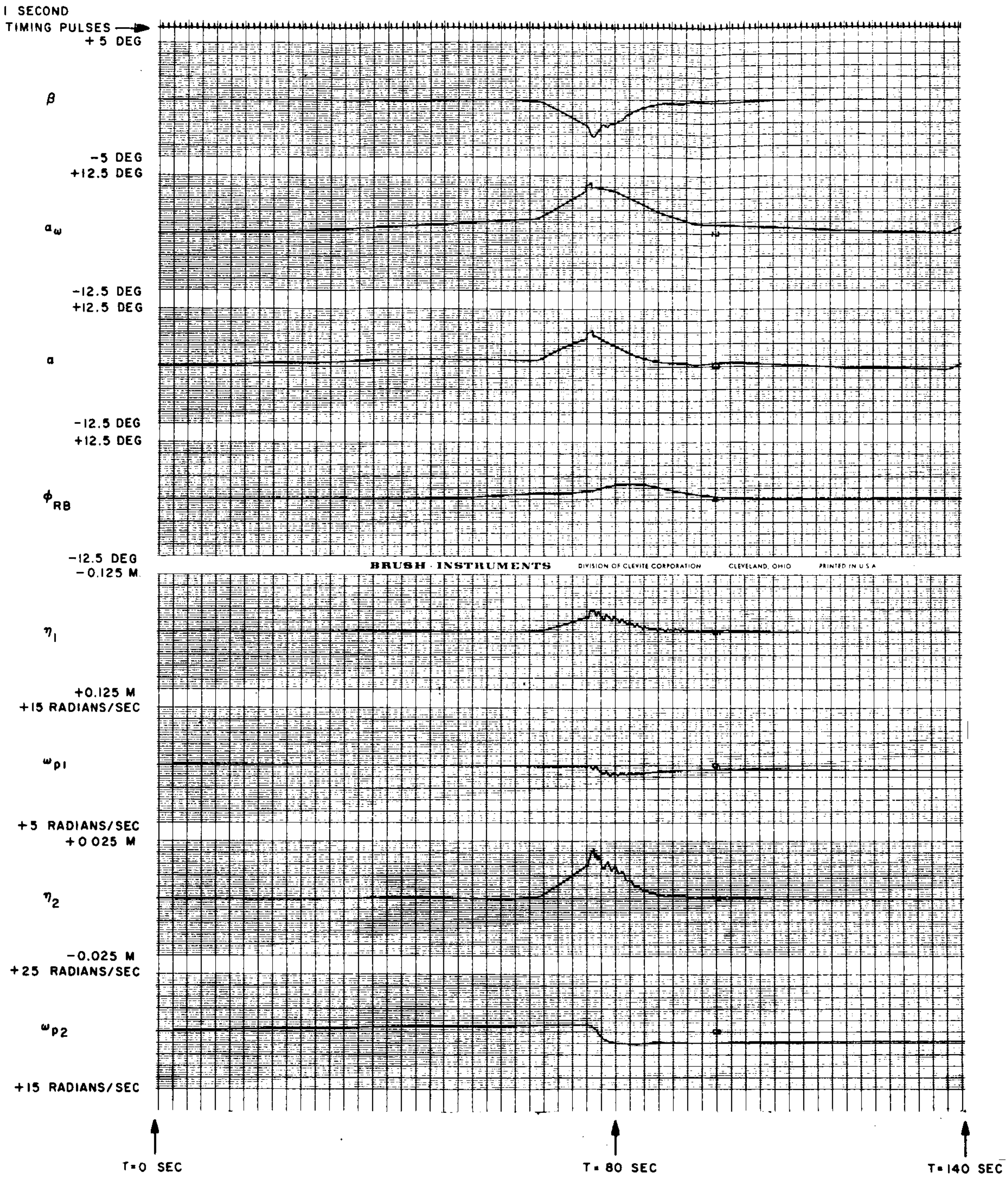

Figure 81A. S-IB-201 Launch Trajectory, Gain Stabilization, Second Mode Frequency Reduced 20 Percent, Filters Tracking

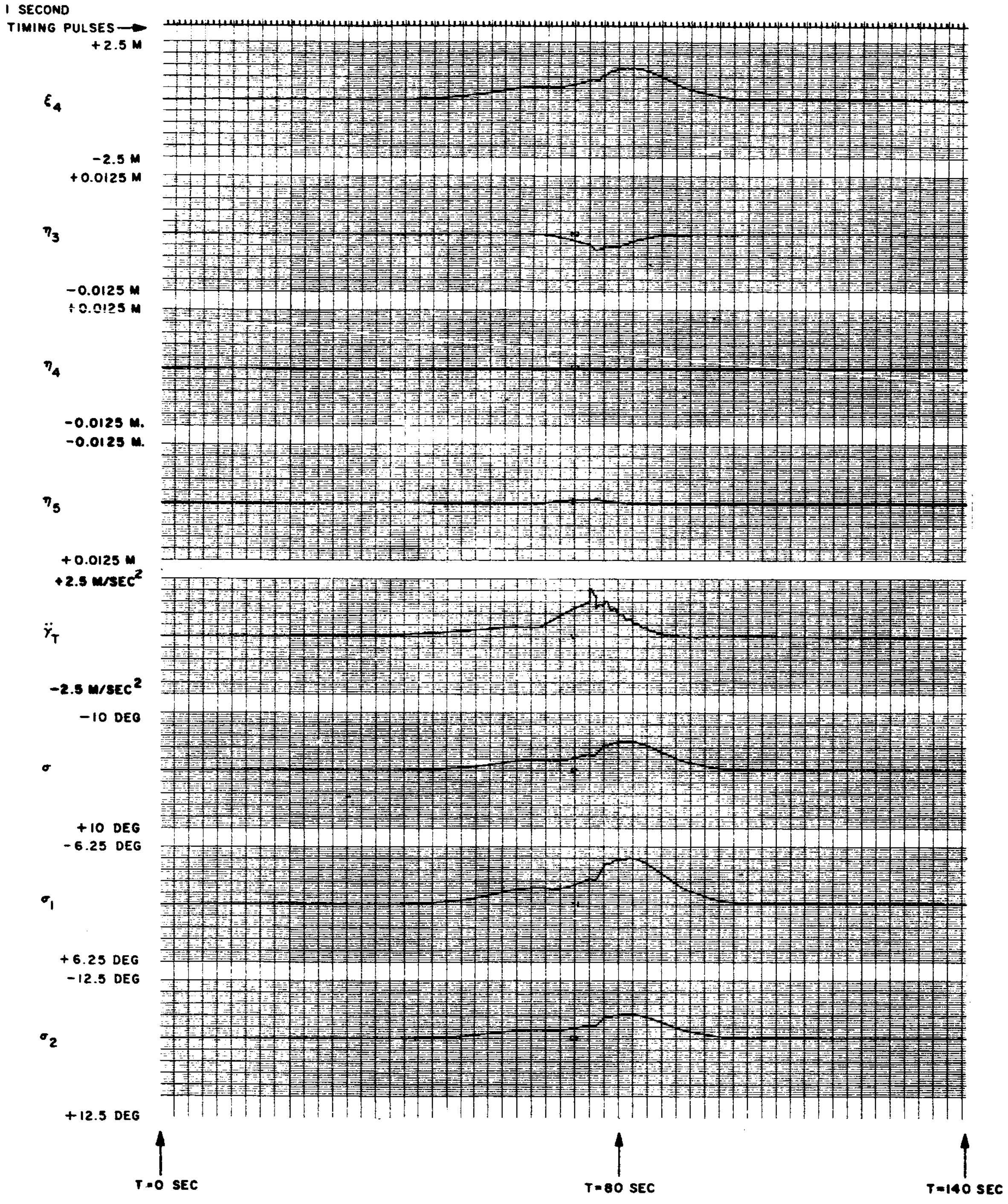

Figure 81B. S-IB-201 Launch Trajectory, Gain Stabilization, Second Mode Frequency Reduced 20 Percent, Filters Tracking

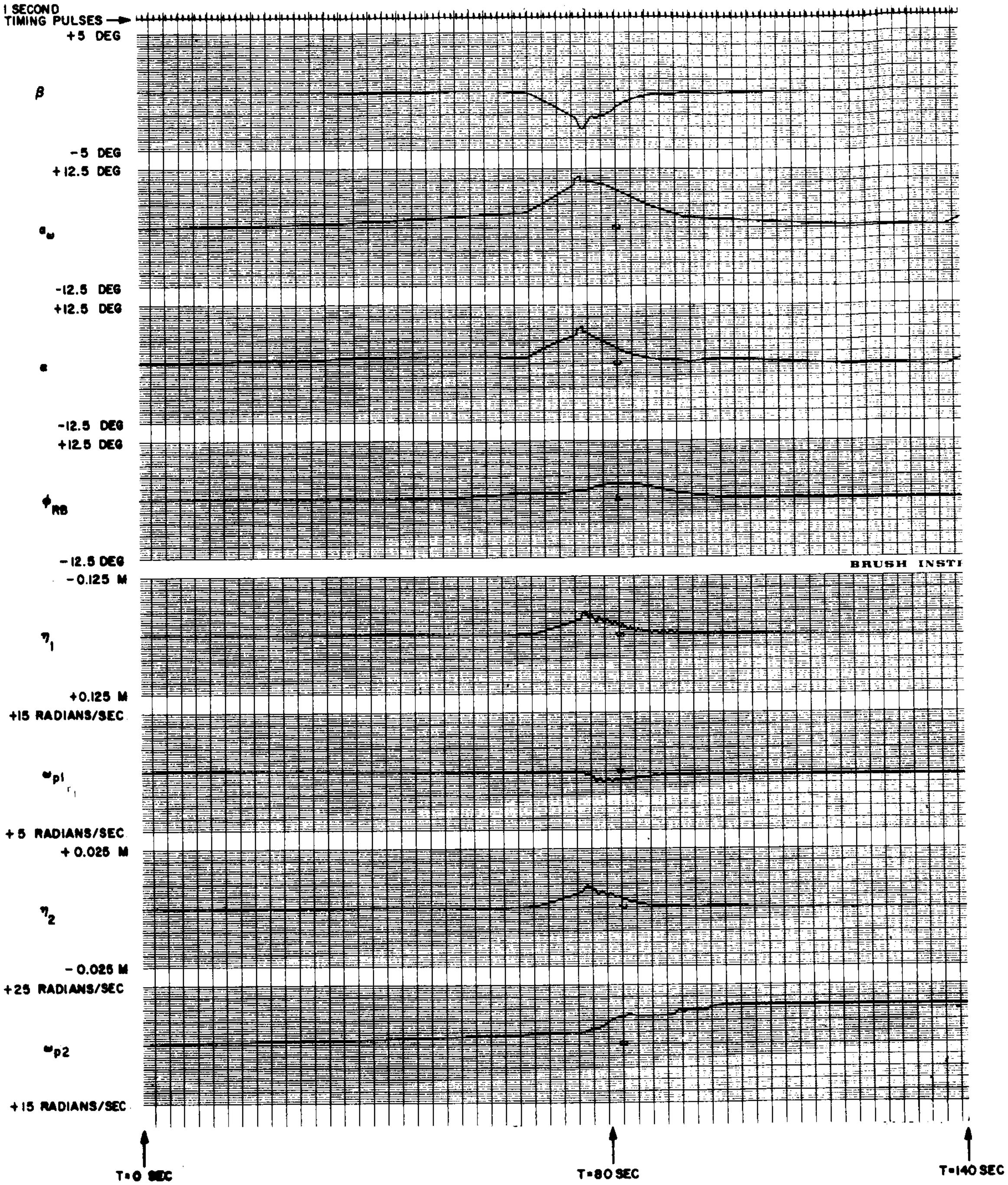

Figure 82A. S-IB-201 Launch Trajectory, Gain Stabilization, Second Mode Frequency Increased 20 Percent, Filters Tracking

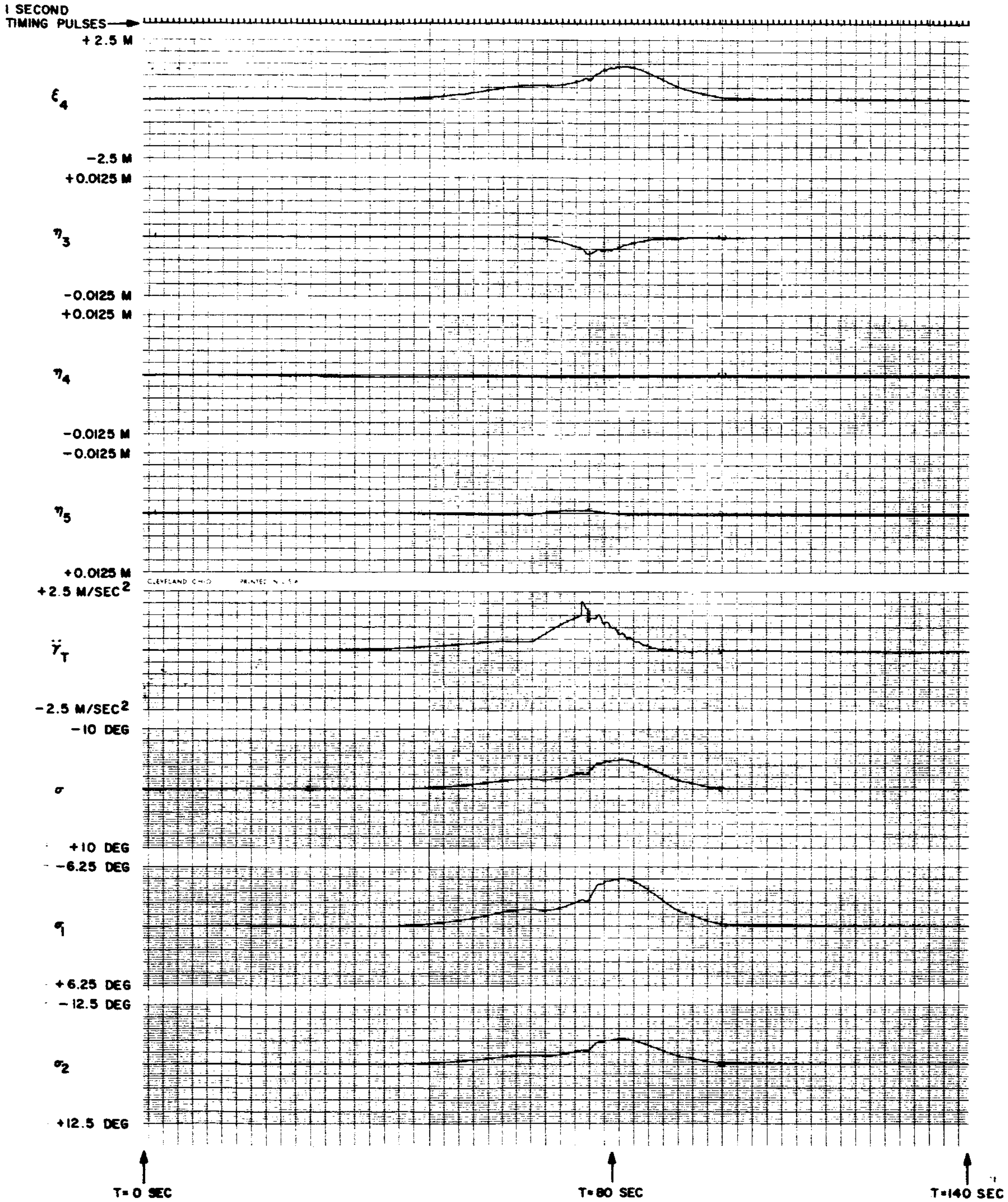

Figure 82B. S-IB-201 Launch Trajectory, Gain Stabilization, Second Mode Frequency Increased 20 Percent, Filters Tracking

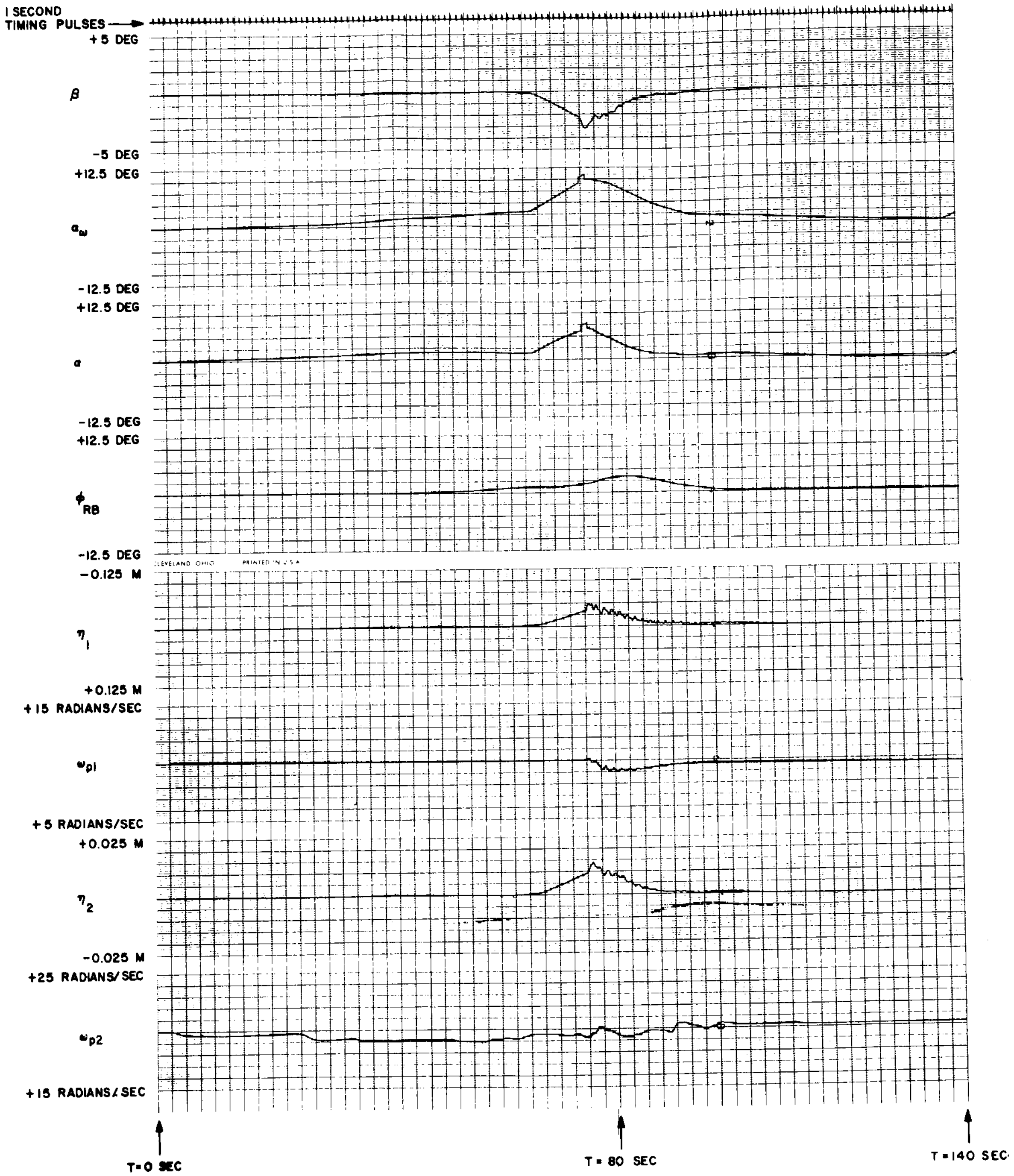

Figure 83A. S-IB-201 Launch Trajectory, Gain Stabilization, Second Mode Slope Increased 12 dB, Filters Tracking

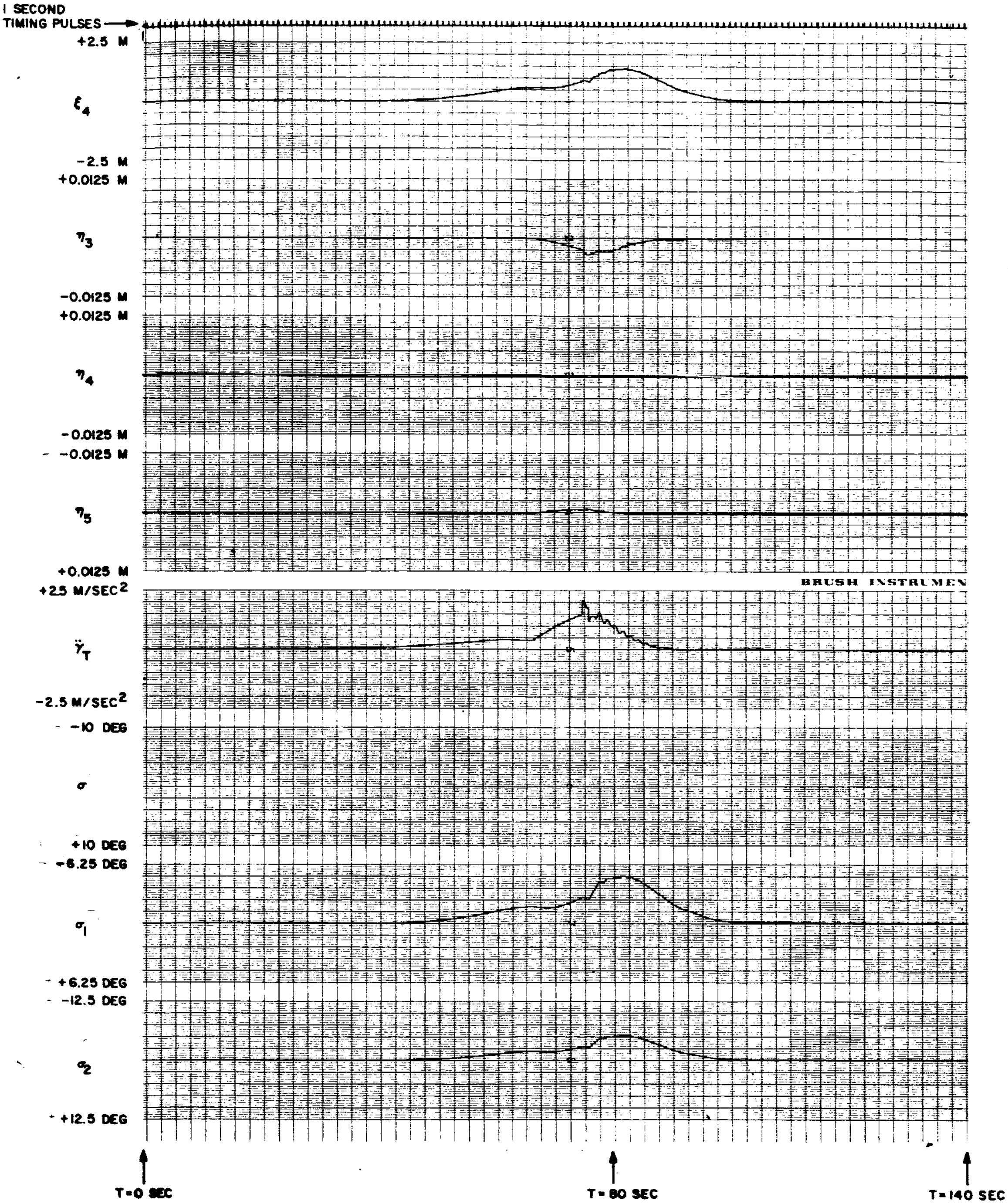

Figure 83B. S-IB-201 Launch Trajectory, Gain Stabilization, Second Mode Slope Increased 12 dB, Filters Tracking

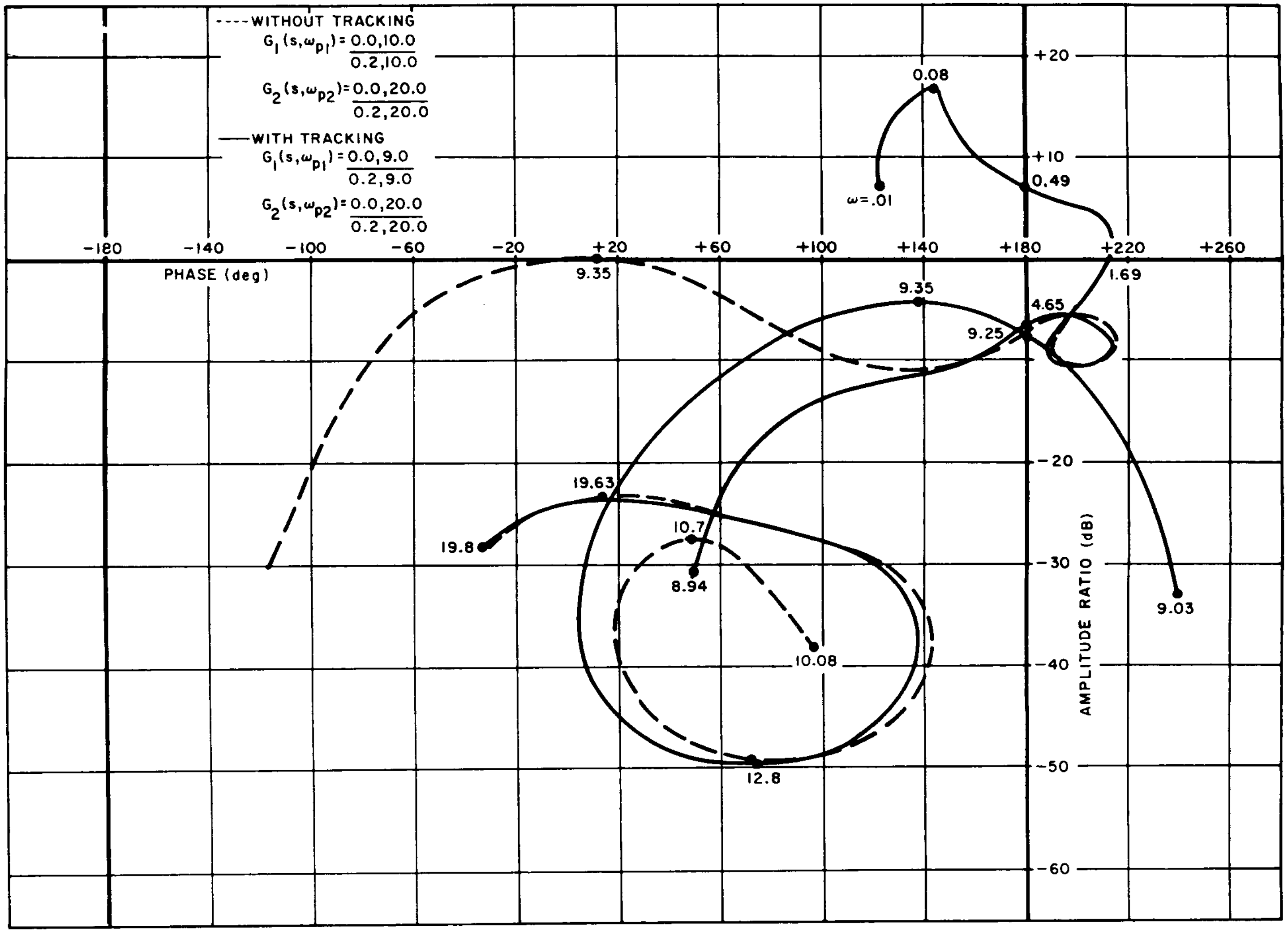

Figure 84. Gain-Phase Plot, Gain Stabilization, With and Without Tracking, Nominal Bending Parameters, T = 80 Seconds

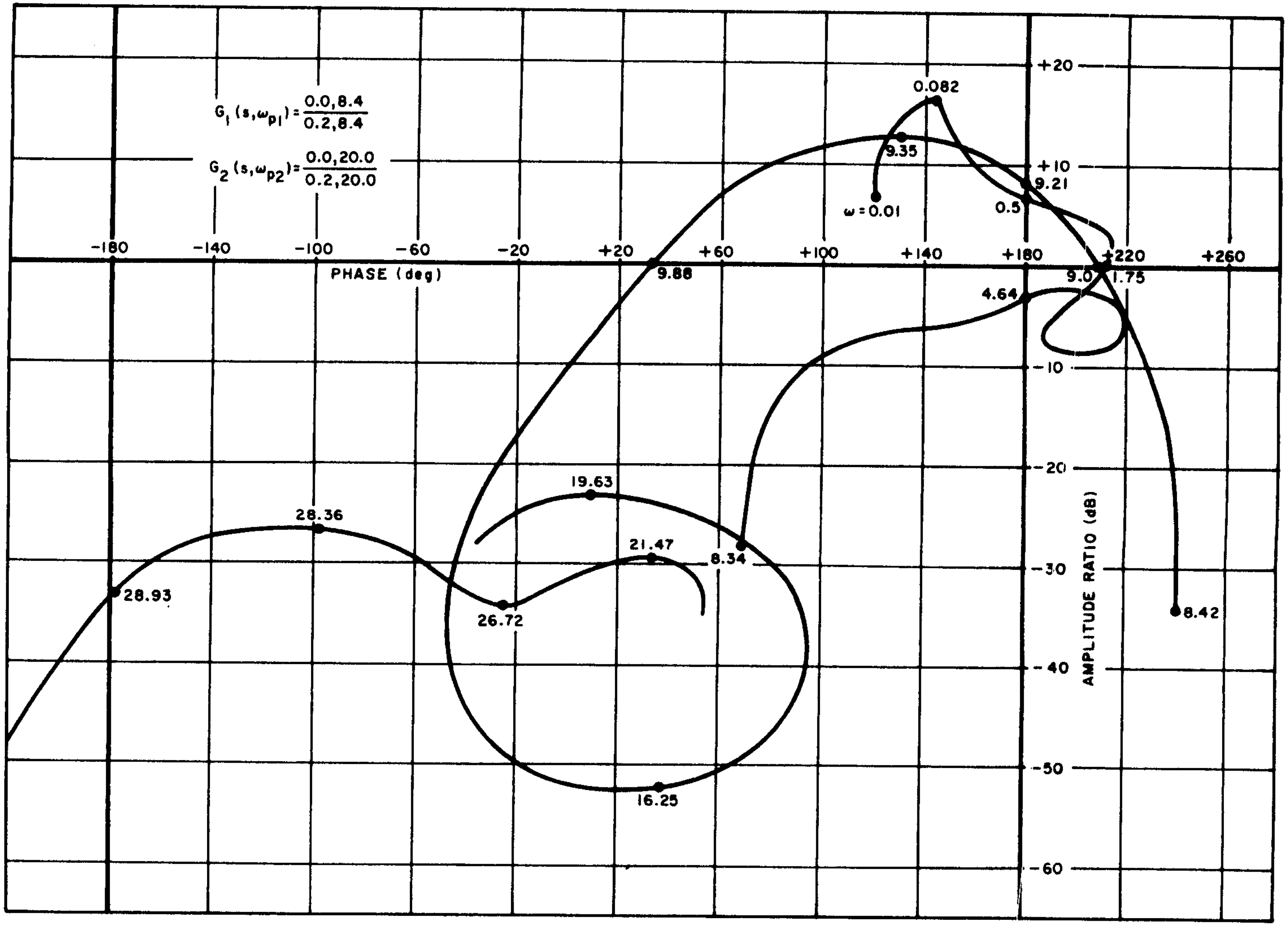

Figure 85. Gain-Phase Plot, Gain Stabilization, First Mode Filter Tracked to ω_{p1} = 8.4 rad/sec, Nominal Bending Parameters, T = 80 Seconds

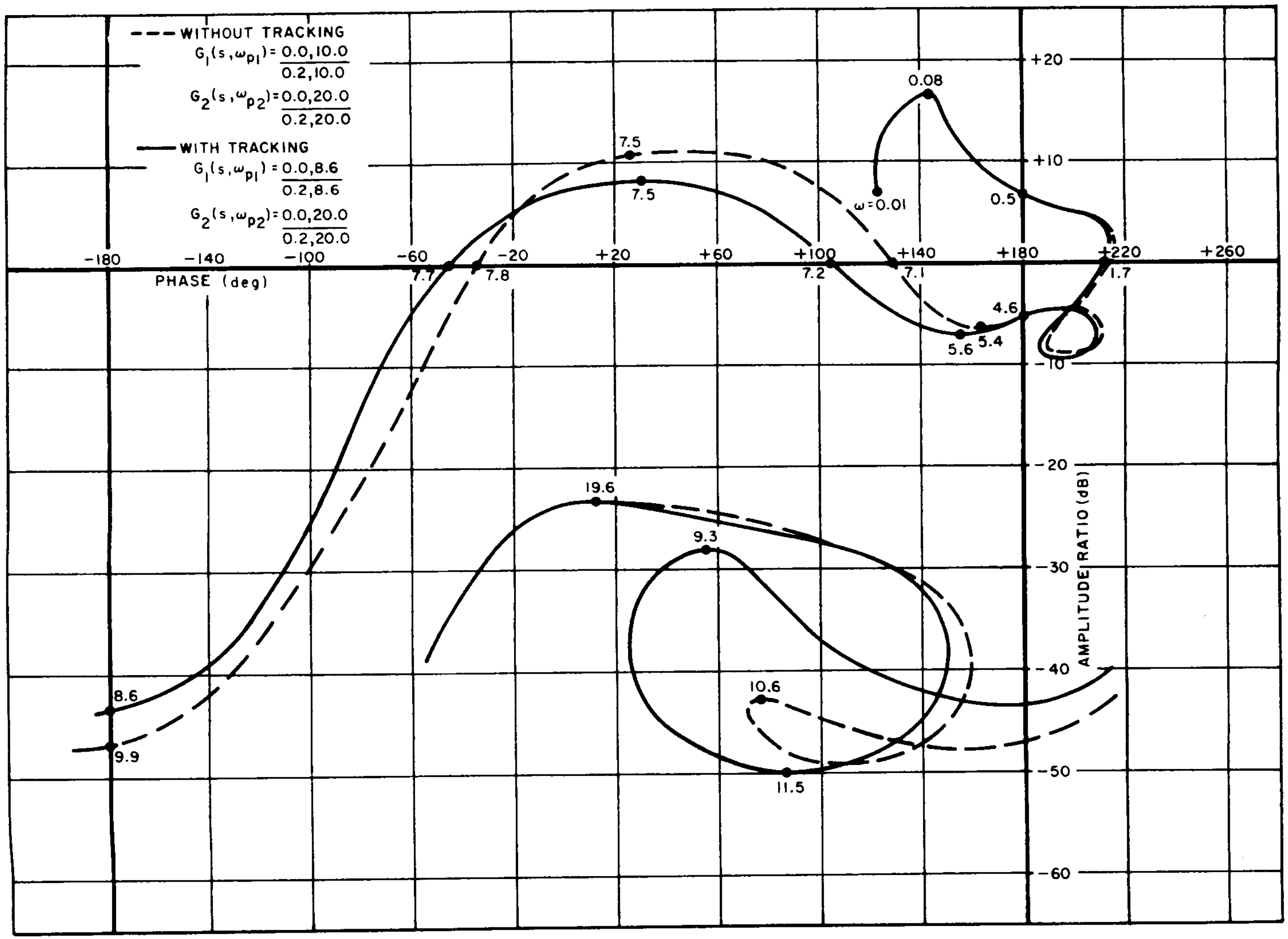

Figure 86. Gain-Phase Plot, Gain Stabilization, With and Without Tracking, First Mode Frequency Reduced 20 Percent, T = 80 Seconds

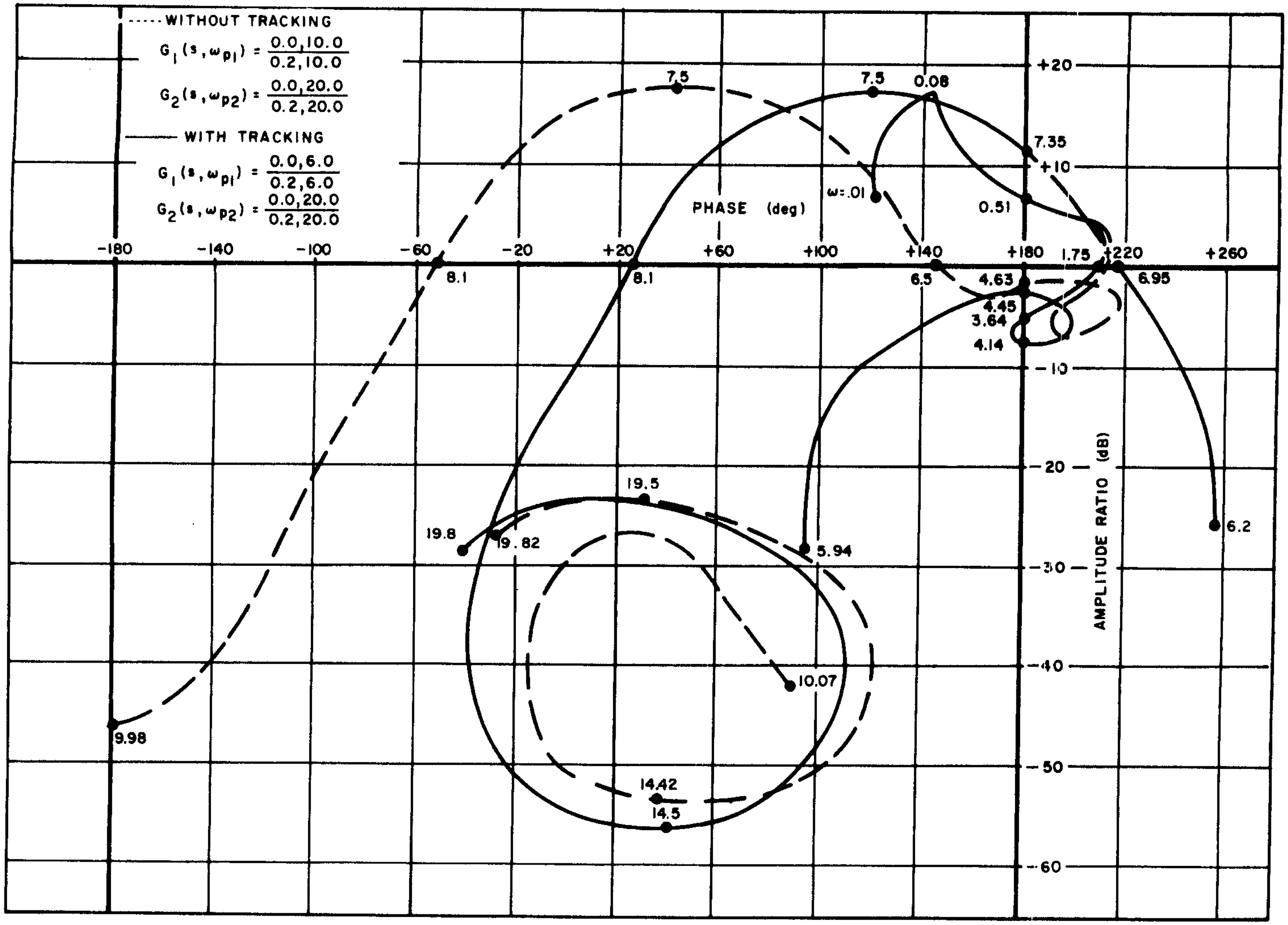

Figure 87. Gain-Phase Plot, Gain Stabilization, With and Without Tracking, First Mode Frequency Reduced 20 Percent, First Mode Slope Increased 6 dB, T = 80 Seconds

TABLE 1

AMPLITUDE OF DC AND SECOND HARMONIC COMPONENTS OF DEMODULATOR OUTPUT

$e_{in} = A \sin \omega_a t, \quad e_r = C \sin (\omega_a t + \phi)$

Demodulator Type	Amplitude of DC Output	Amplitude of $2\omega_a$ Component
Multiplier $e_d = e_r \cdot e_{in}$	$\frac{AC \cos \phi}{2}$	$\frac{AC}{2}$
Chopper $e_d = \mathrm{SGN}\,(e_r) \cdot e_{in}$	$\frac{2A \cos \phi}{\pi}$	$\frac{2A}{3\pi} \sqrt{10 - 6 \cos 2\phi}$
Double Chopper $e_d = \mathrm{SGN}\,(e_r) \cdot \mathrm{SGN}\,(e_{in})$	$1 - \frac{2\phi}{\pi}$	$\frac{2}{\pi} \sqrt{2 - 2 \cos 2\phi}$

TABLE 2

AMPLITUDE AND PHASE ANGLE OF DEMODULATOR REFERENCE

Demodulator Reference Transfer Function $G(s,\omega_p) = \frac{e_r(S)}{e_{in}(S)}$	Amplitude C of Demodulator Reference for $e_{in} = A \sin \omega_a t$	Phase Angle ϕ of Demodulator Reference for $e_{in} = A \sin \omega_a t$
High-Pass $\dfrac{\frac{S^2}{\omega_p^2}}{\frac{S^2}{\omega_p^2} + \frac{2\zeta_p S}{\omega_p} + 1}$	$\dfrac{A\omega_a^2}{\sqrt{\left(\omega_p^2 - \omega_a^2\right)^2 + (2\zeta_p\omega_a\omega_p)^2}}$	$180° - \tan^{-1} \dfrac{2\zeta_p\omega_a\omega_p}{\omega_p^2 - \omega_a^2}$
Low-Pass $\dfrac{-1}{\frac{S^2}{\omega_p^2} + \frac{2\zeta_p S}{\omega_p} + 1}$	$\dfrac{A\omega_p^2}{\sqrt{\left(\omega_p^2 - \omega_a^2\right)^2 + (2\zeta_p\omega_a\omega_p)^2}}$	$180° - \tan^{-1} \dfrac{2\zeta_p\omega_a\omega_p}{\omega_p^2 - \omega_a^2}$
All-Pass $\dfrac{\frac{S^2}{\omega_p^2} - 1}{\frac{S^2}{\omega_p^2} + \frac{2\zeta_p S}{\omega_p} + 1}$	$\dfrac{A\left(\omega_a^2 + \omega_p^2\right)}{\sqrt{\left(\omega_p^2 - \omega_a^2\right)^2 + (2\zeta_p\omega_a\omega_p)^2}}$	$180° - \tan^{-1} \dfrac{2\zeta_p\omega_a\omega_p}{\omega_p^2 - \omega_a^2}$

TABLE 3

AMPLITUDE OF DC COMPONENT OF DEMODULATOR OUTPUT $e_{in} = A \sin \omega_a t$

Demodulator Reference Transfer Function $G(s,\omega_p)$	Demodulator Type		
	Multiplier $e_d = e_r \cdot e_{in}$	Chopper $e_d = \text{SGN}\ (e_r) \cdot e_{in}$	Double Chopper $e_d = \text{SGN}\ (e_r) \cdot \text{SGN}\ (e_{in})$
High-Pass $\dfrac{\dfrac{S^2}{\omega_p^2}}{\dfrac{S^2}{\omega_p^2} + \dfrac{2\zeta_p S}{\omega_p} + 1}$	$\dfrac{A^2\omega_a^2\left(\omega_a^2 - \omega_p^2\right)}{2\left[\left(\omega_a^2 - \omega_p^2\right)^2 + (2\zeta_p\omega_a\omega_p)^2\right]}$	$\dfrac{2A\left(\omega_a^2 - \omega_p^2\right)}{\pi\sqrt{\left(\omega_a^2 - \omega_p^2\right)^2 + (2\zeta_p\omega_a\omega_p)^2}}$	$-1 + \dfrac{2}{\pi}\tan^{-1}\dfrac{2\zeta_p\omega_a\omega_p}{\omega_p^2 - \omega_a^2}$
Low-Pass $\dfrac{-1}{\dfrac{S^2}{\omega_p^2} + \dfrac{2\zeta_p S}{\omega_p} + 1}$	$\dfrac{A^2\omega_p^2\left(\omega_a^2 - \omega_p^2\right)}{2\left[\left(\omega_a^2 - \omega_p^2\right)^2 + (2\zeta_p\omega_a\omega_p)^2\right]}$	$\dfrac{2A\left(\omega_a^2 - \omega_p^2\right)}{\pi\sqrt{\left(\omega_a^2 - \omega_p^2\right)^2 + \left(2\zeta_p\omega_a\omega_p^2\right)^2}}$	$-1 + \dfrac{2}{\pi}\tan^{-1}\dfrac{2\zeta_p\omega_a\omega_p}{\omega_p^2 - \omega_a^2}$
All-Pass $\dfrac{\dfrac{S^2}{\omega_p^2} - 1}{\dfrac{S^2}{\omega_p^2} + \dfrac{2\zeta_p S}{\omega_p} + 1}$	$\dfrac{A^2\left(\omega_a^2 + \omega_p^2\right)\left(\omega_a^2 - \omega_p^2\right)}{2\left[\left(\omega_a^2 - \omega_p^2\right)^2 + (2\zeta_p\omega_a\omega_p)^2\right]}$	$\dfrac{2A\left(\omega_a^2 - \omega_p^2\right)}{\pi\sqrt{\left(\omega_a^2 - \omega_p^2\right)^2 + (2\zeta_p\omega_a\omega_p)^2}}$	$-1 + \dfrac{2}{\pi}\tan^{-1}\dfrac{2\zeta_p\omega_a\omega_p}{\omega_p^2 - \omega_a^2}$

TABLE 4

TRACKING TIME OF ADAPTIVE TRACKING FILTER WITH MULTIPLIER-TYPE DEMODULATOR $e_{in} = A \sin \omega_a t$

Demodulator Reference Transfer Function $G(s,\omega_p)$	Time for the Adaptive Tracking Filter to Track From $\frac{\omega_p}{\omega_a} = X_1$ to $\frac{\omega_p}{\omega_a} = X_2$
High-Pass $\dfrac{\frac{S^2}{\omega_p^2}}{\frac{S^2}{\omega_p^2} + \frac{2\zeta_p S}{\omega_p} + 1}$	$\frac{2\omega_a}{A^2K_a}\left[\left(1 - 4\zeta_p^2\right)(X_2 - X_1) - \frac{\left(X_2^3 - X_1^3\right)}{3} + 2\zeta_p^2 \text{ LN} \left\| \frac{(1 + X_2)(1 - X_1)}{(1 - X_2)(1 + X_1)} \right\| \right]$
Low-Pass $\dfrac{-1}{\frac{S^2}{\omega_p^2} + \frac{2\zeta_p S}{\omega_p} + 1}$	$\frac{2\omega_a}{A^2K_a}\left[-\left(\frac{1}{X_2} - \frac{1}{X_1}\right) - (X_2 - X_1) + 2\zeta_p^2 \text{ LN} \left\| \frac{(1 + X_2)(1 - X_1)}{(1 - X_2)(1 + X_1)} \right\| \right]$
All-Pass $\dfrac{\frac{S^2}{\omega_p^2} - 1}{\frac{S^2}{\omega_p^2} + \frac{2\zeta_p S}{\omega_p} + 1}$	$\frac{2\omega_a}{A^2K_a}\left[2\left(1 - \zeta_p^2\right)\left(\tan^{-1} X_2 - \tan^{-1} X_1\right) - (X_2 - X_1) + \zeta_p^2 \text{ LN} \left\| \frac{(1 + X_2)(1 - X_1)}{(1 - X_2)(1 + X_1)} \right\| \right]$

TABLE 5

TIME CONSTANT $\tau(\omega_o)$ OF LINEARIZED MODEL OF FREQUENCY TRACKING SYSTEM $e_{in} = A \sin (\omega_o + \delta\omega_a)t$

Demodulator Reference Transfer Function $G(s,\omega_p)$	Demodulator Type		
	Multiplier $e_d = e_r \cdot e_{in}$	Chopper $e_d = \text{SGN}(e_r) \cdot e_{in}$	Double Chopper $e_d = \text{SGN}(e_r) \cdot \text{SGN}(e_{in})$
High-Pass $\dfrac{\dfrac{S^2}{\omega_p^2}}{\dfrac{S^2}{\omega_p^2} + \dfrac{2\zeta_p S}{\omega_p} + 1}$	$\dfrac{4\zeta_p^2\omega_o}{A^2}$	$\dfrac{\pi\zeta_p\omega_o}{2A}$	$\dfrac{\pi\zeta_p\omega_o}{2}$
Low-Pass $\dfrac{-1}{\dfrac{S^2}{\omega_p^2} + \dfrac{2\zeta_p S}{\omega_p} + 1}$	$\dfrac{4\zeta_p^2\omega_o}{A^2}$	$\dfrac{\pi\zeta_p\omega_o}{2A}$	$\dfrac{\pi\zeta_p\omega_o}{2}$
All-Pass $\dfrac{\dfrac{S^2}{\omega_p^2} - 1}{\dfrac{S^2}{\omega_p^2} + \dfrac{2\zeta_p S}{\omega_p} + 1}$	$\dfrac{2\zeta_p^2\omega_o}{A^2}$	$\dfrac{\pi\zeta_p\omega_o}{2A}$	$\dfrac{\pi\zeta_p\omega_o}{2}$

TABLE 6

AMPLITUDE OF OUTPUT HARMONICS FOR A NOTCH FILTER

$$e_{in} = \sin(9t) + \sin(3t)$$

$$G(s,\omega_p) = \frac{\dfrac{S^2}{\omega_p^2} + 1}{\dfrac{S^2}{\omega_p^2} + \dfrac{2\zeta_p S}{\omega_p} + 1}$$

Tracking Gain K_a	Damping Ratio ζ_p	Average Filter Natural Frequency ω_{po}	Amplitude of Harmonics (rad/sec)			
			(3)	(9)	(15)	(21)
10	0.2	8.911	1.203	0.105	0.160	0.025
10	0.1	8.978	1.366	0.276	0.286	0.011
1	0.2	8.911	1.010	0.049	0.016	0.004
1	0.1	8.978	1.041	0.026	0.034	0.008

TABLE 7

DOMINANT S-IB STRUCTURAL MODE PARAMETERS (SA-201 VEHICLE)

Time	Mode	Frequency (rad/sec)	Deflection Station 100	Slope Station 1690 (meter^{-1})	Generalized Mass $(\text{kg-sec}^2/\text{meter})$
0	1B*	7.97	+0.2047	-0.01654	1142.7
	2B	16.18	-0.13782	+0.00787	2165.2
	4C*	16.18	-0.13778	+0.00787	2255.0
	5C	20.43	+0.18230	+0.01850	2151.7
40	1B	8.64	+0.1713	-0.01496	931.0
	2B	17.59	-0.16850	+0.01181	608.7
	5C	22.06	+0.2067	+0.01929	1591.8
80	1B	8.90	+0.13914	-0.01457	841.19
	2B	19.44	-0.09122	+0.01575	430.7
	3B	28.19	+0.77527	+0.01378	4904.7
100	1B	8.92	+0.1356	-0.01496	605.1
	2B	19.70	-0.06821	+0.01654	416.3
	3B	34.06	+0.9416	-0.00906	6759.0
140	1B	9.21	+0.2210	-0.01339	841.2
	2B	19.78	-0.06165	+0.01575	411.7
	3B	41.12	+0.2251	-0.03937	2953.3

*B - Bending Mode
C - Cluster Mode

APPENDIX A

HARMONIC ANALYSIS OF THE ADAPTIVE TRACKING FILTER

This appendix presents a harmonic analysis of the adaptive tracking filter for an input comprised of two sinusoidal signals. The analysis leads to an infinite set of linear algebraic equations for the amplitudes of the infinite number of harmonics in the output of the filter. Since the higher order harmonics tend to zero, they can be neglected, and a finite number of equations is obtained. A digital computer program is used to solve the resulting set of equations.

Figure A-1 is a simplified block diagram of the adaptive tracking filter. The differential equation of the filter can be obtained by writing the equations for the outputs of the two summing amplifiers and combining these equations using the rules for differential equation "multiplication". The two equations are:

$$\frac{-1}{\omega_p}\frac{d}{dt}\left(\frac{\dot{e}_1}{\omega_p}\right) = e_{in} + 2\zeta_p\frac{\dot{e}_1}{\omega_p} + e_1 \tag{A1}$$

$$-e_{out} = \lambda_a e_1 + \lambda_b\frac{\dot{e}_1}{\omega_p} + \frac{\lambda_c}{\omega_p}\frac{d}{dt}\left(\frac{\dot{e}_1}{\omega_p}\right) \tag{A2}$$

Rearranging (A1) and (A2) gives

$$-e_{in} = \frac{\ddot{e}_1}{\omega_p^2} + \left(\frac{2\zeta_p}{\omega_p} - \frac{\dot{\omega}_p}{\omega_p^3}\right)\dot{e}_1 + e_1 \tag{A3}$$

$$-e_{out} = \frac{\lambda_c}{\omega_p^2}\ddot{e}_1 + \left(\frac{\lambda_b}{\omega_p} - \frac{\lambda_c\dot{\omega}_p}{\omega_p^3}\right)\dot{e}_1 + \lambda_a e_1 \tag{A4}$$

If the filter were time invariant, the transfer function would be

$$\frac{e_{out}}{e_{in}} = \frac{\lambda_c S^2 + \lambda_b \omega_p S + \lambda_a \omega_p^2}{S^2 + 2\zeta_p \omega_p S + \omega_p^2} \tag{A5}$$

The differential equation for this case is

$$\ddot{e}_{out} + 2\zeta_p \omega_p \dot{e}_{out} + \omega_p^2 e_{out} = \lambda_c \ddot{e}_{in} + \lambda_b \omega_p \dot{e}_{in} + \lambda_a \omega_p^2 e_{in} \tag{A6}$$

It is possible to combine (A3) and (A4) to obtain a single differential equation for the adaptive tracking filter which is similar to (A6). Writing (A3) and (A4) in more general form:

$$e_{in} = \sum_{i=0}^{n} a_i(t) \frac{d^i e_1}{dt^i} \tag{A7}$$

$$e_{out} = \sum_{j=0}^{m} b_j(t) \frac{d^j e_1}{dt^j} \tag{A8}$$

The form of equation which is needed is

$$\sum_{k=0}^{m} h_k(t) \frac{d^k e_{out}}{dt^k} = \sum_{l=0}^{n} g_l(t) \frac{d^l e_{in}}{dt^l} \tag{A9}$$

Substituting (A7) and (A8) into (A9) results in an equation involving only e_1 and its derivatives. By equating the coefficients of each derivative a set of $m + n + 1$ equations is obtained for the $m + n + 2$ variables, $h_k(t)$ and $g_l(t)$. One of these variables can be set to one arbitrarily, since (A9) can always be divided by one of its coefficients.

The result of using the above procedure on (A3) and (A4) is the adaptive tracking filter differential equation:

$$\omega_p \ddot{e}_{out} + \left(2\zeta_p \omega_p^2 - \dot{\omega}_p\right) \dot{e}_{out} + \omega_p^3 e_{out}$$

$$= \lambda_c \omega_p \ddot{e}_{in} + \left(\lambda_b \omega_p^2 - \lambda_c \dot{\omega}_p\right) \dot{e}_{in} + \lambda_a \omega_p^3 e_{in} \qquad \text{(A10)}$$

For the purposes of this analysis, $\lambda_b = 2\zeta_z$ and $\lambda_a = \lambda_c = 1$. A further simplification is made by the substitution,

$$e_{out} = e_{in} + e \qquad \text{(A11)}$$

which, with the above λ values, reduces (A10) to:

$$\omega_p \ddot{e} + \left(2\zeta_p \omega_p^2 - \dot{\omega}_p\right) \dot{e} + \omega_p^3 e = 2(\zeta_z - \zeta_p)\, \omega_p^2 \dot{e}_{in} \qquad \text{(A12)}$$

The input is assumed to contain two sinusoidal signals with arbitrary amplitudes and phase angles and is given by the equation

$$e_{in} = A_1 \sin \omega_a t + A_2 \cos \omega_a t + B_1 \sin \omega_b t + B_2 \cos \omega_b t \qquad \text{(A13)}$$

The approach to be used is: determine the time-varying coefficients of (A12); assume a harmonic series solution for e in (A12), solve for the coefficients of this series by equating terms having the same frequency, and use (A11) to find the amplitudes of the output harmonics. For simplicity in computer programming, input frequencies are restricted to integer values unless the amplitude of one of the frequencies is zero.

It is convenient in what follows to represent all signals appearing in the filter by a single harmonic series in exponential form; e.g.,

$$X(t) = \sum_{i=1}^{k} x_i \exp\left(j n_{x_i} \omega t\right) \qquad \text{(A14)}$$

where ω is the largest common subharmonic of both ω_a and ω_b (i.e., $\omega_a = p\omega$ and $\omega_b = q\omega$, where p and q are integers). Since integer frequencies are used, this subharmonic always exists. The results of writing e_{in} and $\dot{e}_{in}$ in the form of (A14) are given by tables A1 and A2.

Unless the tracking loop gain is extremely high, harmonics in the demodulator reference are small compared to the input, and their influence on the frequency tracker can be neglected. Hence the assumption is made that the tracking loop is unaffected by the harmonics which are in the filter. The reference input to the demodulator e_r can then be approximated by evaluating the steady state transfer function between the input and the reference at the input frequencies. The transfer function is

$$F(j\omega_i) = \frac{-\omega_i^2}{\left(\omega_p^2 - \omega_i^2\right) + j2\zeta_p\omega_p\omega_i} \qquad \text{(A15)}$$

where ω_i is an input frequency. Table A3 summarizes the results of writing e_r as an exponential, harmonic series.

The demodulator output is the product of e_{in} and e_r, and it is related to the rate of change of filter frequency by a gain constant:

$$\dot{\omega}_p = K_a \cdot e_r \cdot e_{in} \qquad \text{(A16)}$$

The various frequency components of $\dot{\omega}_p$ are listed in table A4. The component identified by the * in this table must be zero for the steady state assumption to remain valid. Hence

$$(a_2c_1 + a_1c_2 + a_4c_3 + a_3c_4) = 0 \qquad \text{(A17)}$$

Evaluating (A17) in terms of the system parameters leads to the following polynomial which may be solved for ω_{po}, the average filter natural frequency.

$$\left(-A^2\omega_a^2 - B^2\omega_b^2\right)\omega_{po}^6 + \left(A^2\omega_a^4 + 2A^4\omega_a^2\omega_b^2 - 4A^2\zeta_p^2\omega_a^2\omega_b^2 + B^2\omega_b^4 + 2B^2\omega_a^2\omega_b^2 - 4B^2\zeta_p^2\omega_a^2\omega_b^2\right)\omega_{po}^4 + \left(-2A^2\omega_a^4\omega_b^2 + 4A^2\zeta_p^2\omega_a^4\omega_b^2 - A^2\omega_a^2\omega_b^4 - 2B^2\omega_a^2\omega_b^4 + 4B^2\zeta_p^2\omega_a^2\omega_b^4 - B^2\omega_a^4\omega_b^2\right)\omega_{po}^2 + \left(A^2\omega_a^4\omega_b^4 + B^2\omega_a^4\omega_b^4\right) = 0 \qquad \text{(A18)}$$

where,

$$A^2 = A_1^2 + A_2^2$$

$$B^2 = B_1^2 + B_2^2$$

The evaluation of ω_p, ω_p^2, ω_p^3 and $\omega_p^2\dot{e}_{in}$ is straightforward, and the result of this computation is given in tables A5, A6, A7, and A8.

Substituting these series into the system differential equation:

$$\left[\sum_{i=1}^{9} e_i \exp\left(jn_{e_i}\omega t\right)\right]\ddot{e} + \left[2\zeta_p \sum_{i=1}^{25} f_i \exp\left(jn_{f_i}\omega t\right) - \sum_{i=1}^{8} d_i \exp\left(jn_{d_i}\omega t\right)\right]\dot{e} + \left[\sum_{i=1}^{49} g_i \exp\left(jn_{g_i}\omega t\right)\right] e = 2(\zeta_z - \zeta_p)\left[\sum_{i=1}^{36} b_i \exp\left(jn_{b_i}\omega t\right)\right] \qquad \text{(A19)}$$

The unknown e is assumed to be expressible as a series of harmonics of the base frequency ω :

$$e = \sum_{n=-\infty}^{+\infty} c_n \exp\,(jn\omega t)$$

$$\dot{e} = \sum_{n=-\infty}^{+\infty} jn\omega c_n \exp\,(jn\omega t)$$

$$\ddot{e} = \sum_{n=-\infty}^{+\infty} -n^2\omega^2 c_n \exp\,(jn\omega t) \tag{A20}$$

Substituting (A20) into (A19):

$$\begin{aligned}
&-\omega^2 \sum_{i=1}^{9} \sum_{n=-\infty}^{+\infty} e_i n^2 c_n \exp\left[j\left(n + n_{e_i}\right)\omega t\right] \\
&+ j2\zeta_p\omega \sum_{i=1}^{25} \sum_{n=-\infty}^{+\infty} f_i n c_n \exp\left[j\left(n + n_{f_i}\right)\omega t\right] \\
&- j\omega \sum_{i=1}^{8} \sum_{n=-\infty}^{+\infty} d_i n c_n \exp\left[j\left(n + n_{d_i}\right)\omega t\right] \\
&+ \sum_{i=1}^{49} \sum_{n=-\infty}^{+\infty} g_i c_n \exp\left[j\left(n + n_{g_i}\right)\omega t\right] \\
&= 2(\zeta_z - \zeta_p) \sum_{i=1}^{36} b_i \exp\left(jn_{b_i}\omega t\right)
\end{aligned} \tag{A21}$$

This equation can be solved by equating coefficients of the same frequency. To do this, it is first necessary to shift the infinite series on the left hand side of the equation in such a way that a single frequency will result for any value of n. For example, the first term above with $i = 1$ and $m = n + n_{e1}$ becomes:

$$-\omega^2 \sum_{n=-\infty}^{+\infty} e_1 n^2 c_n \exp\left[j\left(n + n_{e_1}\right)\omega t\right] \xrightarrow{m = n + n_{e_1}}$$

$$-\omega^2 \sum_{m=-\infty}^{+\infty} e_1 \left(m - n_{e_1}\right)^2 c_{m - n_{e_1}} \exp\left(jm\omega t\right) \tag{A22}$$

Since m is a dummy variable, and its range is infinite, it can be renamed "n".

Shifting all the infinite series in (A21):

$$-\omega^2 \sum_{n=-\infty}^{+\infty} \sum_{i=1}^{9} e_i \left(n - n_{e_1}\right)^2 c_{n - n_{e_i}} \exp\left(jn\omega t\right)$$

$$+ j2\zeta_p\omega \sum_{n=-\infty}^{+\infty} \sum_{i=1}^{25} f_i \left(n - n_{f_i}\right) c_{n - n_{f_i}} \exp\left(jn\omega t\right)$$

$$- j\omega \sum_{n=-\infty}^{+\infty} \sum_{i=1}^{8} d_i \left(n - n_{d_i}\right) c_{n - n_{d_i}} \exp\left(jn\omega t\right)$$

$$+ \sum_{n=-\infty}^{+\infty} \sum_{i=1}^{49} g_i c_{n - n_{g_i}} \exp\left(jn\omega t\right)$$

$$= 2\left(\zeta_z - \zeta_p\right) \sum_{i=1}^{36} b_i \exp\left(jn_{b_i}\omega t\right) \tag{A23}$$

Equation (A23), evaluated for each value of n, is a linear algebraic equation in up to 91 (=9+25+8+49) unknowns, depending on how many of the terms n_{e_1}, n_{f_1}, -- are different. The set of equations obtained by equating the coefficients of like frequencies (letting n assume various values) may be written in matrix form:

$$\begin{array}{c} \cdot \\ \cdot \\ \cdot \\ n = 1 \\ n = 0 \\ n = -1 \\ \cdot \\ \cdot \\ \cdot \end{array} \left[\begin{array}{ccccc} & \cdot & \cdot & \cdot & \\ & \cdot & \cdot & \cdot & \\ & \cdot & \cdot & \cdot & \\ \cdots & y_{1,-1} & y_{1,0} & y_{1,1} & \cdots \\ \cdots & y_{0,-1} & y_{0,0} & y_{0,1} & \cdots \\ \cdots & y_{-1,-1} & y_{-1,0} & y_{-1,1} & \cdots \\ & \cdot & \cdot & \cdot & \\ & \cdot & \cdot & \cdot & \\ & \cdot & \cdot & \cdot & \end{array} \right] \times \left[\begin{array}{c} \cdot \\ \cdot \\ \cdot \\ c_1 \\ c_0 \\ c_{-1} \\ \cdot \\ \cdot \\ \cdot \end{array} \right] = \left[\begin{array}{c} \cdot \\ \cdot \\ \cdot \\ x_1 \\ x_0 \\ x_{-1} \\ \cdot \\ \cdot \\ \cdot \end{array} \right] \qquad (A24)$$

It is impractical to write a general expression for the $y_{i,j}$ and x_i above, since in a given problem, many of the terms in (A23) will combine. For example, if $\omega_a = 3$, $\omega_b = 1$ then $p = 3$, $q = 1$, and $\omega = 1$. Referring to table A6, note that such terms as $n_{f_3} = -3p + q$ and $n_{f_4} = -2p - 2q$ are the same in this problem. Thus the terms $j2\zeta_p \omega f_3 (n - n_{f_3})$ and $j2 \, _p\omega f_4 (n - n_{f_4})$ in (A23) will add with other terms to form the matrix coefficient of the nth row and the $n - n_{f_3} = n - n_{f_4} = ---$ $n + 8$th column. Note that in this matrix the row and column indexing starts at the center.

While the infinite matrix equation determines all unknown harmonic amplitudes (c_n), only the first few harmonics are of interest. Since the higher order harmonics tend toward zero, the matrix may be truncated at some n_{max} to obtain the lower harmonics. The method used has been to increase n_{max} until the amplitude of the highest harmonic of interest does not change significantly as n_{max} is further increased.

The computational difficulty in evaluating the matrix equation and solving it for the c's, has been overcome with the use of a digital computer. The program, written in Fortran IV for the UNIVAC 1107 , first computes the value of all the variables given in tables A1 through A8. Then for each matrix element $y_{i,j}$, tables A1 through A7 are searched for harmonics corresponding to the row and column being computed. When a match is found, the $y_{i,j}$ element value is increased by the table value multiplied by the appropriate coefficient in equation (A23). The right-hand side of the matrix equation is similarly computed by searching table A8, multiplying the table value by $2(\zeta_z - \zeta_p)$, and adding the result to the appropriate x_i element value. The matrix equation is solved using conventional techniques.

Results of using this program, for both a single-frequency input and the two-frequency input, are presented in the main body of this report.

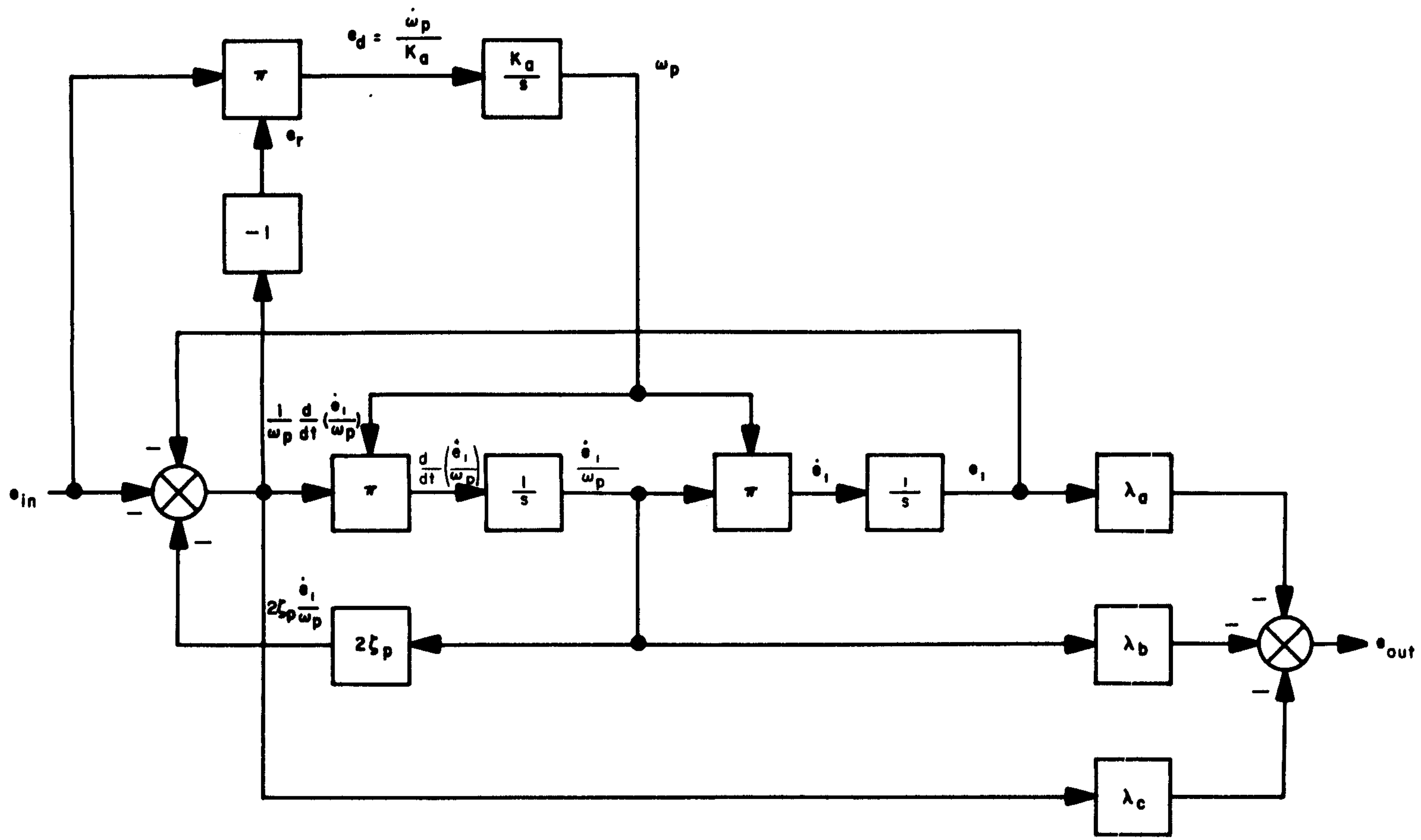

Figure A1. Block Diagram for Derivation of Adaptive Tracking Filter Differential Equation

TABLE A1

$$e_{in} = \sum_{i=1}^{4} a_i \exp\left(jn_{a_i}\omega t\right)$$

i	n_{a_i}	a_i
1	$+p$	$A_2/2 - jA_1/2$
2	$-p$	$A_2/2 + jA_1/2$
3	$+q$	$B_2/2 - jB_1/2$
4	$-q$	$B_2/2 + jB_1/2$

TABLE A2

$$e_{in} = \sum_{i=1}^{4} h_i \exp\left(jn_{h_i}\omega t\right)$$

i	n_{h_i}	h_i
1	$+p$	$jn_{a_1}\omega a_1$
2	$-p$	$jn_{a_2}\omega a_2$
3	$+q$	$jn_{a_3}\omega a_3$
4	$-q$	$jn_{a_4}\omega a_4$

TABLE A3

$e_r = \sum_{i=1}^{4} c_i \exp\left(jn_{c_i}\omega t\right)$		
i	n_{c_i}	c_i
1	+p	$a_1 F\left(jn_{a_1}\omega\right)$
2	-p	$a_2 F\left(jn_{a_2}\omega\right)$
3	+q	$a_3 F\left(jn_{a_3}\omega\right)$
4	-q	$a_4 F\left(jn_{a_4}\omega\right)$

TABLE A4

$$\dot{\omega}_p = \sum_{i=1}^{8} d_i \exp\left(j n_{d_i} \omega t\right)$$		
i	n_{d_i}	d_i
1	$+2p$	$K_a a_1 c_1$
2	$-2p$	$K_a a_2 c_2$
3	$+2q$	$K_a a_3 c_3$
4	$-2q$	$K_a a_4 c_4$
5	$+p \quad +q$	$K_a \left(a_3 c_1 + a_1 c_3\right)$
6	$-p \quad -q$	$K_a \left(a_4 c_2 + a_2 c_4\right)$
7	$+p \quad -q$	$K_a \left(a_4 c_1 + a_1 c_4\right)$
8	$-p \quad +q$	$K_a \left(a_3 c_2 + a_2 c_3\right)$
*	0	$K_a \left(a_2 c_1 + a_1 c_2 + a_4 c_3 + a_3 c_4\right)$

TABLE A5

$\omega_p = \sum_{i=1}^{9} e_i \exp\left(j n_{e_i} \omega t\right)$		
i	n_{e_i}	e_i
1	0	ω_{po}
2	$+2p$	$d_1/j\ n_{d_1}\omega$
3	$-2p$	$d_2/j\ n_{d_2}\omega$
4	$+2q$	$d_3/j\ n_{d_3}\omega$
5	$-2q$	$d_4/j\ n_{d_4}\omega$
6	$+p \quad +q$	$d_5/j\ n_{d_5}\omega$
7	$-p \quad -q$	$d_6/j\ n_{d_6}\omega$
8	$+p \quad -q$	$d_7/j\ n_{d_7}\omega$
9	$-p \quad +q$	$d_8/j\ n_{d_8}\omega$

TABLE A6

$$\omega_p^2 = \sum_{i=1}^{25} f_i \exp\left(jn_{f_i}\omega t\right)$$

i	n_{f_i}	f_i
1	$-4p$	e_3^2
2	$-3p \quad -q$	$2e_3e_7$
3	$-3p \quad +q$	$2e_3e_9$
4	$-2p \quad -2q$	$2e_3e_5 + e_7^2$
5	$-2p$	$2e_1e_3 + 2e_7e_9$
6	$-2p \quad +2q$	$2e_3e_4 + e_9^2$
7	$-p \quad -3q$	$2e_5e_7$
8	$-p \quad -q$	$2e_1e_7 + 2e_3e_8 + 2e_5e_9$
9	$-p \quad +q$	$2e_1e_9 + 2e_3e_6 + 2e_4e_7$
10	$-p \quad +3q$	$2e_4e_9$
11	$-4q$	e_5^2
12	$-2q$	$2e_1e_5 + 2e_7e_8$
13	0	$e_1^2 + 2e_2e_3 + 2e_4e_5 + 2e_6e_7 + 2e_8e_9$
14	$2q$	$2e_1e_4 + 2e_6e_9$

TABLE A6. - Concluded

i	n_{f_i}	f_i
15	$4q$	e_4^2
16	$p \quad -3q$	$2e_5e_8$
17	$p \quad -q$	$2e_1e_8 + 2e_2e_7 + 2e_5e_6$
18	$p \quad +q$	$2e_1e_6 + 2e_2e_9 + 2e_4e_8$
19	$p \quad +3q$	$2e_4e_6$
20	$2p \quad -2q$	$2e_2e_5 + e_8^2$
21	$2p$	$2e_1e_2 + 2e_6e_8$
22	$2p \quad +2q$	$2e_2e_4 + e_6^2$
23	$3p \quad -q$	$2e_2e_8$
24	$3p \quad +q$	$2e_2e_6$
25	$4p$	e_2^2

TABLE A7

$$\omega_p^3 = \sum_{i=1}^{49} g_i \exp\left(jn_{g_i}\omega t\right)$$

i	n_{g_i}	g_i
1	$-6p$	e_3f_1
2	$-5p \quad -q$	$e_3f_2 + e_7f_1$
3	$-5p \quad +q$	$e_3f_3 + e_9f_1$
4	$-4p \quad -2q$	$e_3f_4 + e_5f_1 + e_7f_2$
5	$-4p$	$e_3f_5 + e_1f_1 + e_7f_3 + e_9f_2$
6	$-4p \quad +2q$	$e_3f_6 + e_4f_1 + e_9f_3$
7	$-3p \quad -3q$	$e_3f_7 + e_5f_2 + e_7f_4$
8	$-3p \quad -q$	$e_3f_8 + e_1f_2 + e_5f_3 + e_7f_5 + e_8f_1 + e_9f_4$
9	$-3p \quad +q$	$e_3f_9 + e_1f_3 + e_4f_2 + e_6f_1 + e_7f_6 + e_9f_5$
10	$-3p \quad +3q$	$e_3f_{10} + e_4f_3 + e_9f_6$
11	$-2p \quad -4q$	$e_3f_{11} + e_5f_4 + e_7f_7$
12	$-2p \quad -2q$	$e_3f_{12} + e_1f_4 + e_5f_5 + e_7f_8 + e_8f_2$ $+ e_9f_7$
13	$-2p$	$e_3f_{13} + e_1f_5 + e_2f_1 + e_4f_4 + e_5f_6$ $+ e_6f_2 + e_7f_9 + e_8f_3 + e_9f_8$

TABLE A7. – Continued

i	n_{g_i}		g_i
14	$-2p$	$+2q$	$e_3f_{14} + e_1f_6 + e_4f_5 + e_6f_3 + e_7f_{10} + e_9f_9$
15	$-2p$	$+4q$	$e_3f_{15} + e_4f_6 + e_9f_{10}$
16	$-p$	$-5q$	$e_5f_7 + e_7f_{11}$
17	$-p$	$-3q$	$e_1f_7 + e_3f_{16} + e_5f_8 + e_7f_{12} + e_8f_4 + e_9f_{11}$
18	$-p$	$-q$	$e_1f_8 + e_2f_2 + e_3f_{17} + e_4f_7 + e_5f_9 + e_6f_4 + e_7f_{13} + e_8f_5 + e_9f_{12}$
19	$-p$	$+q$	$e_1f_9 + e_2f_3 + e_3f_{18} + e_4f_8 + e_5f_{10} + e_6f_5 + e_7f_{14} + e_8f_6 + e_9f_{13}$
20	$-p$	$+3q$	$e_1f_{10} + e_3f_{19} + e_4f_9 + e_6f_6 + e_7f_{15} + e_9f_{14}$
21	$-p$	$+5q$	$e_4f_{10} + e_9f_{15}$
22		$-6q$	e_5f_{11}
23		$-4q$	$e_1f_{11} + e_5f_{12} + e_7f_{16} + e_8f_7$
24		$-2q$	$e_1f_{12} + e_2f_4 + e_3f_{20} + e_4f_{11} + e_5f_{13} + e_6f_7 + e_7f_{17} + e_8f_8 + e_9f_{16}$

TABLE A7. – Continued

i	n_{g_i}	g_i
25	0	$e_1f_{13} + e_2f_5 + e_3f_{21} + e_4f_{12} + e_5f_{14} + e_6f_8 + e_7f_{18} + e_8f_9 + e_9f_{17}$
26	2q	$e_1f_{14} + e_2f_6 + e_3f_{22} + e_4f_{13} + e_5f_{15} + e_6f_9 + e_7f_{19} + e_8f_{10} + e_9f_{18}$
27	4q	$e_1f_{15} + e_4f_{14} + e_6f_{10} + e_9f_{19}$
28	6q	e_4f_{15}
29	p -5q	$e_5f_{16} + e_8f_{11}$
30	p -3q	$e_1f_{16} + e_2f_7 + e_5f_{17} + e_6f_{11} + e_7f_{20} + e_8f_{12}$
31	p -q	$e_1f_{17} + e_2f_8 + e_3f_{23} + e_4f_{16} + e_5f_{18} + e_6f_{12} + e_7f_{21} + e_8f_{13} + e_9f_{20}$
32	p +q	$e_1f_{18} + e_2f_9 + e_3f_{24} + e_4f_{17} + e_5f_{19} + e_6f_{13} + e_7f_{22} + e_8f_{14} + e_9f_{21}$
33	p +3q	$e_1f_{19} + e_2f_{10} + e_4f_{18} + e_6f_{14} + e_8f_{15} + e_9f_{22}$
34	p +5q	$e_4f_{19} + e_6f_{15}$
35	2p -4q	$e_2f_{11} + e_5f_{20} + e_8f_{16}$

TABLE A7. - Continued

i	n_{g_i}	g_i
36	$2p \quad -2q$	$e_1f_{20} + e_2f_{12} + e_5f_{21} + e_6f_{16} + e_7f_{23} + e_8f_{17}$
37	$2p$	$e_1f_{21} + e_2f_{13} + e_3f_{25} + e_4f_{20} + e_5f_{22} + e_6f_{17} + e_7f_{24} + e_8f_{18} + e_9f_{23}$
38	$2p \quad +2q$	$e_1f_{22} + e_2f_{14} + e_4f_{21} + e_6f_{18} + e_8f_{19} + e_9f_{24}$
39	$2p \quad +4q$	$e_2f_{15} + e_4f_{22} + e_6f_{19}$
40	$3p \quad -3q$	$e_2f_{16} + e_5f_{23} + e_8f_{20}$
41	$3p \quad -q$	$e_1f_{23} + e_2f_{17} + e_5f_{24} + e_6f_{20} + e_7f_{25} + e_8f_{21}$
42	$3p \quad +q$	$e_1f_{24} + e_2f_{18} + e_4f_{23} + e_6f_{21} + e_8f_{22} + e_9f_{25}$
43	$3p \quad +3q$	$e_2f_{19} + e_4f_{24} + e_6f_{22}$
44	$4p \quad -2q$	$e_2f_{20} + e_5f_{25} + e_8f_{23}$
45	$4p$	$e_1f_{25} + e_2f_{21} + e_6f_{23} + e_8f_{24}$

TABLE A7. – Concluded

i	n_{g_i}	g_i
46	$4p \quad +2q$	$e_2f_{22} + e_4f_{25} + e_6f_{24}$
47	$5p \quad -q$	$e_2f_{23} + e_8f_{25}$
48	$5p \quad +q$	$e_2f_{24} + e_6f_{25}$
48	$6p$	e_2f_{25}

TABLE A8

$$\omega_p^2 \dot{e} = \sum_{i=1}^{36} b_i \exp\left(j n_{b_i} \omega t\right)$$

i	n_{b_i}	b_i
1	$-5p$	h_2f_1
2	$-4p \quad -q$	$h_2f_2 + h_4f_1$
3	$-4p \quad +q$	$h_2f_3 + h_3f_1$
4	$-3p \quad -2q$	$h_2f_4 + h_4f_2$
5	$-3p$	$h_1f_1 + h_2f_5 + h_3f_2 + h_4f_3$
6	$-3p \quad +2q$	$h_2f_6 + h_3f_3$
7	$-2p \quad -3q$	$h_2f_7 + h_4f_4$
8	$-2p \quad -q$	$h_1f_2 + h_2f_8 + h_3f_4 + h_4f_5$

TABLE A8. – Continued

i	n_{b_i}	b_i
9	$-2p \quad +q$	$h_1f_3 + h_2f_9 + h_3f_5 + h_4f_6$
10	$-2p \quad +3q$	$h_2f_{10} + h_3f_6$
11	$-p \quad -4q$	$h_2f_{11} + h_4f_7$
12	$-p \quad -2q$	$h_1f_4 + h_2f_{12} + h_3f_7 + h_4f_8$
13	$-p$	$h_1f_5 + h_2f_{13} + h_3f_8 + h_4f_9$
14	$-p \quad +2q$	$h_1f_6 + h_2f_{14} + h_3f_9 + h_4f_{10}$
15	$-p \quad +4q$	$h_2f_{15} + h_3f_{10}$
16	$-5q$	h_4f_{11}
17	$-3q$	$h_1f_7 + h_2f_{16} + h_3f_{11} + h_4f_{12}$
18	$-q$	$h_1f_8 + h_2f_{17} + h_3f_{12} + h_4f_{13}$
19	q	$h_1f_9 + h_2f_{18} + h_3f_{13} + h_4f_{14}$
20	$3q$	$h_1f_{10} + h_2f_{19} + h_3f_{14} + h_4f_{15}$
21	$5q$	h_3f_{15}
22	$p \quad -4q$	$h_1f_{11} + h_4f_{16}$
23	$p \quad -2q$	$h_1f_{12} + h_2f_{20} + h_3f_{16} + h_4f_{17}$
24	p	$h_1f_{13} + h_2f_{21} + h_3f_{17} + h_4f_{18}$
25	$p \quad +2q$	$h_1f_{14} + h_2f_{22} + h_3f_{18} + h_4f_{19}$

TABLE A8. - Concluded

i	n_{b_i}	b_i
26	$p + 4q$	$h_1 f_{15} + h_3 f_{19}$
27	$2p - 3q$	$h_1 f_{16} + h_4 f_{20}$
28	$2p - q$	$h_1 f_{17} + h_2 f_{23} + h_3 f_{20} + h_4 f_{21}$
29	$2p + q$	$h_1 f_{18} + h_2 f_{24} + h_3 f_{21} + h_4 f_{22}$
30	$2p + 3q$	$h_1 f_{19} + h_3 f_{22}$
31	$3p - 2q$	$h_1 f_{20} + h_4 f_{23}$
32	$3p$	$h_1 f_{21} + h_2 f_{25} + h_3 f_{23} + h_4 f_{24}$
33	$3p + 2q$	$h_1 f_{22} + h_3 f_{24}$
34	$4p - q$	$h_1 f_{23} + h_4 f_{25}$
35	$4p + q$	$h_1 f_{24} + h_3 f_{25}$
36	$5p$	$h_1 f_{25}$

APPENDIX B

S-IB-201 VEHICLE EQUATIONS AND DATA

Vehicle equations and data used in the Phase I study were supplied by Marshall Space Flight Center. With the one exception of assuming all aerodynamic loading to be concentrated at the rigid body aerodynamic center of pressure, the equations used are identical to the complete set of pitch-yaw equations appearing in NASA memo no. R-ASTR-F-65-6.

Figure B-1 defines the relevant vehicle geometry; figures B-2 and B-3 define the rigid body and bending coordinate system employed. The complete set of vehicle pitch plane equations are as follows:

Pitching Moment Equation:

$$\ddot{\phi} = -C_1\alpha - C_2\beta + \frac{57.3\ F}{I_x}\sum_i \left[l_G Y_i'(x_G) - Y_i(x_G) \right] \eta_i$$

$$+ \frac{57.3}{I_x}\sum_k m_{sk} l_{sk} \ddot{\xi}_k + \frac{57.3(F - D)}{I_x}\sum_k \frac{m_{sk}}{m}\xi_k \qquad \text{(B1)}$$

Acceleration of Vehicle C.G. Normal to Flight Path:

$$\ddot{Z} = \frac{F - D}{57.3\ m}\phi_R + \frac{R'}{57.3\ m}\beta + \frac{qSC_{N_\alpha}\alpha}{57.3\ m} - \sum_i \frac{F}{m} Y_i'(x_G)\eta_i$$

$$- \sum_k \frac{m_{sk}}{m}\ddot{\xi}_k \qquad \text{(B2)}$$

Sloshing Equation (k^{th} slosh mode):

$$\ddot{\xi}_k = -2\zeta_{sk}\omega_{sk}\dot{\xi}_k - \omega_{sk}^2\xi_k + \frac{l_{sk}}{57.3}\ddot{\phi}_R + \frac{F - D}{57.3\ m}\phi_R$$

$$- \ddot{Z} - \sum_i Y_i\ (x_{sk})\ \ddot{\eta}_i \qquad \text{(B3)}$$

Bending Equation (i^{th} mode):

$$\ddot{\eta}_i = -2\zeta_{Bi}\omega_{Bi}\dot{\eta}_i - \omega_{Bi}^2\eta_i + \frac{R'Y_i\ (x_G)}{57.3\ M_i}\beta$$

$$+ \frac{S_E Y_i\ (x_G) + I_E Y_i'\ (x_G)}{57.3\ M_i}\ddot{\beta} - \sum_k \frac{m_{sk}}{M_i} Y_i\ (x_{sk})\ \ddot{\xi}_k$$

$$+ \frac{qSC_{N_\alpha}}{57.3\ M_i} Y_i\ (x_{CP})\ \alpha + \frac{qSC_{N_\alpha}}{57.3\ M_i} Y_i\ (x_{CP}) \sum_j Y_j'\ (x_{CP})\ \eta_j$$

$$+ \frac{F}{M_i} Y_i\ (x_G) \sum_j Y_j'\ (x_G)\ \eta_j \qquad \text{(B4)}$$

Control Sensor Equations (At Instrument Unit):

Attitude Gyro:

$$\phi = \phi_R - 57.3 \sum_i Y_i'\ (x_{IU})\ \eta_i \qquad \text{(B5)}$$

Rate Gyro:

$$\dot{\phi} = \dot{\phi}_R - 57.3 \sum_i Y_i'\ (x_{IU})\ \dot{\eta}_i \qquad \text{(B6)}$$

Accelerometer:

$$\ddot{Y}_T = \frac{qSC_{N_\alpha}}{57.3\ m}\alpha + \frac{R'}{57.3\ m}\beta - \frac{l_A}{57.3}\ddot{\phi}_R + \sum_i Y_i\ (x_{IU})\ \ddot{\eta}_i$$

$$- \sum_i \left[\frac{FY_i'\ (x_G)}{m} - \frac{F - D}{m} Y_i'\ (x_{IU})\right] \eta_i - \sum_k \frac{m_{sk}}{m}\ddot{\xi}_k \qquad \text{(B7)}$$

Angle of Attack:

$$\alpha = \phi_R + \alpha_W - 57.3 \frac{\ddot{Z}}{V_m} \qquad \text{(B8)}$$

These equations were used for all point trajectory studies. For the launch trajectory simulation, certain simplifications were required to fit the problem on a single fully-complemented EAI 231-R analog computer. This was accomplished by eliminating nonessential coupling terms. The equations thus simplified are as follows:

Pitching Moment Equation:

$$\ddot{\phi}_R = -C_1\alpha - C_2\beta + \frac{57.3\ F}{I_x}\left[l_G Y_1'\ (x_G) - Y_1\ (x_G)\right]\eta_1$$

$$+ \frac{57.3}{I_x}\sum_k m_{sk} l_{sk}\ddot{\xi}_x + \frac{57.3\ (F - D)}{I_x}\sum_k \frac{m_{sk}}{m}\xi_k \qquad \text{(B9)}$$

Acceleration of Vehicle C.G. Normal to Flight Path:

$$\ddot{Z} = \frac{F - D}{57.3\ m}\phi_R + \frac{R'}{57.3\ m}\beta + \frac{qSC_{N_\alpha}\alpha}{57.3\ m} - \sum_k \frac{m_{sk}}{m}\ddot{\xi}_k \qquad \text{(B10)}$$

Sloshing Equation:

$$\ddot{\xi}_k = -2\zeta_{sk}\omega_{sk}\dot{\xi}_k - \omega_{sk}^2\xi_k + \frac{l_{sk}}{57.3}\ddot{\phi}_R + \frac{F - D}{57.3\ m}\phi_R - \ddot{Z} - Y_1\ (x_{sk})\ \ddot{\eta}_1 \qquad \text{(B11)}$$

First Mode Bending Equation:

$$\ddot{\eta}_1 = -2\zeta_{B1}\omega_{B1}\dot{\eta}_1 - \omega_{B1}^2\eta_1 + \frac{R'Y_1\ (x_G)}{57.3\ M_1}\beta + \frac{S_E Y_1\ (x_G) + I_E Y_1'\ (x_G)}{57.3\ M_1}\ddot{\beta} - \sum_k \frac{m_{sk}}{M_1} Y_1\ (x_{sk})\ \ddot{\xi}_k \qquad \text{(B12)}$$

$(i + 1)^{th}$ Mode Bending Equation:

$$\ddot{\eta}_{i+1} = -2\zeta_{Bi+1}\omega_{Bi+1}\dot{\eta}_{i+1} - \omega_{Bi+1}^2\eta_{i+1} + \frac{R'Y_{i+1}\ (x_G)}{57.3\ M_{i+1}}\beta + \frac{S_E Y_{i+1}\ (x_G) + I_E Y_{i+1}'\ (x_G)}{57.3\ M_{i+1}}\ddot{\beta} \qquad \text{(B13)}$$

Control Sensor Equations:

Attitude Gyro:

$$\phi = \phi_R - 57.3 \sum_i Y_i'\ (x_{IU})\ \eta_i \qquad \text{(B14)}$$

Rate Gyro:

$$\dot{\phi} = \dot{\phi}_R - 57.3 \sum_i Y_i'\ (x_{IU})\ \dot{\eta}_i \qquad \text{(B15)}$$

Accelerometer:

$$\ddot{Y}_T = \frac{qSC_{N_\alpha}\alpha}{57.3\ m} + \frac{R'}{57.3\ m}\beta - \frac{l_A}{57.3}\ddot{\phi}_R - \sum_i \left[\frac{FY_i'\ (x_G)}{m}\right]\eta_i - \sum_k \frac{m_{sk}}{m}\ddot{\xi}_k \tag{B16}$$

Angle of Attack:

$$\alpha = \phi_R + \alpha_W - 57.3\ \frac{\dot{Z}}{V_m} \tag{B17}$$

Data was supplied for the S-IB-201 vehicle payload combination. All structural mode data was obtained from NASA memo no. R-ASTR-F-65-6. As a result of reviewing this data, it was determined that the bending problem was adequately described by the first three bending modes (1B, 2B, 3B) and the fourth and fifth tank cluster modes (4C, 5C). This determination was made by assuming that each mode was uncoupled and being forced at its natural frequency by the control engines. The relative amplitude of each mode detected by a rate sensor located at the instrument unit (Sta 1690) was then used as an indication of the relative significance of each mode. This relationship, readily obtained from equations (B4) and (B6), is

$$\dot{\eta}_i\ (IU) = R'\beta\ \frac{Y_i\ (x_G)}{57.3\ M_i}\ \frac{1}{2\zeta_{Bi}\omega_{Bi}}\ Y_i'\ (x_{IU}) \tag{B18}$$

By assuming a unit thrust amplitude $(R'\beta = 1)$ and a damping ratio of 0.01 for all modes, this relationship simplifies to

$$\dot{\eta}_i\ (I_U) = \frac{Y_i\ (x_G)}{M_i\omega_{Bi}}\ Y_i'\ (x_{IU}) \tag{B19}$$

Not all of the five modes are equally significant at each flight time. For the critical flight times at which point trajectory studies were conducted, the modes listed below are the most significant, and were consequently those used for the point studies.

T = 0	1B 2B 4C 5C
T = 40	1B 2B 5C
T = 80	1B 2B 3B
T = 100	1B 2B 3B
T = 140	1B 2B 3B

The assumption of uncoupled modes is invalidated when the control system loop is closed. However, the inherent attenuation resulting from compensation networks and the actuation system tend to increase the frequency weighting, thus further reducing the significance of the higher frequency modes.

Propellant slosh mode data was obtained from NASA memo no. R-ASTR-F-65-6. A review of this data indicated that the dominant slosh mode was that of the SIV-B Lox tank. This was verified by examining the effect of each slosh mode on the first mode bending frequency. The amount by which the first mode frequency changed was used as an indication of the relative coupling of each slosh mode.

The complete set of data used in the Phase I study is summarized in tables B1 through B8. Included are the five structural modes previously noted and the SIV-B slosh mode.

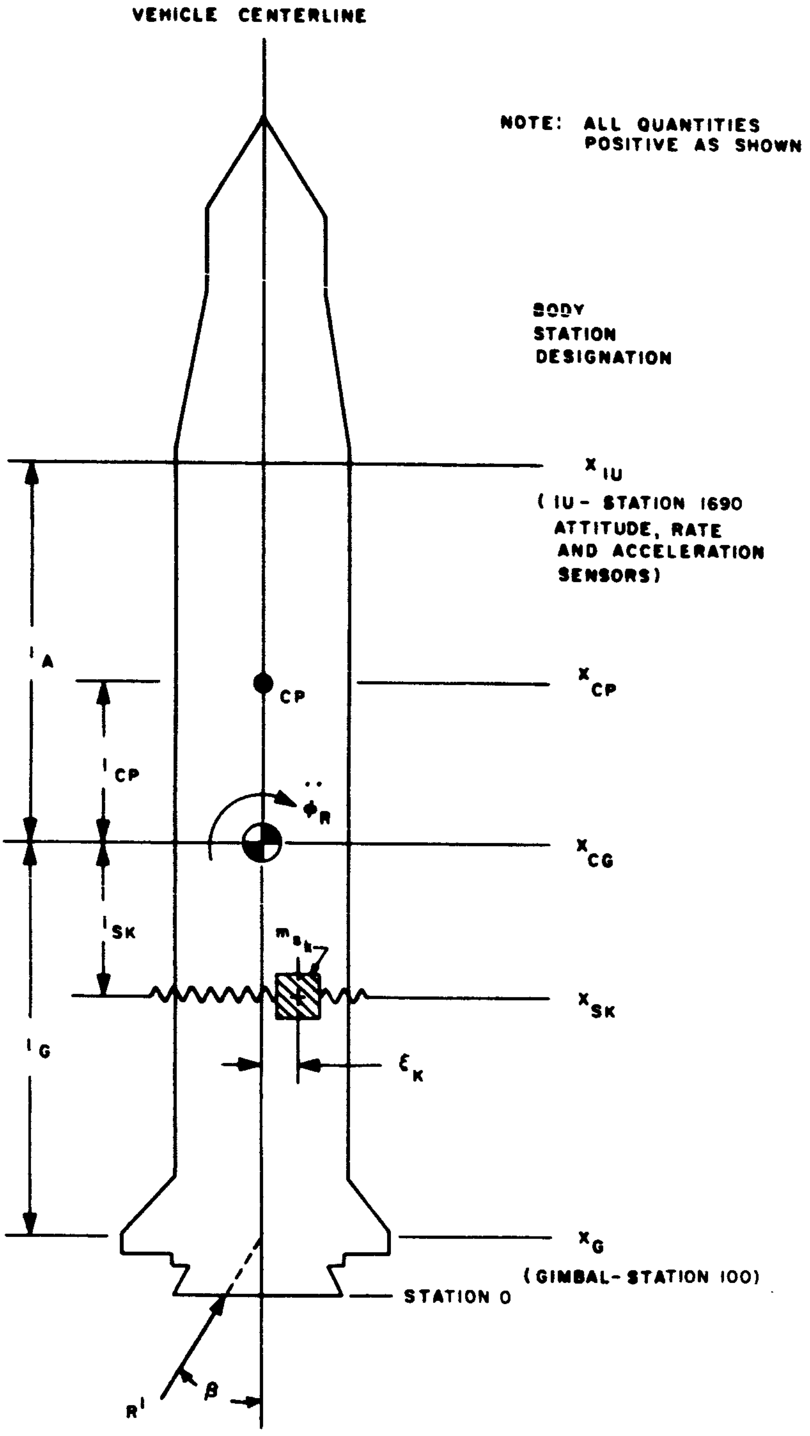

Figure B1. Vehicle Geometry

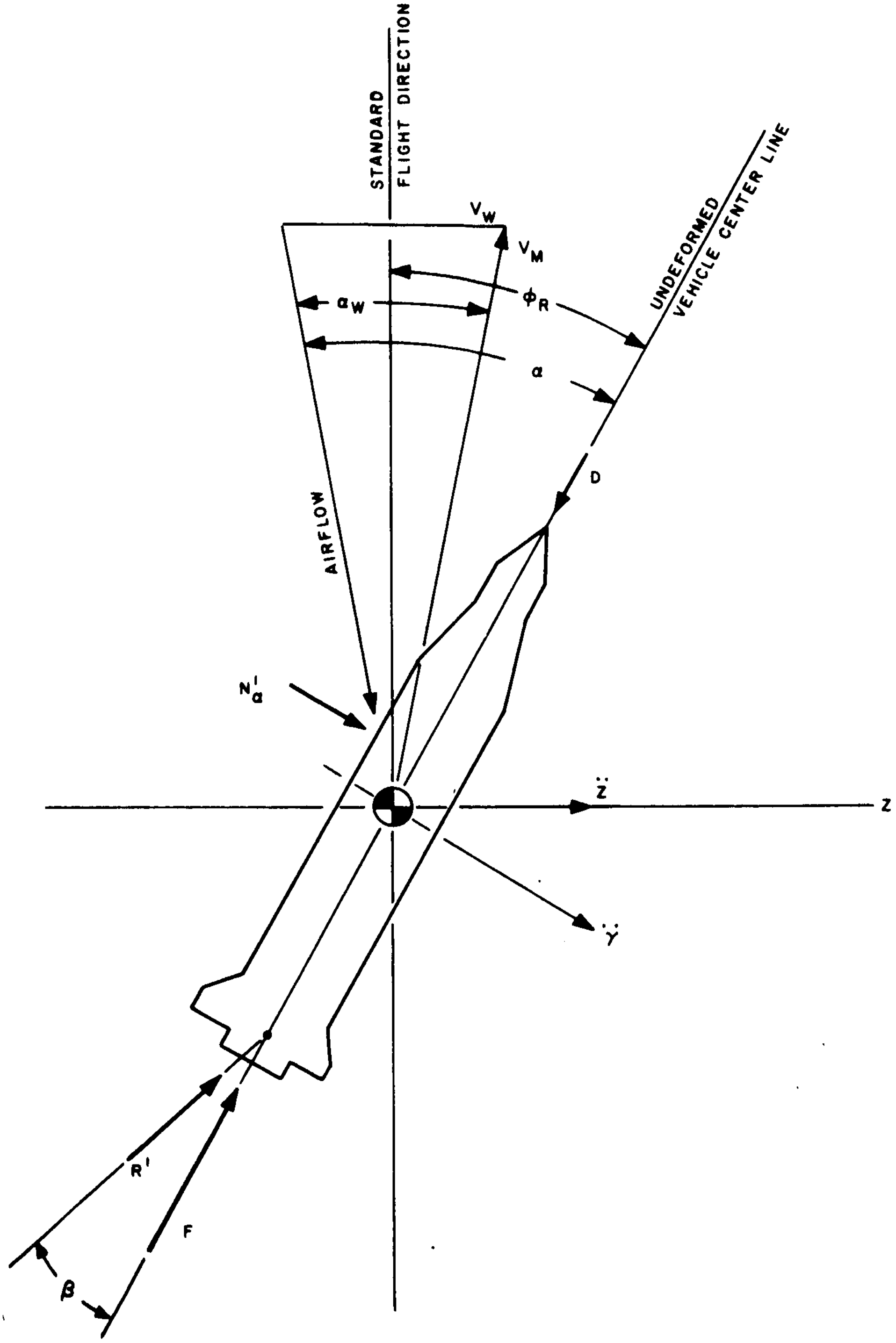

Figure B2. Rigid Body Coordinate System

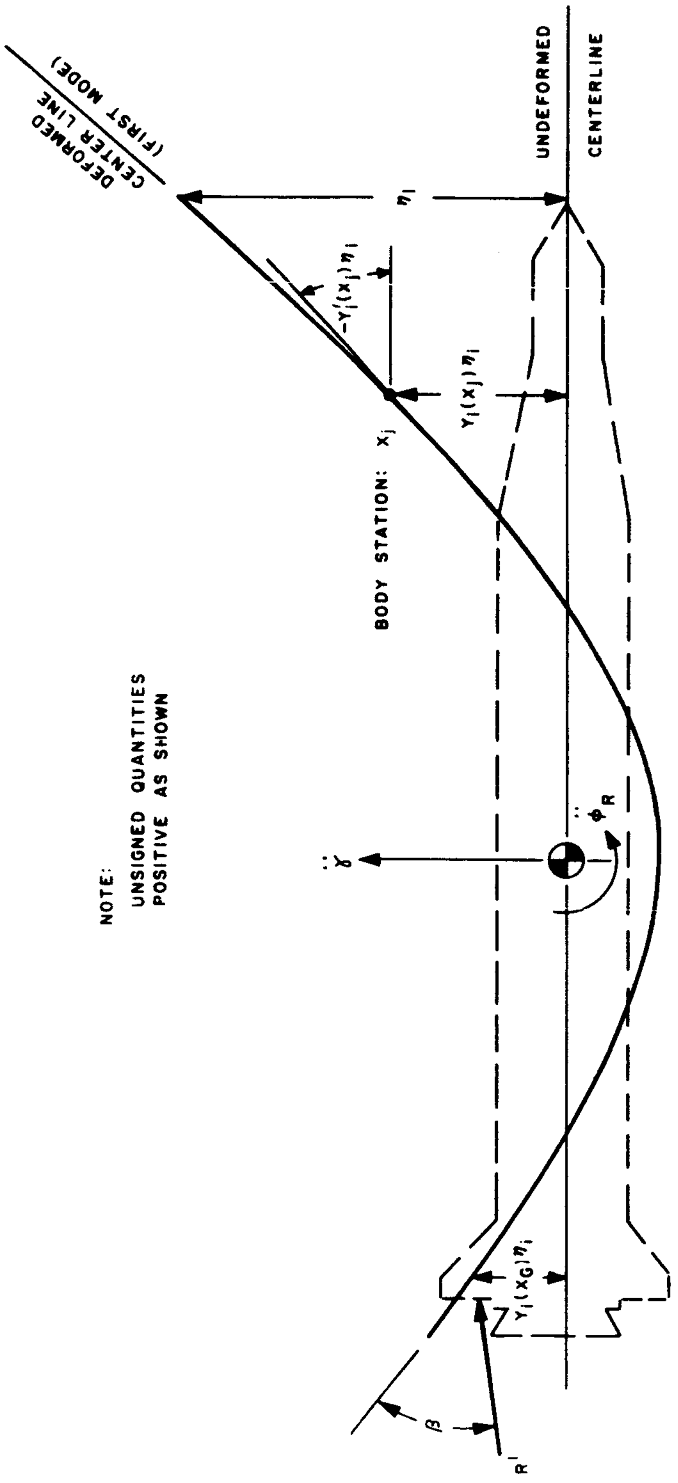

Figure B3. Bending Coordinate System

TABLE B1

RIGID BODY PARAMETERS

Parameter	Units	Flight Time (seconds)							
		0	20	40	60	80	100	120	140
C_1	1/sec^2	0	-0.01192	-0.05875	+0.01492	-0.43679	-0.2910	-0.06162	-0.00418
C_2	1/sec^2	0.73686	0.7468	0.76137	0.8046	0.8798	1.0117	1.2887	2.0834
F	Kg	726,209	738,657	755,987	780,278	800,643	809,790	807,721	396,956
R'	Kg	363,104	369,328	377,994	390,139	400,322	404,895	403,860	198,478
D	Kg	1,500.1	7,295.7	18,571.3	54,124.9	64,683.8	21,451.2	4,199.9	604.6
q	Kg/m^2	0	222	1,133	2,567	3,039	1,516	440	95
S	m^2	33.45	33.45	33.45	33.45	33.45	33.45	33.45	33.45
C_{N_α}	---	5.85	5.85	5.91	7.1	6.0	5.26	4.75	4.06
I_x	Kg-m-sec^2	8,113,060	8,073,561	8,056,147	8,008,431	7,842,111	7,437,743	6,570,943	4,802,586
I_E	Kg-m-sec^2	464	464	464	464	464	464	464	464
S_E	Kg-sec^2	337	337	337	337	337	337	337	337
m	Kg-sec^2/m	60,763	55,035	49,281	43,536	37,784	32,076	26,408	20,798
l_G	m	16.464	16.235	16.227	16.516	17.234	18.585	20.968	25.205
l_A	m	26.530	26.759	26.759	26.530	25.785	24.410	22.060	17.763
V_m	---	0	62.2	156	293.2	480.9	783.7	1,229.2	1,815.6

TABLE B2

BODY STATION - INCHES

Station-Inches	Flight Time (seconds)							
	0	20	40	60	80	100	120	140
x_{IU}	1,690	1,690	1,690	1,690	1,690	1,690	1,690	1,690
x_{CP}	825	830	822	743	1,000	1,151	1,153	1,153
x_{CG}	748	739	739	750	779	832	926	1,092
x_{S4}	1,110	1,110	1,110	1,110	1,110	1,110	1,110	1,110
x_G	100	100	100	100	100	100	100	100

TABLE B3

SLOSH MODE PARAMETERS
(SIV-B LOX TANK)

Parameter	Units	Flight Time (seconds)							
		0	20	40	60	80	100	120	140
ω_{S4}	rad/sec	3.24	3.46	3.65	3.9	4.25	4.75	5.35	5.97
ζ_{S4}	---	0.03	0.03	0.03	0.03	0.03	0.03	0.03	0.03
m_{S4}	Kg-sec^2/m	1,560	1,560	1,560	1,560	1,560	1,560	1,560	1,560
l_{S4}	m	-9.2	-9.5	-9.5	-9.2	-8.5	-7.1	-4.7	-0.5

TABLE B4

BENDING PARAMETERS
FIRST BENDING MODE

Parameter	Units	Flight Time (seconds)							
		0	20	40	60	80	100	120	140
ζ_{B_1}	---	0.01	0.01	0.01	0.01	0.01	0.01	0.01	0.01
ω_{B_1}	rad/sec	7.9733	8.3440	8.6394	8.8216	8.8970	8.9159	8.9473	9.2111
M_1	Kg-sec^2/m	1,142.7	1,018.2	931.03	877.18	841.19	605.12	841.21	866.17
$Y_1(x_{IU})$	---	0.045	0.015	-0.005	-0.020	-0.022	-0.027	-0.020	-0.030
$Y_1(x_{CP})$	---	-0.16	-0.16	-0.16	-0.140	-0.180	-0.165	-0.160	-0.15
$Y_1(x_{S4})$	---	-0.140	-0.152	-0.160	-0.162	-0.170	-0.170	-0.165	-0.155
$Y_1(x_G)$	---	0.2047	0.1911	+0.1713	0.1522	0.13914	0.1356	0.1494	0.2210
$Y_1'(x_{IU})$	1/m	-0.016535	-0.015748	-0.014961	-0.014174	-0.014567	-0.014961	-0.014567	-0.013386
$Y_1'(x_{CP})$	1/m	0.00354	0.00354	0.00433	0.00984	-0.00197	-0.00433	-0.00433	-0.00275
$Y_1'(x_G)$	1/m	0.01772	0.01811	0.01732	0.01614	0.01496	0.01496	0.01575	0.01850

TABLE B5

BENDING PARAMETERS
SECOND BENDING MODE

Parameter	Units	Flight Time (seconds)							
		0	20	40	60	80	100	120	140
ζ_{B_2}	---	0.01	0.01	0.01	0.01	0.01	0.01	0.01	0.01
ω_{B_2}	rad/sec	16.179	16.663	17.5992	18.699	19.440	19.704	19.773	19.786
M_2	Kg-sec^2/m	2,165.2	2,093.7	608.69	537.21	430.65	416.30	411.81	411.70
$Y_2(x_{IU})$	---	-0.220	-0.220	-0.205	-0.190	-0.170	-0.167	-0.160	-0.160
$Y_2(x_{CP})$	---	0.08	0.09	0.115	0.140	0.107	0.070	0.070	0.07
$Y_2(x_{S4})$	---	-0.020	-0.010	+0.025	+0.060	+0.075	+0.080	+0.082	+0.082
$Y_2(x_G)$	---	-0.13782	-0.15967	-0.1685	-0.1468	-0.09122	-0.06821	-0.05623	-0.06165
$Y_2'(x_{IU})$	1/m	0.007874	0.009843	0.011811	0.013780	0.015748	0.016535	0.015748	0.015748
$Y_2'(x_{CP})$	1/m	0.00826	0.00748	0.00748	0	0.01023	0.01181	0.01181	0.01181
$Y_2'(x_G)$	1/m	-0.01772	-0.02165	-0.02165	-0.02087	-0.01378	-0.01142	-0.01063	-0.01023

TABLE B6

BENDING PARAMETERS
THIRD BENDING MODE

Parameter	Units	Flight Time (seconds)							
		0	20	40	60	80	100	120	140
ζ_{B_3}	---	0.01	0.01	0.01	0.01	0.01	0.01	0.01	0.01
ω_{B_3}	rad/sec	25.567	25.842	26.911	30.023	28.186	34.061	39.257	41.111
M_3	Kg-sec^2/m	1,216.9	1,449.5	2,308.0	5,762.7	4,904.7	6,759.0	4,262.5	2,953.3
$Y_3(x_{IU})$	---	0.055	0.07	0.125	0.30	0.207	0.550	0.820	0.900
$Y_3(x_{CP})$	---	-0.119	-0.14	-0.235	-0.730	-0.050	-0.020	-0.160	-0.21
$Y_3(x_{S4})$	---	+0.085	+0.085	+0.050	-0.02	+0.070	-0.100	-0.280	-0.320
$Y_3(x_G)$	---	0.1340	0.1598	0.2188	0.3156	0.77527	0.9416	0.5551	0.2251
$Y_3'(x_{IU})$	1/m	0.007480	0.012992	0.012992	0	0.013780	-0.009055	-0.023622	-0.039370
$Y_3'(x_{CP})$	1/m	-0.01380	-0.03149	-0.03937	-0.07283	-0.02756	-0.06181	0.7874	-0.09055
$Y_3'(x_G)$	1/m	0.01386	-0.03307	0.04921	0.08661	0.14173	0.21969	0.15748	0.08661

TABLE B7

BENDING PARAMETERS
FOURTH CLUSTER MODE

Parameter	Units	Flight Time (seconds)							
		0	20	40	60	80	100	120	140
ζ_{B_4}	---	0.01	0.01	0.01	0.01	0.01	0.01	0.01	0.01
ω_{B_4}	rad/sec	16.185	16.663	18.171	21.168	26.861	38.082	70.654	86.375
M_4	Kg-sec^2/m	2,255.0	2,165.3	108,136.0	8,025.7	900,000.0	1.527 x 10^7	8,160.6	1.066 x 10^5
$Y_4(x_{IU})$	---	-0.220	-0.210	-0.20	-0.10	+0.300	+1.0	-0.70	-2.9
$Y_4(x_{CP})$	---	0.08	0.095	+0.14	0.270	0.1	0	0.41	0.8
$Y_4(x_{S4})$	---	-0.015	0	+0.05	+0.10	+0.1	0	+0.63	+0.60
$Y_4(x_G)$	---	-0.13778	-0.15962	-0.12705	+0.11	+0.71078	+0.8222	+0.43617	+1.509
$Y_4'(x_{IU})$	1/m	0.009449	0.008661	0.013520	0.01693	0.015748	-0.023622	-0.02756	+0.55118
$Y_4'(x_{CP})$	1/m	+0.00787	+0.00709	+0.01220	+0.03425	-0.02322	-0.07874	+0.12598	+0.01181
$Y_4'(x_G)$	1/m	-0.01772	-0.02165	-0.03425	-0.04527	+0.04331	+0.73228	+0.12992	+1.0354

TABLE B8

BENDING PARAMETERS
FIFTH CLUSTER MODE

Parameter	Units	Flight Time (seconds)							
		0	20	40	60	80	100	120	140
ζ_{B_5}	---	0.01	0.01	0.01	0.01	0.01	0.01	0.01	0.01
ω_{B_5}	rad/sec	20.426	20.923	22.067	24.291	36.907	52.854	52.854	52.854
M_5	Kg-sec^2/m	2,151.7	1,700.1	1,591.8	2,309.0	11,805.0	3.470 x 10^5	3.489 x 10^5	3.469 x 10^5
$Y_5(x_{IU})$	---	-0.125	-0.117	-0.082	+0.002	+0.69	+0.92	---	---
$Y_5(x_{CP})$	---	0.225	0.207	0.155	0.027	-0.50	-0.25	---	---
$Y_5(x_{S4})$	---	+0.133	+0.130	+0.140	+0.128	-0.25	-0.3	---	---
$Y_5(x_G)$	---	0.1823	0.1545	0.2067	0.4016	0.23505	0.88369	---	---
$Y'_5(x_{IU})$	1/m	0.018504	0.018504	0.019291	0.018110	-0.003937	-0.55118	---	---
$Y'_5(x_{CP})$	1/m	0.01417	0.01063	0.00394	-0.00708	-0.08070	-0.01181	-0.01181	-0.01181
$Y'_5(x_G)$	1/m	0.01771	0.01417	0.02362	0.06147	0.10630	0.39370	0.39370	0.39370